

# **Investigation of Fluorination Methodologies for the Application in Positron Emission Tomography**



Oliver Macaulay Gray

Submitted in fulfilment of the requirements for the degree of Doctor of  
Philosophy

Bedson Building, School of Natural and Environmental Sciences

Newcastle University

September 2022

## Abstract

The use of fluorinated compounds has become increasingly popular within recent decades, especially within the fields of pharmaceuticals, agrochemicals, and fine chemicals. Incorporation of fluorine into a compound has various effects on the chemical properties of a molecule. In the pharmaceutical industry, around 20% of the commercially available pharmaceuticals contain fluorine<sup>a</sup>. Fluorine incorporation has profound effects on the pharmacokinetics and physiochemical properties of a compound, such as the adsorption, distribution, and increased metabolic stability.

An emerging area of fluorine chemistry is the application of the unnatural isotope fluorine-18 in radiochemical labelling for positron emission tomography (PET). PET is a non-invasive nuclear imaging technique that is used to observe biological and physiological functions in the body, including blood flow, metabolism and to probe disease progression. Fluorine-18 is the most clinically relevant radioisotope for PET imaging; however the universal uptake of PET is limited and there is an urgent unmet clinical need to expand the range of the fluoro-radiopharmaceuticals that are readily available and open the way for the benefits that the power medical imaging offers in the diagnosis and management of disease.

The work herein describes the investigation into a nucleophilic and electrophilic fluorination methodology. The study of an iron (II) acetylacetonate initiated electrophilic fluorination method led to the discovery of a practical route to the thiodifluoromethylene group using Selectfluor<sup>TM</sup>. Subsequent mechanistic investigation has allowed the synthesis of a number of difluorinated compounds in moderate to excellent yields.

---

<sup>a</sup> As of 2020.

## Acknowledgements

I would first like to thank my supervisor Dr Michael Carroll, for your guidance and help throughout my PhD. You have shaped me into the chemist and researcher I am today. Without your support and wise words, it would have been a far more difficult undertaking to finish. It has been a pleasure to work in your group, and I cannot thank you enough for the opportunity you gave me all those years ago.

My thanks also extends to Dr James Knight. Your supervision this last year has been incredibly helpful. I am so grateful for the help and guidance you provided. It was much appreciated you taking on the task of supervising me.

I would like to thank High Force Research and the ERDF for funding this project and allowing me to have this opportunity to gain valuable knowledge and experience I will use for the rest of my career.

I would like to thank Dr Paul Waddell for small molecule crystallography. Dr Corinne Wills and Dr Casey Dixon, I would like to thank you for helping me with the excessive use of the NMR especially with the kinetics studies.

To the Johnston Lab, my friends and colleagues that I had the pleasure working with. You made the last four years bearable. I have had a fantastic time working alongside you and I wish you all good luck in your own research (which I miss listening to).

To my friends and family, your unwavering support has not gone unnoticed. You have helped me get through some of the most stressful years of my life. Knowing that I have you all there beside me has allowed me to achieve my potential. I cannot thank you all enough.

I would especially like to thank my lovely wife, Rachel. My research has meant the world to me, as do you. You have had to put up with the highs and the lows, sacrificed and patiently waited. Like you always say, "It will all be worth it in the end".

## Table of Contents

Chapter 1. Introduction.....	1
1.1 Positron Emission Tomography.....	1
1.2 Radioisotopes Used in PET .....	2
1.3 Fluorine-18 Production and Incorporation .....	4
1.3.1 Electrophilic Fluorination .....	5
1.3.2 Nucleophilic Fluorination .....	7
1.4 2-[ <sup>18</sup> F]Fluoro-2-deoxy-D-Glucose ([ <sup>18</sup> F]FDG).....	7
Chapter 2. Nucleophilic Fluorination using a Manganese (III) Salen Catalyst .....	13
2.1 Background .....	13
2.2 Nucleophilic Fluorination – Initial Reactions .....	16
2.2.1 Rucaparib and Deprotection of Benzyl Groups .....	18
2.3 Optimisation.....	20
2.3.1 Mn(salen)OTs .....	20
2.3.3 Fluoride Sources .....	20
2.3.3 By-product Identification.....	22
2.3.4 Practical Aspects.....	23
2.4 Mechanism of Oxygen Transfer.....	24
2.4.1 Proposed Mechanism .....	24
2.4.2 Radical Scavenger Reactions.....	25
2.4.3 Oxidant Test Reactions.....	25
2.4.3.1 Epoxidation Reactions .....	26
2.4.3.2 Fluorination Test with Oxidants.....	27
2.5 Alternative Manganese Catalysts .....	27
2.5.1 Manganese Salen Fluoride Complexes .....	28
2.5.1.1 Substituted Salen Derivatives .....	32
2.5.2 Salen Derivatives and Other Transition Metals .....	33
2.5.2.1 Alternative Transition Metals .....	33
2.6 Conclusions and Future Work .....	34
2.7 Experimental.....	35
Chapter 3. Electrophilic Fluorination via Iron (II) Acetylacetonate Radical Initiators. 44	
3.1 Background .....	44
3.2 Initial Reactions.....	47

3.3	Optimisation of Initial Reactions .....	47
3.3.1	Fluorination of Acetylacetonate Ligand.....	47
3.3.2	Synthesis of Fe(acetylacetonate) <sub>2</sub> .....	54
3.3.3	Synthesis of Substituted Fe(acetylacetonate) <sub>2</sub> .....	59
3.3.3.1	Characterisation of Fe(acac) <sub>2</sub> Derivatives .....	61
3.4	Testing of the Fe(x-acetylacetonate) <sub>2</sub> Derivatives and Process Optimisation ...	67
3.4.1	Process Optimisation – Degassing Solvent .....	69
3.4.2	Testing of the Fe(x-acetylacetonate) <sub>2</sub> Derivatives.....	70
3.4.3	Process Optimisation.....	71
3.4.3.1	Reaction Time .....	71
3.4.3.2	Reaction Temperature .....	72
3.4.3.3	Kinetics Experiment .....	73
3.4.3.4	Alternative Fluorine Source .....	74
3.4.3.5	Addition of Additives .....	75
3.4.4	Optimisation Conclusion .....	76
3.5	Fluorination of Wider Range of Substrates .....	77
3.5.1	Radical Stability.....	80
3.5.2	Chain Length Investiagtion.....	81
3.6	Conclusions and Future Work .....	83
3.7	Experimental.....	84
Chapter 4. A Practical Route to the Thiodifluoromethylene Group .....		96
4.1	Current Methodology .....	96
4.1.1	Direct Fluorination .....	96
4.1.1.1	Electrolysis.....	96
4.1.1.2	Nucleophilic Fluorination .....	97
4.1.1.3	Electrophilic Fluorination .....	98
4.1.2	Indirect Synthesis .....	100
4.2	Initial Reactions.....	101
4.3	Optimisation.....	103
4.3.1	Reaction Conditions .....	103
4.3.1.1	Practical Measures .....	103
4.3.1.2	Fluorine Source .....	105
4.3.1.2.1	Alternative Counter Ion to BF <sub>4</sub> .....	106
4.3.2	Tetrafluoroborate Counter Ion Investigation.....	108

4.3.2.1 Lewis Acid Addition.....	108
4.3.2.2 Additional Fluoride Sources .....	109
4.3.3 Conclusion to Optimisation.....	110
4.4 Mechanism Identification .....	110
4.4.1 Sulfone Compounds .....	113
4.4.2 Kinetics Studies.....	113
4.4.3 Radical Reactions and Scavengers .....	115
4.5 Substrate Scope .....	116
4.5.1 Thioacetonitrile Compounds.....	118
4.5.1.2 Fluorinated Substrates.....	120
4.5.2 Electron Withdrawing Group and Hyperconjugation Effect.....	121
4.5.3 Effects of Substituents within the Aromatic-Thioether System.....	121
4.5.4 Hammett Plot .....	123
4.5.5 Electron Rich Ring Systems .....	126
4.6 Further Functionalisation .....	127
4.6.1 Raney-Nickel Desulfurisation .....	127
4.7 Conclusions and Future Work.....	130
4.8 Experimental.....	131
Appendix. ....	144
Appendix A Crystal Structure Refinement for Compound <b>2.25</b> .....	144
Appendix A Crystal Structure Refinement for Compound <b>2.30</b> .....	150
Appendix A Crystal Structure Refinement for Compound Fe(acac) <sub>3</sub> .....	157
Appendix A Crystal Structure Refinement for Compound Fe(3-chloroacac) <sub>3</sub> .....	162

## Table of Figures

Figure 1.1. Structure of EDTA and DOTA. ....	3
Figure 1.2. Electrophilic fluorinating reagents. ....	6
Figure 1.3. 2-[ <sup>18</sup> F]Fluoro-2-deoxy-D-glucose ([ <sup>18</sup> F]FDG). ....	10
Figure 1.4. Accumulation of glucose and [ <sup>18</sup> F]FDG within a cell .....	12
Figure 2.1. Structures of the Katsuki and Jacobsen Mn (III) salen complexes. ....	17
Figure 2.2. Rucaparib. ....	24
Figure 2.3. Structures of <b>2.12</b> , the monofluorinated <b>2.13</b> and the by-products <b>2.25</b> and <b>2.26</b> . ....	28
Figure 2.4. Crystal structure of <b>2.25</b> . ....	29
Figure 2.5. <sup>19</sup> F NMR spectrum of the mixture of <b>2.13</b> and <b>2.26</b> . <b>2.13</b> is the overlapping doublet of quartets (-166.5) whilst <b>2.26</b> is the quartet (-87.2 ppm) .....	29
Figure 2.6. The salen ligands which were used in the synthesis of Mn(salen)F type compounds. ....	35
Figure 2.7. <sup>19</sup> F NMR of Mn(salen)F spectrum. ....	35
Figure 2.8. Crystal structure of the Mn(salen)F using ( $\pm$ )- <b>2.29</b> as a ligand. ....	36
Figure 2.9. Bond lengths of the Mn-F bonds. ....	37
Figure 2.10. Bond angles between Mn-F-Mn and F-Mn-F (Top) and the coordinating water molecule (Bottom). ....	38
Figure 2.11. Structure of the Mn(salen)Cl complexes. ....	39
Figure 2.12. Structure of the VO(salen)Cl ( $\pm$ )- <b>2.31</b> . ....	40
Figure 3.1. Structures of the substrates investigated during the initial reactions. ....	54
Figure 3.2. 5,6-Dimethoxy-1-indanone and mono-fluorinated products. ....	55
Figure 3.3. <sup>19</sup> F NMR spectrum of the crude reaction mixtures at temperatures 0 °C, RT and 55 °C. ....	56
Figure 3.4. Structures of the substituted acetylacetonone derivatives used. ....	60
Figure 3.5 Electrostatic potential of some of the substituted acetylacetonone derivatives. ....	62
Figure 3.6. <sup>1</sup> H NMR spectrum of Fe(acac) <sub>3</sub> . ....	65
Figure 3.7. <sup>1</sup> H NMR of Fe(acac) <sub>2</sub> over a period of about a week (Top) and the stacked <sup>1</sup> H NMR of Fe(acac) <sub>2</sub> over a period of 10 days in a sealed J Young NMR tube under an N <sub>2</sub> atmosphere (Bottom) .....	68
Figure 3.8. Structure of the substituted Fe(acac) <sub>2</sub> derivatives <b>3.11-17</b> . ....	69

Figure 3.9. Photos of the substituted Fe(acac) <sub>2</sub> derivatives.....	70
Figure 3.10. <sup>1</sup> H NMR of the Fe(acac) <sub>2</sub> derivatives. ....	71
Figure 3.11a. <sup>13</sup> C NMR of Fe(acac) <sub>2</sub> .....	72
Figure 3.12. Anaerobic setups that were tested .....	74
Figure 3.13. Crystal structures of iron (III) acetylacetonate (Left) and iron (III) 3-chloroacetylacetonate .....	76
Figure 3.14. Structures of Fe(acac) <sub>2</sub> tetramer (left), and the mononuclear bis-ligand adducts: trans (middle) and cis (right). (Right).....	76
Figure 3.15. Graph of ln(concentration) vs. time.....	84
Figure 3.16. Structures of the substrates investigated. ....	88
Figure 3.17. Structure of Amitriptyline™. ....	90
Figure 3.18. p-Cymene <b>3.38</b> and the two potential fluorinated products. ....	92
Figure 3.19. Proposed coordination to allow lone pair stabilisation of the radical intermediates.....	93
Figure 4.1. Colour difference when using one equivalent (left) and two equivalents (right).....	118
Figure 4.2. Electrophilic fluorinating agents used.....	118
Figure 4.3. Reactivity series for the electrophilic fluorinating reagents .....	119
Figure 4.4a. <sup>19</sup> F NMR of <b>4.39</b> . Residual BF <sub>4</sub> peak at -151 ppm.....	120
Figure 4.5. Concentration vs time for the fluorination of 4.34 followed by <sup>19</sup> F NMR. ....	127
Figure 4.6. <sup>19</sup> F NMR at various time points .....	127
Figure 4.7. -ln[product] vs time for the kinetics reaction of 4.4 (0 h to 10 h). ....	128
Figure 4.8. The substrates investigated during the substrate scoping experiments. Majority of the compounds were commercially available. ....	130
Figure 4.9. Stacked <sup>19</sup> F NMR spectrum of the <b>4.48</b> (top) and <b>4.52</b> (bottom).....	132
Figure 4.10. <sup>19</sup> F NMR spectrum of the 'rotamers'. ....	132
Figure 4.11. Concentration vs time for the p-substituted derivatives of 4.1. ....	137
Figure 4.12. Hammett plot for the p-substituted derivatives of 4.1.....	138
Figure 4.13. <sup>19</sup> F NMR spectrum of the desulfurisation reaction of <b>4.35</b> .....	143



## Table of Tables

Table 1.1. Properties of radionuclides. 2-4.....	2
Table 2.1. Yields of <b>2.13</b> when using Mn(salen)Cl as a catalyst in the presence of radical scavengers.....	32
Table 3.1. The pK <sub>a</sub> and enol:keto ratio of the ligands <b>3.11-3.17</b> . <sup>1</sup> pK <sub>a</sub> calculated using the freely accessible web server MolGpka ( <a href="https://xundrug.cn/molgpka">https://xundrug.cn/molgpka</a> ) <sup>5,2</sup> The enol percentage was calculated from <sup>1</sup> H NMR integrating the CH <sup>e</sup> /CH <sub>2</sub> <sup>k</sup> , CH <sub>3</sub> <sup>e</sup> /CH <sub>3</sub> <sup>k</sup> and the CH <sup>k</sup> /OH <sup>e</sup> of the acetylaceton derivatives. <sup>19</sup> F and <sup>1</sup> H NMR was used to calculate the %enol of <b>3.16</b> . CDCl <sub>3</sub> was used as the solvent for all the NMR. * %Enol are in accordance with those published. <sup>3,6-11</sup> .....	63
Table 3.2. Yields of the Fe(acac) <sub>2</sub> complexes and the colour.....	70
Table 3.3. Conversion of ligands to the fluorinated ligands in mol%. .....	77
Table 3.4. Yields of the benzylic fluorination product using some of the derivatives synthesised. ....	78
Table 3.5. Yields of the benzylic fluorination products for the model substrates <b>3.4</b> and <b>3.26</b> . .....	80
Table 3.6. Yields of the fluorinated products when using <b>3.21</b> and <b>3.24</b> as the radical initiators. ....	81
Table 3.7. Yields of the benzylic fluorination products at times 4, 8, 24 h and 3 days. ....	82
Table 3.8. Yields of the fluorinated products of the substrates investigated. ....	89
Table 3.9. Radical energies and monofluorinated benzylic product yields. ....	91
Table 4.1. Yields of the geminal difluoroproduct <b>4.33</b> with the addition of Lewis acids, following geminal fluorination method. ....	122
Table 4.2. Yields of the geminal difluoro-products of <b>4.1</b> and <b>4.34</b> when using radical scavengers.....	129
Table 4.3. The highest yielding substrates. ....	133
Table 4.4. Yields of the difluorothiomethylene products from the p-substituted aromatic thioethers. ....	135
Table 4.5. Rate of formation of difluoro-product.....	137
Table 4.6. The %conversion of <b>4.76</b> to <b>4.77</b> over a period of 24-168 h.....	142

## Table of Schemes

Scheme 1.1 The mixture of products from fluorination of 1,4 -ketoesters.....	6
Scheme 1.2. Phenol deoxyfluorination reaction proposed by Ritter et al. ....	8
Scheme 1.3. Use of the modified PhenoFluor for [ <sup>18</sup> F]fluoride incorporation. ....	8
Scheme 1.4. Deoxyfluorination reported by Doyle et al.....	8
Scheme 1.5. An example of a radiochemical protocol used by Toste et al.....	10
Scheme 1.6. General method for the introduction of [ <sup>18</sup> F]difluorocarbenes via O-H, S-H or N-H insertion.....	10
Scheme 1.7. Synthesis of [ <sup>18</sup> F]FDG by electrophilic fluorination (Wolf, 1976 ). ....	13
Scheme 1.8. Nucleophilic method of [ <sup>18</sup> F]FDG production.....	13
Scheme 2.1. Epoxidation using Mn(salen)X catalysts.....	17
Scheme 2.2. Epoxidation of indene.....	18
Scheme 2.3. Mechanism of oxygen transfer for the epoxidation. Mechanism A: concerted, mechanism B: via radical and mechanism C: manganaoxtane intermediate. Ligands omitted for clarity.....	19
Scheme 2.4. Asymmetric aerobic oxidation of cinnamic alcohol. ....	20
Scheme 2.5. Fluorination of 4-ethyl-1,1'-biphenyl using Mn(salen)Cl and a fluorine source.....	20
Scheme 2.6. Groves et al late stage benzylic C-H fluorination using [ <sup>18</sup> F]fluoride....	20
Scheme 2.7. Synthesis of salen-ligand (±)-N,N'-bis(3,5-di-tert-butylsalicylidene)-1,2-cyclohexanediamine <b>(±)-2.16</b> .....	22
Scheme 2.8. Synthesis of Jacobsen's catalyst <b>(±)-2.04</b> .....	22
Scheme 2.9. Synthesis of iodosobenzene <b>2.18</b> .....	23
Scheme 2.10. Fluorination of ethyl-1,1'-biphenyl <b>2.12</b> .....	23
Scheme 2.11. Radiochemical transformation of borylated Rucaparib precursor to [ <sup>18</sup> F]Rucaparib. ....	25
Scheme 2.12. Radiofluorination of an Olaparib derivative by Pimlott et al. ....	25
Scheme 2.13. N-Benzylmethylamine fluorination and subsequent imine formation and hydrolysis. i AgF 1.25 Equiv., Mn(salen)Cl, PhIO, 50 °C, 6 h.....	25
Scheme 2.14. Synthesis of Mn(Salen)OTs <b>(±)-2.24</b> from <b>(±)-2.04</b> and AgOTs.....	26
Scheme 2.15. Catalytic cycle proposed by Groves et al for the installation of the benzylic fluorine. Salen ligand omitted for clarity. ....	31
Scheme 2.16. Addition of pyridine N-oxide to the catalyst.....	32

Scheme 2.17. Epoxidation of styrene <b>2.27</b> .....	33
Scheme 3.1. Benzylic fluorination reported by Lectka et al.....	53
Scheme 3.2. The dehydrohalogenation and E <sub>1</sub> cB reaction mechanisms. ....	56
Scheme 3.3. Fluorinated acetylacetonate by-products.....	57
Scheme 3.4. Potential mechanism of the fluorination of the acetylacetonate ligand. 58	
Scheme 3.5. The outcome of the equilibrium when blocking groups and electronic changes occur altering the keto:enol equilibrium and pK <sub>a</sub> of the α-carbonyls.....	60
Scheme 3.6. Conjugation and the resonance forms of 3.14. ....	64
Scheme 3.7. Fluorination reactions using model substrates <b>3.4</b> and <b>3.26</b> .....	77
Scheme 3.8. Proposed mechanism by Lectka et al modified for iron (II).....	79
Scheme 3.9. Fluorination reaction of <b>3.04</b> at an elevated temperature of 50 °C.....	82
Scheme 3.10. NMR kinetics experiment using <b>3.26</b> as the substrate. ....	83
Scheme 3.11. First order reaction. ....	83
Scheme 3.12. Resonance of the benzylic radicals stabilised by the p-nitro and o-nitro-group. ....	90
Scheme 4.1. Anodic mono- and difluorination of propargyl sulfides. ....	110
Scheme 4.2. Anodic fluorination of arylthioalkynes. ....	110
Scheme 4.3. Hydrofluorination of alkynyl sulfides using 70% Py•HF. ....	111
Scheme 4.4. Halogen exchange reaction using TREAT•3HF to synthesise gem-difluoroalkylsulfanyl carbonyl compounds. ....	111
Scheme 4.5. Fluorination using IF <sub>5</sub> and TREAT•3HF.....	111
Scheme 4.6. Fluorination of thioanisole with XeF <sub>2</sub> . ....	112
Scheme 4.7. Difluorination of sulfonamides using NaHMDS/KHMDS and NFSI ...	112
Scheme 4.8. Fluorination and subsequent cross-coupling to form protected L-4-[sulfono(difluoromethyl)]phenylalanine.....	113
Scheme 4.9. Synthesis of difluoro-β-ketosulfonone using Selectfluor™ and [Hbim]BF <sub>4</sub> . .....	113
Scheme 4.10. Synthesis and application of bromodifluorosulfanylmethane, a gem-difluoromethylene building block. ....	113
Scheme 4.11. Synthesis of difluorosulfanylacetate. ....	114
Scheme 4.12. Structure of the sulfur containing substrate <b>4.1</b> and the benzylic product <b>4.32</b> and the thiodifluoro-product <b>4.33</b> . ....	115
Scheme 4.13. The reaction of <b>4.34</b> with Selectfluor™ and Fe(acac) <sub>2</sub> derivatives. .	115

Scheme 4.14. The synthesis of <b>4.39</b> by ion exchange using ammonium hexafluorophosphate.....	120
Scheme 4.15. Investigation into the Lewis Acid addition using <b>4.01</b> as the substrate. .....	122
Scheme 4.16. Potential mechanistic options for the formation of thiodifluoromethylene group-.....	125
Scheme 4.17. Fluorination of 2-(phenylthio)acetonitrile.....	131
Scheme 4.18. The initial nucleophilic attack of the sulfur lone pair on Selectfluor™. .....	136
Scheme 4.19. Formation of the transition state and the S-F bond.....	139
Scheme 4.20. Difluorination to synthesise gem-difluoro-bisarylic derivatives. ....	140
Scheme 4.21. General Mozingo reduction. Formation of a thioacetal followed by desulfurisation to an alkane. ....	141
Scheme 4.22. Desulfurisation of <b>4.76</b> using Raney-Nickel. ....	141
Scheme 4.23. The desulfurisation reaction of <b>4.35</b> to <b>4.78</b> . ....	142

## Abbreviations

Ache	Acetylcholine esterase
AP <sup>+</sup>	Affinity Purification
Ar	Aryl
b.p	Boiling Point
BCHe	Butylcholine esterase
Br	Broad
CS <sub>N</sub> Ar	Concerted Nucleophilic Aromatic Substitution
CT	Computed Tomography
d	Doublet
DABCO	1,4-Diazabicyclo[2.2.2]octane
DAST	Diethylaminosulfur trifluoride
DCM	Dichloromethane
dd	Doublet of Doublets
ddd	Doublet of Doublet of Doublets
DMF	Dimethylformamide
DMSO	Dimethyl sulfoxide
DNA	Deoxyribose nucleic acid
E <sub>1</sub> CB	Elimination, Unimolecular, Conjugate Base
EDTA	Ethylenediaminetetraacetic acid
ee	Enantiomeric Excess
E <sub>max</sub>	Electromotive Force
Equiv.	Equivalent
EWG	Electron Withdrawing Group
FDG	Fluorodeoxyglucose
FLT	Fluorothymidine
FPT	Freeze-Pump-Thaw
FT-IR	Fourier Transform Infrared Spectroscopy
g	Gram
Gem	Geminal
GLUT	Glucose Transporter Proteins
h	Hour
HIV/AIDS	Human Immunodeficiency Virus/Acquired Immunodeficiency Syndrome
Hz	Hertz

J	Coupling Constant Measured in Hertz
keV	Kiloelectron Volt
LDA	Lithium Diisopropylamide
m	Multiplet
m.p	Melting Point
<i>m</i> -CPBA	<i>Meta</i> -Chloroperbenzoic Acid
MeCN	Acetonitrile
MeV	Megaelectron Volt
MHz	Megahertz
mL	Millilitre
mm	Millimetre
mmol	Millimoles
MRI	Magnetic Resonance Imaging
MS	Multiple Sclerosis
NFSI	<i>N</i> -Fluorobenzenesulfonamide
NMR	Nuclear Magnetic Resonance
ODS	Ozone Depleting Substance
PARP	Poly(ADP-ribose)polymerase
Pent.	Pentet
PET	Positron Emission Tomography
Ph	Phenyl
ppm	Parts Per Million
Py	Pyridine
q	Quartet
R <sub>f</sub>	Retardation Factor
RCC	Radiochemical Conversion
RCY	Radiochemical Yield
RT	Room Temperature
s	Singlet
S <sub>N</sub> 2	Nucleophilic Substitution, 2 <sup>nd</sup> Order
S <sub>N</sub> Ar	Nucleophilic Aromatic Substitution
SPECT	Single Photon Emission Computed Tomography
t	Triplet
t <sub>1/2</sub>	Half-life
TEDA	Triethylenediamine

TEMPO (2,2,6,6)-Tetramethylpiperidin-1-yl)oxyl  
TLC Thin Layer Chromatography  
TOF Time of Flight  
TREAT•3HF Triethylamine Trihydrofluoride

## Chapter 1 - Introduction

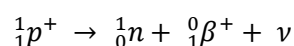
### 1.1 Positron Emission Tomography

Positron Emission Tomography (PET) is a non-invasive nuclear imaging technique that is used to measure biological and physiological function under both healthy and pathological conditions.<sup>1</sup> PET can not only be used to probe processes at the molecular level such as blood flow and metabolism but can also be used to determine the state of a disease and monitor its progression. This information can be used to evaluate the efficacy of a drug and select appropriate treatment protocols.<sup>2-4</sup> PET has a sensitivity orders of magnitude greater than that of other imaging techniques. Techniques such as magnetic resonance imaging (MRI), computed tomography (CT), ultrasound or X-rays tend to provide detailed anatomical images (namely structural images) but give limited information on a molecular scale whereas PET, because of the sensitivity, can monitor *in vivo* metabolic or molecular events as well as drug distribution, pharmacokinetics and pharmacodynamics.<sup>5,6</sup> Another imaging technique which utilises radiotracers is single photon emission computed tomography (SPECT). This technique uses a combination of a radiotracer with CT to acquire images.

	Sensitivity / mol L <sup>-1</sup>	Spatial Resolution (FWHM) / mm	Contrast Resolution
CT	-	0.5 – 0.6	Low to moderate
MRI	10 <sup>-3</sup> – 10 <sup>-5</sup>	1 -2	High
SPECT	10 <sup>-10</sup> – 10 <sup>-5</sup>	4 – 15	Very high
PET	10 <sup>-11</sup> – 10 <sup>-12</sup>	4 – 10	Very high

Table 1.1. Properties of various imaging techniques.<sup>7</sup>

PET relies on the use of a targeted molecule containing a positron-emitting radionuclide. The radionuclide decays via positron emission (Equation 1.1) resulting in a positron ( $\beta^+$ ) being emitted from the nucleus of the atom.<sup>8,9</sup>



Equation 1.1. Positron emission.



As the positron travels through matter it loses energy, due to interactions with other electrons and nuclei, where it eventually comes to rest and combines with an electron. This results in a positron-electron annihilation event where the mass of the two particles is converted into energy in the form of two electromagnetic photons which are emitted 180° apart from one another with an energy of 511 keV. Scintillation detectors (detectors with an inorganic crystal known as a scintillator) detect the two 511 keV photons and emit visible light photon themselves (scintillation) which are then detected by the coupled photodetectors and are converted into an electrical signal.<sup>9</sup> Most modern scintillators are made of lutetium-yttrium oxyorthosilicate, a highly dense material.<sup>10</sup>

## 1.2 Radioisotopes Used in PET

The commonly used radioactive isotopes (radionuclides) in PET are <sup>11</sup>C, <sup>13</sup>N, <sup>15</sup>O, <sup>18</sup>F, <sup>64</sup>Cu, <sup>68</sup>Ga, <sup>89</sup>Zr and <sup>124</sup>I (Table 1). The preferred 'physiological' radionuclides for labelling organic radiopharmaceuticals are <sup>11</sup>C, <sup>13</sup>N and <sup>15</sup>O as these elements are already present in many bioactive molecules and therefore should not affect the *in vivo* activity of these molecules. However, these preferred radionuclides have short half-lives (time taken for 50% of the radioactive atoms to decay) which limits synthetic and imaging routes.<sup>1</sup>

<b>Radionuclide</b>	<b>Half-life (t<sub>1/2</sub>)</b>	<b>% β<sup>+</sup> Decay</b>	<b>E<sub>max</sub> (MeV)</b>	<b>Mean Range in Water (mm)</b>
Carbon-11	20.4 min	100	0.959	1.1
Nitrogen-13	9.96 min	100	1.197	1.5
Oxygen-15	2.05 min	100	1.738	2.5
Fluorine-18	109.8 min	97	0.635	0.6
Copper-64	12.8 h	19	0.656	0.6 <sup>a</sup>
Gallium-68	68.3 h	89	1.898	2.9
Zirconium-89	78.4 h	22	0.396	1.2
Iodine-124	4.17 days	23	2.13	3.5 <sup>a</sup>

Table 1.2. Properties of radionuclides.<sup>13-15</sup> <sup>a</sup> Estimated values taken from reference 15.

The physical and chemical characteristics of an isotope determines the suitability for PET imaging, and therefore careful consideration is needed when determining the appropriate radionuclide for imaging. The half-life (t<sub>1/2</sub>), positron energy (E<sub>max</sub>) and

percentage positron emission are considered to be some of the more important characteristics.

The half-life needs to be of a sufficient time to allow the chemical incorporation of the radionuclide into the target molecule but also match the biological timescale of the process that is being investigated in a clinical setting.<sup>14</sup> An example of this would be the use of oxygen-15 as a radionuclide, as this has a very short half-life (2.05 min), its incorporation into a target molecule using long complex synthetic methods is impractical and is therefore far from ideal for measuring slow biological processes. The short half-life would result in the majority of the oxygen-15 decaying before any meaningful data can be obtained during the scan.<sup>14</sup>

The resolution of the image is largely determined by the positron energy of the radionuclide with higher resolution images being produced from lower energy decay processes. This is a consequence of high energy positrons travelling further through the body before thermalising and annihilating. As this is the detection event and it occurs remotely from the site of the radiolabelled pharmaceutical there is a greater uncertainty in the latter's position and so results in reduced resolution image. For example, fluorine-18 has a positron energy of 0.635 MeV and travels a mean distance through water (or the body of a patient) of 0.6 mm and a maximum of 2.4 mm, whereas gallium-68 travels a much greater distance of 2.9 mm because of a higher positron energy of 1.898 MeV.

Some radionuclides require specific chelating functionality to enable incorporation of the metal ion into the target molecule. These radionuclides tend to be radiometals (<sup>64</sup>Cu, <sup>68</sup>Ga and <sup>89</sup>Zr) and the chelating groups (e.g. EDTA and DOTA analogues) provide relatively thermodynamically and kinetically stable systems.<sup>14,16</sup> These specific chelating groups can prove to be somewhat limiting.

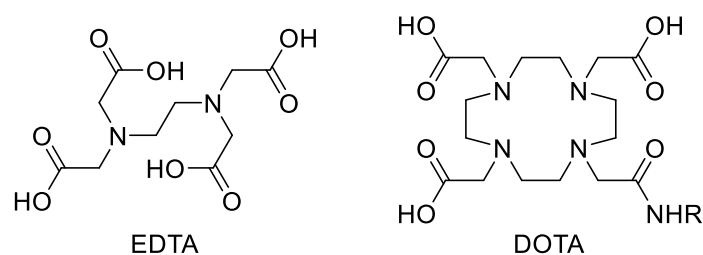


Figure 1.1. Structure of EDTA and DOTA.

Fluorine-18 is the most clinically relevant radionuclide and is often referred to as the 'isotope of choice' for PET. With a suitably long half-life ( $t_{1/2} = 109.8$  min), longer multistep radiosynthesis, purification and pharmaceutical formulation can be conducted without significant loss of radioactivity.<sup>17</sup> The half-life is favourable for measuring longer biological processes, such as metabolism. A much longer half-life, relative to the half-lives of  $^{11}\text{C}$ ,  $^{13}\text{N}$  or  $^{15}\text{O}$ , allows transport to off-site facilities and imaging centres that are unable to produce fluorine-18 themselves or the labelled radiopharmaceutical and still retain levels of radioactivity suitable for PET scans. Being able to deliver a radionuclide to an imaging centre means that patients do not have to travel to a specialised imaging centre which has an on-site production facility. Other radionuclides with shorter half-lives tend to be produced in centralised dual production and imaging facilities as transport is severely limited.

### 1.3 Fluorine-18 Production and Incorporation

The production method of fluorine-18 is dependent on the fluorination technique that is used to incorporate the fluorine-18 into the target molecule. There are two main fluorination techniques that are used to incorporate fluorine-18 into a target precursor molecule: electrophilic fluorination and nucleophilic fluorination.

If electrophilic fluorination methods are being used, then the fluorine-18 is produced initially as  $^{18}\text{F}\text{F}_2$  gas. This is done in two ways. The first uses neon gas as a target containing 0.1-2%  $\text{F}_2$  as a carrier which is then bombarded with deuterons (deuterium nucleus). Fluorine-18 is obtained as  $^{18}\text{F}\text{F}_2$  gas by the nuclear reaction  $^{20}\text{Ne}(d, \alpha)^{18}\text{F}$ , and yielding a drier form of fluorine-18. The second method is a bombardment method using a nickel target charged with oxygen-18 enriched  $\text{O}_2$ . This is then irradiated with protons to give fluorine-18 via the nuclear reaction  $^{18}\text{O}(p, n)^{18}\text{F}$ . Isotopic exchange occurs when the target is filled with a noble gas and  $^{19}\text{F}\text{F}_2$  mixture and irradiated a second time.<sup>1</sup> The neon route is an older way of producing fluorine-18, while the 'double shoot' method is an improved method on the 'single shot'.

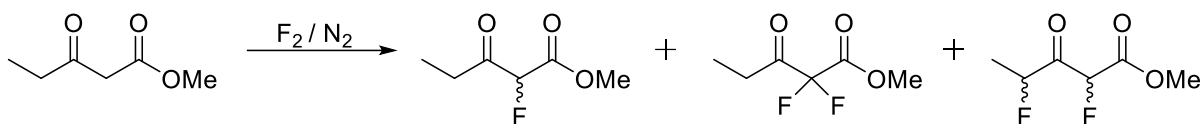
The limitation of electrophilic fluorine-18 production is the low specific activity due to them being carrier-added methods (100-600 MBq/ $\mu\text{mol}$ ).<sup>18</sup> Specific activity is the amount of radioactivity per unit mass of the nuclide and it is often critical to have high specific activity for PET imaging. If a biological target is saturated with the non-radioactive fluorine-19 isotopologue of the radiopharmaceutical meaningful images

cannot be obtained.<sup>11</sup> Radiopharmaceuticals of low specific activity cannot be used to probe biological targets that are in low concentrations, e.g. neurotransmitter receptors.

In general, fluorine-18 production for nucleophilic fluorination methods have a higher specific activity (in the range of  $10^2$  GBq/ $\mu$ mol, orders of magnitude different to electrophilic).<sup>18</sup> This is because the production does not require the use of carrier [ $^{19}\text{F}$ ] $\text{F}_2$  gas; the method is described as non-carrier added. Fluorine-18 is produced using proton bombardment of oxygen-18 enriched water target and produced via the nuclear reaction  $^{18}\text{O}(p, n)^{18}\text{F}$ . The fluorine-18 is produced in the form of aqueous [ $^{18}\text{F}$ ]fluoride, where the water is removed by either distillation or a resin column with a base being added generating  $\text{M}[^{18}\text{F}]\text{F}$ .<sup>1</sup> A common problem with this method is the difficulty in producing very anhydrous [ $^{18}\text{F}$ ]fluoride. Fluoride ions in an aqueous solution can form hydrogen bonds to water molecules which reduce the reactivity of the fluoride ions. For nucleophilic reactions it is critical to have reactive fluoride ions in an anhydrous environment to increase the nucleophilicity of the fluoride, therefore they require drying techniques such as azeotropic distillation with MeCN. Techniques that are used for fluorine-19 can be impractical when used with fluorine-18 as reactions with fluorine-18 are typically conducted on a nanomole scale. However, the nucleophilic method of fluorine-18 production is currently the more practical method to prepare radiopharmaceuticals with a high specific activity and with larger amounts of activity allowing for production of multiple doses which can be transported.

### 1.3.1 Electrophilic Fluorination

The [ $^{18}\text{F}$ ] $\text{F}_2$  gas that is produced can be used as an electrophilic fluorination reagent as most polyfunctional biologically active molecules have electron rich groups which will react; however, fluorine gas is violently reactive and is hard to handle. [ $^{18}\text{F}$ ] $\text{F}_2$  gas is not suitable for complex compounds with functional groups that can be easily oxidised. These usually give poor regioselectivity and a mixture of products that require extensive HPLC separation (Scheme 1.1). If there is a clearly identified reactive site on relatively simple compounds, it can be used in industry as a fluorinating agent.<sup>14,15</sup>



Scheme 1.1 The mixture of products from fluorination of 1,4 -ketoesters..

$[^{18}\text{F}]\text{F}_2$  gas is more often used as a progenitor and converted into less reactive and more selective fluorinating reagents. Several reagents have been prepared from  $[^{18}\text{F}]\text{F}_2$  to increase the radiochemical yield (RCY) and selectivity, these include: hypofluorites (acetylhypofluorite ( $[^{18}\text{F}]\text{AcOF}$ ) and trifluoroacetyl hypofluorite ( $[^{18}\text{F}]\text{CF}_3\text{COOF}$ )), *N*-fluoropyridinium salts, *N*-fluorobenzenesulfonimide ( $[^{18}\text{F}]\text{NFSI}$ ),  $[^{18}\text{F}]\text{Selectfluor}^{\text{TM}}$  and  $[^{18}\text{F}]\text{XeF}_2$  (Fig. 1.2). These reagents, from a fluorine-19 perspective, are more stable and easier to handle than elemental fluorine, with ‘fluorinating power’ from mild to moderate depending on the structure.<sup>16</sup> When considering fluorine-18, these reagents benefit from increased selectivity but require an additional step to synthesise, thus complicating automation. They also can introduce additional impurities into the process which will require removal.

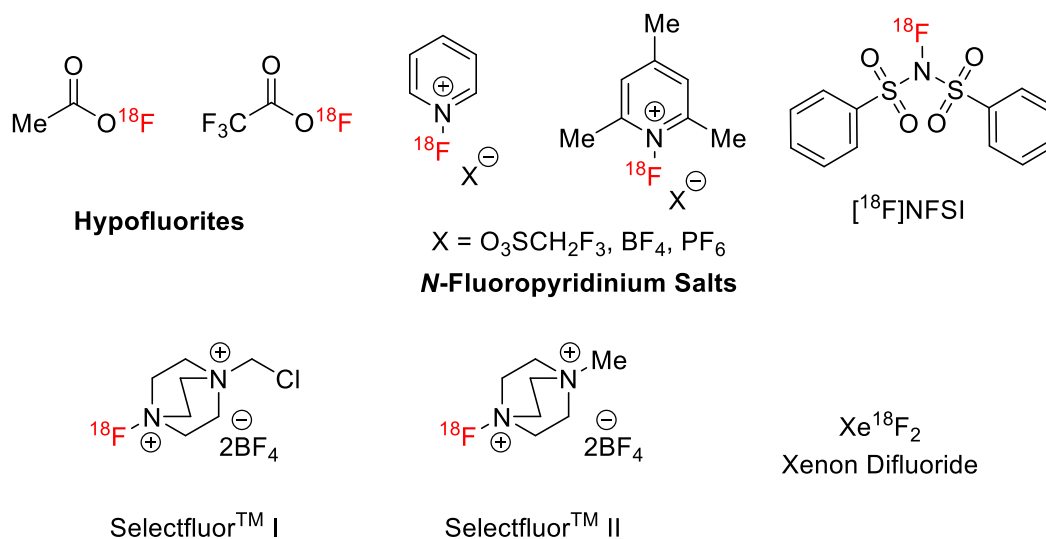


Figure 1.2. Electrophilic fluorinating reagents.

Electrophilic  $[^{18}\text{F}]\text{F}_2$  and derivatives allow the labelling of electron-rich systems (e.g. aromatic rings, alkenes and activated methylene groups) and fluoro-decarboxylation of carboxylic acids.  $[^{18}\text{F}]\text{Selectfluor}^{\text{TM}}$  can be prepared with higher specific activity using  $[^{18}\text{F}]\text{F}_2$ , using an electrical discharge chamber, and has been demonstrated to be more selective than elemental fluorine. It can be used to prepare fluoroaromatic and difluoromethylarenes.<sup>17</sup>

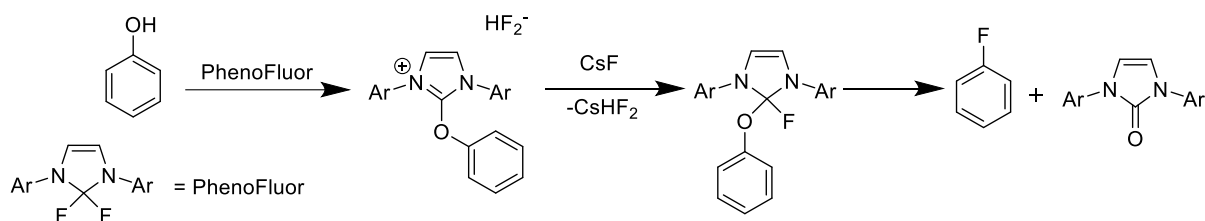
Historically relevant radiopharmaceuticals have been prepared by electrophilic fluorination methods, over time these have been replaced with nucleophilic fluorination methods due to the greater amount of activity and the higher specific activity (orders of magnitude different).<sup>21</sup>

### 1.3.2 Nucleophilic Fluorination

Early nucleophilic methods centred around the Balz-Schiemann reaction. Radiosynthetic methods would convert aniline into [<sup>18</sup>F]fluoroarenes via the thermal or photodecomposition of a diazonium tetrafluoroborate salt in the presence of a source of [<sup>18</sup>F]fluoride. This initial method has significantly lower specific activity, compared to modern nucleophilic methods, due to the potential for fluoride exchange between the [<sup>18</sup>F]fluoride and the fluorine-19 present in the tetrafluoroborate.<sup>22</sup>

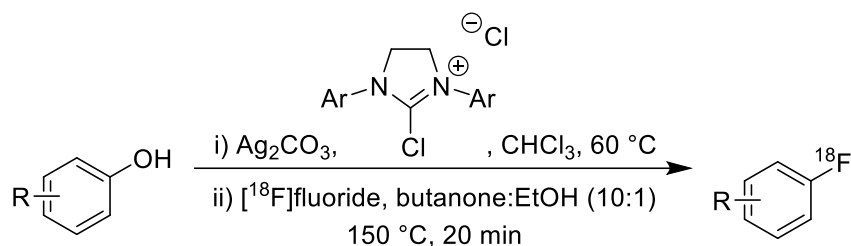
More recent methods have focused on the use of phase transfer catalysts, such as Kryptofix [2.2.2]<sup>TM</sup> and 18-crown-6. These increase the solubility of the fluoride in organic solvents. Paired with poorly nucleophilic bases (typically carbonates, e.g. K<sub>2</sub>CO<sub>3</sub>), the [<sup>18</sup>F]fluoride can be introduced into a molecule usually via an S<sub>N</sub>2 or S<sub>N</sub>Ar reaction.

A recent example of nucleophilic fluorination as a method of incorporation was demonstrated by Ritter *et al.*<sup>23</sup> Fluorine-18 and fluorine-19 were incorporated into small molecules via a concerted nucleophilic aromatic substitution (C<sub>S</sub>NAr) using Phenofluor. Despite nucleophilic aromatic substitution (S<sub>N</sub>Ar) being widely used and is the most common method to generate fluorine-18 containing arenes for use in PET, the arenes must contain an electron-withdrawing group to sufficiently stabilise the build-up of negative charge during the formation of the Meisenheimer complex. Many contain strong π-acceptors in the ortho or para positions. This does limit the substrate scope which can be used for this reaction, and many tend to require complex starting materials, however, the proposed C<sub>S</sub>NAr reaction from Ritter *et al* is not limited to electron poor arenes as it does not proceed via a Meisenheimer complex. Instead the reaction proceeds via a phenol deoxyfluorination reaction. The rate of which is greater for electron deficient substrates but is not limited to these (Scheme 1.2).



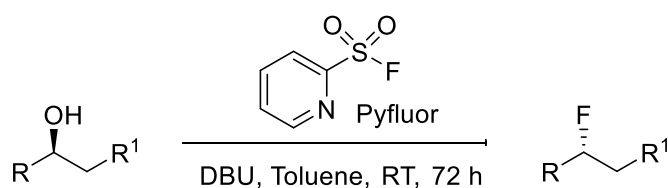
Scheme 1.2. Phenol deoxyfluorination reaction proposed by Ritter *et al.*

Fluorine-18 would be desirable in the use of Ritter's  $\text{CS}_{\text{NAr}}$  reaction but the two equivalents of fluorine inherent to PhenoFluor and the additional fluoride used renders the initial reaction useless. In order to access fluorine-18 incorporation, the PhenoFluor was modified (Scheme 1.3). This reaction has good tolerance for amines, phenols, thioethers and amides, however, carboxylic acids are not tolerated and do not fluorinate.



Scheme 1.3. Use of the modified PhenoFluor for  $[^{18}\text{F}]$ fluoride incorporation.

Another deoxyfluorination reaction which can selectively incorporate fluorine-18 into a molecule was described by Doyle *et al* (Scheme 1.4) using 2-pyridinesulfonyl fluoride (Pyfluor), an alternative fluorinating reagent for diethylaminosulfur trifluoride (DAST).<sup>24</sup> DAST readily fluorinates alcohols, however, the selectivity is not limited to these. Ketones and aldehydes will fluorinate when using DAST to give geminal difluoro-products. DAST violently decomposes above 50 °C, is expensive and has limited functional group tolerance and can form various elimination side products which complicate purification.



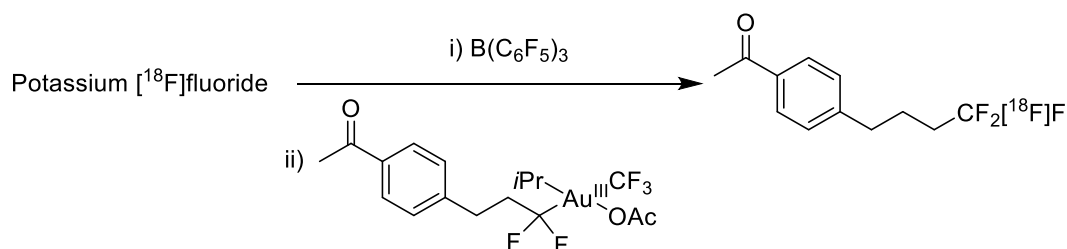
Scheme 1.4. Deoxyfluorination reported by Doyle *et al.*

Thermally stable variants of DAST (Deoxo-fluor and Xtalfluor) have been established which offer improvements but are expensive. Doyle *et al* found that electron deficient aryl and heteroaryl sulfonyl fluorides outperformed perfluorobutanesulfonyl fluoride, deoxofluor and DAST in selectivity towards the fluorinated product over the elimination product. Pyfluor gave 79% yield and a high selectivity (20:1 fluorinated product:elimination product). The deoxyfluorination occurs via a base assisted addition of the substrate alcohol to the sulfonyl fluoride.

Fluorine can be introduced into a molecule by incorporating the trifluoromethyl group. Trifluoromethyl groups are a crucial pharmaceutical moiety.<sup>25</sup> The strong, non-interacting C-F bonds, while lending metabolic stability, limit the chemical transformations that can be used to link these units to a substrate molecule. The incorporation of fluorine-18 using trifluoromethyl groups adds even more complexity to the situation. General nucleophilic fluorination methods used with fluorine-18 for radiosynthesis are incompatible with the stereoelectronic demands of the trifluoromethyl group. The most common method is to react a "CF<sub>2</sub>" precursor with [<sup>18</sup>F]fluoride to form the relevant CF<sub>3</sub> moiety prior to incorporation into the desired molecule via an organocopper intermediate.

Toste *et al* describes a catalytic fluoride-rebound mechanism for the formation of C(sp<sup>3</sup>)-CF<sub>3</sub> bonds (Scheme 1.5).<sup>25</sup> A class of Au(III) complexes were discovered to form the trifluoromethyl group when treated with boranes. This reaction can be conducted catalytically with tris(pentafluorophenylborane), and the trifluoromethyl group is formed via nucleophilic reductive elimination using a suitable fluoride source. The Au(III) intermediate complexes described are considered inert functional groups, requiring exceptionally strong acids, such as CF<sub>3</sub>SO<sub>3</sub>H, or elemental halogens in order to cleave the Au-C bond. The synthetically tolerant metal complexes formed during this reaction allowed for the development to a radiochemical protocol using potassium [<sup>18</sup>F]fluoride and Kryptofix[2.2.2]<sup>TM</sup>.





Scheme 1.5. An example of a radiochemical protocol used by Toste *et al.*

Another method to fluorine-18 incorporation was highlighted by Gouverneur *et al* (Scheme 1.6).<sup>26</sup> Carbenes have many applications in inorganic and organometallic chemistry, however, there has been little work to establish their use in radiochemistry, especially in the field of PET. Difluorocarbenes can be activated to participate in various chemical transformations including insertions, cycloadditions and cross-coupling reactions giving rise to many fluorine-19 containing molecules. The use of  $[^{18}\text{F}]$ difluorocarbenes has not been well established and their occurrence in the literature is rare. A novel  $[^{18}\text{F}]$ difluorocarbene reagent prepared by Gouverneur *et al* showed broad reactivity towards O-H, S-H and N-H insertions as well as cross-coupling reactions. The novel fluorine-18 containing reagent was prepared by nucleophilic substitution of (bromofluoromethyl)-(4-*tert*-butyl)phenyl)sulfane with  $[^{18}\text{F}]$ fluoride followed by an oxidation using  $\text{RuCl}_3/\text{NaIO}_4$ . The novel reagent can then be reacted with an alcohol, thiol or amine to insert the  $[^{18}\text{F}]$ difluorocarbene (Scheme 1.5).



X = O, S or N

Scheme 1.6. General method for the introduction of  $[^{18}\text{F}]$ difluorocarbenes via O-H, S-H or N-H insertion.

#### 1.4 2- $[^{18}\text{F}]$ Fluoro-2-deoxy-D-Glucose ( $[^{18}\text{F}]$ FDG)

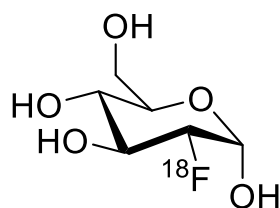


Figure 1.3. 2- $[^{18}\text{F}]$ Fluoro-2-deoxy-D-glucose ( $[^{18}\text{F}]$ FDG).

2-[<sup>18</sup>F]Fluoro-2-deoxy-D-glucose ([<sup>18</sup>F]FDG) is an analogue of glucose in which the hydroxyl group at the 2-position has been replaced by a fluorine atom (Fig. 1.3).

[<sup>18</sup>F]FDG is currently the major fluorinated tracer used in routine clinical PET.<sup>19</sup> Other radiotracers and radioligands are used in PET, however [<sup>18</sup>F]FDG accounts for around 90-95% of all PET conducted being extensively used within the fields of oncology, cardiology and neurology.<sup>20</sup> The first synthesis of [<sup>18</sup>F]FDG was published in 1976 by Ido and co-workers following a long collaboration with researchers at the National Institute of Health (NIH) who had been working with  $\beta$ -emitting 2-[<sup>14</sup>C]deoxyglucose, which [<sup>18</sup>F]FDG was modelled after, and the technique of autoradiography.<sup>21</sup> This technique had illustrated that radiolabelled glucose analogues can be used as a metabolic tracer to map regional brain function. Carbon-11 was initially chosen as the nuclide to radiolabel with; however, it was decided that fluorine-18 would be more suitable due to the nuclide's more practical radiological characteristics which would allow for transport of the radiolabelled tracer between their two research sites (Brookhaven National Laboratory (BNL) and the University of Pennsylvania). Within the same year as the first synthesis was published, [<sup>18</sup>F]FDG was first administered to humans.<sup>21</sup> Initially [<sup>18</sup>F]FDG was being used for assessment of myocardial viability and evaluation of recurrent brain tumours, but with the development of PET scanners which could rapidly obtain high-quality images [<sup>18</sup>F]FDG was transformed into a major player in the oncological imaging field.<sup>19</sup>

[<sup>18</sup>F]FDG is used to measure glucose metabolism. Cancer cells, along with a number of other cells, have increased glycolysis along with an increase in glucose metabolism and enhanced glucose transport, with an increase in the number of glucose transporter proteins (GLUT) on the surface of the cell, in particular GLUT-1 and to a lesser extent GLUT-3. This is due to an overexpression of the gene responsible for coding these proteins.<sup>19</sup> [<sup>18</sup>F]FDG enters the cell by glucose transport proteins (GLUT), the same used by glucose, through the cell membrane. Once within the cell, [<sup>18</sup>F]FDG undergoes the same metabolic pathway as glucose and is phosphorylated by hexokinase to generate [<sup>18</sup>F]FDG-6-phosphate. However, this metabolite is now not a substrate for further metabolism due to the need of a hydroxyl group at position two and is therefore stuck within the cell (Fig. 1.4).<sup>19,1</sup>

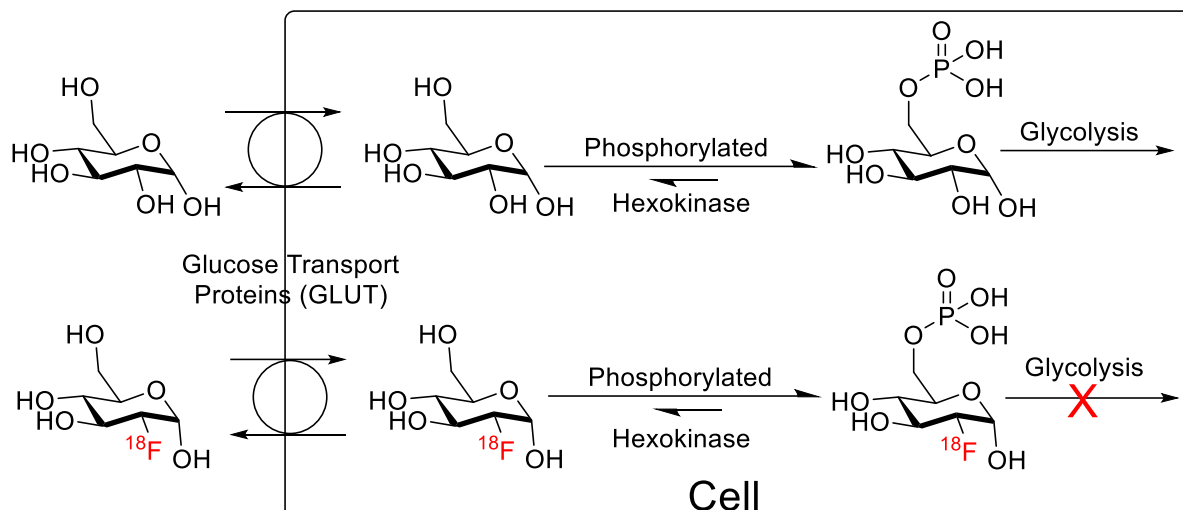
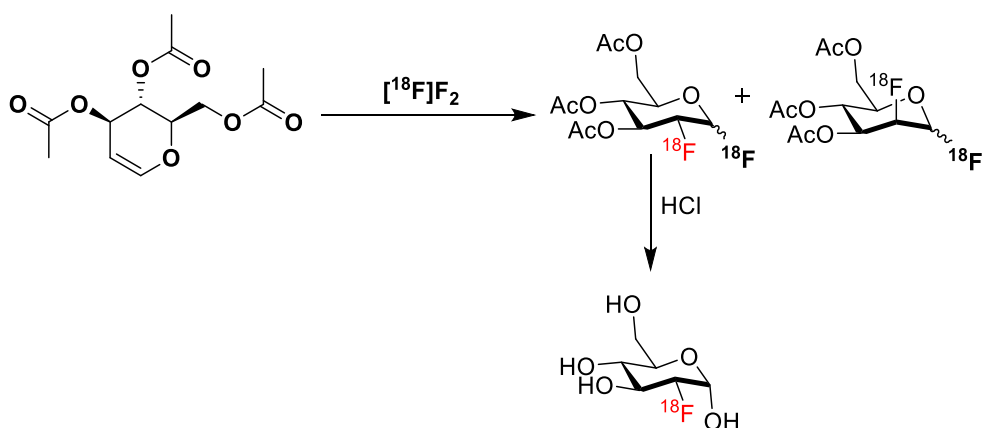


Figure 1.4. Accumulation of glucose and  $[^{18}\text{F}]\text{FDG}$  within a cell .

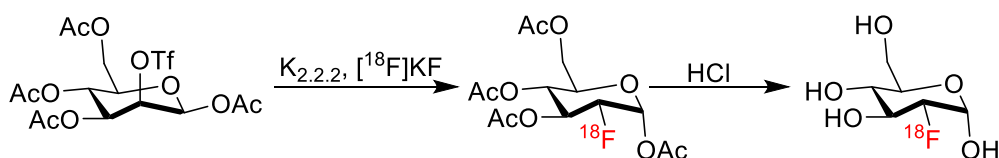
$[^{18}\text{F}]\text{FDG}$  accumulates within the cell in proportion to the metabolism of glucose and creates a gradient between the cancerous cells and the surrounding tissues which is highly favourable for detecting cancerous cells and tumours. These cells and tumours can be characterised by the elevated levels of glucose consumption which is visualised on the PET scan.

The use of  $[^{18}\text{F}]\text{FDG}$  in detection of cancer cells is suboptimal as the relative contribution of glycolysis and glucose transport varies according to the tumour type, and areas within the tumour as most are heterogeneous, with  $[^{18}\text{F}]\text{FDG}$  uptake being influenced by a number of other parameters such as tumour proliferation, hypoxia and blood glucose levels.<sup>19</sup>  $[^{18}\text{F}]\text{FDG}$  does also accumulate in some normal tissues, e.g. the brain and bladder, and uptake is increased in macrophages present in inflammatory infiltrate which results in an accumulation in both malignant tumours and benign inflammatory lesions.<sup>19,1</sup>  $[^{18}\text{F}]\text{FDG}$  uptake in cancerous cells is far from being fully understood.



Scheme 1.7. Synthesis of [ $^{18}\text{F}$ ]FDG by electrophilic fluorination (Wolf, 1976).

The original synthesis of [ $^{18}\text{F}$ ]FDG used electrophilic fluorination (Scheme. 1.7).<sup>22</sup> The precursor 3,4,6-tri-*O*-acetyl-D-glucal was treated with [ $^{18}\text{F}$ ]F<sub>2</sub> which produced a 3:1 mixture of fluorine-18 labelled difluoro-glucose and difluoro-mannose derivatives, with the possibility to form regioisomers of the difluoro-glucose at the anomeric position. The difluoro-glucose derivative is then treated with hydrochloric acid (HCl) to remove the acetyl protecting groups giving [ $^{18}\text{F}$ ]FDG. The reaction gave a low yield (8%) of the [ $^{18}\text{F}$ ]FDG and took around 2 h to synthesise. An improvement to the electrophilic fluorination method was to use the easier to control secondary reagent acetylhypofluorite ([ $^{18}\text{F}$ ]AcOF), which was produced *in-situ* from [ $^{18}\text{F}$ ]F<sub>2</sub>, which gave a higher yield. One problem associated with this method is that only half of the radioactive fluorine atoms are incorporated into the molecule while a second issue is the lower specific activity due to the method of fluorine-18 production being carrier-added.



Scheme 1.8. Nucleophilic method of [ $^{18}\text{F}$ ]FDG production.

The method that is most commonly used today is nucleophilic substitution which was first conducted in 1986 after the use of Kryptofix [2.2.2]<sup>TM</sup> was discovered to increase the reactivity of [ $^{18}\text{F}$ ]fluoride.<sup>7</sup> 1,3,4,6-Acetyl-2-*O*-trifluoromethanesulfonyl- $\beta$ -D-mannopyranose is used as the precursor which is treated with a [ $^{18}\text{F}$ ]fluoride source and Kryptofix [2.2.2]<sup>TM</sup> to give as high as a 95% incorporation of [ $^{18}\text{F}$ ]fluoride (Scheme 1.8). This method comes with the benefit of using a non-carrier-added source of

[<sup>18</sup>F]fluoride resulting in a much higher specific activity than the electrophilic alternative.<sup>22,27</sup>

There is an urgent unmet clinical need to expand the range of radiopharmaceuticals that are readily available and thus the therapeutic areas which can benefit from the power medical imaging offers in the diagnosis and management of disease. Despite rapid global expansion of PET technology, universal take-up of this technology has remained somewhat limited. This is due to the challenges of new diagnostic agent discovery and the provision of sufficient quantities of materials to facilitate the translation to a clinical setting. Many fluorine-18 probes that would be of use are inaccessible due to the lack of fluorination chemistry that is available. C-F bonds are challenging to add into a complex molecule especially in the presence of a variety of functional groups.

## References

1. O. Jacobson and X. Chen, *Curr. Top. Med. Chem.*, 2010, **10**, 1048-1059
2. A. Berger, *BMJ*, 2003, **326**, 1449
3. X. Huang, W. Liu, H. Ren, R. Neelamegam, J. M. Hooker and J. T. Groves, *J. Am. Chem. Soc.*, 2014, **136**, 6842-6845
4. W. Liu, X. Huang, M. S. Placzek, S. W. Krska, P. McQuade, J. M. Hooker and J. T. Groves, *Chem. Sci.*, 2018, **9**, 1168-1172
5. M. Rudin and R. Weissleder, *Nature Reviews Drug Discovery*, 2003, **2**, 123-131
6. P. W. Miller, N. J. Long, R. Vilar and A. D. Gee, *Angew. Chem. Int. Ed.*, 2008, **47**, 8998-9033
7. E. Lin and A. Alessio, *J. Cardiovasc. Comput. Tomogr.* 2009, **3**, 403-408
8. D. L. Bailey, D. W. Townsend, P. E. Valk and M. N. Maisey, *Positron Emission Tomography: Basic Sciences*, Springer London, London, 2005
9. Z. Li and P. S. Conti, *Adv. Drug Delivery Rev.*, 2010, **62**, 1031-1051
10. M. Lowdon, P. G. Martin, M. W. J. Hubbard, M. P. Taggart, D. T. Connor, Y. Verbelen, P. J. Sellin and T. B. Scott, *Sensors*, 2019, **19**, 3828
11. H.-J. Biersack and L. M. Freeman, *Clinical Nuclear Medicine*, Springer Berlin Heidelberg, 2007
12. Z. Cai and C. J. Anderson, *J. Labelled Comp. Radiopharm.*, 2014, **57**, 224-230
13. E. Lee, A. S. Kamlet, D. C. Powers, C. N. Neumann, G. B. Boursalian, T. Furuya, D. C. Choi, J. M. Hooker and T. Ritter, *Science*, 2011, **334**, 639-642
14. K. Adachi, Y. Ohira, G. Tomizawa, S. Ishihara and S. Oishi, *J. Fluorine Chem.*, 2003, **120**, 175-183
15. O. Jacobsen, D. O. Kiesewetter and X. Chen, *Bioconjugate Chem.*, 2015, **26**, 1-18
16. M. M. Alauddin, *Am. J. Nucl. Med. Mol. Imaging*, 2012, **2**, 55-79
17. E. L. Cole, M. N. Stewart, R. Littich, R. Hoareau and P. J. H. Scott, *Curr. Top Med. Chem.*, 2014, **14**, 875-900
18. R. Cheng, PhD Thesis, Newcastle University, 2021
19. O. Couturier, A. Luxen, J. P. Chatal, J. P. Vuillez, P. Rigo and R. Hustinx, *Eur. J. Nucl. Med. Mol. Imaging*, 2004, **31**, 1182-1206
20. H. H. Coenen, P. H. Elsinga, R. Iwata, M. R. Kilbourn, M. R. A. Pillai, M. G. R. Rajan, H. N. Wagner Jr. and J. J. Zaknun, *Nucl. Med. Biol.*, 2010, **37**, 727-740
21. A. Alavi and M. Reivich, *Semin. Nucl. Med.*, 2002, **32**, 2-5

22. S. Yu, *Biomed. Imaging Intervention J.*, 2006, **4**, e57
23. C. N. Neumann, J. M. Hooker and T. Ritter, *Nature*, 2016, **534**, 369
24. M. K. Nielsen, C. R. Ugaz, W. Li and A. G. Doyle, *J. Am. Chem. Soc.*, 2015, **137**, 9571-9574
25. M. D. Levin, T. Q. Chen, M. E. Neubig, C. M. Hong, C. A. Theulier, I. J. Kobylanskii, M. Janabi, J. P. O'Neil and F. D. Toste, *Science*, 2017, **356**, 1272
26. J. B. I. Sap, C. F. Meyer, J. Ford, N. J. W. Straathof, A. B. Dürr, M. J. Lelos, S. J. Paisey, T. A. Mollner, S. M. Hell, A. A. Trabanco, C. Genicot, C. W. am Ende, R. S. Paton, M. Tredwell and V. Gouverneur, *Nature*, 2022, **606**, 102
27. J. S. Fowler and T. Ido, *Semin. Nucl. Med.*, 2002, **32**, 6-12

## Chapter 2 – Nucleophilic Fluorination using a Manganese (III) Salen Catalyst

### 2.1. Background

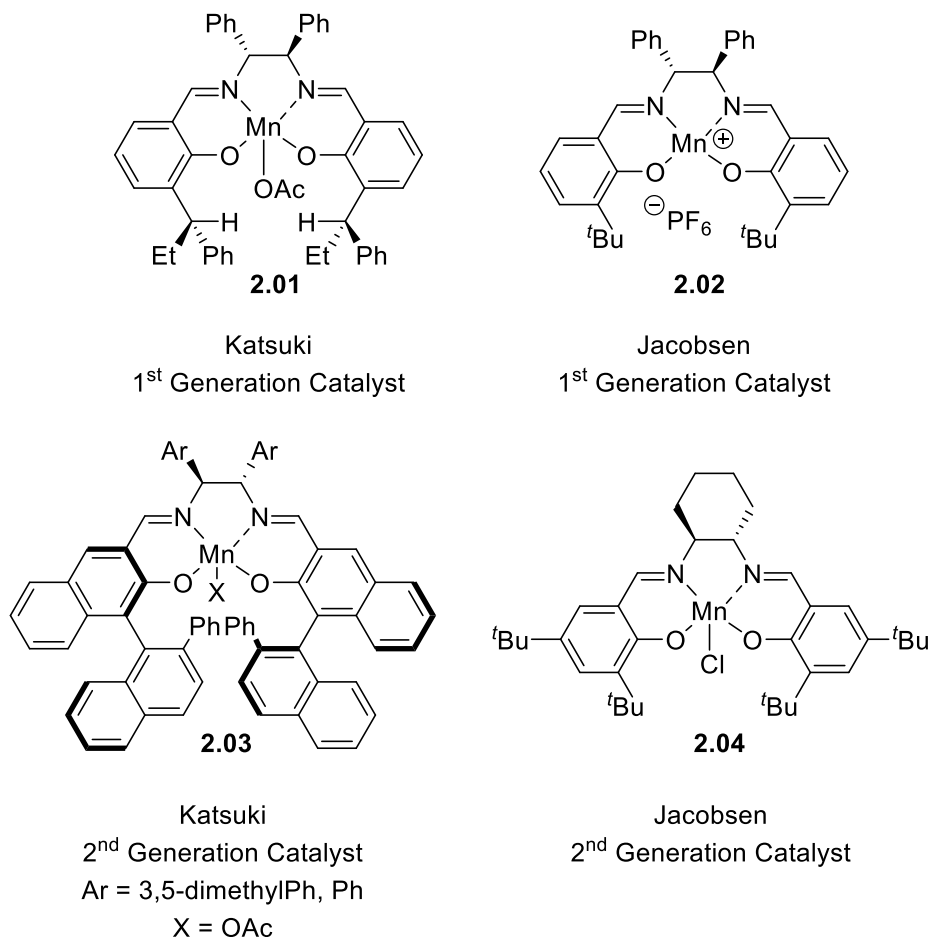
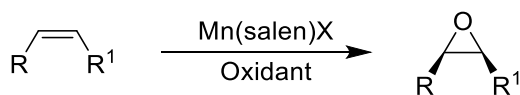


Figure 2.1. Structures of the Katsuki and Jacobsen Mn (III) salen complexes.

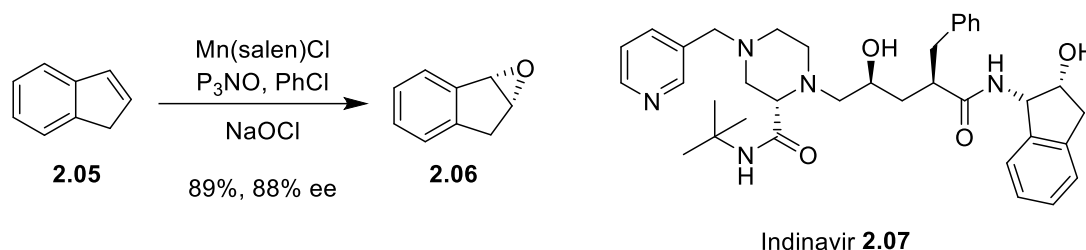
Since 1990 when Jacobsen and Katsuki independently synthesised chiral manganese (III) salen complexes (**2.01** and **2.02**) from 1,2-diamine compounds and salicylaldehyde derivatives, there has been an interest in manganese (III) salen complexes for a variety of catalytic reactions (Fig. 2.1).<sup>1-4</sup> These catalysts have opened synthetic routes which allow for the fine-control and introduction of stereocentres into a number of organic molecules.



Scheme 2.1. Epoxidation using Mn(salen)X catalysts.

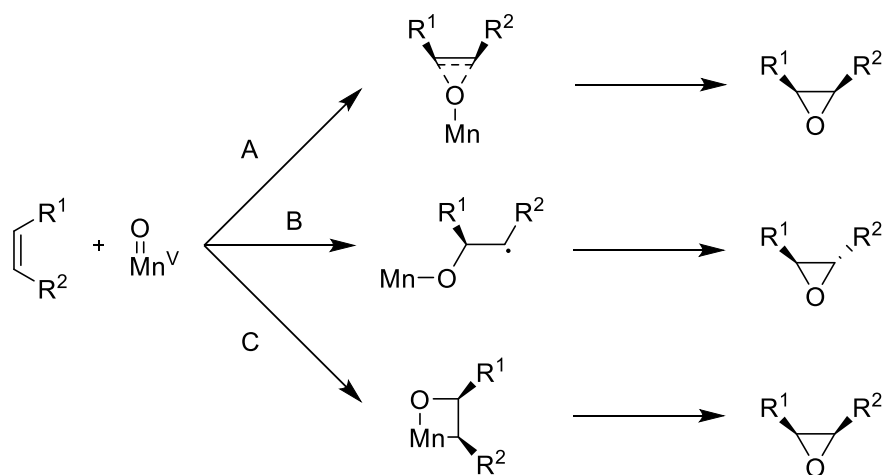


The most common use of these complexes is for the catalytic enantioselective epoxidation of simple alkenes (Scheme 2.1). The best results are obtained when conducted on *cis*-alkenes, however Katsuki *et al* have developed an alternate range of substituted catalysts which work well on *trans*-alkenes.<sup>5</sup> One particular example of importance is the enantioselective epoxidation of indene **2.05**, the precursor compound for the highly active antiretroviral drug Indinavir **2.07** used to treat HIV/AIDS (Scheme 2.2).<sup>6</sup>



Scheme 2.2. Epoxidation of indene.

Iodosobenzene (PhIO) and sodium hypochlorite (NaOCl) are the oxidants of choice but oxidants like *meta*-chloroperbenzoic acid, hydrogen peroxide and iodosylmesitylene have also been used. Stoichiometric amounts of the oxidants are required in order to oxidise the manganese (III) species to an oxo-manganese (V) species, which are postulated to be the catalytically active species. The high degree of enantioselectivity is thought to arise from the large bulky *tert*-butyl groups on the salen ligand. These groups hinder the approach of the alkene, especially if also containing bulky groups, from the side of the complex and directs it away avoiding unfavourable steric interactions and forces the alkenes approach over the diamine where the stereochemistry of the diamine translates to epoxidations with high ee's.<sup>1,2</sup>



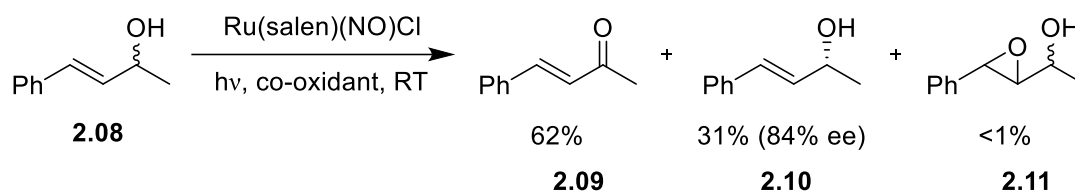
Scheme 2.3. Mechanism of oxygen transfer for the epoxidation. Mechanism A: concerted, mechanism B: via radical and mechanism C: manganoaxetane intermediate. Ligands omitted for clarity.

The mechanism of oxygen transfer is complex and not fully understood. There are thought to be three mechanisms through which the epoxide formation occurs (Scheme 2.3). A concerted oxygen transfer (pathway A), a pathway which proceeds via radical intermediate (pathway B) and a manganoaxetanes intermediate (pathway C) are all possible pathways. A mixture of *cis*- and *trans*- epoxides were observed in early examples of the Jacobsen-Katsuki epoxidations, however alkyl-substituted derivatives gave only *cis*-products. This gives support to a radical intermediate for conjugated alkenes (the radical intermediate allowing for rotation around the C-C bond resulting in both epoxides) while a concerted pathway is more likely for alkyl-substituted alkenes. However, there are examples, e.g. *cis*- $\beta$ -methylstyrene, where it becomes clear that there is strong dependency on the oxidant, the catalyst, and any additives.<sup>7</sup>

The ease of the synthesis of the salen ligands is highly advantageous and allows for fine tuning of the ligands steric properties to best suit the alkene substrate of choice, by choosing appropriate diamines and salicylaldehyde precursors. The transition metal at the centre of the complex is not limited to manganese, there have been a number of complexes synthesised over the years which utilise a range of transition metals such as chromium, titanium, and cobalt.<sup>8,9</sup> Katsuki *et al* investigated the use of ruthenium as the metal centre.<sup>4</sup> The ruthenium catalysts were initially used as an epoxidation catalyst and in hetero Diels-Alder reactions via photoactivation<sup>b</sup>. Further

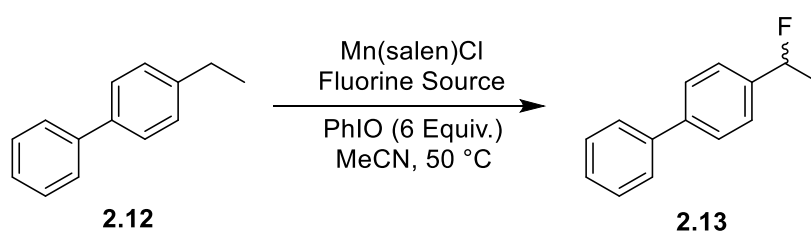
<sup>b</sup> This discovery was quite serendipitous. The reaction proceeded nicely during sunny weather and was worse when it was cloudy.

investigations into the photoactivation led Katsuki to discover their use as a catalyst for asymmetric aerobic oxidation of alcohols (Scheme 2.4).<sup>10</sup>



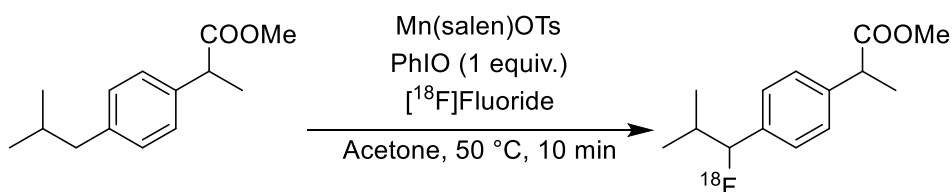
Scheme 2.4. Asymmetric aerobic oxidation of cinnamic alcohol.

Choudary *et al* has illustrated the use of the Mn (III) salen complexes as efficient acylation catalysts of alcohols.<sup>11</sup> Use of the Mn (III) salen complexes in the catalysis of transesterification of  $\beta$ -keto esters has also been reported.<sup>12</sup>



Scheme 2.5. Fluorination of 4-ethyl-1,1'-biphenyl using Mn(salen)Cl and a fluorine source.

Groves *et al* has used the Jacobsen epoxidation catalysts, Mn(salen)Cl, and utilised it in a heteroatom transfer mechanism, specifically for the use in nucleophilic fluorinations. Groves reported a high conversion (81%) with a moderate yield of the fluorinated product (60%) when using TREAT•3HF as the fluoride source.



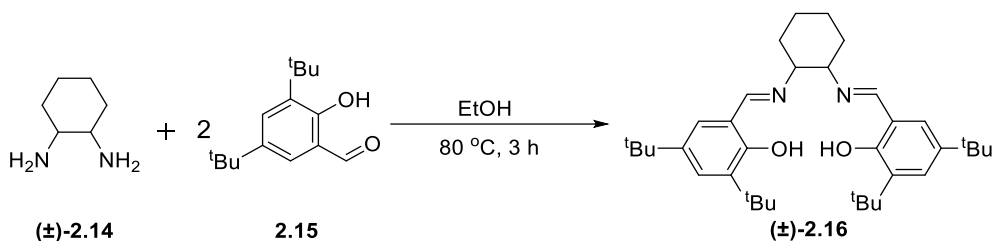
Scheme 2.6. Groves *et al* late stage benzylic C-H fluorination using [<sup>18</sup>F]fluoride.

Their group has also taken this method further and utilised this for fluorine-18 incorporation (Scheme 2.6).<sup>13</sup> Groves *et al* used a tosylate variation of the Jacobsen epoxidation catalyst, which afforded the highest radiochemical conversions (65% for ibuprofen test substrate). When tested on a wider range of substrates the radiochemical conversion ranged from 20 to 68% and a wide range of functional groups were tolerated, including but not limited to esters, amides, imides, ketones and heterocycles.

The aim of the work described within this chapter is to evaluate the utilisation of the manganese salen catalysts reported by Groves *et al* for nucleophilic fluorination of small molecules. The effectiveness this class of catalysts would have for production of fluorinated molecules on an industrial scale process, with particular focus on the yield of the fluorinated targets and for the use in fluorine-18 radiolabelling, is to be assessed. The results reported within this chapter are from experimental work based off the research conducted by Groves and his research group at Princeton University.<sup>14,15</sup>

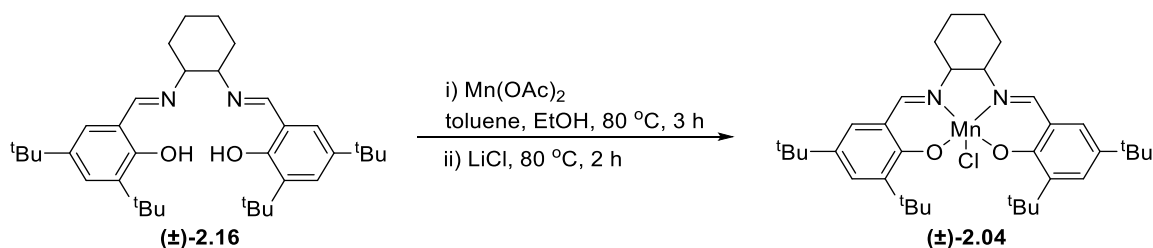
## 2.2. Nucleophilic Fluorination – Initial Reactions

Initial reactions used manganese(salen)Cl as the catalyst. The salen ligand, ( $\pm$ )-*N,N'*-bis(3,5-di-*tert*-butylsalicylidene)-1,2-cyclohexanediamine **2.16** was synthesised from ( $\pm$ )-1,2-diaminocyclohexane ( $\pm$ )-**2.14** and 3,5-di-*tert*-butylsalicylaldehyde **2.15** as a yellow solid in a good yield of 77% (Scheme 2.7).<sup>16</sup>



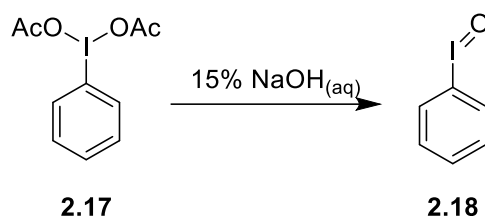
Scheme 2.7. Synthesis of salen-ligand ( $\pm$ )-*N,N'*-bis(3,5-di-*tert*-butylsalicylidene)-1,2-cyclohexanediamine ( $\pm$ )-**2.16**.

The manganese catalyst (Jacobsen's catalyst) ( $\pm$ )-**2.04** was synthesised according to the literature by heating ( $\pm$ )-**2.16** and Mn(OAc)<sub>2</sub> at reflux for 3 h and further 2 h after the addition of LiCl giving the catalyst as a brown powder (Scheme 2.8).<sup>16,17</sup> FT-IR was used to confirm the successful synthesis of the catalyst as NMR is not possible due to the paramagnetic nature of manganese resulting in broadening of the peaks. The FT-IR taken of the catalyst was compared with the literature ( $\pm$ )-**2.04** and showed the successful synthesis of the catalyst in good yield (77%).<sup>16,17</sup> It was noted that dropwise addition of the salen to the suspension of Mn(OAc)<sub>2</sub> over the course of an hour was required for a higher yielding generation of the catalyst (yield increased from 41% to 77%).



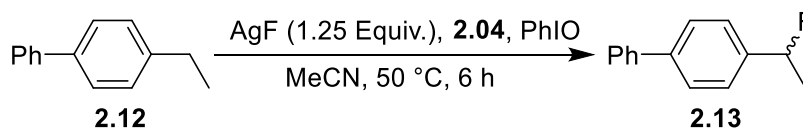
Scheme 2.8. Synthesis of Jacobsen's catalyst ( $\pm$ )-**2.04**.

Nucleophilic fluorination using a manganese catalyst requires an oxidant to achieve the higher oxidation states of manganese (Mn<sup>V</sup>) required, previously explained in chapter 2.1.



*Scheme 2.9. Synthesis of iodosobenzene 2.18.*

Iodosobenzene **2.18** was the oxidant used in the literature, however it had to be synthesised due to the reagent no longer being commercially available.<sup>18</sup> Diacetoxyiodobenzene **2.17** was dispersed in 15% w/w aqueous NaOH and stirred at room temperature for 4 h (Scheme 2.9) in which time a precipitate had formed. After washing, this gave the desired iodosobenzene as a pale-yellow solid in a good yield of 76%. The product was not rigorously dried<sup>c</sup> due to an increased risk of fire or explosion on rigorous drying.<sup>18,19</sup>

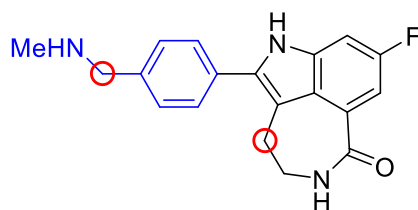


*Scheme 2.10. Fluorination of ethyl-1,1'-biphenyl 2.12.*

4-Ethyl-1,1'-biphenyl **2.12** was used as the test substrate for the fluorination reactions using ( $\pm$ )-**2.04**. **2.12** was used by Groves *et al*, where it gave a yield of 58% for the fluorinated product after 6-9 h. Silver fluoride (AgF) was used as the fluorine source and iodosobenzene (PhIO) as the oxidant. ( $\pm$ )-4-(1-Fluoroethyl)-1,1'-biphenyl **2.13** was shown by <sup>19</sup>F NMR, a peak at -166 ppm corresponding to the literature value confirming the fluorination at the benzylic position had occurred, however in a very low yield (<1% isolated yield).

<sup>c</sup> The PhIO was dried on the filter overnight. PhIO should not be dried in a vacuum oven or at high temperatures for extended periods of time.

### 2.2.1. Rucaparib and Deprotection of Benzyl Groups

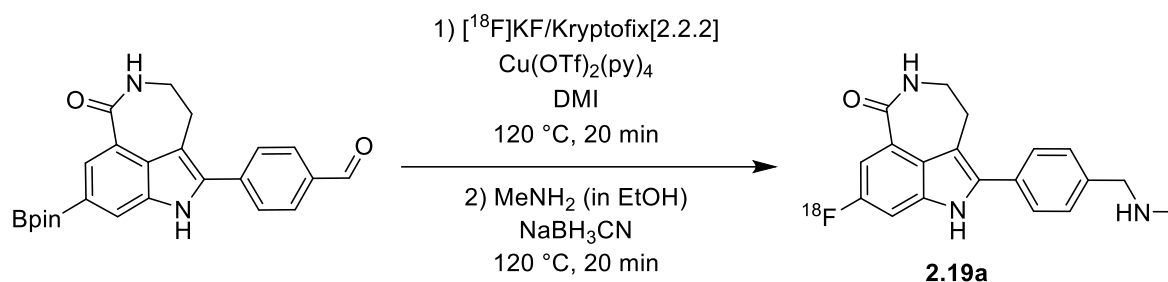


2.19

Figure 2.2. Rucaparib. Benzylic positions highlighted in red. *N*-Benzylmethylamine model compound highlight in blue.

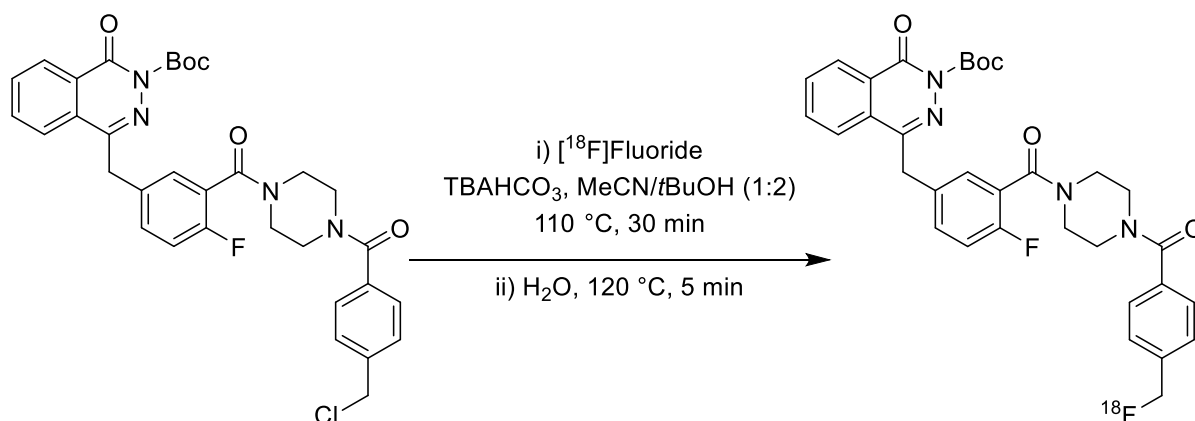
Rucaparib **2.19** (sold under the brand name Rubraca) is a poly(ADP-ribose) polymerase (PARP) inhibitor (Fig. 2.2). PARP is important in the DNA base excision repair pathway of single DNA strand breaks. When a single strand break occurs in DNA, PARP1 and PARP2 connect the break using their DNA binding domains. PARP is activated when anticancer drugs damage the DNA of cancer cells.<sup>20</sup> [<sup>18</sup>F]Fluorodeoxyglucose and 3'-deoxy-3'-[<sup>18</sup>F]fluorothymidine (FLT) are used as metabolism biomarkers in tumours and markers for DNA synthesis and cell proliferation respectively. The uptake of these compounds can be used to determine the impact of Rucaparib in clinical studies and treatment. These biomarkers, however, detect the slower secondary effects of the Rucaparib uptake but if Rucaparib could be fluorinated in the benzylic positions (Fig. 2.2) this would allow the potential for the derivatives of Rucaparib to be developed and used as a PET tracer, removing the need for secondary imaging biomarkers and allow the direct study of the PARP inhibitors.

Gouverneur *et al* has recently published a copper-mediated radiosynthetic route to [<sup>18</sup>F]Rucaparib.<sup>21</sup> A borylated Rucaparib precursor, accessible from a novel bis-halogenated tricyclic indole, was used as the substrate to fluorinate in a one-pot fluorination reaction followed by a reductive amination to afford [<sup>18</sup>F]Rucaparib **2.19a** (Scheme 2.11). [<sup>18</sup>F]KF was used as the nucleophilic source of fluorine-18 with Kryptofix[2.2.2]<sup>TM</sup> in the presence of Cu(OTf)<sub>2</sub>(py)<sub>4</sub>. [<sup>18</sup>F]Rucaparib was synthesised in an activity yield of 11% and a molar activity of 30 GBq/μmol.



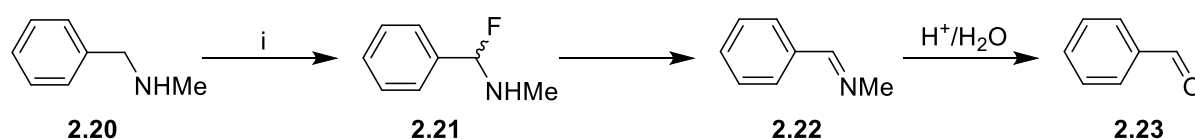
Scheme 2.11. Radiochemical transformation of borylated Rucaparib precursor to [<sup>18</sup>F]Rucaparib.

Other related PARP inhibitors have been investigated for the use in PET. Pimlott *et al* managed to radiofluorinate the PARP inhibitor Olaparib by modifying one of the amide groups from a cyclopropyl ring to a chlorophenyl precursor. The fluorine-18 was incorporated into the chloro-precursor using [<sup>18</sup>F]fluoride in a nucleophilic substitution in the presence of a base (tetrabutylammonium hydrogencarbonate) (Scheme 2.12).<sup>22</sup>



Scheme 2.12. Radiofluorination of an Olaparib derivative by Pimlott *et al*.

An initial fluorination reaction using Rucaparib was attempted but was unsuccessful. The <sup>19</sup>F NMR showed no fluorination had occurred at either benzylic position. Rucaparib is poorly soluble in MeCN, and this could have caused the lack of fluorination. Due to the high cost of Rucaparib and the small amount of material available, model substrates were investigated before conducting any further experiments on Rucaparib.



Scheme 2.13. *N*-Benzylmethylamine fluorination and subsequent imine formation and hydrolysis. *i* AgF 1.25 Equiv., Mn(salen)Cl, PhIO, 50 °C, 6 h.

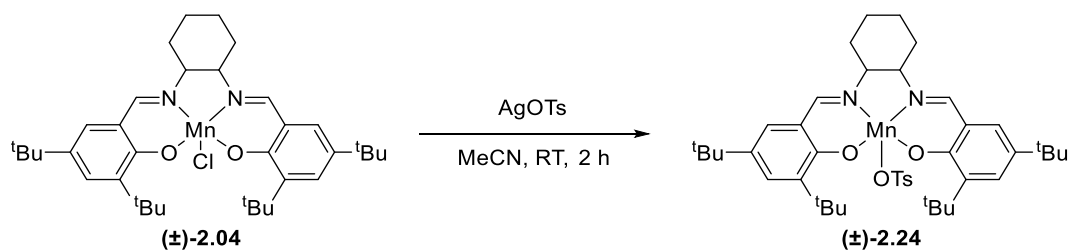


*N*-Benzylmethylamine was used as a model compound for one of the benzylic positions on Rucaparib. Using Mn(salen)Cl as the catalyst and iodosobenzene as the oxidant, **2.20** was reacted following the initial procedure for fluorination (Scheme 2.13). The desired benzylic fluorination only occurred in trace amounts as determined by <sup>19</sup>F NMR spectroscopy, however, there was a number of different by-products present in the <sup>1</sup>H NMR spectrum. On the <sup>1</sup>H NMR, a peak at 9.86 ppm corresponds to benzaldehyde **2.23** being formed; this suggests that fluorination did occur but the adjacent lone pair on the nitrogen would facilitate the fluorine being eliminated to form an imine (supported by the peaks at 8.10-8.26 ppm) Hydrolysis of the imine, either in the reaction due to water in the solvent or during work-up, would give the aldehyde seen. A potential application of this reaction could be in the use of the removal of benzyl groups; a benzyl deprotection method.

### 2.3. Optimisation

The fluorination of test substrate **2.12** illustrated the need for optimisation of the reaction in order to increase the yield of the desired fluorinated products.

#### 2.3.1. Mn(Salen)OTs



Scheme 2.14. Synthesis of Mn(Salen)OTs **(±)-2.24** from **(±)-2.04** and AgOTs.

Catalyst **(±)-2.04** with a chloride counterion was used as the initial catalyst<sup>d</sup>. The literature has shown that the counterion on the Mn[salen]X can affect the fluorination reaction and, in some cases, increase the yield of the desired fluorinated product, e.g. trace amounts for RCC for the Mn(salen)Cl, while Mn(salen)OTs gives an RCC of 53%.<sup>23</sup> Mn(Salen)OTs **(±)-2.24** was synthesised in an 83% yield from **(±)-2.04** and silver *p*-toluenesulfonate by stirring the reaction mixture at room temperature for 2 h (Scheme 2.14). Analysis of the product using FT-IR, the addition of bands at 1030 and

<sup>d</sup> This was due to the relatively simple synthetic process (2 steps) and the commercial availability of the catalyst.

1006 cm<sup>-1</sup> confirmed the presence of the sulfur-oxygen double bond present in the tosylate group.

Fluorination of **2.12** using this modified catalyst, Mn(Salen)OTs (**±**)-**2.24**, resulted in similar yields (<1%) to that of Mn(Salen)Cl therefore the catalysts were used interchangeably.

### 2.3.2. Fluoride Sources

Firstly, alternate fluoride sources were investigated after the low yields obtained when using AgF in combination with (**±**)-**2.04**. Again ethyl-1,1'-biphenyl **2.12** was used as the test substrate for these reactions to allow comparison of the results obtained.

Initially AgF was used as the source of fluoride ions based on the reported methodology, however, low yields (<5%) were obtained for a range of substrates. In an attempt to improve the conversion, more forcing conditions were used in order to achieve higher yields of the desired product **2.13**, these are highlighted below with a focus on the equivalents of the fluoride source.

AgF is poorly soluble in acetonitrile, therefore cesium fluoride (CsF) was used as an alternative fluoride source to overcome the poor solubility and need for a use of an excess of AgF but showed a decrease in yield of **2.13** compared with AgF, with only trace amounts of **2.13** showing in the <sup>19</sup>F and <sup>1</sup>H NMR spectra meaning it was not possible to isolate the product from using CsF.

With CsF only fluorinating **2.12** in trace amounts greater equivalents of AgF were investigated. It was found that the yield of **2.13** varied depending on the stoichiometry of AgF in relation to the substrate. Three equivalents resulted in yields ranging from 1-4% while 5.5 equivalents resulted in an increased yield of 19%. However, the yield of **2.13** was not consistent with repeats of the experiment giving a wide range of yields (1-19%).

Additional fluoride sources were then tested. Tetramethylammonium fluoride tetrahydrate and tetraethylammonium fluoride were used with only trace amounts of the desired fluorinated product being formed. Potassium fluoride (KF) was used in conjunction with the phase transfer catalyst 18-crown-6 as a source of fluoride. The literature uses KF/18-crown-6 with additional additives such as AgOTf and K<sub>2</sub>CO<sub>3</sub>, both of these conditions were tested. When KF/18-crown-6 was used along with

AgOTf there was no fluorination of **2.12**, however, when used with  $K_2CO_3$  the KF/18-crown-6 fluorinated **2.12** in a yield of 5%. Due to the low yields when using KF, no further experimentation using KF was conducted.

Triethylamine trihydrofluoride (TREAT•3HF) was used along with silver (I) fluoride and catalysts ( $\pm$ )-**2.04** and ( $\pm$ )-**2.24** (Mn(salen)OTs) at 0.2 equivalents. In using this dual-fluorine source, yields (15-19%) similar to solely using AgF (5.5 equivalents) were obtained. This method does limit the substrate scope. The use of TREAT•3HF creates an acidic reaction mixture which, at the elevated temperature (50 °C) and the long reaction times (6-9 h), can lead to the hydrolysis of acid sensitive groups such as esters. 3-Phenylpropylacetate was used as a substrate to test whether acid sensitive groups can tolerate the fluorination conditions, and this led to the hydrolysis of the ester. The exposed alcohol group formed from the hydrolysis interfered with the reaction and resulted in no fluorinated products forming.

Another complication when using TREAT•3HF is there is an excess of fluoride. This would lead to a decrease in the specific activity of fluorine-18 when used in a fluorine-18 radiolabelling application. This would reduce the yield of the fluorine-18 radiolabelled compounds.

### 2.3.3. By-product Identification

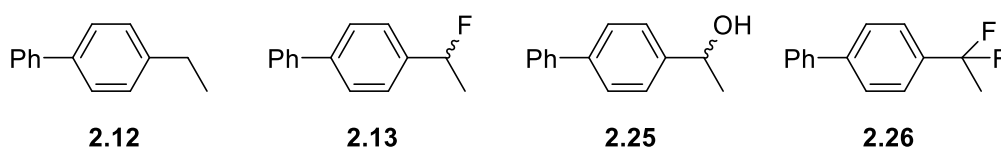


Figure 2.3. Structures of **2.12**, the monofluorinated **2.13** and the by-products **2.25** and **2.26**.

A large-scale (1 g) experiment on ethyl-1,1'-biphenyl using ( $\pm$ )-**2.04** and AgF (5.5 equiv.) allowed the isolation, by preparative TLC, of by-products from the fluorination reaction. The hydroxy product **2.25** was identified and isolated as a white solid in a 5% yield. This is most likely from the presence of water or oxygen in the reaction, suggesting the reaction is sensitive to oxygen and/or water and needs strict anaerobic and anhydrous conditions to increase the yield of the desired fluorinated product. The hydroxy product most likely forms from the trapping of a radical intermediate via an oxo-manganese species, similar to the proposed mechanism of the epoxidation

synthesis from alkenes by Jacobsen and Katsuki. **2.25** was recrystallised from toluene and a crystal structure was obtained confirming the proposed structure.

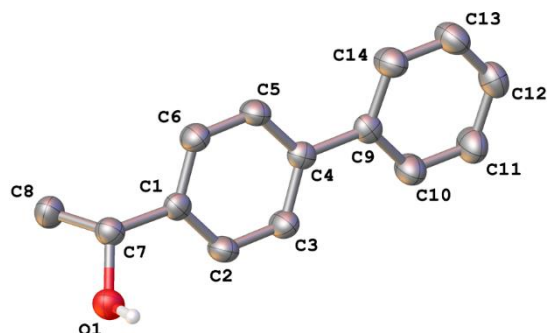


Figure 2.4. Crystal structure of **2.25**.

The large-scale reaction also resulted in the identification of the difluorosubstituted compound **2.26** which co-eluted with the latter portion of **2.13** and was isolated from the crude reaction as part of a mixture as shown by the  $^{19}\text{F}$  NMR (Fig. 2.5).

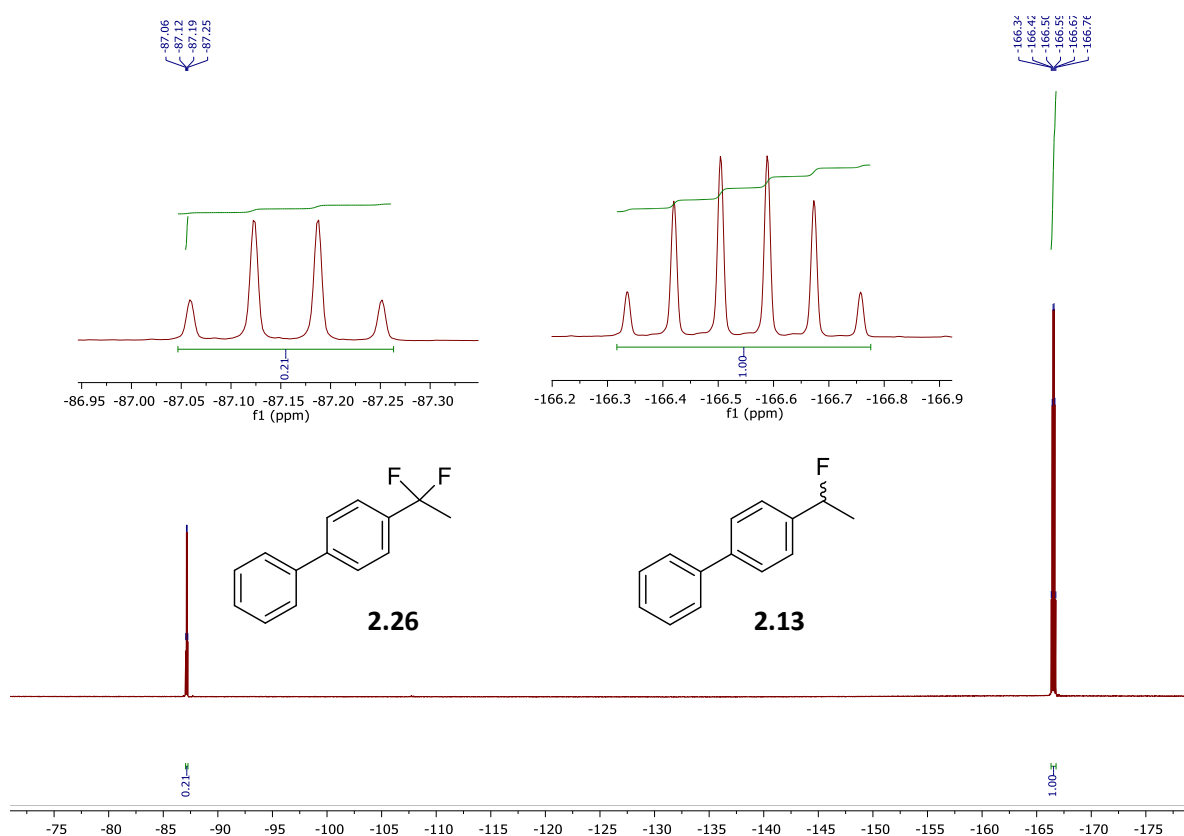


Figure 2.5.  $^{19}\text{F}$  NMR spectrum of the mixture of **2.13** and **2.26**. **2.13** is the overlapping doublet of quartets (-166.5) whilst **2.26** is the quartet (-87.2 ppm)

#### 2.3.4. Practical Aspects

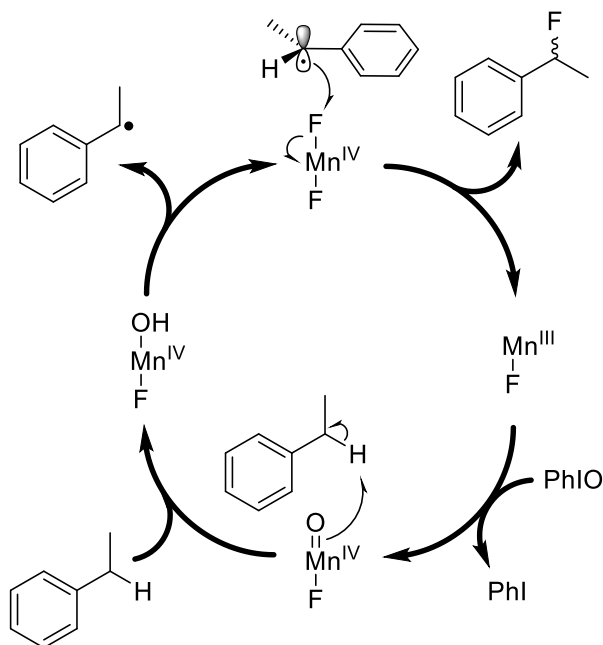
The effect of practical changes to the underlying methodology was also tested. For example several experiments used acetonitrile that had been degassed by sparging with nitrogen overnight and this showed little to no change in the yield of **2.13** and **2.25** was still present. This suggests that the transfer of oxygen in the reaction to form the hydroxyl by-product, which was thought to decrease the yield of the desired fluorinated product, might not be from oxygen in the solvent but through other sources such as water or the oxidant (PhIO) itself. The reason behind the use of degassed solvent was to reduce the amount of the oxidative product present and subsequently increase the yield of the fluorinated products.

#### 2.4. Mechanism and Oxygen Transfer

The presence of the hydroxy product **2.25**, despite the use of anhydrous and degassed MeCN, suggests the hydroxyl-group is installed via a mechanism within the reaction. Further investigation into the proposed reaction mechanism by Groves *et al* was conducted.

##### 2.4.1. Proposed Mechanism

The mechanism, for fluorine-19 reactions, proposes a radical intermediate which abstracts the fluorine from a difluoromanganese (IV) reactive fluorine transfer intermediate. This is thought to be analogous to the mechanism, again proposed by Groves, of the benzylic fluorination using a manganese porphyrin catalyst.<sup>14</sup> A benzylic radical is formed on the substrate from the  $[\text{Mn}^{\text{V}}(\text{O})(\text{salen})\text{F}]$  complex abstracting a benzylic hydrogen, this radical then abstracts a fluorine from the active difluoromanganese species. This in turn regenerates the resting Mn (III) catalyst and the cycle repeats (Scheme 2.15).



Scheme 2.15. Catalytic cycle proposed by Groves et al for the installation of the benzylic fluorine. Salen ligand omitted for clarity.

Given the low yields and the by-products observed with the test substrate **2.12**, a closer look into the mechanism was conducted.

#### 2.4.2. Radical Scavenger Reactions

The identification of the hydroxyl by-product **2.25** led to investigations into the mechanism proposed by Groves and the transfer of oxygen to the substrate.<sup>14,15,23</sup> A series of reactions were conducted using radical scavengers with the aim to suppress the formation and propagation of the radical pathway proposed. The use of TEMPO (15 mol%) resulted in similar yields of **2.13** (8% and 11%, Mn(salen)Cl and Mn(salen)OTs respectively) as previous reactions (5-19%). This is surprising given the proposed radical intermediate. The **2.25** by-product was not observed when using TEMPO and Mn(salen)Cl but still remained in a 5% yield when using Mn(salen)OTs as the catalyst.

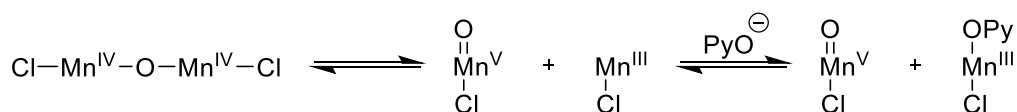
Radical Scavenger	Yield / %
TEMPO	8 <sup>a</sup>
Hydroquinone	1 <sup>b</sup>
Butylated Hydroxytoluene	3 <sup>b</sup>
$\alpha$ -Tocopherol	2 <sup>b</sup>
Galvinoxyl	3 <sup>b</sup>

Table 2.1. Yields of **2.13** when using  $Mn(salen)Cl$  as a catalyst in the presence of radical scavengers.  
<sup>a</sup> Isolated yield, <sup>b</sup> Yield calculated by NMR using 2-fluorotoluene as an internal standard.

The use of radical scavengers showed no significant change in the yield of the desired fluorinated product **2.13**. A possible explanation to the small decrease in the yield is that the radical being produced in the catalytic cycle is closely bound to the manganese centre of the catalyst and is therefore not a 'free radical'.

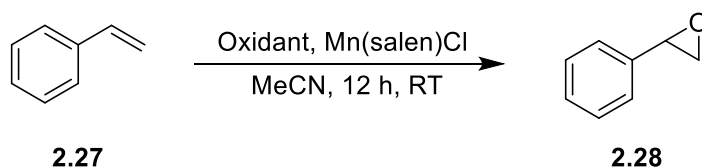
#### 2.4.3. Oxidant Test Reactions

As previously mentioned in Chapter 2.1, the  $Mn(salen)Cl$  catalysts were originally designed to be used for the epoxidation of alkenes. An oxidant, typically  $NaOCl$  or iodosobenzene, is used to oxidise the alkene to the epoxide. Due to the similarity of the proposed mechanism by Groves *et al* of the fluorination and the established mechanism for the Jacobsen epoxidation, several oxidants commonly used in epoxidation chemistry were tested as alternative oxidants to iodosobenzene. These included urea hydrogen peroxide, 3-chloroperbenzoic acid (*m*-CPBA) and oxone<sup>®</sup>.<sup>24,25</sup> Pyridine *N*-oxide was also used in some epoxidation reactions as a co-oxidant with the possibility that the pyridine *N*-oxide regenerates the manganese-oxo complex, which is proposed as the active catalytic intermediate, or that it occupies the vacant axial coordination site stabilising the intermediate and shifting the equilibrium towards the  $Mn^V$ -oxo complex, hence maintaining the catalytic cycle (Scheme 2.16). Therefore, in addition to the oxidants stated above, pyridine *N*-oxide will also be tested as a co-oxidant.<sup>26</sup>



Scheme 2.16. Addition of pyridine *N*-oxide to the catalyst.

#### 2.4.3.1. Epoxidation Reactions



Scheme 2.17. Epoxidation of styrene **2.27**.

A common example of the epoxidation of an alkene is using styrene **2.27** (Scheme 2.17). Styrene is commonly used as the model compound for evaluating epoxidation catalysis. The majority of the oxidants tested have been used to epoxidise styrene. When using urea hydrogen peroxide or oxone<sup>®</sup> as the oxidant only trace amounts of the styrene epoxide was evident by analysis by <sup>1</sup>H NMR spectroscopy. The results from the urea hydrogen peroxide and oxone<sup>®</sup> reactions can be accounted for by the poor solubility of both reagents in acetonitrile which has led to the poor yields of the epoxide.

Iodosobenzene does generate styrene epoxide at around a 50% conversion (by <sup>1</sup>H NMR spectroscopy) when used on its own, however, when used with pyridine *N*-oxide the conversion increases to around 70%. *m*-CPBA also successfully leads to styrene epoxide, also giving a conversion of around 50%, which increases to around 60% with the addition of pyridine *N*-oxide. As a result of their compatibility with the catalytic system, all of these alternate oxidants were taken forward to be tested under fluorination conditions.

#### 2.4.3.2. Fluorination Test with Oxidants

Test fluorination reactions were conducted using **2.12** as the model substrate. Attempted fluorination using high levels of urea hydrogen peroxide as the oxidant (7 equiv.) was carried out, however, no fluorination was evident by <sup>19</sup>F NMR spectroscopy. This reaction was conducted at 55 °C, following the same procedure for the iodosobenzene, which may have caused the urea hydrogen peroxide to decompose (decomposition temperature approx. 55-60 °C and the evolution of gas on addition of the urea hydrogen peroxide to the hot reaction mixture).<sup>27</sup> As a result, the temperatures used in this reaction means that urea hydrogen peroxide is not a viable oxidant. *m*-CPBA also gave trace amounts of **2.13** by <sup>19</sup>F NMR spectroscopy although



a large amount of starting material remained along with the hydroxy product **2.25**, as seen by  $^1\text{H}$  NMR spectroscopy and TLC.

Iodosobenzene was used in conjunction with pyridine *N*-oxide (as the co-oxidant). At one equivalent of pyridine *N*-oxide, the yield of **2.13** (by  $^{19}\text{F}$  NMR spectroscopy) was only 3%, a decrease in the yield previously seen without the use of a co-oxidant. It is proposed that this could be a result of the co-oxidant occupying the axial coordination site blocking the fluorine ligand from coordinating which stops the formation of the active form of the catalyst. Increasing the reaction time (4 h to 8 h) and increasing the equivalents of pyridine *N*-oxide (5 equiv.) resulted in a yield of 6%. The pyridine *N*-oxide occupying the axial coordination site should lead to a decrease in yield of the fluorinated product. However, the greater equivalents of pyridine *N*-oxide could result in a greater shift of the equilibrium, proposed by Jacobsen (Scheme 2.13), and allow for a greater amount of the  $\text{Mn}^{\text{V}}$ -oxo complex to be present within the reaction medium therefore increasing the yield relative to the yield observed with one equivalent of pyridine *N*-oxide.<sup>26</sup>

In summary the use of alternative and co-oxidants resulted in a reduced yield of the desired fluorination product and iodosobenzene has been found to be the best option for the oxidant in this reaction.

## 2.5. Alternative Manganese Catalysts

From the mechanism, a number of intermediates are proposed in the catalytic cycle, one such intermediate being  $\text{Mn}(\text{salen})\text{F}$ .

### 2.5.1. Manganese Salen Fluoride Complexes

The radical scavenger studies (Chapter 2.4.2) found that a radical intermediate, if formed, would most likely be located closely to the manganese centre, within the solvent cage, due to the presence of radical scavengers having little effect on the yield of the desired fluorinated product **2.13**. As Groves suggests that the  $\text{Mn}(\text{Salen})\text{F}$  and  $\text{Mn}(\text{Salen})\text{F}_2$  are both catalytic intermediates, the impact of a series of independently prepared  $\text{Mn}(\text{Salen})\text{F}$  compounds was of interest. These were used to

test whether the proposed benzylic radical is a separate free radical or bound to the manganese and the fluorine is added via an intermolecular transition state.

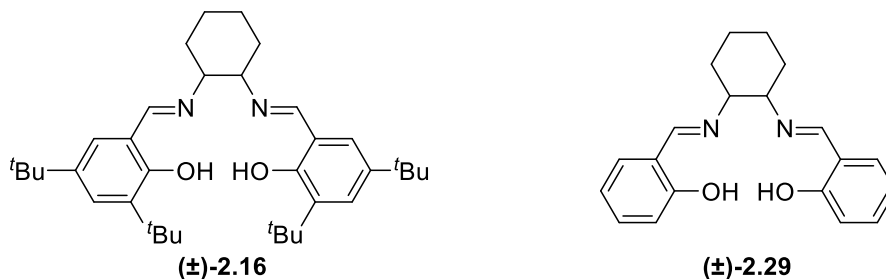


Figure 2.6. The salen ligands which were used in the synthesis of Mn(salen)F type compounds.

The synthesis of Mn(Salen)F type compounds was attempted using two different salen ligands; **(±)-2.16** and **(±)-2.29** (Fig. 2.6). The salen ligands were treated with manganese (III) fluoride and triethylamine in MeOH for 40 min while being heated at reflux.<sup>29</sup>

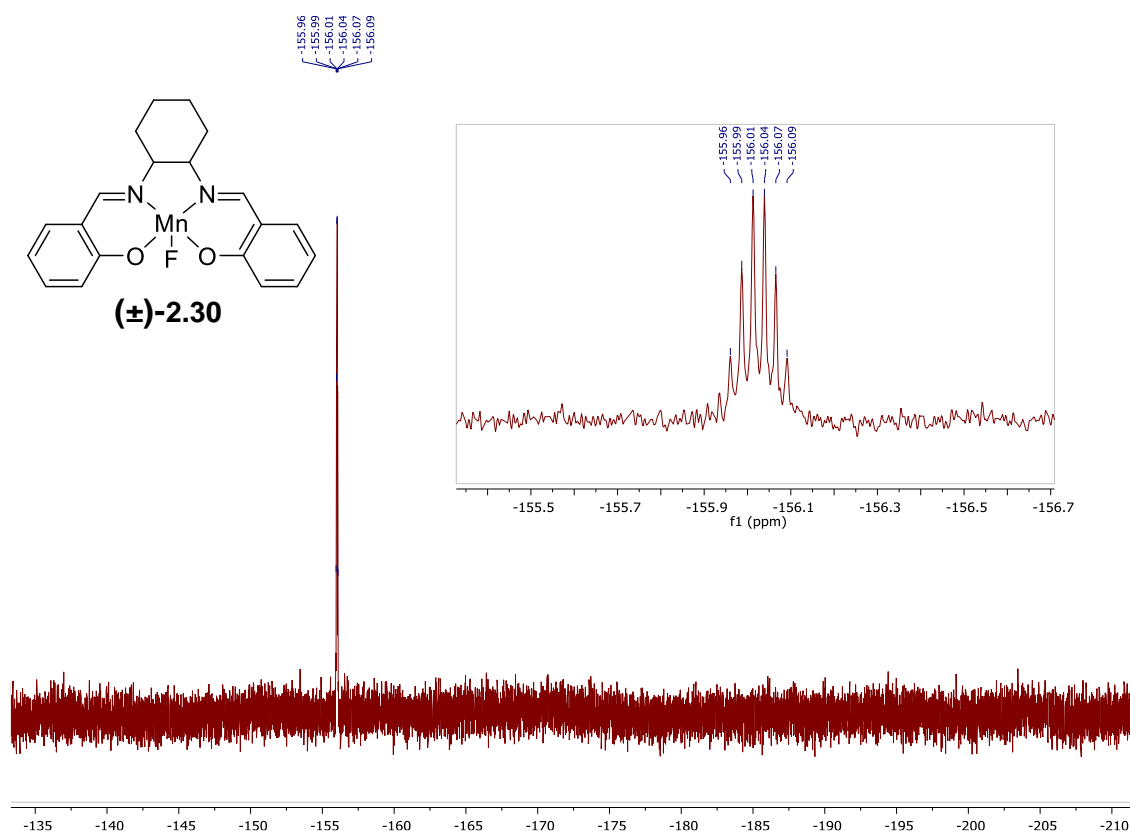


Figure 2.7. <sup>19</sup>F NMR of Mn(salen)F spectrum.

When using **(±)-2.16** as the initial salen ligand, the formation of the Mn-F compound was unsuccessful as no signals were evident by <sup>19</sup>F NMR analysis. However, when using **(±)-2.29** as the ligand the synthesis of the Mn-F compound was successful with

the  $^{19}\text{F}$  NMR spectrum showing one peak (-156 ppm) with a splitting pattern of a sextet demonstrating the coupling to the manganese ( $I = 5/2$ ) (Fig. 2.7). The low signal to noise ratio of this compound is due to the poor solubility of these types of complexes in organic solvents however it was possible to recrystallize this material allowing a crystal structure to be obtained (Fig. 2.8).

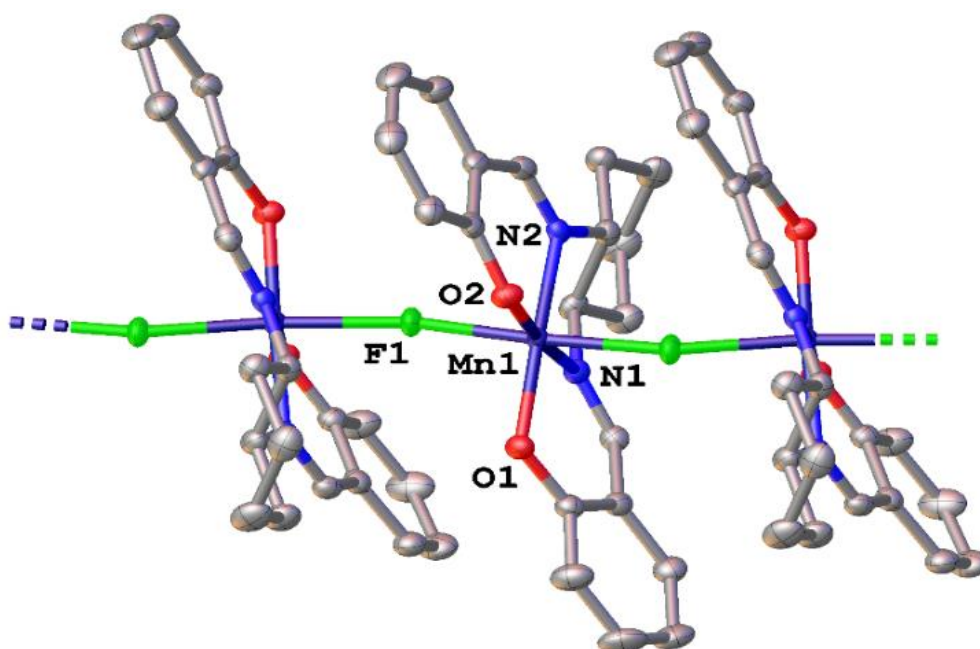


Figure 2.8. Crystal structure of the  $\text{Mn}(\text{salen})\text{F}$  using  $(\pm)\text{-2.29}$  as a ligand.

It is interesting that, in the solid state,  $(\pm)\text{-2.30}$  adopts a 1D coordination polymeric structure, with the coordination via a manganese-fluorine-manganese bond. The crystal structure of the coordination polymer illustrates that the Mn(III) is the central atom of a distorted octahedral coordination complex formed by the equatorial coordination of the tetradentate salen and the axial coordination of two fluoride ligands. The bond lengths for the Mn-F bonds are 2.038 Å and 2.035 Å for the fluorine below and above the Mn(III) central atom respectively (Fig. 2.9).

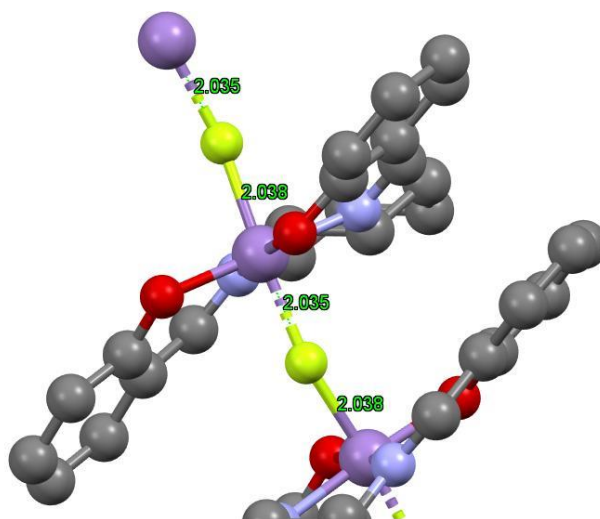


Figure 2.9. Bond lengths of the Mn-F bonds.

All manganese centres are equivalent in the unit cell packing, giving the bridging fluoride Mn-F-Mn a bond angle of  $160.53^\circ$  and the F-Mn-F a bond angle of  $171.86^\circ$  (Fig. 2.10). The salen ligand with the large cyclohexane group results in the alternating orientation of the salen ligand by  $180^\circ$  around the Mn(II) central atom. It is interesting to note that a molecule of water has been shown to be incorporated into the crystal structure of ( $\pm$ )-**2.30**. This molecule engages in hydrogen bonding to the oxygen atoms on the salen ligand and to the fluorine atom present but does not coordinate to the Mn(III) central atom (Fig. 2.10). This is further supported by literature data which has shown that similar complexes are obtained as hydrates and that by heating the complexes at  $100^\circ\text{C}$  for 2 h the water is removed with no change to the FT-IR spectrum, other than those associated with the O-H vibrations. The success of this method for the removal of water suggests that the water molecule is only loosely associated and therefore non-coordinating.<sup>26</sup>

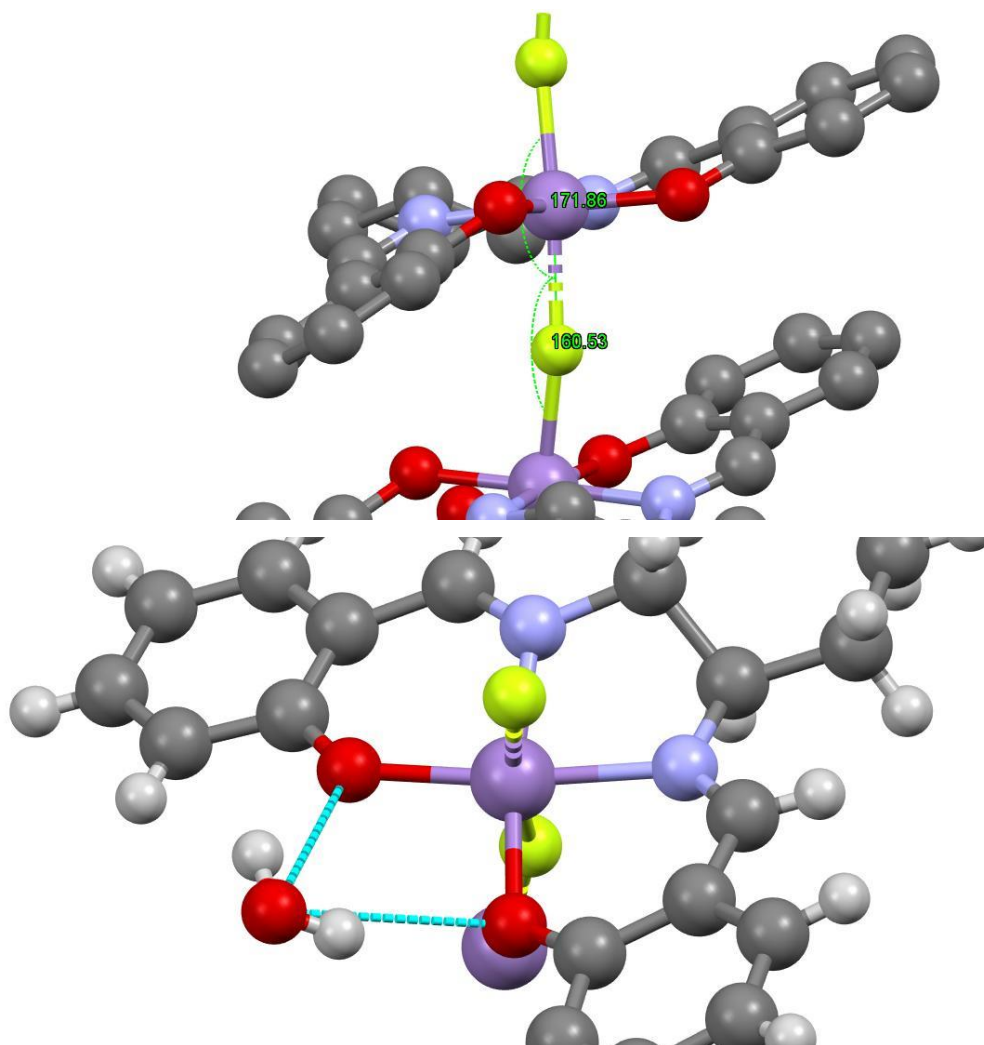


Figure 2.10. Bond angles between Mn-F-Mn and F-Mn-F (Top) and the coordinating water molecule (Bottom).

In solution, the  $^{19}\text{F}$  NMR spectrum shows one fluorine peak, that of -156 ppm (sextet), suggesting the polymer breaks down into the Mn(salen)F monomer. The polymer would have a greater splitting pattern if bound to both manganese centres (greater than the sextet observed for **(±)-2.30**). This would agree with the literature on similar Mn(salen)F type compounds.<sup>28</sup> Birk found that polymeric Mn(salen)F complexes break down into the monomeric form of Mn(salen)F when in solution.<sup>27</sup>

In light of the results above, Mn(salen)F **(±)-2.30** was used as a catalyst for the fluorination of **2.12** (AgF/TREAT·HF as sources of fluorine and PhIO as the oxidant) which gave a yield of 11% for the mono-fluorinated product **2.13**. This low yield could be due to the poor solubility of the of **(±)-2.30** in MeCN or by removing the *tert*-butyl groups from the salen ligand this has reduced the activity of the catalyst. The solubility of the Mn(salen)F and some salen ligands is problematic. These type of compounds

[Mn(salen)F] are proposed as an intermediate and precipitation out of the reaction would result in a low yielding fluorination reaction. The nucleophilic fluorination reaction using Mn(salen)Cl is homogeneous, with the catalyst being able to dissolve in MeCN easily with minimal intervention. The Mn(salen)F class of catalysts may not function under heterogeneous conditions and therefore would need ligands which convey improved solubility in the reaction solvents, such as MeCN.

Further work into the Mn(salen)F compounds for the use as nucleophilic fluorination catalysts is needed, particularly the development of ligand systems to overcome the poor solubility of these species.

#### 2.5.1.1. Substituted Salen Derivatives

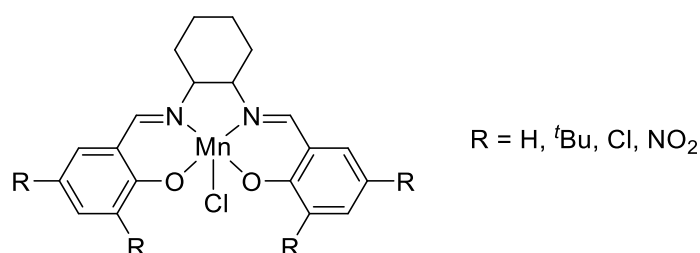


Figure 2.11. Structure of the Mn(salen)Cl complexes.

The substituted salen derivatives of (**±**)-**2.16** (previously stated in 2.5.1) were used to synthesise Mn(salen)Cl type complexes (Fig. 2.11). The complexes were then used as the catalysts for the fluorination of **2.12** in order to test whether the groups on the aromatic ring have an effect on the catalytic potential.

From work conducted by M. Alsaffar, the use of the dichloro-substituted Mn(salen)Cl gave promising results when fluorinating 5,6-dimethoxyindanone.<sup>30</sup> The 3,5-dinitrosalen ligand was synthesised, however the very poor solubility of this ligand meant the formation of the Mn(salen)Cl and the Mn(salen)F complexes were not achieved.

#### 2.5.2. Salen Derivatives and Other Transition Metals

Due to the still low yields of the desired fluorinated product and with few options left for functional group modification of the salen ligand, alternative transition metals to manganese were also investigated.

### 2.5.2.1. Alternative Transition Metals

Manganese is not the only transition metal which can be used for fluorination reactions. In recent years there have been a lot of interest in this field and a number of transition metals have been found to catalyse fluorination reactions, e.g. vanadium and iron.

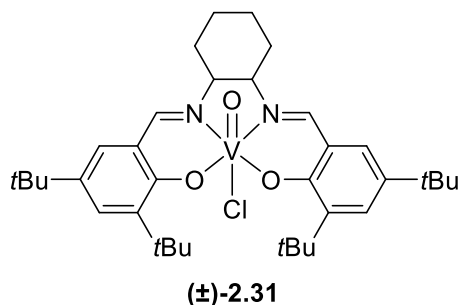


Figure 2.12. Structure of the VO(salen)Cl (**±**)-2.31.

A variation of the M(salen)Cl complex was synthesised in a 42% yield using vanadium oxychloride (VOCl<sub>3</sub>) and ligand (**±**)-2.16 in THF.<sup>31</sup> This complex differs from the Mn(salen)X complexes with the presence of the axial oxy-group. The reason behind using the VO(salen)Cl complex was that it resembles the MnO(salen)Cl catalytic intermediate of the catalytic cycle proposed by Groves.<sup>14,15</sup> The VO(salen)Cl was therefore tested as a catalyst for nucleophilic fluorination using **2.12** as the model substrate, and following the optimised conditions<sup>e</sup> used for Mn(salen)Cl. Only trace amounts of the fluorinated product **2.13** were present by <sup>19</sup>F NMR analysis, and therefore it appears that the VO(salen)Cl would not be a suitable option for use as a fluorination catalyst.

In order to increase the yield of the desired product **2.13**, direct synthesis of the potential key VO(salen)F complex was attempted using VOF<sub>3</sub> as the source of the vanadium. However, the synthesis was unsuccessful, no fluorine peaks were present in the <sup>19</sup>F NMR spectrum of the crude reaction mixture before and/or after work-up. Given these results further investigation into the alternative transition metal catalysts was not conducted at this time.

<sup>e</sup> Both AgF (5.5 Equiv.), PhIO, 50 °C, 6-9 h and TREAT•3HF (0.2 Equiv.), AgF(3.0 Equiv.), PhIO, 50 °C, 6-9 h were attempted.

## 2.6. Conclusion and Future Work

In this chapter nucleophilic fluorination of small molecules was attempted, using Mn(salen)Cl as a catalyst. Following low yields during the initial investigation and the identification of the hydroxyl by-product **2.25** a series of optimisation experiments were conducted in order to increase the yield of the mono-fluorination product.

An investigation into the choice of fluoride source and the oxidant, gave the highest yield for the fluorination of **2.12** using AgF and PhIO. Close inspection of the mechanism proposed by Groves gave rise to the Mn(salen)F complex and its use as a catalyst. The yield of **2.13** did not increase, giving a yield of 11%. The synthesis of Mn(salen)F type complexes opens up the possibility of further work into the area with more complex salen ligands, which can allow fine-tuning of the ligand properties, and the potential fluorination capacity of the catalyst.

Early work into different transition metals was conducted. A VO(salen)Cl complex was synthesised and tested as a fluorination catalyst with no fluorination observed. Experimental work into different metals was being conducted by another group member, M. Alfasir. This work is currently ongoing.

For an industrial process, a low yield for the incorporation of fluorine-19 into the target molecule is not of great benefit. However, fluorine-18 incorporation does not require high yields and the yields achieved within this work would be substantial enough to potentially allow for a good radiochemical conversion. The next steps of the investigation of Mn(salen)Cl catalysed fluorination would be to test the catalyst and the optimised conditions using fluorine-18.

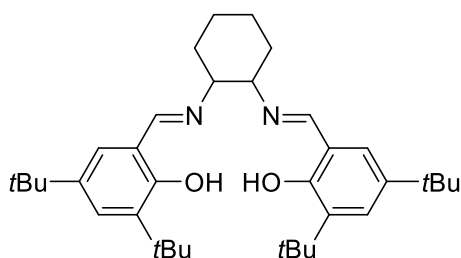


## 2.7. Chapter 2 Experimental

Starting materials were purchased from commercial sources and were used without further purification.  $^1\text{H}$ ,  $^{13}\text{C}$  and  $^{19}\text{F}$  NMR spectra were recorded using Bruker Avance II 400 MHz and Bruker Avance III 300 MHz spectrometer, with a residual protic solvent used as the reference for  $^1\text{H}$  and  $^{13}\text{C}$  NMR spectroscopy and an external reference of  $\text{CFCl}_3$  for  $^{19}\text{F}$  NMR studies. Infrared spectroscopy were recorded using Varian 800 FT-IR spectrometer. Melting points were recorded on a Gallenkamp MF-370 melting point apparatus and are uncorrected. LCMS data was recorded on an LCMS Agilent Infinity II R90 UPLC + MSD XT instrument and HRMS data was recorded on a LCMS/MS (QToF) Waters Acquity UPLC + Xevo G2-XS instrument.

Acetonitrile was dried using 3 Å molecular sieves and degassed via sparging overnight with nitrogen and stored under nitrogen prior to use. The water content was measured (in ppm) using Karl-Fischer Coulometry. Acetonitrile used in the reactions had between 10-80 ppm water content.

### (±)-*N,N'*-Bis(3,5-di-*tert*-butylsalicylidene)-1,2-cyclohexanediamine (±)-2.16

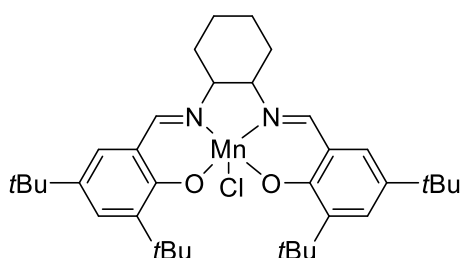


(±)-1,2-Diaminocyclohexane (4.27 mL, 35.55 mmol) was added to EtOH (50 mL). 3,5-Di-*tert*-butylsalicylaldehyde (6.05 g, 25.82 mmol) was dissolved in EtOH (100 mL) and the solution was added dropwise to the diamine-ethanol solution over 1 h. The reaction mixture was heated at reflux for 3 h and then cooled in an ice-bath for 1 h. The yellow precipitate was removed by filtration and washed with cold EtOH (2 × 40 mL) and left to dry for 2 h. The preliminary product was taken up in DCM (60 mL) and washed with distilled water (2 × 25 mL). The organic layer was dried with anhydrous  $\text{MgSO}_4$  overnight and the solvent was removed by in vacuo to give (±)-*N,N'*-bis(3,5-di-*tert*-butylsalicylidene)-1,2-cyclohexanediamine as a yellow solid (5.46 g, 9.99 mmol, 77%).  $\nu_{\text{max}}$  (neat/ $\text{cm}^{-1}$ ) 2952, 2861, 1626, 1439, 1251, 1173, 1095, 877, 772  $\text{cm}^{-1}$ ;  $^1\text{H}$  NMR (

300 MHz, CDCl<sub>3</sub>)  $\delta_{\text{H}}$  13.64 (2H, br, s, OH), 8.23 (2H, s, N=CH), 7.22 (2H, d,  $J=2.4$  Hz, aromatic H), 6.91 (2H, d,  $J=2.4$  Hz, aromatic H), 3.25 (2H, d,  $J=9.4$  Hz, N-CH), 1.93-1.37 (8H, m, CH<sub>2</sub>), 1.34 (18H, s, CH<sub>3</sub>), 1.16 (18H, s, CH<sub>3</sub>) ppm; <sup>13</sup>C NMR (300 MHz, CDCl<sub>3</sub>)  $\delta_{\text{C}}$  165.9 (CH), 158.0 (C), 139.9 (C), 136.4 (C), 126.8 (CH), 126.1 (C), 117.9 (CH), 72.4 (CH), 35.0 (C), 34.0 (CH<sub>2</sub>), 33.3 (C), 31.4 (CH<sub>3</sub>), 29.4 (CH<sub>3</sub>), 24.4 (CH<sub>2</sub>) ppm;  $m/z$  (TOF MS ES+ HRMS) 546.4185 [M]<sup>+</sup>. Found: [M+H]<sup>+</sup> 547.4305.

*Analytical data corresponds to the literature*<sup>1</sup>

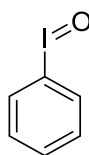
(±)-*N,N'*-Bis(3,5-di-*tert*-butylsalicylidene)-1,2-cyclohexanediamino manganese(III) chloride (±)-2.04



The (±)-salen ligand (2.50 g, 4.56 mmol) was dissolved in toluene (50 mL) and added dropwise to Mn(OAc)<sub>2</sub> (4.09 g, 23.64 mmol) in EtOH (80 mL). The reaction was heated at reflux for 3 h. LiCl (1.08 g, 25.38 mmol) was added to the reaction mixture and heated at reflux for a further 2 h and then was cooled in an ice-bath for 1.5 h. The reaction mixture was washed with distilled water (2 × 70 mL) and the organic layer was dried with anhydrous MgSO<sub>4</sub> and the solvent was removed in vacuo to give (±)-*N,N'*-bis(3,5-di-*tert*-butylsalicylidene)-1,2-cyclohexanediaminomanganese(III) chloride as a brown powder (2.25 g, 3.53 mmol, 77%).  $\nu_{\text{max}}$  (neat/cm<sup>-1</sup>) 2949, 1613, 1535, 1433, 1310, 1252, 1174, 1029, 836, 780, 748, 567, 543, 484 cm<sup>-1</sup>.

*Analytical data corresponds with a sample received from Sigma Aldrich.*

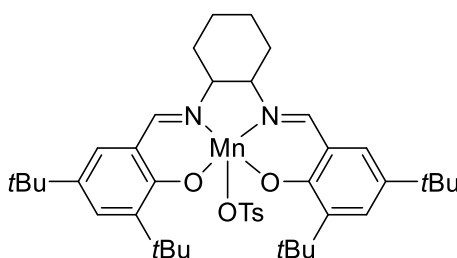
Iodosylbenzene 2.18<sup>30</sup>



Diacetoxyiodobenzene (5.07 g, 15.73 mmol) was dispersed in aqueous NaOH 15% w/w (19 mL) and stirred at room temperature for 4 h. The solid was removed by filtration then washed with water (2 × 30 mL), chloroform (30 mL) then acetone (30 mL). The product was air dried on the Büchner filter for overnight, giving a pale-yellow solid (2.62 g, 11.91 mmol, 76%). <sup>1</sup>H NMR (300 MHz, d<sub>4</sub>-MeOH) δ<sub>H</sub> 7.83-7.68 (2H, m, CH), 7.47-7.11 (3H, m, CH) ppm.

*Analytical data corresponds with the literature*<sup>32</sup>

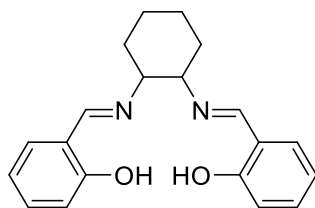
(±)-N,N'-Bis(3,5-di-*tert*-butylsalicylidene)-1,2-cyclohexanediamino manganese(III) tosylate (±)-2.24<sup>33</sup>



[(±)Salen-Mn][Cl] (0.21 g, 0.31 mmol) was dissolved in acetonitrile (5 mL) and stirred at room temperature for 1 h. Silver *p*-toluenesulfonate (0.10 g, 0.31 mmol) was added to the reaction mixture and left to stir at room temperature for 2 h. The reaction mixture was filtered and the solvent was removed *in vacuo* giving a brown powder (0.21 g, mmol, 83%). ν<sub>max</sub> (neat/cm<sup>-1</sup>) 2952, 2864, 1617, 1530, 1432, 1312, 1252, 1031 cm<sup>-1</sup>.

*Analytical data corresponds with the literature*<sup>33</sup>

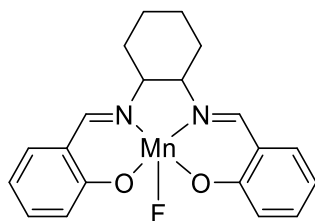
(±)-N,N'-Bis(salicylidene)-1,2-cyclohexanediamine (±)-2.29<sup>34</sup>



1,2-Diaminocyclohexane (4.27 mL, 35.55 mmol) was dissolved in EtOH (50 mL). Salicylaldehyde (7.55 mL, 71.10 mmol) was dissolved in EtOH (100 mL) and added dropwise to the reaction mixture over 1 h and heated at reflux for 3 h. The solution was allowed to cool overnight and the precipitate was removed by filtration and washed with EtOH (100 mL) giving the product as a yellow solid (8.18 g, 25.37 mmol, 71%).  $\nu_{\max}$  (neat/cm<sup>-1</sup>) 2926, 2843, 1626, 1499, 1278, 1148, 844, 757 cm<sup>-1</sup>; <sup>1</sup>H NMR (300 MHz, CDCl<sub>3</sub>)  $\delta_{\text{H}}$  13.32 (2H, s, phenol), 8.29 (2H, s, N=CH), 7.30 - 7.23 (2H, m, aromatic H), 7.20 – 7.16 (2H, m, aromatic H), 6.93 (2H, d,  $J=8.2$ , aromatic H), 6.81 (2H, t,  $J=7.3$ , aromatic H), 3.38 – 3.35 (2H, m, CH), 2.03 – 1.86 (4H, m, CH<sub>2</sub>), 1.84 – 1.67 (2H, m, CH<sub>2</sub>), 1.56 – 1.44 (2H, m, CH<sub>2</sub>) ppm.

*Analytical data corresponds with the literature<sup>34</sup>*

(±)-N,N'-Bis(salicylidene)-1,2-cyclohexanediamino manganese(III) fluoride (±)-2.30

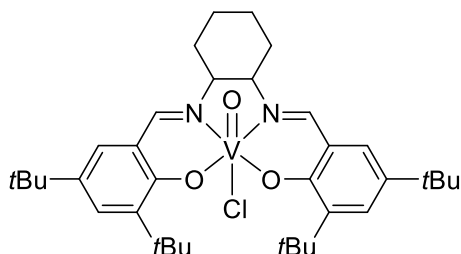


(±)-N,N'-Bis(salicylidene)-1,2-cyclohexanediamine (1.36 g, 4.19 mmol) was partially dissolved in MeOH (40 mL) and manganese (III) fluoride (0.45 g, 4.03 mmol) was added followed by triethylamine (0.61 mL, 8.06 mmol). The reaction was heated at reflux for 35 min when water (2.5 mL) was added and the reaction was heated at reflux for a further 5 min. The solvent was removed *in vacuo* giving a brown powder (0.48 g, 1.22 mmol, 30%).  $\nu_{\max}$  (neat/cm<sup>-1</sup>) 3365, 2929, 1639, 1596, 1542, 1445, 1307, 1196,

1144, 1039, 906, 747, 616, 563, 465  $\text{cm}^{-1}$ .  $^{19}\text{F}$  NMR (300 MHz,  $\text{d7-DMF}$ )  $\delta_{\text{F}}$  -156.0 (sextet,  $J = 7.5$  Hz, Mn-F) ppm.

See Appendix for crystal structure.

(±)-*N,N'*-Bis(3,5-di-*tert*-butylsalicylidene)-1,2-cyclohexanediamino oxo-vanadium (V) chloride (±)-2.31<sup>31</sup>



(±)-*N,N'*-Bis(3,5-di-*tert*-butylsalicylidene)-1,2-cyclohexanediamine (1.00 g, 1.83 mmol) was dissolved in THF (20 mL) and  $\text{VOCl}_3$  (0.23 mL, 2.42 mmol) was added whilst stirring. The reaction was stirred for 30 min at RT then the solvent was removed *in vacuo*. The product was isolated by column chromatography (3:1 EtOAc:Hexane then 1:1:1 EtOAc:Hexane:MeOH) and the dark green fractions were collected. The solvent was removed *in vacuo* giving a dark green powder (498 mg, 0.77 mmol, 42%).  $R_f$  0.2 (1:1:0.25 EtOAc:Hexane:MeOH);  $\nu_{\text{max}}$  (neat/ $\text{cm}^{-1}$ ) 3321, 2951, 1615, 1552, 1248, 968, 844, 759, 594, 490  $\text{cm}^{-1}$ ;  $^1\text{H}$  NMR (300 MHz,  $\text{CDCl}_3$ )  $\delta_{\text{H}}$  8.72 (1H, s, HC=N), 8.58 (1H, s, HC=N), 7.76 (1H, d,  $J = 2.1$  Hz, aromatic CH), 7.71 (1H, d,  $J = 2.3$  Hz, aromatic CH), 7.56 (1H, d,  $J = 2.2$  Hz, aromatic CH), 7.53 (1H, d,  $J = 2.1$  Hz, aromatic CH), 4.47 (1H, t,  $J = 10.8$  Hz, HC-N), 3.79 (1H, t,  $J = 10.8$  Hz, HC-N), 2.75 (1H, d,  $J = 10.4$ ,  $\text{CH}_2$ ), 2.51 (1H, d,  $J = 10.4$ ,  $\text{CH}_2$ ), 2.11 – 2.07 (4H, m,  $\text{CH}_2$ ), 1.74 – 1.71 (2H, m,  $\text{CH}_2$ ), 1.53 (9H, s,  $\text{C}(\text{CH}_3)_3$ ), 1.51 (9H, s,  $\text{C}(\text{CH}_3)_3$ ), 1.38 (9H, s,  $\text{C}(\text{CH}_3)_3$ ), 1.36 (9H, s,  $\text{C}(\text{CH}_3)_3$ ) ppm;  $^{13}\text{C}$  NMR (300 MHz,  $\text{CDCl}_3$ )  $\delta_{\text{C}}$  165.0, 161.5, 160.2, 144.2, 144.1, 136.0, 135.3, 132.2, 131.7, 128.4, 122.1, 121.0, 35.9, 35.7, 34.7, 34.6, 31.6, 31.5, 30.7, 30.0, 29.8, 29.2, 24.7, 24.2 ppm;  $m/z$  (TOF MS ES+ HRMS) 611.3418  $[\text{M-Cl}]^+$ . Found:  $[\text{M-Cl}]^+$ , 611.3436.

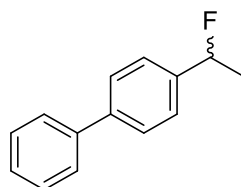
Analytical data corresponds with the literature<sup>31</sup>

### General Procedure for Nucleophilic Fluorination using Mn(salen)Cl Catalysts

Method A: To an oven-dried Schlenk flask under an N<sub>2</sub> atmosphere, Mn(salen)Cl (0.22 mmol, 20 mol%), AgF (6.00 mmol) and substrate (1.1 mmol) were added followed by degassed anhydrous MeCN (2 mL). The reaction mixture was heated to 50 °C. PhIO (6.60 mmol) was added in small portions (10 mg/2 min) over 6-9 h. MeCN (1 mL) was added for every two equivalents of oxidant. The reaction mixture was allowed to cool to RT and DCM (5 mL) was added to dilute the reaction mixture. The reaction mixture was passed through a Celite plug. The crude reaction mixture was concentrated *in vacuo* and products isolated by chromatographic techniques (e.g. prepTLC, column chromatography or flash column chromatography).

Method B: To an oven-dried Schlenk flask under an N<sub>2</sub> atmosphere, Mn(salen)Cl (0.22 mmol, 20 mol%), AgF (3.3 mmol) and substrate (1.10 mmol) were added followed by degassed anhydrous MeCN (1 mL). TREAT•3HF (0.1 mL) is dissolved in MeCN (1.5 mL) and is added to the Schlenk flask. The reaction mixture was heated to 50 °C. PhIO (6.00 mmol) was added in small portions (10 mg/2 min) over 6-9 h. MeCN (1 mL) was added for every two equivalents of oxidant. The reaction mixture was allowed to cool to RT and DCM (5 mL) was added to dilute the reaction mixture. The reaction mixture was passed through a Celite plug. The crude reaction mixture was concentrated *in vacuo* and products isolated by chromatographic techniques (e.g. prepTLC, column chromatography or flash column chromatography).

#### 4-(1-Fluoroethyl)-1,1'-biphenyl **2.13**<sup>15</sup>

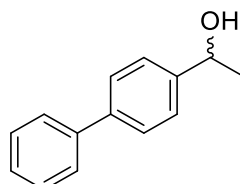


From 4-ethyl-1,1'-biphenyl using Method A, white solid (42 mg, 0.21 mmol, 19%). R<sub>f</sub> 0.28 (petrol 40-60). <sup>1</sup>H NMR (400 MHz, CDCl<sub>3</sub>) δ<sub>H</sub> 7.53-7.47 (5H, m, aromatic CH), 7.37-7.30 (4H, m, aromatic CH), 5.57 (1H, dq, *J* = 48.0, 6.3 Hz, CH), 1.58 (3H, dd, *J* = 23.8, 6.5 Hz, CH<sub>3</sub>) ppm; <sup>13</sup>C NMR (400 MHz, CDCl<sub>3</sub>) δ<sub>C</sub> 141.3 (d, *J* = 2.1), 140.7, 140.5

(d,  $J = 19.6$ ), 128.9, 127.5, 127.3, 127.2, 125.8 (d,  $J = 7.2$ ), 90.8 (d,  $J = 167.8$  Hz, CHF), 22.9 (d,  $J = 25.0$  Hz, CH<sub>3</sub>) ppm; <sup>19</sup>F NMR (300 MHz, CDCl<sub>3</sub>) δ<sub>F</sub> -166.5 ppm.

*Analytical data corresponds with the literature*<sup>15</sup>

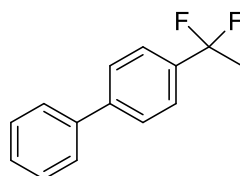
#### 1-([1,1'-Biphenyl]-4-yl)ethan-1-ol **2.25**



An isolated by-product when using Method A on **2.12** as the substrate. White solid (10 mg, 0.05 mmol, 5%). R<sub>f</sub> 0.25 (Petrol 40-60); mp 96-98 °C; ν<sub>max</sub> (neat/cm<sup>-1</sup>) 3288, 3030, 2971, 1597, 1485, 1404, 1067, 1004, 893 cm<sup>-1</sup>; <sup>1</sup>H NMR (300 MHz, CDCl<sub>3</sub>) δ<sub>H</sub> 7.54-7.48 (5H, m, aromatic CH), 7.40 – 7.35 (4H, m, aromatic CH), 4.88 (1H, q,  $J = 6.3$  Hz, CH), 1.67 (1H, s, br, OH), 1.47 (3H, d,  $J = 6.7$  Hz, CH<sub>3</sub>) ppm; <sup>13</sup>C NMR (300 MHz, CDCl<sub>3</sub>) δ<sub>C</sub> 114.8, 140.9, 140.5, 128.8, 127.3, 127.1, 125.9, 70.2, 25.2 ppm.

*See Appendix for crystal structure. Analytical data corresponds against a sample obtained from Apollo Scientific.*

#### 4-(1,1-Difluoroethyl)-1,1'-biphenyl **2.26**



In product mixture (mono:di, 1:0.11), as a pale-yellow oil (85 mg) from Method A reaction on **2.12**. R<sub>f</sub> 0.28 (petrol 40-60); <sup>1</sup>H NMR (300 MHz, CDCl<sub>3</sub>) δ<sub>H</sub> 7.68 – 7.62 (5H, m, aromatic CH), 7.52 – 7.44 (4H, m, aromatic CH), 2.01 (3H, t,  $J = 18.1$  Hz, CH<sub>3</sub>); <sup>13</sup>C NMR (400 MHz, CDCl<sub>3</sub>) δ<sub>C</sub> 143.4, 140.3, 137.5, 129.1, 128.0, 127.7, 127.5, 125.1 (t,  $J = 6.0$  Hz), 122.0, 26.0 (t,  $J = 30.2$  Hz, CH<sub>3</sub>) ppm; <sup>19</sup>F NMR (300 MHz, CDCl<sub>3</sub>) δ<sub>F</sub> -87.2 (2F, q,  $J = 18.2$  Hz) ppm.

### General Conditions for the Epoxidation Reactions

Styrene (0.40 mmol) was added to CD<sub>3</sub>CN (4 mL), Mn(salen)Cl (0.08 mmol, 20 mol%) was added and allowed to dissolve. The oxidant (0.80 mmol) was added and left to stir at RT for 16 h. The reaction mixture was taken up into an NMR tube and <sup>1</sup>H NMR was taken of the reaction mixture.

### General Conditions for Radical Scavenger Reactions

To an oven-dried Schlenk flask under an N<sub>2</sub> atmosphere, Mn(salen)Cl (0.22 mmol, 20 mol%), AgF (6.00 mmol) and substrate (1.1 mmol) were added followed by degassed anhydrous MeCN (2 mL) and the radical scavenger (15 mol%). The reaction mixture was heated to 50 °C. PhIO (6.60 mmol) was added in small portions (10 mg/2 min) over 6-9 h. MeCN (1 mL) was added for every two equivalents of oxidant. The reaction mixture was allowed to cool to RT and DCM (5 mL) was added to dilute the reaction mixture. The reaction mixture was passed through a Celite plug. The crude reaction mixture was concentrated *in vacuo* and products isolated by chromatographic techniques (e.g. prepTLC, column chromatography or flash column chromatography).



## References

1. E. N. Jacobsen, W. Zhang, A. R. Muci, J. R. Ecker and L. Deng, *J. Am. Chem. Soc.*, 1991, **113**, 7063-7064
2. W. Zhang, J. L. Loebach, S. R. Wilson and E. N. Jacobsen, *J. Am. Chem. Soc.*, 1990, **112**, 2801-2803
3. R. Irie, K. Noda, Y. Ito, N. Matsumoto and T. Katsuki, *Tetrahedron Asymmetry*, 1991, **2**, 481-494
4. R. Irie, T. Uchida and K. Matsumoto, *Chem. Lett.*, 2015, **44**, 1268-1283
5. J. Clayden, N. Greeves, S. Warren, *Organic Chemistry*, Oxford University Press, Oxford, 2nd edn, 2012, 41, 1122-1123
6. A. K. Ghosh, G. Bilcer and G. Schiltz, *Synthesis Stuttg*, 2001, **15**, 2203-2229
7. T. Linker, *Angew. Chem. Int. Ed. Engl.*, 1997, **36**, 2060-2062
8. T. Katsuki, *Adv. Synth. Catal.*, 2002, **344**, 131-147
9. S. E. Schaus, B. D. Brandes, J. F. Larrow, M. Tokunaga, K. B. Hansen, A. E. Gould, M. E. Furrow and E. N. Jacobsen, *J. A. Chem. Soc.*, 2002, **124**, 1307-1315
10. K. Masutani, T. Uchida, R. Irie and T. Katsuki, *Tetrahedron Lett.*, 2000, **41**, 5119
11. M. L. Kantam, B. Bharathi, C. R. V. Reddy and B. M. Choudary, *J. Mol. Catal. A*, 2001, **168**, 69-73
12. M. L. Kantam, V. Neeraja, B. Bharathi and C. V. Reddy, *Catal. Lett.*, 1999, **62**, 67-69
13. X. Huang, W. Liu, H. Ren, R. Neelamegam, J. M. Hooker and J. T. Groves, *J. Am. Chem. Soc.*, 2014, **136**, 6842-6845
14. W. Liu and J. T. Groves, *Acc. Chem. Res.*, 2015, **48**, 1727-1735
15. W. Liu and J. T. Groves, *Angew. Chem. Int. Ed.*, 2013, **52**, 6024-6027
16. X. Xi, J. Shao, X. Hu and Y. Wu, *RSC Advances*, 2015, **5**, 80772-80778
17. R. Cheng, PhD Thesis, Newcastle University, 2021
18. L. I. Dixon, M. A. Carroll, G. J. Ellames and T. J. Gregson, *Org. Synth.*, 2014, **91**, 60-71
19. L. I. Dixon, M. A. Carroll, T. J. Gregson, G. J. Ellames, R. W. Harrington and W. Clegg, *Org. Biomol. Chem.*, 2013, **11**, 5877-5884
20. G. S. de Almeida, PhD Thesis, Newcastle University, 2012

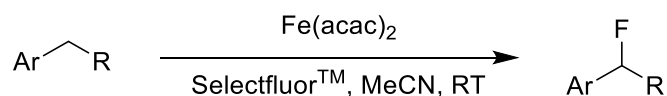
21. Z. Chen, G. Destro, F. Guibbal, C. Y. Chan, B. Cornelissen and V. Gouverneur, *Org. Lett.*, 2021, **23**, 7290-7294
22. F. Zmuda, A. Blair, M. C. Liuzza, G. Malviya, A. J. Chalmers, D. Lewis, A. Sutherland and S. L. Pimlott, *J. Med. Chem.*, 2018, **61**, 4103-4114
23. X. Huang, W. Liu, H. Ren, R. Neelamegam, J. M. Hooker and J. T. Groves, *J. Am. Chem. Soc.*, 2014, **136**, 6842-6845
24. B. M. Andrus and W. Benjamin, *Tetrahedron Letters*, 2000, **41**, 1013-1014
25. L. Song and C. Lee, *Chem. Commun.*, 2000, **24**, 2415-2416
26. E. N. Jacobsen, L. Deng, Y. Furukawa and L. E. Martínez, *Tetrahedron*, 1994, **50**, 4323-4334
27. T. Birk, PhD Thesis, University of Copenhagen, 2012
28. R. Matyáš, J. Selesovsky, V. Pelikán, M. Szala, S. Cudziło, W. A. Trzciński and M. Gozin, *Propellants Explos. Pyrotech.*, 2017, **42**, 198-203
29. T. Brik, K. S. Pedersen, S. Piligkos, C. Aa. Thuesen, H. Weihe and J. Bendix, *Inorg. Chem.*, 2011, **50**, 5312-5314
30. M. Alfasir, PhD Thesis, Newcastle University, 2022
31. Y. N. Belokon, V. I. Maleev, M. North and D. L. Usanov, *Chem. Commun.*, 2006, 4614-4616
32. P. M. Matos, W. Lewis, J. C. Moore and R. A. Stockman, *Org. Lett.*, 2018, **12**, 3674-3677
33. X. Xi, J. Shao, X. Hu and Y. Wu, *RSC Advances*, 2015, **5**, 80772-80778
34. J. Cheng, Y. Li, R. Sun, J. Liu, F. Gou, X. Zhou, H. Xiang and J. Liu, *J. Mater. Chem. C.*, 2015, **3**, 11099-11110



## Chapter 3 - Electrophilic Fluorination via Iron (II) Acetylacetonate Radical Initiators

### 3.1. Background

There are a number of electrophilic fluorination methods and reagents available. All rely on a source of  $F^+$  as the reactive fluorine. The most commonly used bench-top stable, commercially available electrophilic fluorinating reagent is Selectfluor<sup>TM</sup>. Selectfluor<sup>TM</sup> has been used in a variety of way to fluorinate compounds with nucleophilic functionality. In recent years, the focus has shifted to look at transition metal catalysed reactions with Selectfluor<sup>TM</sup>.



Scheme 3.1. Benzylic fluorination reported by Lectka *et al.*

Lectka *et al* reports a mild, one-pot synthesis of monofluorinated benzylic substrates using commercially available iron (II) acetylacetonate and Selectfluor<sup>TM</sup> (Scheme 3.1).<sup>1</sup> A variety of substrates underwent benzylic fluorination in good to excellent yields and selectivity. It was found that substrates which contained carbonyls preferentially fluorinated at the benzylic position rather than the more favourable  $\alpha$ -carbon. The method demonstrated a high functional group tolerance with the substrates being investigated including aryl ketones, esters, ketones, amides and halogenated substrates all being tolerant to the fluorination conditions. The majority of substrates tested also did not undergo dehydrohalogenation upon the work-up, something which is a common problem in benzylic halogenation reactions.

The work described within this chapter will focus on the electrophilic fluorination of small molecules for incorporation of fluorine-19, with the aim to provide an easy and efficient method to be utilised for small to medium scale production within a laboratory. A wide range of functionalisation is to be considered to allow for the development of a method which can be used for the design of a number of different fluorinated compounds.

### 3.2. Initial Reactions

Iron (II) acetylacetonate was used in an electrophilic fluorination reaction using Selectfluor™. This reaction, due to the long reaction time (24 h) and the use of electrophilic fluorine source (lower specific/molar activity) means that it is not ideal for fluorine-18 reactions although novel selectivity would still make this approach viable. However, the conditions are suitable for the introduction of fluorine-19 into a target molecule as the restrictions highlighted are not applicable although product yield and practicalities become important.

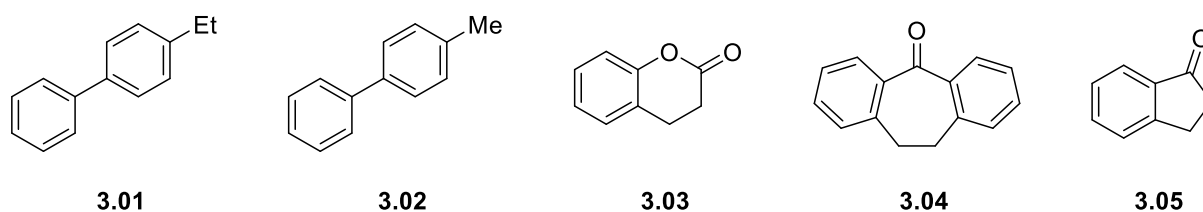


Figure 3.1. Structures of the substrates investigated during the initial reactions.

Several substrates were tested with the majority of the substrates (Fig. 3.1), including those specified in the literature, not showing any fluorination (**3.01**, **3.02**, **3.03** and **3.05**). Substrates **3.02** and **3.03** have been observed to fluorinate in the literature using  $\text{Fe}(\text{acac})_2$ .<sup>1</sup> The difference between the findings in the literature and what was observed in the experiments conducted at Newcastle University will be explained in this chapter. 5,6-Dimethoxy-1-indanone **3.06** did fluorinate at two different positions:  $\alpha$  to the carbonyl group and the benzylic position (Fig. 3.2).

**3.06** was chosen as a model substrate for the Alzheimer's drug Donepezil (Fig. 3.2). While other work within the group was to determine the AChE/BChE selectivity of the 2-, 3- and 4- fluorobenzyl Donepezil, the work described herein details the optimisation of the direct fluorination methodology.

Donepezil has two benzylic positions which could be fluorinated (highlighted in Figure 3.2). However, from reactions previously reported in Chapter 2, the benzylic position adjacent to the nitrogen has already been eliminated as a potential site for the fluorination due to the lack of stability of the fluorinated product, i.e. elimination of the fluorine by the lone pair on the nitrogen. Therefore, the remaining position on the indanone ring (highlighted in red, Fig. 3.2) was chosen as preferred position for fluorination.

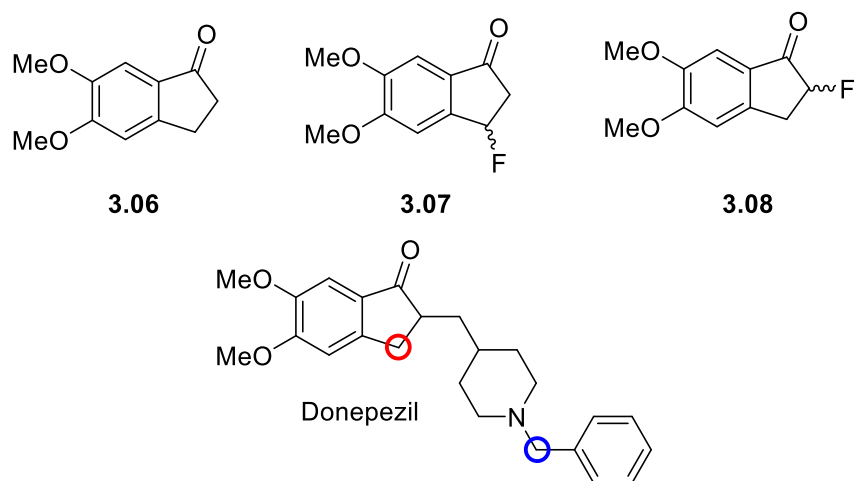
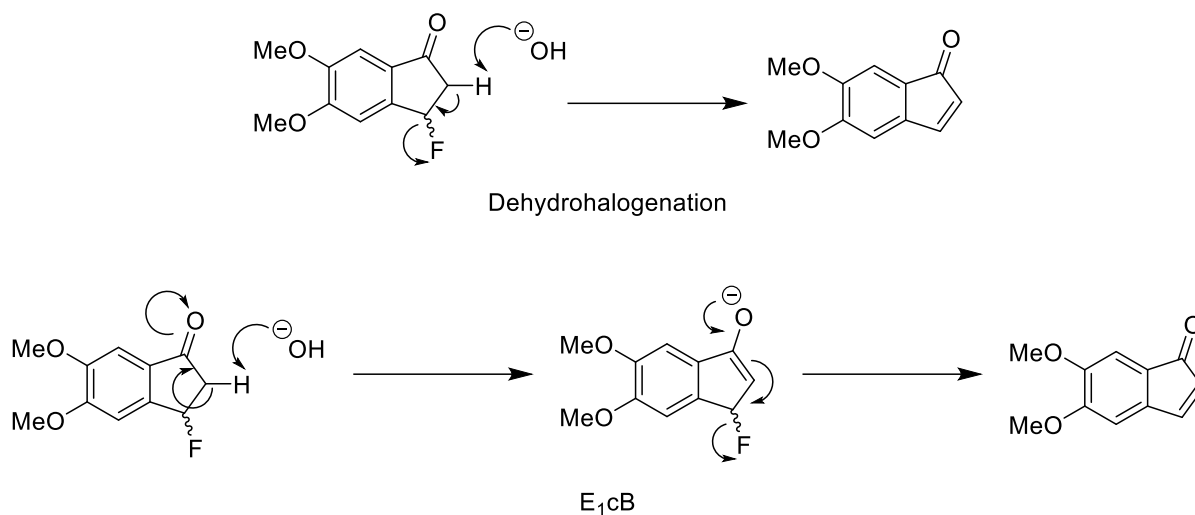


Figure 3.2. 5,6-Dimethoxy-1-indanone and mono-fluorinated products.

On a small scale (50 mg), the two possible fluorinated products were present in similar amounts at 1.54:1.00 for **3.07**:**3.08**, however, when the reaction was carried out on a larger scale (10 g) the fluorination ratio was around 0.12:1.00 for **3.07**:**3.08**, indicating an apparent reversal in the selectivity of the reaction and enabling isolation of **3.08** in 29%. It should be noted that **3.07** is unstable if left in solution which may account for the difference due to the extended processing times of the larger scale reaction. This was seen in the  $^1\text{H}$  and  $^{19}\text{F}$  NMR data of samples taken in  $\text{CDCl}_3$  over a period of more than three days, and after about a week, **3.07** cannot be detected at all by either  $^1\text{H}$  or  $^{19}\text{F}$  NMR spectroscopy. Possible mechanisms for the decomposition are dehydrohalogenation to form a double bond or it may be that **3.07** decomposes and regenerates the starting material **3.06** or via an  $\text{E}_{1\text{cB}}$  mechanism (Scheme 3.2).<sup>2</sup> It should be noted that **3.08** seems to be stable in solution, however, the potential by-products of the decomposition of **3.07** have not been detected.



Scheme 3.2. The dehydrohalogenation and E<sub>1</sub>cB reaction mechanisms.

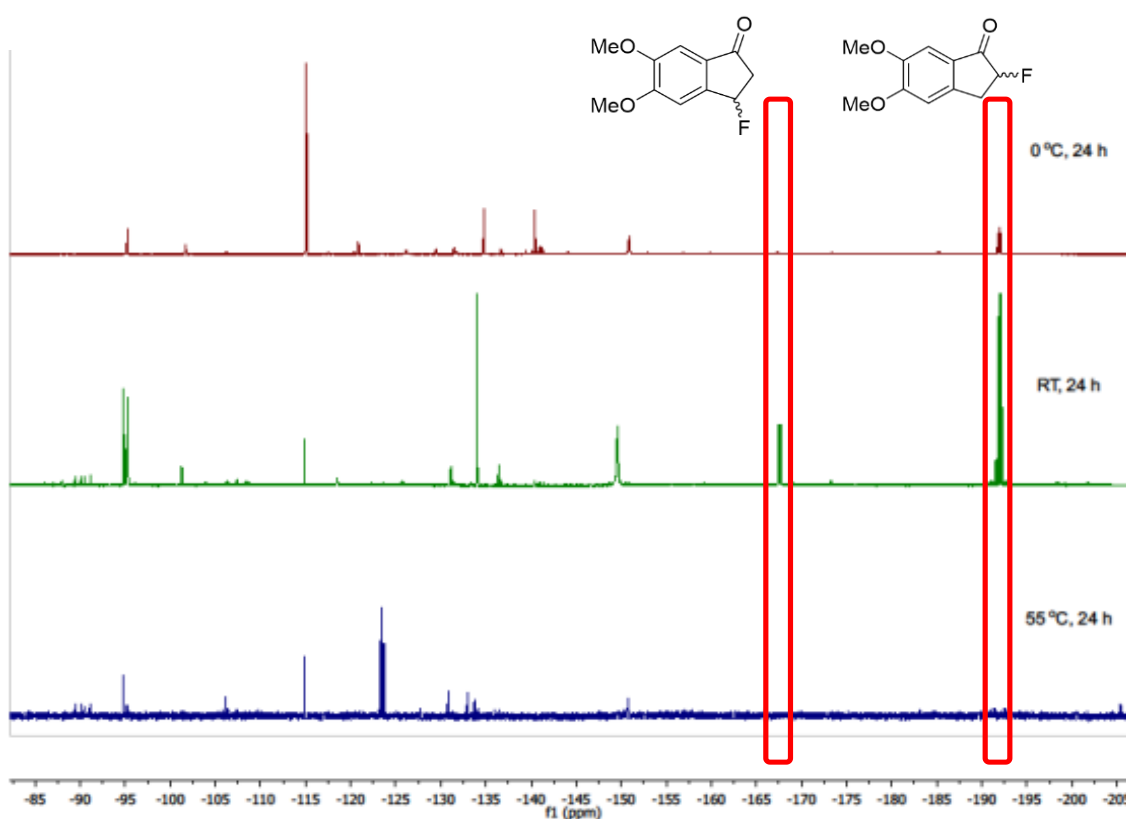


Figure 3.3. <sup>19</sup>F NMR spectrum of the crude reaction mixtures at temperatures 0 °C, RT and 55 °C.

It was initially thought that **3.07** was the kinetic product and **3.08** the thermodynamic product due to the greater stability of **3.08**. To investigate whether this was the case the reaction was conducted at different temperatures (0 °C, RT and 55 °C) and analysed at 24 h. At room temperature the ratio of **3.07**:**3.08** was 0.5:1, while at 0 °C the ratio decreased to 0.15:1.00 (**3.0**:**3.08**). At 55 °C, neither **3.07** nor **3.08** was evident by NMR (Fig. 3.3). This would suggest that **3.08** is both the kinetic and thermodynamic

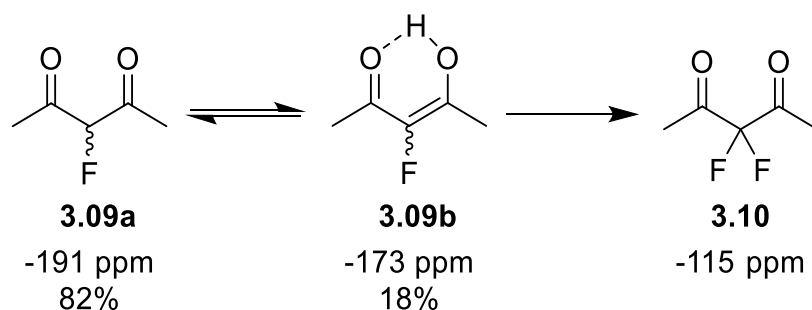
product while **3.07** is a different product which forms more slowly and is less stable than **3.08**. These results highlight a potential route to selectively synthesise **3.08** over **3.07**. However, analysis at 24 h may potentially be too long to measure the kinetic product accurately. If **3.07** decomposes via a mechanism which reforms the indanone starting material this could, in theory, cycle through to **3.08**. Further work into this area of research would require a shorter analysis time or analysis via  $^{19}\text{F}$  NMR monitored in real-time.

Investigation into  $\text{Fe}(\text{acac})_3$  showed that some fluorination of **3.06** does occur, with the major product being **3.08**. However, when **3.06** is reacted with Selectfluor<sup>TM</sup> in the absence of any  $\text{Fe}(\text{acac})_x$  the amount of the fluorinated products observed corresponds with that of seen when  $\text{Fe}(\text{acac})_3$  is used, therefore suggesting that  $\text{Fe}(\text{acac})_3$  does not contribute to the fluorination mechanism. When the commercial  $\text{Fe}(\text{acac})_2$  is present in the reaction there is an increase in yield of **3.08** (4% to 12% by  $^{19}\text{F}$  NMR using an internal standard) but a decrease in the yield of the benzylic fluorination product **3.07**, suggesting some involvement, albeit a small one.

### 3.3. Optimisation of Initial Reactions

The small increase in yield from the commercial  $\text{Fe}(\text{acac})_2$  suggested that the  $\text{Fe}(\text{acac})_2$  is involved with the reaction. A series of experiments were designed to probe the reaction in an attempt to optimise the fluorination.

#### 3.3.1. Fluorination of Acetylacetonate Ligand



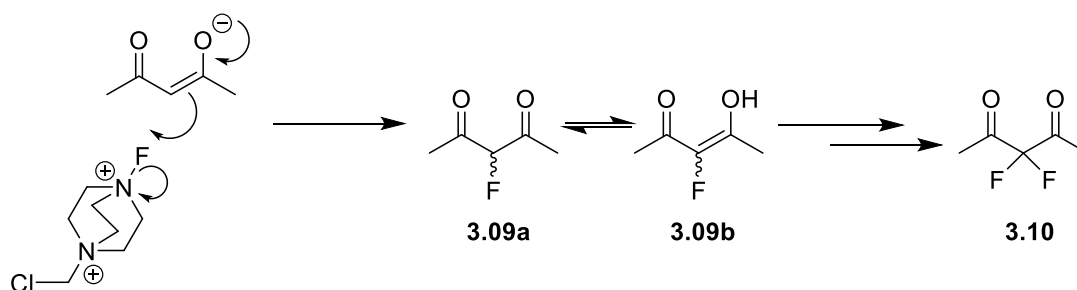
*Scheme 3.3. Fluorinated acetylacetonate by-products.*

From the initial work conducted using 5,6-dimethoxy-1-indanone **3.06** as the substrate, other fluorinated compounds are present in the  $^{19}\text{F}$  NMR spectrum. A peak around -191 ppm (doublet of heptets) and at -173 ppm (heptet) are present in the majority of the test reactions with fluorination of the acetylacetonate ligand the most likely cause,



with the literature suggesting **3.09a/3.09b** (Scheme 3.3) as the most likely fluorination position corresponding to these peaks.<sup>3</sup> Isolation of the fluorinated ligand was not successful due to the low molecular weight and volatility of the compounds. Another peak present in the <sup>19</sup>F NMR spectrum is -115 ppm, which the literature data suggests is the di-fluorinated species **3.10** again originating from the catalyst (Scheme 3.3). The difluoroacetylacetonate by-product **3.10** is one of the major compounds observed in the <sup>19</sup>F NMR spectrum when **3.6** is used as the substrate (1:2:4 ratio of **3.10:3.07:3.08**) and hence work, detailed later in this chapter, was conducted to reduce the amount of these by-products. The **3.09a** and **3.09b** occur in a ratio of 82:18 **3.09a:3.09b** in the reaction. This correlates to the equilibrium ratio of the keto/enol forms when acetylacetonate is fluorinated using fluorine gas in formic acid conducted by R. D. Chambers *et al* (mono-fluorinated product observed a keto-enol content of ~15% which reduces to ~10% if left for 2 months due to the slow keto tautomer re-formation).<sup>3</sup> The substituted acetylacetonate compounds which were investigated were all in the keto-form at the end of the process, apart from 3-fluoro-2,4-pentanedione.

Fluorination of the ligand most likely results from the deprotonation at the methylene group, due to relatively acidic protons, forming the enol that then collapses back to the keto-form and captures a fluorine from Selectfluor™ (Scheme 3.4). This can occur twice, with the second fluorination occurring faster from the increased acidity of the remaining proton, and result in the difluoro-product. The initial deprotonation may not need to occur as the enolate form of acetylacetonate ligand will be the predominant form when bonded to the iron (II) centre and is the predominant form as the free ligand (enol:keto ratio of ~81:19 for acetylacetonate)<sup>4</sup>, therefore could fluorinate directly.



Scheme 3.4. Potential mechanism of the fluorination of the acetylacetonate ligand.

The presence of the fluorinated acetylacetonate, both the mono- and di-fluorinated ligands, is significant. Although, the amount of the acetylacetonate ligand within the reaction relative to the substrate is small (<0.2-0.4 equivalents) reducing or eliminating

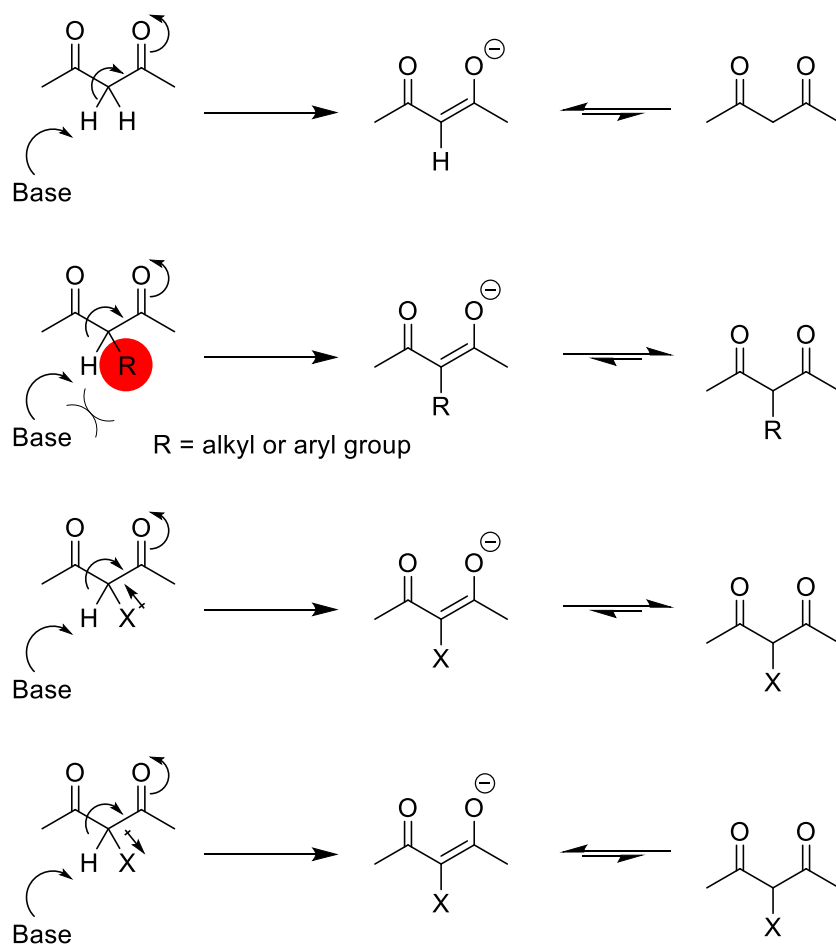
the fluorination should increase the yield of the desired fluorinated products by increasing the amount of Selectfluor™ available for fluorination. There are two possible methods to reduce the fluorination of the ligand:

1 - using blocking groups

2 - changing the pK<sub>a</sub> of the α-protons

The introduction of sterically bulky groups hinders the acidic protons which in turn reduces the likelihood of the enolate forming. The introduction of a single alkyl group would also increase the electron density at the remaining α-proton, via inductive effects, and reduce the pK<sub>a</sub> and overall limiting the amount of enol forming from tautomerisation. Changing the pK<sub>a</sub> of the α-protons would alter the diketo:ketoenol equilibrium, which could favour the diketo tautomer reducing the likelihood of the fluorination occurring via the enolate (Scheme 3.5).

This has been illustrated by work conducted by J. L. Burdett and M. T. Rogers, who investigated the keto-enol tautomerisation of β-dicarbonyls using NMR spectroscopy.<sup>4</sup> Their work showed that substitution of bulky groups in the α-position results in steric hinderance between the methyl- and the bulky groups, particularly in the enol tautomer. The increase in steric hinderance, paired with the inductive effect that alkyl groups have increasing the α-protons electron density, causes a large reduction in the percentage enol tautomer for such compounds relative to acetylacetone (3-methyl-2,4-pentanedione 30% enol tautomer reduced from 81% enol tautomer observed with acetylacetone). If the substituted groups are electron withdrawing, e.g. Cl, the lower electron density of the α-protons results in an increase of the enol tautomer (an increase from 81% to 94%). It is worth noting that hexafluoroacetylacetone exists exclusively in the enol tautomer due to the strong electron-withdrawing effects of the CF<sub>3</sub> groups.



*Scheme 3.5. The outcome of the equilibrium when blocking groups and electronic changes occur altering the keto:enol equilibrium and  $pK_a$  of the  $\alpha$ -carbonyls.*

A number of substituted acetylacetone ligands **3.11-3.17** (Fig. 3.4), with a range of steric and electronic properties affecting the  $pK_a$  and accessibility of the acidic protons, were investigated for the synthesis of iron (II) complexes.

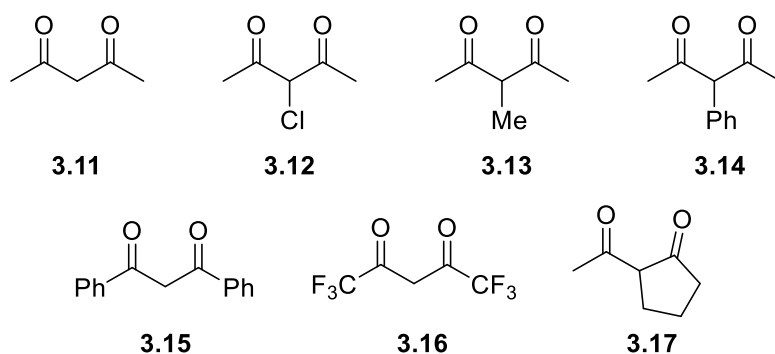


*Figure 3.4. Structures of the substituted acetylacetone derivatives used.*

The ligands **3.12** and **3.13** (3-chloro-2,4-pentanedione and 3-methyl-2,4-pentanedione) are both commercially available and inexpensive making these ligands

suitable choices for large scale production of the iron (II) complexes.<sup>f</sup> With a methyl group at the  $\alpha$ -carbonyl position, **3.13** has increased steric hinderance, therefore the acidic hydrogen is less accessible, and the inductive effect of the methyl group lowers the  $pK_a$ . 1,3-Diphenyl-1,3-propanedione **3.15** is also commercially available and inexpensive, with the two phenyl-groups having an electron-withdrawing effect lowering the  $pK_a$  of the acidic hydrogens, allowing for a broad  $pK_a$  range to be studied. 3-Phenyl-2,4-pentanedione **3.14** was synthesised from iodobenzene and acetylacetone, using CuI (8 mol%) as a catalyst, in the presence of potassium carbonate, in a yield of 32%.<sup>5</sup> The large phenyl-group allows for the investigation into a large steric hinderance at the methylene protons, with little effect on the  $pK_a$ . Hexafluoroacetylacetone **3.16** was used as a ligand for an extreme change in  $pK_a$ . The two  $CF_3$  groups cause a strong electron-withdrawing effect resulting in the increased acidity of the methylene protons, with very little steric hinderance from the  $CF_3$  groups.

---

<sup>f</sup> **3.12** £58.00/100 g (Sigma Aldrich), **3.13** £52.80/100 g (Sigma Aldrich) and **3.14** £69.60/25 g (Sigma Aldrich) (as of 19/06/2022).

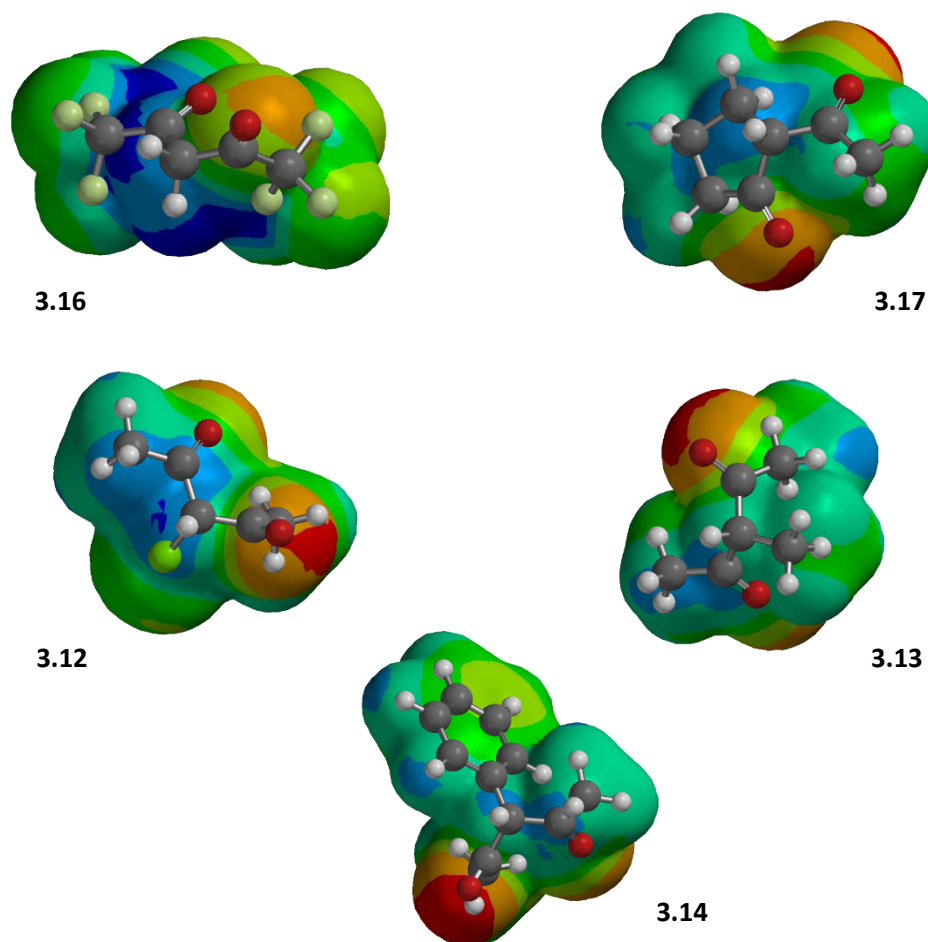


Figure 3.5 Electrostatic potential of some of the substituted acetylacetonone derivatives. Blue denotes a region of low electron density while red denotes a region of higher electron density.

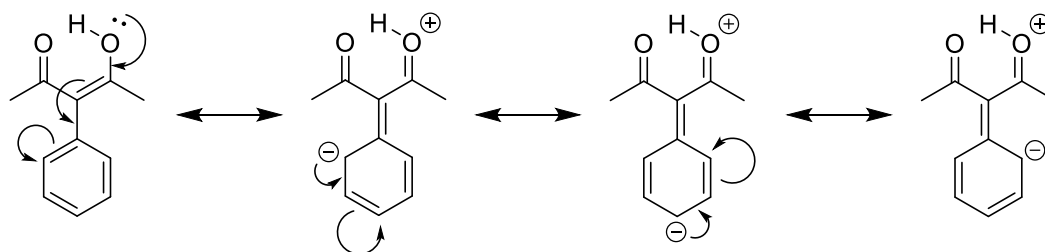
Figure 3.5 illustrates the influence the different groups on acetylacetonone have on the  $pK_a$  of the methylene proton(s). The electrostatic potential was mapped using Spartan18, with darker blue regions indicating an area of low electron density and the red regions being that of high electron density. Low electron density in the region of the methylene proton(s) results in more acidic methylene proton(s), and hence a lower  $pK_a$ . The electron-withdrawing groups Cl and  $CF_3$  result in the region around the methylene proton(s) being a much darker blue than the region around those of **3.8** (3-Me). It is interesting to note that the keto-enol structure is reflected in the electrostatic potential mapping in Figure 3.5. One side of the 1,3-dicarbonyl group is mapped in blue while the other red, this reflects the keto-enol structure.

Ligand	pK <sub>a</sub> <sup>1</sup>	%Enol <sup>2*</sup>
<b>3.11</b>	9.6	86
<b>3.12</b>	9.1	95
<b>3.13</b>	10.0	41
<b>3.14</b>	10.1	100
<b>3.15</b>	8.6	100
<b>3.16</b>	5.3	100
<b>3.17</b>	11.0	48

Table 3.1. The pK<sub>a</sub> and enol:keto ratio of the ligands **3.11-3.17**. <sup>1</sup> pK<sub>a</sub> calculated using the freely accessible web server MolGpka (<https://xundrug.cn/molgpka>)<sup>6,2</sup>. The enol percentage was calculated from <sup>1</sup>H NMR spectra integrating the CH<sup>e</sup>/CH<sub>2</sub><sup>k</sup>, CH<sub>3</sub><sup>e</sup>/CH<sub>3</sub><sup>k</sup> and the CH<sup>k</sup>/OH<sup>e</sup> of the acetylacetonone derivatives. <sup>19</sup>F and <sup>1</sup>H NMR spectroscopy were used to calculate the %enol of **3.16**. CDCl<sub>3</sub> was used as the solvent for all the NMR. \* %Enol are in accordance with those published.<sup>4,7-12</sup>

The pK<sub>a</sub> of the ligands **3.11-3.17** are shown in Table 3.1. These values were calculated using the freely accessible web server MolGpka (<https://xundrug.cn/molgpka>).<sup>6</sup> The results follow the general observations from J. L. Burdett and M. T. Rogers, with the ligands that contain alkyl and blocking groups, e.g. 3-Me (**3.13**), 3-Ph (**3.14**) and 2-acetylcyclopentan-1-one (**3.17**) having a higher pK<sub>a</sub> relative to acetylacetonone (**3.11**). Also, the ligands containing electron withdrawing groups, such as Cl (**3.12**), CF<sub>3</sub> (**3.16**) and Ph (**3.15**), have much lower pK<sub>a</sub>'s, especially that of hexafluoroacetylacetonone.

Despite the phenyl ring acting as a blocking group, **3.14** is found entirely as the keto-enol form. This can be attributed to the electronic effects the phenyl-group has on the stability of the enol. Through conjugation, resulting in a series of resonance forms, the energy of the keto-enol tautomer is reduced leading to a more stable tautomeric form which is further stabilised by the hydrogen-bond interaction from the enol alcohol and the oxygen of the ketone (Scheme 3.6). The β-diketo tautomer is of a higher energy due to the lack of conjugation and therefore the keto-enol is the preferred tautomer. It should also be noted that the phenyl ring, being flat, can rotate out of the way and therefore reduce the effectiveness of the blocking group.



Scheme 3.6. Conjugation and the resonance forms of 3.14.

The reduction in the keto-enol tautomer would, in theory, reduce the amount of the fluorination observed of the acetylacetonate ligand which should lead to higher yields of the desired fluorinated product. Steric hindrance may play a significant role in the reduction of the keto-enol tautomerisation and hence a reduction in the amount of the fluorinated acetylacetonate ligands. **3.13** and **3.17** have increased steric hindrance and this is showcased in the low %enol observed in the  $^1\text{H}$  NMR spectra. Isopropyl and *tert*-butyl groups would introduce increased steric hindrance, however these ligands were not tested. These two compounds are easily synthesised<sup>9</sup> and therefore would be ideal ligands to test in the future.

### 3.3.2. Synthesis of Fe(acetylacetonate)<sub>2</sub>

In order to test the synthesis of the substituted Fe(acac)<sub>2</sub> compounds, Fe(acac)<sub>2</sub> was synthesised from iron (II) chloride and acetylacetonate using a modified literature procedure of Buckingham *et al.*<sup>13</sup> The IR data suggests the formation of Fe(acac)<sub>2</sub> after extensive drying and comparison with commercial Fe(acac)<sub>2</sub> which has a broad OH band at 3000-3500 cm<sup>-1</sup> which was removed when dried following the same dry-down procedure used in the synthesis of Fe(acac)<sub>2</sub>. The broad OH band in the commercial Fe(acac)<sub>2</sub> is likely due to improper storage and frequent use without drying. This sensitivity to water could explain the low yields, and in some cases the lack of fluorinated products when using substrates reported by Lectka *et al.*<sup>1</sup> The water combined in the catalyst may solvate the iron centre of the Fe(acac)<sub>2</sub> preventing the necessary interactions for the fluorination to occur. The IR data suggested a successful synthesis of iron acetylacetonate compound, however, the oxidation state of the iron centre cannot be clearly deduced from FT-IR alone. Iron (II) is very susceptible to oxidation to iron (III), in the presence of air or moisture, and commercial

<sup>9</sup> 3-(1,1-dimethylethyl)-2,4-Pentanedione is synthesized using acetylacetonate and *tert*-butylalcohol with sulfuric acid in DCM at 23 °C for 16 h and 3-Isopropyl-2,4-pentanedione is synthesised using 2-iodopropane and acetylacetonate in the presence of K<sub>2</sub>CO<sub>3</sub> in acetone at 120 °C for 60 h.<sup>15</sup>

$\text{Fe}(\text{acac})_2$  is usually contaminated with  $\text{Fe}(\text{acac})_3$ .<sup>14</sup> This may also contribute to the low yields observed for the substrates tested and the low reproducibility of the fluorination reactions as reduced iron (II) content would lead to reduced fluorination yields. Therefore it was deemed essential to determine the relative amounts of the iron oxidation states and  $^1\text{H}$  NMR was used to investigate the amount of iron (III) contamination present in the synthetic and commercial compounds.

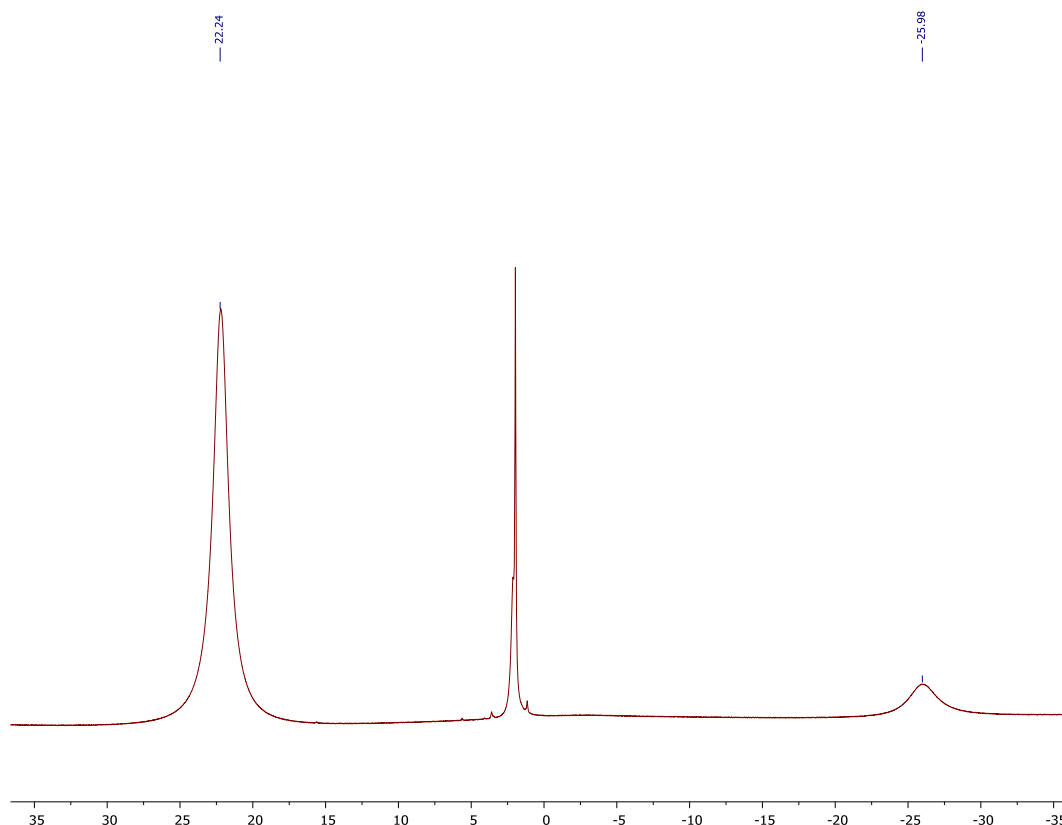


Figure 3.6.  $^1\text{H}$  NMR spectrum of  $\text{Fe}(\text{acac})_3$ .

From the  $^1\text{H}$  NMR spectrum of the synthesised  $\text{Fe}(\text{acac})_2$ , there was a significant amount of iron (III) contamination shown by an intense peak at 22 ppm and a weak peak at -26 ppm (Fig. 3.6). In the case of iron (II), the intense peak should occur at -26 ppm ( $\text{CH}_3$ ) and a weaker peak occurring around 22-25 ppm ( $\text{CH}$ ) in  $\text{CD}_3\text{CN}$ .<sup>14</sup> The peaks observed in the  $^1\text{H}$  NMR are those of the coordinative saturation of the complex  $\text{Fe}(\text{acac})_3$  and assigned the  $\text{CH}_3$  (22 ppm) and  $\text{CH}$  protons (-26 ppm).

After these findings, extensive anaerobic measures were used to reduce the likelihood of causing iron (III) contamination in the synthesis of  $\text{Fe}(\text{acac})_2$ , however after persistent presence of the contamination (identified by  $^1\text{H}$  NMR) the conclusion that the iron (III) was a result of the iron (II) chloride being used as the source of iron.



During storage, the iron (II) chloride had become either “wet” (e.g. through exposure to a humid environment) or exposed to air over a prolonged period of time with either case resulting in the iron (II) chloride being oxidised to iron (III) chloride<sup>h</sup>; therefore iron (II) chloride tetrahydrate was used as the source of iron (II) for the proceeding synthesis. The use of the tetrahydrate in the preparation of Fe(acac)<sub>2</sub> has been documented within the literature. The water content during preparation does not affect the synthesis of the iron (II) complex as water is the solvent in the synthesis of the complexes. However, the water used as the solvent must be thoroughly degassed<sup>i</sup> prior to use to reduce the likelihood of the oxidation of the iron (II) to iron (III). It was found that the water of crystallisation in the iron (II) chloride tetrahydrate does not affect the iron (II) oxidation state during the storage provided the material is stored correctly. Water content becomes a problem once the Fe(acac)<sub>2</sub> has been synthesised and is used under fluorination conditions.

Synthesis of iron (II) acetylacetonate was successful in a good yield (78%). The <sup>1</sup>H NMR spectrum showed a sharp peak at -25 ppm and a peak at 28 ppm which corresponds to the Fe(acac)<sub>2</sub> (Fig. 3.7). Other peaks seen in the NMR are solvent peaks and water contamination (10 ppm) from the deuterated DMSO. The absence of the broad peak at 22 ppm, corresponding to Fe(acac)<sub>3</sub>, is indicative of a successful synthesis. If exposed to air or moisture, after the preparation of the Fe(acac)<sub>2</sub>, there is a gradual oxidation of the Fe(acac)<sub>2</sub> to Fe(acac)<sub>3</sub> which can be seen by the increase of a peak at 25 ppm and the decrease of the peak at -25 ppm (Fig. 3.7 bottom). If left under an N<sub>2</sub> atmosphere, the Fe(acac)<sub>2</sub> remains as iron (II) even after a period of about 10 days.

Overtime, and with frequent use, the Fe(acac)<sub>2</sub> compounds do oxidise while in storage, despite stringent methods to reduce this oxidation (e.g. Schlenk techniques and high positive pressures of nitrogen when exposing flasks to air). If frequently used the Fe(acac)<sub>2</sub> was found to have a shelf-life of about one month under extensively anaerobic and anhydrous storage conditions before colour changes (usually from orange-brown to dark red) and the characteristic iron (III) peak appearing in the <sup>1</sup>H

---

<sup>h</sup> The CoA could not be used to determine whether the batch was wet before delivery from Fluorochem. Water content by Karl Fisher was not tested. The batch was 98% pure by NMR assay.

<sup>i</sup> Degassing was achieved by sparging the water with N<sub>2</sub> gas for 24 h prior to the synthesis of Fe(acac)<sub>2</sub>. Freeze-pump-thaw would have been a more thorough option but was deemed to be a higher risk [of the flask cracking] due to the expansion of the ice when frozen.

NMR spectrum was observed. Blatant exposure to air resulted in a rapid exothermic reaction and immediate colour change, which when analysed gave the same  $^1\text{H}$  NMR as the  $\text{Fe}(\text{acac})_3$ .

Extra care should be taken when handling large quantities of the iron (II) acetylacetonate material (>5 g) and the exposure to air should be kept to a minimum. The rapid oxidation can result in a lot of heat being generated which could lead to injury or ignition of flammable materials. Disposal of the iron (II) acetylacetonate requires gradual controlled exposure to air in order to oxidise the material to the air stable iron (III) acetylacetonate.

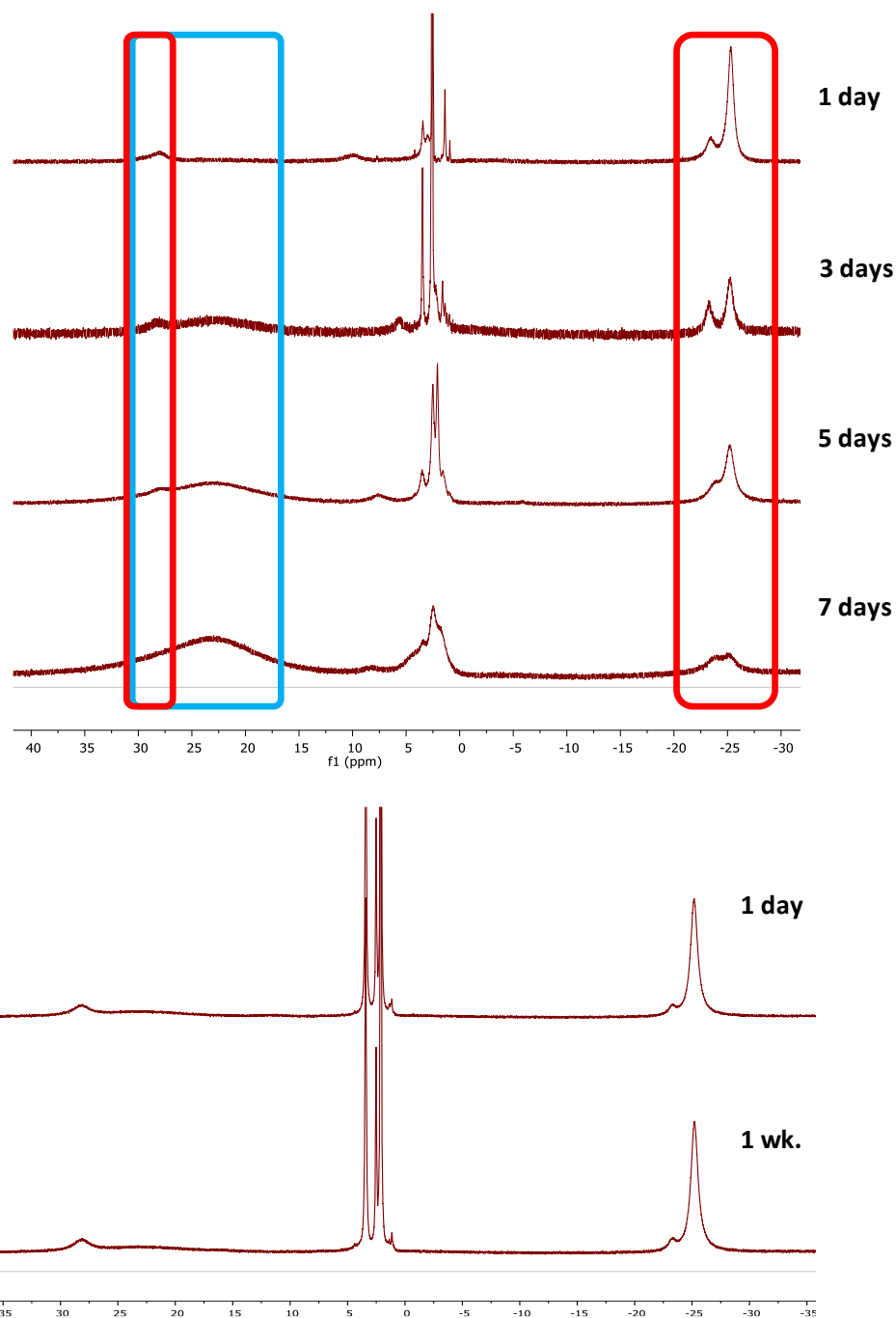


Figure 3.7. <sup>1</sup>H NMR of Fe(acac)<sub>2</sub> over a period of about a week (Top) and the stacked <sup>1</sup>H NMR of Fe(acac)<sub>2</sub> over a period of 10 days in a sealed J Young NMR tube under an N<sub>2</sub> atmosphere (Bottom). Fe(acac)<sub>2</sub> highlighted in red and Fe(acac)<sub>3</sub> highlighted in blue

Use of, freshly prepared Fe(acac)<sub>2</sub>, as the fluorination catalyst, still resulted in a large proportion of the acetylacetonate ligand undergoing reaction. Therefore, the substituted Fe(acac)<sub>2</sub> compounds bearing functionalised acac derivatives were synthesised in an attempt to reduce the amount of fluorination occurring at the methylene protons of the ligand.

### 3.3.3. Synthesis of Substituted Fe(acetylacetonate)<sub>2</sub>

A number of substituted iron (II) acetylacetonate complexes **3.18-3.24** (Fig. 3.8), with a range of steric and electronic properties affecting the pK<sub>a</sub> and accessibility of the methylene protons (explained above in 3.3.1), were synthesised using the ligands **3.11-3.17**.

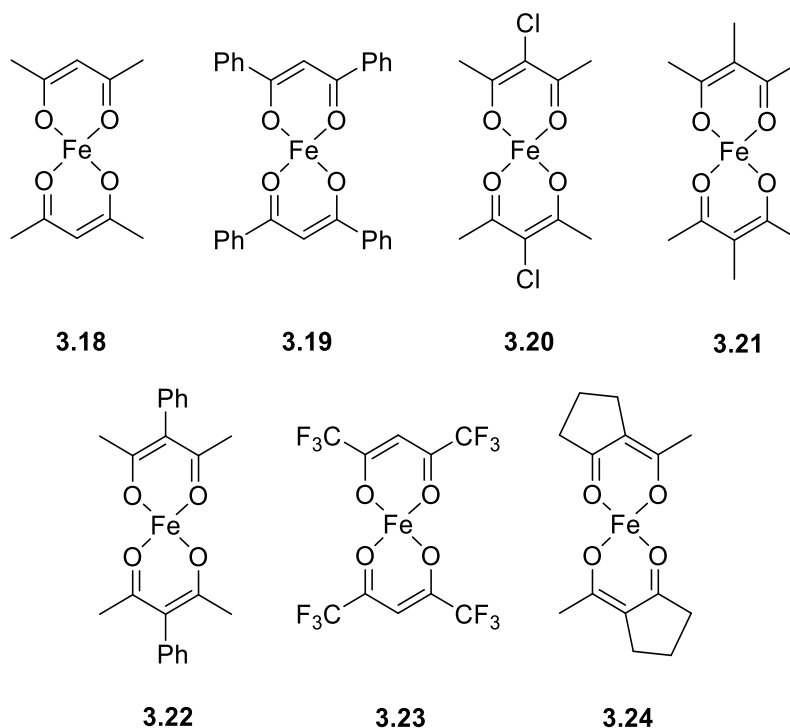


Figure 3.8. Structure of the substituted Fe(acac)<sub>2</sub> derivatives **3.11-17**.

These derivatives were synthesised following modifications to the literature procedure used previously to synthesise Fe(acac)<sub>2</sub> after optimisation. An aqueous solution of iron (II) chloride tetrahydrate was added to an aqueous solution of the substituted acetylacetonate ligand and piperidine to form the substituted Fe(acac)<sub>2</sub> complexes. After removal of the solvent via cannula, and drying the residual wet cake under vacuum, gave the desired products as powders in various yields as highlighted in Table 3.2.

Fe(acac) <sub>2</sub> Complex	Yield / %	Colour as Fe <sup>II</sup>	Colour as Fe <sup>III</sup>
<b>3.18</b>	90	Reddish-brown	Dark red
<b>3.19</b>	87	Navy-blue	Red
<b>3.20</b>	95	Dark Brown	Red
<b>3.21</b>	92	Brown	Dark red
<b>3.22</b>	89	Dark Brown	Dark red
<b>3.23</b>	58	Bluish-purple	Red
<b>3.24</b>	93	Light Brown	Dark red

Table 3.2. Yields of the Fe(acac)<sub>2</sub> complexes and the colour.

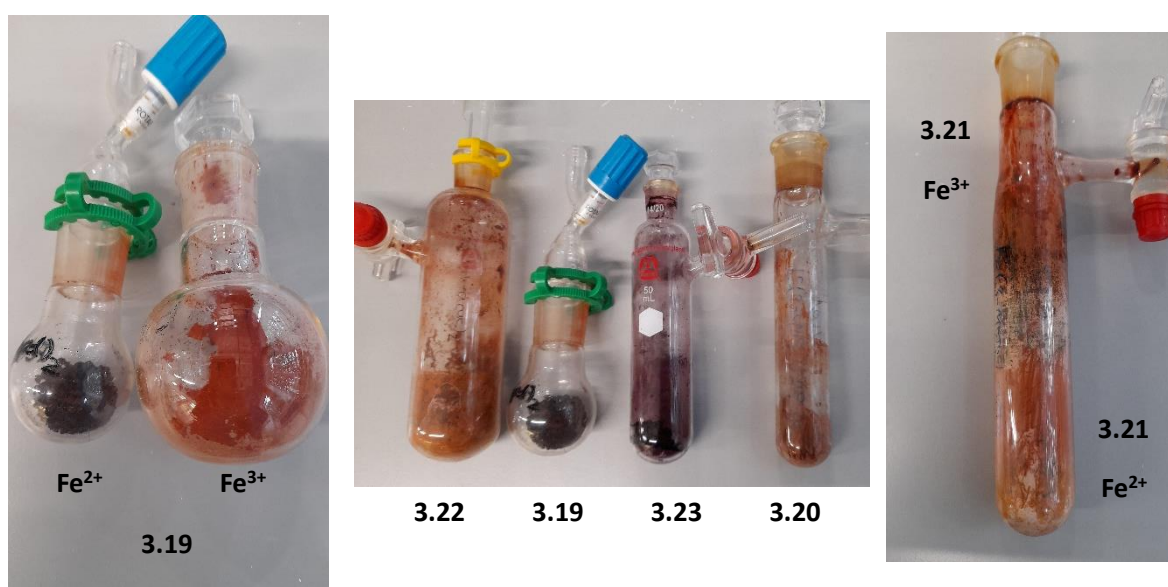


Figure 3.9. Photos of the substituted Fe(acac)<sub>2</sub> derivatives. **Left:** **3.19** as in the iron (II) and iron (III) oxidation states. **Middle** (from left to right): **3.22**, **3.19**, **3.23** and **3.20** as iron (II) complexes. **Right:** **3.21** in iron (II) oxidation state (note the iron (III) complex formation in the upper regions of the flask denoted by the darker reddish-brown colour where it has oxidised overtime and through prolonged use).

The majority of the complexes were synthesised in good yield and purity (based on <sup>1</sup>H NMR). The low yield from **3.23** is due to the high volatility associated with metal complexes using hexafluoroacetylacetonate as the ligand.<sup>16</sup> During the drying process, while heated under reduced pressure, the metal complex sublimes, and some is lost through the vacuum. This is an acceptable loss of yield; a dry material is needed in order for the fluorination to work and the complex not to oxidise during storage.

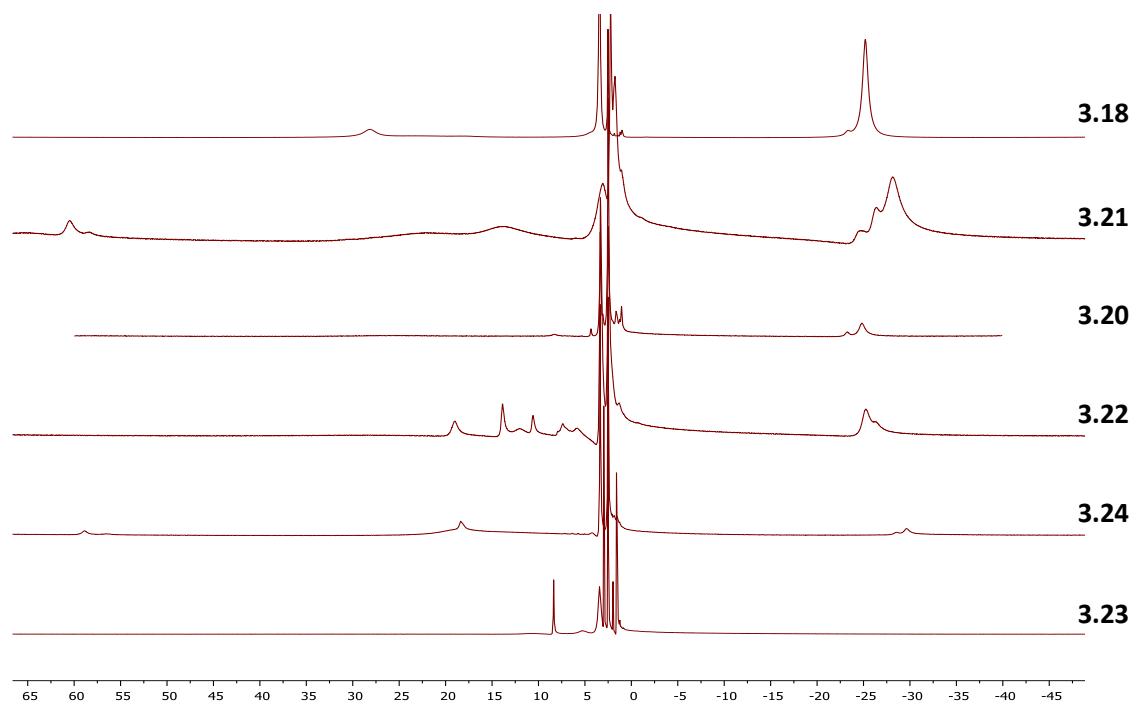


Figure 3.10.  $^1\text{H}$  NMR of the  $\text{Fe}(\text{acac})_2$  derivatives.

### 3.3.3.1. Characterisation of $\text{Fe}(\text{acac})_2$ Derivatives

Due to their sensitivity it is not surprising that there is a lack of characterisation of such  $\text{Fe}(\text{acac})_2$  complexes within the literature, even more so for the substituted derivatives. Full characterisation is difficult to obtain due to the susceptibility to oxidation, making some analytical methods difficult to conduct (e.g. mass spectrometry and UV-vis).

As of writing, there is currently no  $^{13}\text{C}$  NMR of iron (II) acetylacetonate complexes within the literature. Due to constraints resulting from the need for extensive spectrometer time (multiday experiments are required), only the NMR spectra of three complexes were taken. A  $^{13}\text{C}$  NMR was taken of derivatives **3.18**, **3.23** and **3.24** (Fig. 3.11a-c).

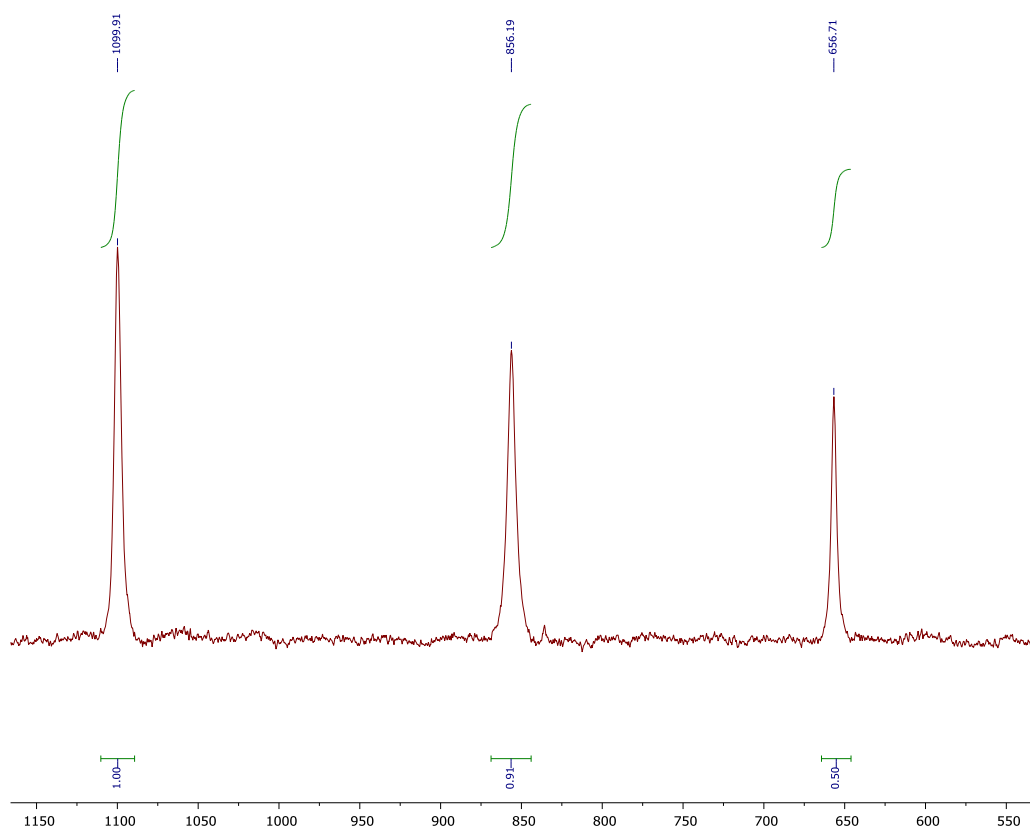


Figure 3.11a.  $^{13}\text{C}$  NMR of  $\text{Fe}(\text{acac})_2$ .

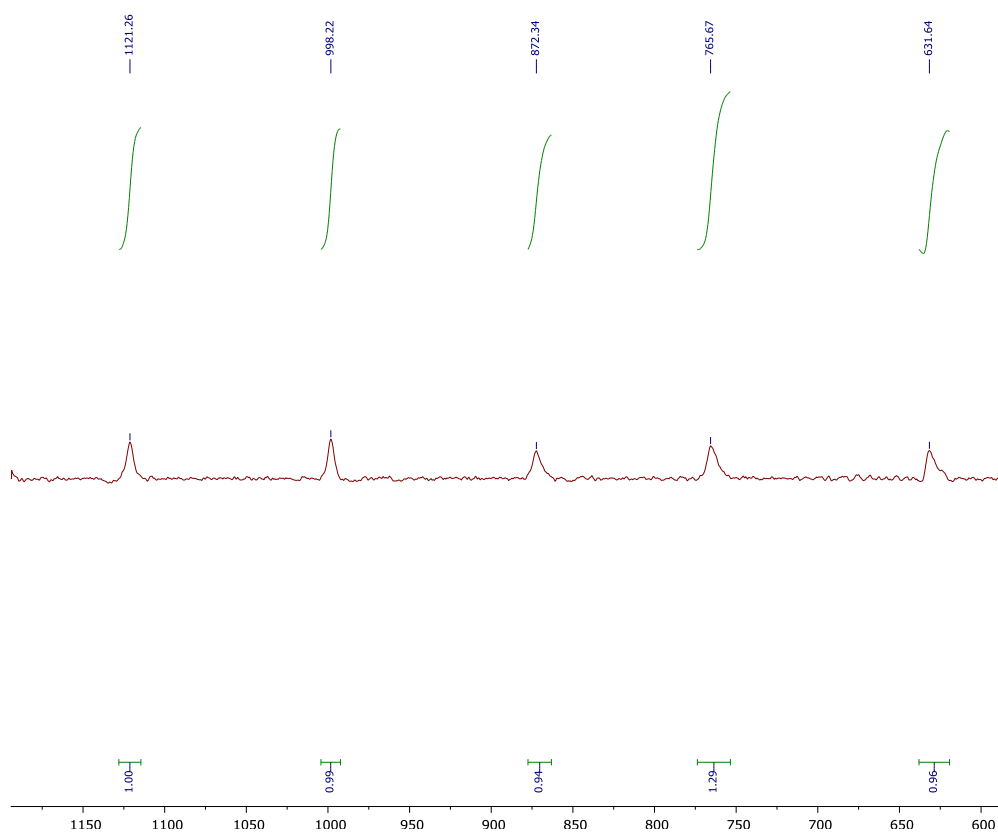


Figure 3.11b.  $^{13}\text{C}$  NMR of  $\text{Fe}(\text{acetylcyclopentanone})_2$ .

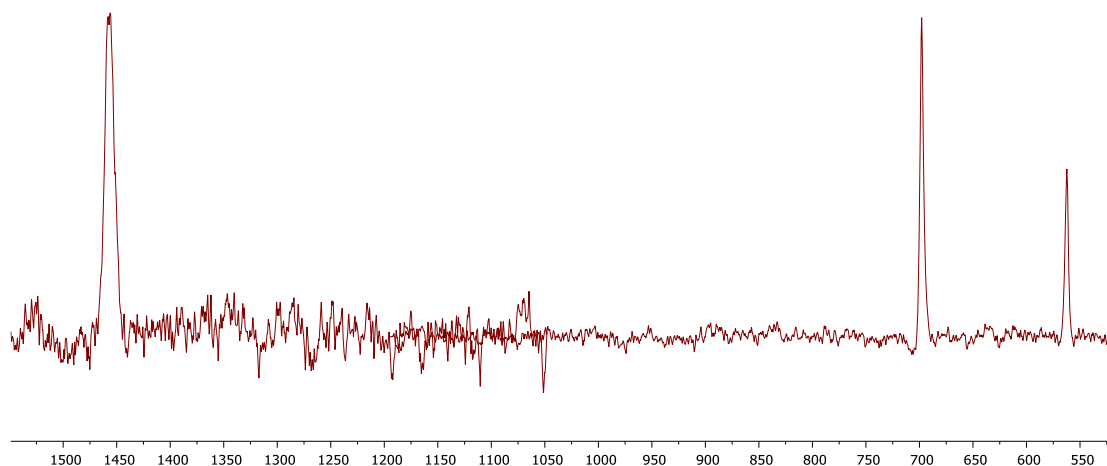


Figure 3.11c.  $^{13}\text{C}$  NMR of  $\text{Fe}(\text{hexafluoroacetylacetonate})_2$ .  $^{13}\text{C}$  NMR is a superposed spectrum of two NMRs of overlapping regions.

Obtaining crystal structures of the iron (II) complexes also proved a challenge. Attempts were made to grow crystals suitable for x-ray crystallography, however, the crystals grown under these conditions were not of a quality which would give good x-ray diffraction and allow a structure to be obtained. A number of different anaerobic set-ups were tested (Fig. 3.12).



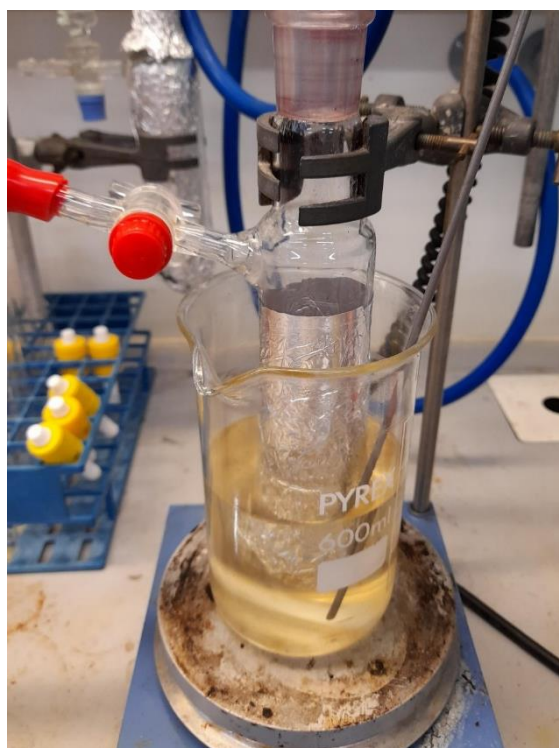


Figure 3.12. Anaerobic setups that were tested. Layering using two different solvents (Top Left), slow evaporation using controlled flow of  $N_2$  to remove solvent (Top Right) and sublimation (Bottom Middle).

The layering technique allowed for the slow diffusion of solvents into one another and did not result in any formation of crystals. More promising results came from using the slow evaporation and sublimation methods. Slow evaporation under  $N_2$  was achieved using a Schlenk flask and an oil bubbler. A positive pressure of  $N_2$  through the system

resulted in the slow evaporation of the recrystallisation solvent and this was controlled via the Schlenk flask stopcock (Fig. 3.12, Top Right). Small crystals eventually formed, however, these gave poor diffraction patterns and no crystal structure was obtained. Sublimation was possible for complex **3.16**. Under a vacuum, while being heated, the fine powder sublimes to a pale purple gas which was drawn towards the vacuum where it cooled undergoing deposition, forming very thin hair-like crystals, on the upper cooler regions of the Schlenk flask (Fig. 3.12, Bottom Middle). Tin foil was used to create a temperature gradient along the length of the Schlenk flask, gradually thinning out to a single sheet. Unfortunately these crystals, again, were not of a quality in which x-ray diffraction could give a crystal structure. This method had an increased occurrence of twinning, where a formed crystal would seed another, growing two or more crystals at the same site reducing the quality of the crystals grown.

The complex, time and equipment consuming setups meant that only a small number of attempts with suitable solvents could be tested. The crystallisation of the iron (II) complexes was only attempted with a limited number of solvents and only on a small number of the synthesised complexes (**3.18**, **3.21**, **3.23** and **3.24**). Within the literature, there are only a few examples of crystal structures from neat  $\text{Fe}(\text{acac})_2$  complexes.<sup>14,17</sup>  $\text{Fe}(\text{acac})_2$  is reported to crystallise in the form of a tetramer with two O-bridged dinuclear units, further held together by a long Fe-C bond from an adjoining central carbon atom of an acetylacetonate unit with the inner Fe atom of another (Fig. 3.13). The vast majority of the  $\text{Fe}(\text{acac})_2$  complexes with crystal structures within the literature have full coordination saturation from neutral donor ligands including weakly binding solvent molecules, e.g. THF, EtOH and pyridine, to give mononuclear bis-ligand adducts. The bis-aqua adduct has been crystallographically characterised with *trans* geometry as have other derivatives using the hexafluoroacetylacetonate ligand with the axial ligands being molecules such as THF and *o*-diaminobenzene. In the presence of chelating ligands, e.g.  $\text{Me}_2\text{NCH}_2\text{CH}_2\text{NMe}_2$  and 2-(2-pyridyl)-4,6-bis(trifluoromethyl)pyrimidine, a *cis* geometry has been observed and characterised crystallographically.<sup>14</sup>

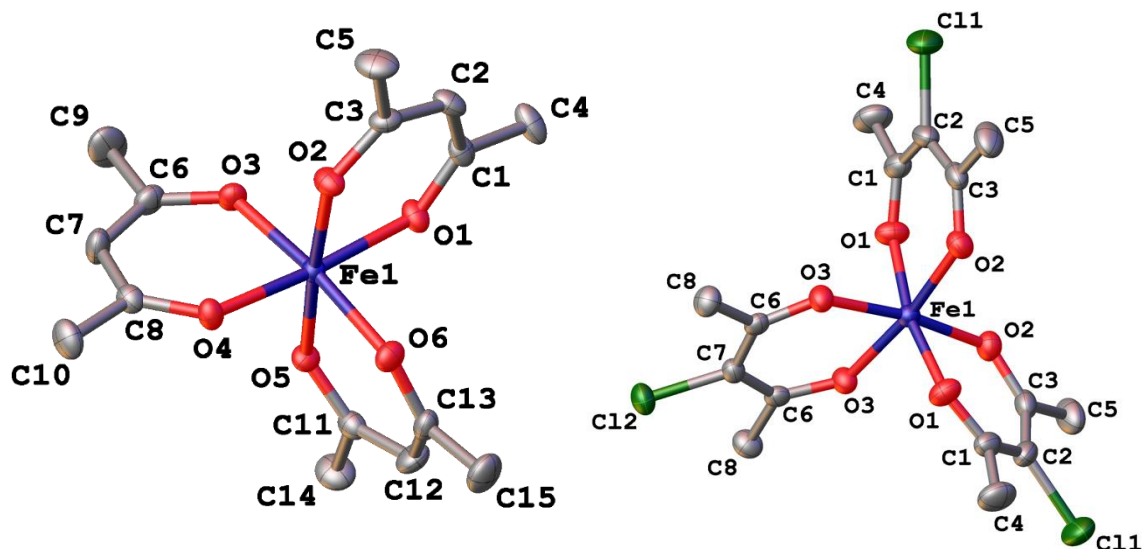


Figure 3.13. Crystal structures of iron (III) acetylacetonate (Left) and iron (III) 3-chloroacetylacetonate

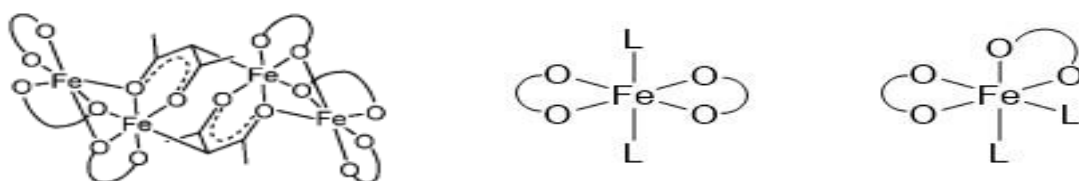
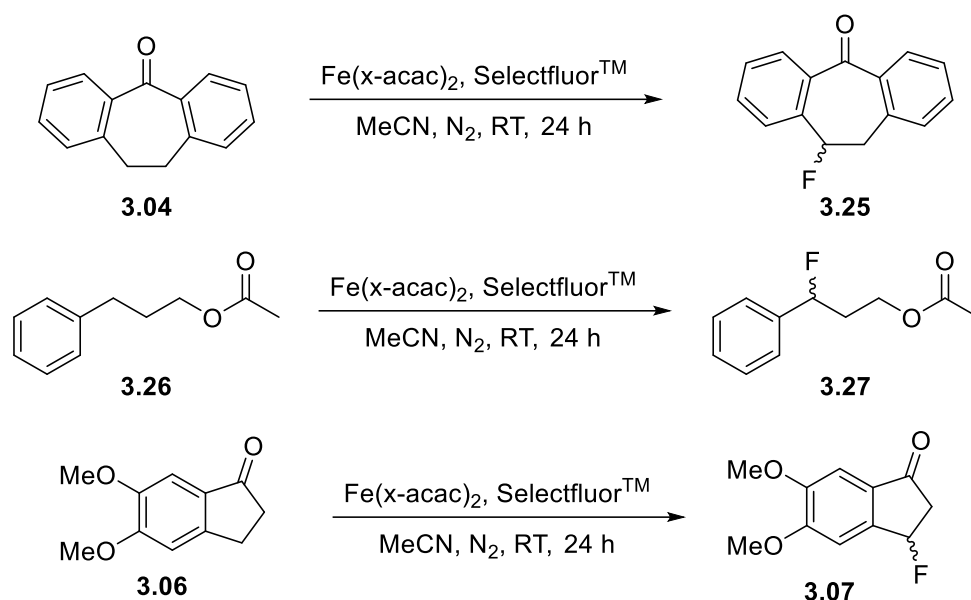


Figure 3.14. Structures of Fe(acac)<sub>2</sub> tetramer (left), and the mononuclear bis-ligand adducts: trans (middle) and cis (right). (Right).

The iron (III) complexes are far easier to experimentally set up; with these complexes being stable under aerobic conditions. The crystal structures of complexes **3.11** and **3.13** were obtained for the iron (III) oxidation state (Fig. 3.14). The iron (III) complexes have an octahedral arrangement around the iron (III) centre, while the proposed geometry of the iron (II) acetylacetonate complexes are tetrahedral.<sup>18</sup>

Further work into the characterisation would be of interest and future work would be aimed at obtaining the <sup>13</sup>C NMRs of the remaining complexes and crystal structures of the iron (II) acetylacetonates.

### 3.4. Testing of the Fe(x-acetylacetonate)<sub>2</sub> Derivatives and Process Optimisation



Scheme 3.7. Fluorination reactions using model substrates **3.04** and **3.26**.

The synthesised derivatives were used as catalysts in the fluorination reaction. Dibenzosuberone **3.04** and 3-phenylpropyl acetate **3.26** were used as model substrates for the fluorination reactions (Scheme 3.7). Previous fluorination methods were tested using 4-ethylbiphenyl and 5,6-dimethoxyindanone, however, under these conditions 4-ethylbiphenyl does not fluorinate and 5,6-dimethoxyindanone has competing sites for the fluorination which would complicate the optimisation.

Acetylacetonate Ligand	Fluorinated Ligand Conversion		
	Monofluoro keto / mol%	Monofluoro enol / mol%	Difluoro / mol%
<b>3.11</b>	0	0	4
<b>3.12</b>	74	-	-
<b>3.13</b>	33	-	-
<b>3.14</b>	87	-	-
<b>3.15</b>	30	2	68
<b>3.16</b>	0	0	0
<b>3.17</b>	54	0	-

Table 3.3. Conversion of ligands to the fluorinated ligands in mol%.

Table 3.3 illustrates the degree of fluorination of the acetylacetonate ligands. Paradoxically, the acetylacetonate **3.11** and hexafluoroacetylacetonate **3.16** ligands,

which are likely to fluorinate, have very little conversion to the fluorinated ligand (keto, enol and difluoro forms). This can be explained by the fluorinated acetylacetonate derivatives of **3.11** and **3.16** have low boiling points. The ligand conversions were calculated by  $^{19}\text{F}$  NMR spectroscopy using an internal standard from the crude reaction mixture after the work-up and solvent removal *in vacuo*. The solvent removal process would have also removed these low boiling point compounds resulting in the low conversion observed.

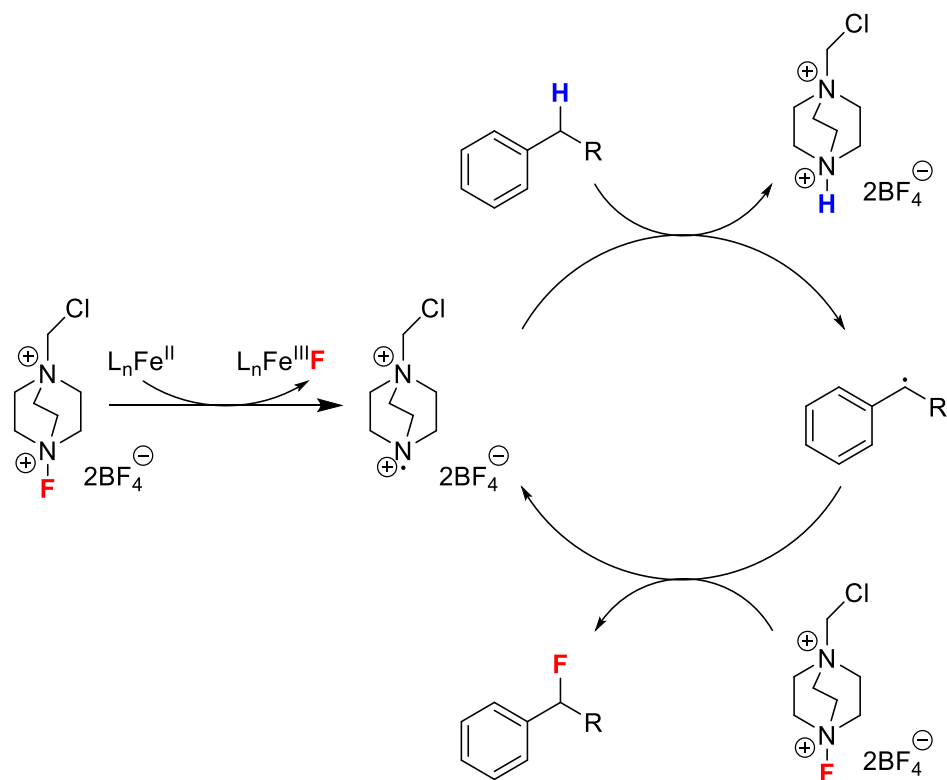
Initial reaction using some of the iron (II) acetylacetonate derivatives showed little change in the yield of the desired fluorination product (Table 3.4).

Substrate	<b>3.18</b>	<b>3.19</b>	<b>3.20</b>	<b>3.21</b>
Dibenzosuberone	3%	N/A	9%	10%
3-Phenylpropyl Acetate	0%	3%	Trace	5%

Table 3.4. Yields of the benzylic fluorination product using some of the derivatives synthesised.

From the initial reactions, it can be seen that the yields of the fluorinated products were still low despite modification to the acetylacetonate ligand and high iron (II) purity. However, there is an increase in the yields when using the modified iron (II) acetylacetonate complexes, especially **3.21** which gave increased yields in both the model substrates.

In the literature, a copper system has been extensively researched by Lectka *et al.* The literature proposes the mechanism of the copper reaction to be catalytic via the Selectfluor<sup>TM</sup> radical dication ( $\text{TEDA}^{2+}$ ) and has been suggested that this mechanism is an analogous fluorination reaction, and is therefore applicable to the iron (II) acetylacetonate reaction (Scheme 3.8).<sup>19</sup>



Scheme 3.8. Proposed mechanism by Lectka *et al* modified for iron (II).

Applying this mechanism to the iron (II) acetylacetonate, the iron (II) from the  $\text{Fe}(\text{acac})_2$  reduces the Selectfluor™ liberating fluoride generating the radical dication via a single electron transfer reaction. The radical dication abstracts the benzylic hydrogen from the substrate molecule (due to the relatively weak C-H bond at the benzylic position and the stabilisation the formed radical would receive from the aromatic ring). This forms a radical at the benzylic position which is able to abstract a fluorine from the Selectfluor™ regenerating the catalytic radical dication species.

As previously observed, the lack of fluorination when using  $\text{Fe}(\text{acac})_3$  is a direct result of the inability of the iron (III) to initiate a single electron transfer reaction. The need for the oxidation state of the iron to be iron (II) was of paramount importance, therefore any conditions which would lead to the oxidation of the iron (II) to iron (III) needed to be removed.

#### 3.4.1. Process Optimisation – Degassing Solvent

The acetonitrile used as the solvent for the fluorination reaction contains oxygen dissolved within it. A study conducted by I. Klimant *et al* has showed that the concentration of dissolved oxygen in acetonitrile can be somewhere in the region of

2.60 ± 0.15 mM.<sup>20</sup> The original method for removing this oxygen was sparging the acetonitrile with nitrogen overnight, however a more efficient process for the removal of dissolved oxygen is freeze-pump-thaw (FPT). The use of solvent degassed by FPT resulted in a significant increase in yield of the desired fluorinated products when using the model substrates **3.4** and **3.26**, and **3.21** as the radical initiator (10% to 19% and 3% to 36% for **3.04** and **3.26** respectively). The higher yields can be explained by the electrophilic fluorination reaction being sensitive to oxygen. The oxygen can oxidise the iron (II) to iron (III) but can also quench the reaction by trapping the radicals formed halting the reaction progress which results in low yields. FPT removes a greater amount of the dissolved oxygen present in the solvent allowing the radical initiation step to commence and the TEDA<sup>2+</sup> formed catalysing the reaction leading to fluorination and fewer oxidation products occurring. All reactions conducted from this point forward used the FPT degassed solvent.

#### 3.4.2. Testing of the Fe(x-acetylacetonate)<sub>2</sub> Derivatives

The substituted iron (II) acetylacetonates were tested under fluorination conditions, using the FPT degassed acetonitrile, as radical initiators. The yields of the benzylic fluorination products of the substrates **3.04** and **3.26** varied, with the highest yields observed with the iron (II) complexes **3.21** and **3.24** (Table 3.5).

Substrate	Radical Initiator						
	<b>3.18</b>	<b>3.19</b>	<b>3.20</b>	<b>3.21</b>	<b>3.22</b>	<b>3.23</b>	<b>3.24</b>
<b>3.04</b>	3%	4%	9%	19%	6%	4%	12%
<b>3.26</b>	6%	N/A	11%	36%	2%	2%	37%

Table 3.5. Yields of the benzylic fluorination products for the model substrates **3.04** and **3.26**.

**3.21** and **3.24** have a smaller degree of the keto-enol tautomer (41% and 48% respectively) as the free ligand. This reduction of the keto-enol tautomerisation and the sterically hindered methine proton, result in a smaller amount of the ligand becoming fluorinated which has led to a higher yield of fluorinated product. The yield of the benzylic fluorination correlates with the degree of keto-enol:keto-keto tautomerisation. Those complexes which have ligands with a high degree of keto-enol tautomer, e.g. **3.19**, **3.22** and **3.23** (100% keto-enol tautomer), have low yields of the benzylic fluorination product using both model substrates. **3.18** and **3.20** both fall somewhere in between. The higher yields observed with **3.20** despite the 95% keto-

enol tautomer is likely due to there being only one available proton at the methylene position reducing the amount of Selectfluor™ being consumed fluorinating the free ligand. Fe(acac)<sub>2</sub> **3.18** has two available protons to be abstracted and therefore would consume a greater amount of Selectfluor™ in the process of being fluorinated reducing the overall yield of the benzylic fluorination product.

From the testing of the radical initiators, **3.21** and **3.24** both result in higher yields of the benzylic fluorinated product. When using **3.04** and **3.26** as test substrates and two substrates used in substrate scoping studies ((3-chloropropyl)benzene and 4-phenyl-2-butanone) it is clear that **3.21** gives higher yields of the fluorinated products over a wider range of substrates. On top of these results, 3-methyl-2,4-pentanedione is a cheaper starting material and was commercially available at the time and was therefore used as the preferred substituted iron (II) acetylacetonate derivative.

Substrate	Yield of Product using 3.21 / %	Yield of Product using 3.24 / %
<b>3.04</b>	19	12
<b>3.26</b>	36	37
<b>(3-Chloropropyl)benzene</b>	30	14
<b>4-Phenyl-2-butanone</b>	37	30

Table 3.6. Yields of the fluorinated products when using **3.21** and **3.24** as the radical initiators.

### 3.4.3. Process Optimisation

Once the optimal radical initiator was identified (**3.21**), further investigation into the reaction conditions was conducted in order to improve the yield of the desired benzylic fluorinated product.

#### 3.4.3.1. Reaction Time

The length of the reaction time was investigated. Using the model substrates, reaction times of 4, 8, 24 h and 3 days were tested (Table 3.7).

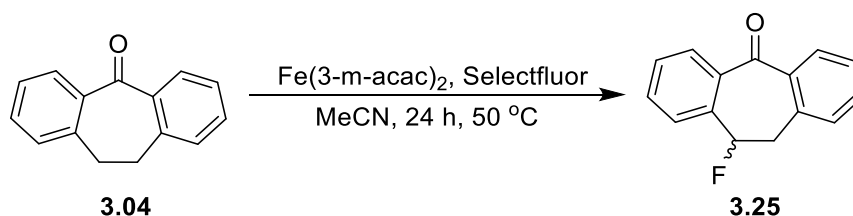


Substrate	4 h	8 h	24 h	3 Days
<b>3.04</b>	8%	14%	19%	6%
<b>3.26</b>	N/A	27% <sup>a</sup>	30% <sup>a</sup>	6%

Table 3.7. Yields of the benzylic fluorination products at times 4, 8, 24 h and 3 days. <sup>a</sup> is an average yield of three reactions.

Initial reactions suggested that the optimum reaction time would be between 8 and 24 h, dependent on the substrate. The highest yields were observed around 24 h, however there is only a small increase in the yield from 8 h to 24 h suggesting that the reaction comes to completion between these two times. A kinetics experiment was conducted, detailed later within this chapter, which gives a clearer illustration of the optimum timeframe. If left for 3 days, the yield dramatically reduces to 6%. From these reactions, it was decided that reactions were to be conducted over 24 h but further work into the kinetics of the reaction was conducted to investigate the timeframe of the reaction further.

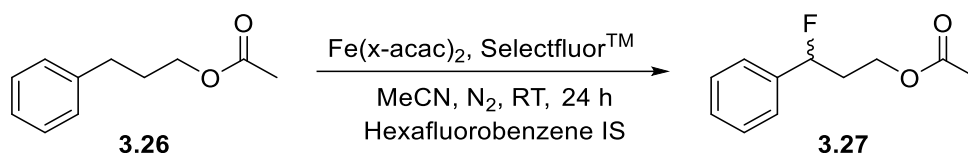
#### 3.4.3.2. Reaction Temperature



Scheme 3.9. Fluorination reaction of **3.04** at an elevated temperature of 50 °C.

Reactions were conducted at higher temperatures to investigate whether elevated temperatures increase the yield of the desired fluorinated products. **3.04** was used as the test substrate and was reacted with iron complex **3.21** and Selectfluor<sup>TM</sup> at an elevated temperature of 50 °C (Scheme 3.9). This led to the reduction in yield of **3.25** to <1% with an increased number of fluorinated by-products observed by <sup>19</sup>F NMR, albeit in similar amounts to **3.25** (<1%), which were not isolated. Due to the increased number of by-products and poor yield it is clear that conducting the reaction at elevated temperatures does not aid in increasing the yield of the desired fluorinated product. Other temperatures were not investigated, and it may be that temperatures between ambient and 50 °C would increase the yield of **3.25**. Further investigation into the reaction temperature would be a focus of future work.

### 3.4.3.3. Kinetics Experiment



Scheme 3.10. NMR kinetics experiment using **3.26** as the substrate.

A kinetics experiment was conducted, monitoring the reaction by  $^{19}\text{F}$  NMR spectroscopy using hexafluorobenzene as an internal standard, with **3.26** as the reaction substrate (Scheme 3.10). The reaction was monitored over 24 h. The first 10 h of the reaction has the fastest rate of reaction. This begins to plateau around this time and there is a slow increase in the concentration of **3.27** over the next 14 h.



Scheme 3.11. First order reaction.

Assuming first order kinetics,  $k_1$  is the rate determining step, as  $k_2$  the radical intermediate is far more reactive than the benzylic starting material **3.26** (Scheme 3.11). Therefore, it can be assumed that the  $[\text{product } \mathbf{3.27}] = -[\text{reagent } \mathbf{3.26}]$  (Equation 3.1).

$$\text{rate} = \frac{d[\mathbf{3.27}]}{dt} = -\frac{d[\mathbf{3.26}]}{dt}$$

Equation 3.1. Rate of the first order reaction using **3.26**.

The rate order is first order assuming no other reaction pathways and that the catalytic cycle proposed by Lectka *et al* is correct. With an excess of Selectfluor<sup>TM</sup> and the broad assumption of full conversion of  $\text{Fe}^{2+}$  to  $\text{Fe}^{3+}$  by single electron transfer to Selectfluor<sup>TM</sup> to form  $\text{TEDA}^{2+\bullet}$  radical dication, it can be assumed that the reaction is first order with approx. 10 mol% (i.e. 10x less) catalytic  $\text{TEDA}^{2+\bullet}$  within the reaction at the start compared to the **[3.26]**.

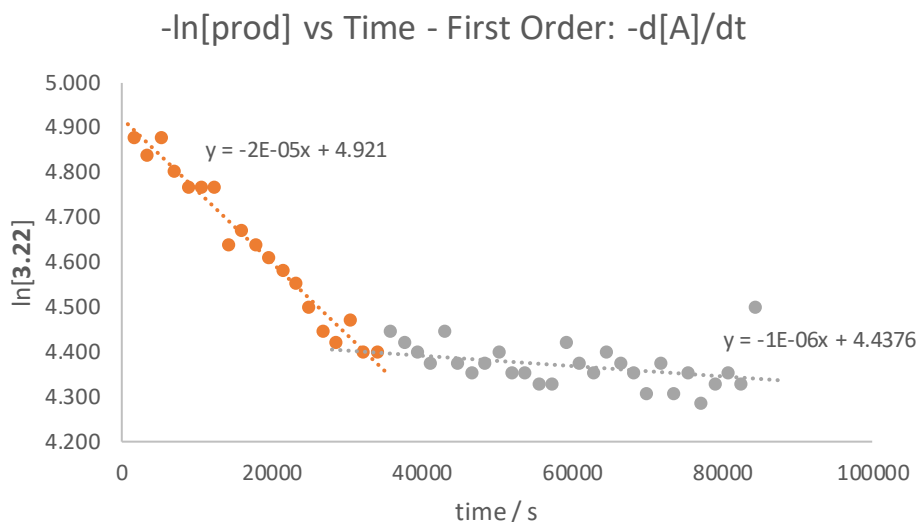


*Figure 3.15. Graph of ln(concentration) vs. time.*

As the reaction starts to slow down, [TEDA<sup>2+</sup>] reduces or the [3.26] ≈ [TEDA<sup>2+</sup>] and this would result in the decrease in the rate seen around 10 h (Figure 3.15). The rate order for the next 14 h is most likely first order but at a slower rate of reaction. This is likely to plateau later beyond the data points collected after 24 h. It should be noted that a plateau is to be expected at the very start of the reaction as the reagents start to react, however the time delay in obtaining the first NMR data points has meant this has been missed.

From the kinetics experiment, the reaction is near completion at 10 h. However, due to logistics a 24 h timeframe is more appropriate. It can be determined that a reaction time greater than 24 h would not increase the yield of the desired fluorinated products significantly. It has been observed that extended reaction times result in significantly reduced yields of the fluorinated products (Chapter 3.4.3.1). The data collected from the kinetics experiment further supports the reaction time experiments conclusion and therefore the time frame of the reaction was kept at 24 h.

#### 3.4.3.4. Alternate Fluorine Source

Selectfluor™ was used as the primary fluorinating reagent throughout the initial fluorination reactions. Selectfluor™ is relatively cheap and commercially available, easy to handle and stable over long periods of time. To conduct a thorough investigation into the fluorination reaction initiated by the iron (II) acetylacetonate

complexes, other electrophilic fluorinating reagents that were also tested, these were *N*-fluorobenzenesulfonimide (NFSI) and *N*-fluoropyridinium triflate.

Fluorination attempts using these fluorine sources did not result in the desired fluorination products using **3.04** and **3.26** as the substrates. Both NFSI and *N*-fluoropyridinium triflate are weaker fluorinating reagents than Selectfluor™.<sup>21</sup> It could be that the lower reactivity of these reagents limits the fluorinating 'power' and therefore are unable to fluorinate the substrates. The likelihood is that it is due to these fluorinating reagents being unable to form the catalytic radical dication (NFSI forming a neutral nitrogen radical and *N*-fluoropyridinium triflate forming a radical cation) which produces the benzylic radicals. This suggests that Selectfluor™ is crucial to the catalytic mechanism and is required in order to produce the benzylic radicals which react to form the benzylic fluorinated products.

A dual fluorination source was also investigated, using Selectfluor™ and *N*-fluoropyridinium triflate as the two sources of fluorine. This allowed the necessary Selectfluor™ to be present, reacting with the iron (II) forming the catalytic TEDA<sup>2+</sup> radical dication and the *N*-fluoropyridinium triflate serving as the fluorine source to generate the desired product. This should not impact the catalytic cycle, proposed by Lectka *et al*, as *N*-fluoropyridinium triflate has been shown not to react when used as a fluorine source (individually) and should therefore provide additional fluorine to be scavenged by the benzylic radicals formed by the TEDA<sup>2+</sup>. This dual fluorine source did fluorinate **3.26**, however only in a 10% yield (by <sup>19</sup>F NMR spectroscopy), this is a reduction in yield from the 37% observed for this reaction using Selectfluor™ on its own and thus conveyed no benefit.

#### 3.4.3.5. Addition of Additives

Based upon the proposed mechanism and kinetics experiments, a series of different additives were investigated in order to increase the yield of the desired fluorination product. From the kinetics experiment, it can be seen that the reaction is complete at around 10 hours, with only a small increase in the yield of the desired fluorinated product after this time. The initial rate is relatively quick compared to the rate of reaction after 10 hours, it was therefore assumed that a remedial addition of either the

Selectfluor™ or the radical initiator around this time (8 h) would reinitiate the reaction and lead to greater yield of the fluorinated product.

Selectfluor™, iron complex **3.21** and both Selectfluor™ and **3.21** were added to the reaction after 8 hours, using **3.26** as the substrate. The yield of the fluorinated **3.26** in these reactions (30-37%) were similar to that of reactions conducted without the additional charges of initiator or Selectfluor™. This suggests that the additional charges of Selectfluor™ and initiator does not reinitiate the reaction and increase the yield of the fluorinated product.

In the proposed mechanism the iron (II) undergoes a single electron transfer to the Selectfluor™ which produces the TEDA<sup>2+</sup> radical dication which is the active catalyst within the reaction, while the iron (II) is the radical initiator. A redox buffer could, in theory, result in the reduction of the iron (III), generated from the single electron transfer to iron (II) which would be able to reinitiate the reaction. Iron (III) has been shown to be reduced by ascorbic acid to iron (II).<sup>22</sup> Ascorbic acid was added to the reaction as a redox buffer (10 mol%), in the aim to reduce the iron (III) generated in the reaction. However addition of ascorbic acid to the reaction resulted in a reduction of yield of the fluorinated product of **3.26** to 2% (from ~37%).

The benzylic fluorination products are susceptible to autohydrolysis with the elimination of HF under acidic conditions. This elimination was a potential cause of the low yields observed with the fluorination reactions using iron (II) acetylacetonates as radical initiators. In order to reduce the likelihood of the elimination occurring, a base was added to the reaction in order to remove any acidic environment that is present. Li<sub>2</sub>CO<sub>3</sub> was used as the base (10 mol%), however this also resulted in a reduction in yield of the desired fluorination product of **3.26** to 5%. When both the redox buffer and base were used in combination a yield of 10% was achieved. This suggests that the pH of the reaction medium may be critical to controlling the reaction and attaining higher yields of the desired fluorinated products. Further work would be required to investigate the effect pH has on the reaction.

#### 3.4.4. Optimisation Conclusion

In conclusion, the optimised conditions were found to be:

- Iron complex **3.21**, Fe(3-methylacetylacetonate)<sub>2</sub>

- MeCN, degassed by freeze-pump-thaw
- Anhydrous MeCN (10-80 ppm analysed by Karl-Fisher) should be used to minimise oxidative products
- Selectfluor™ as the fluorine source
- Reaction time of 10-24 h
- Reaction temperature of room temperature/ambient

The addition of additives (ascorbic acid and base) and remedial additions of Selectfluor™ and **3.21** did not improve the yield of the desired fluorinated product and therefore should not be added.

### 3.5. Fluorination of Wider Range of Substrates

Based on the changes implemented through the optimisation process, a wider range of substrates were then tested. The substrates tested had a range of functionalisation (Fig. 3.16).

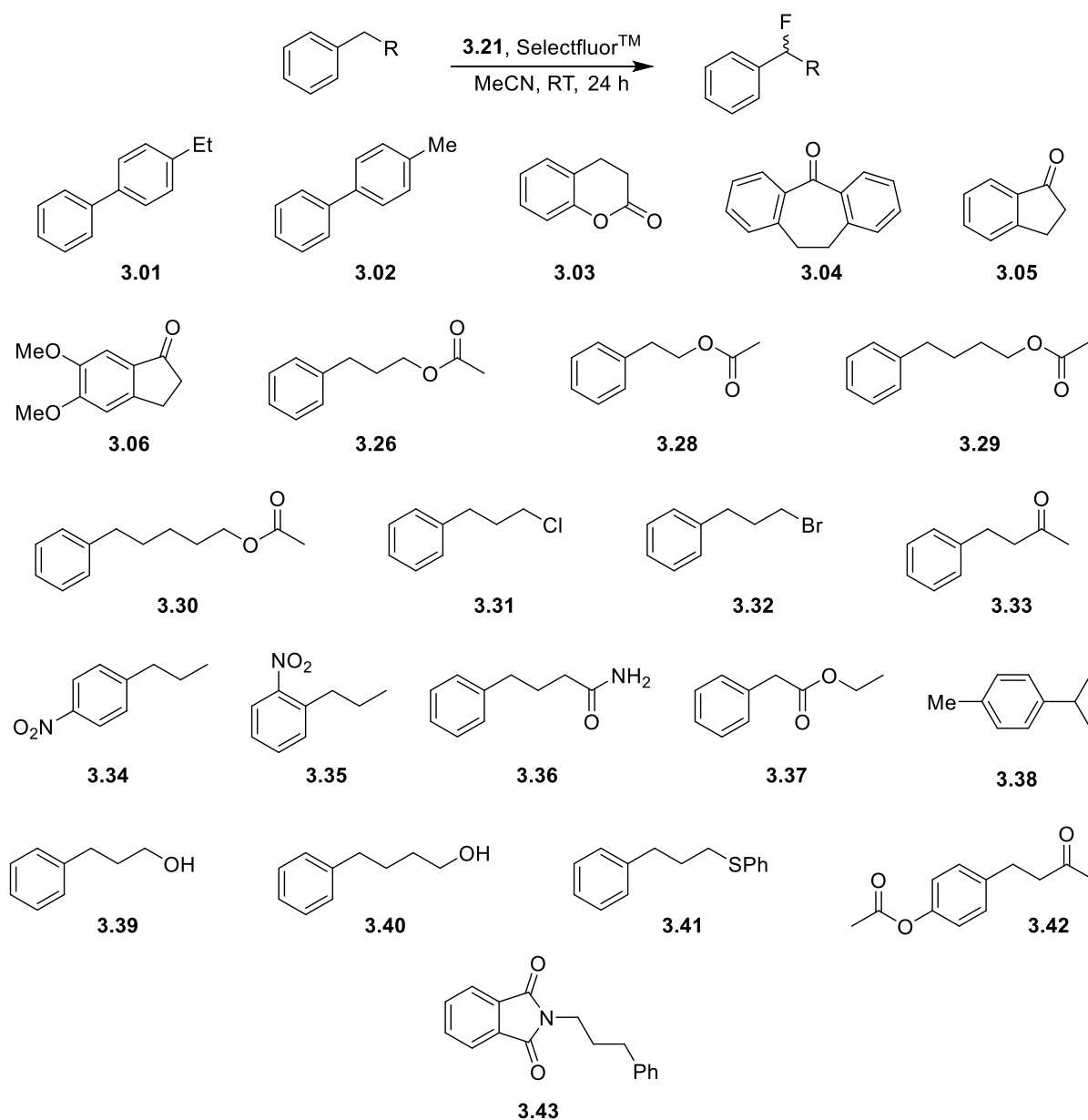


Figure 3.16. Structures of the substrates investigated.

The substrates fluorinated in a variety of yields depending on the motifs within the molecule, ranging from 0 to 40%. The yields of the fluorinated products are summarised in Table 3.8.

Entry	Substrate	Yield / %
1	3.01	<1
2	3.02	<1
3	3.03	0
4	3.04	19
5	3.05	0
6	3.06	0
7	3.26	40
8	3.28	10
9	3.29	36
10	3.30	13
11	3.31	30
12	3.32	18
13	3.33	37
14	3.34	0
15	3.35	0
16	3.36	2
17	3.37	1
18	3.38	10*
19	3.39	0
20	3.40	0
21	3.41	6
22	3.42	1
23	3.43	0

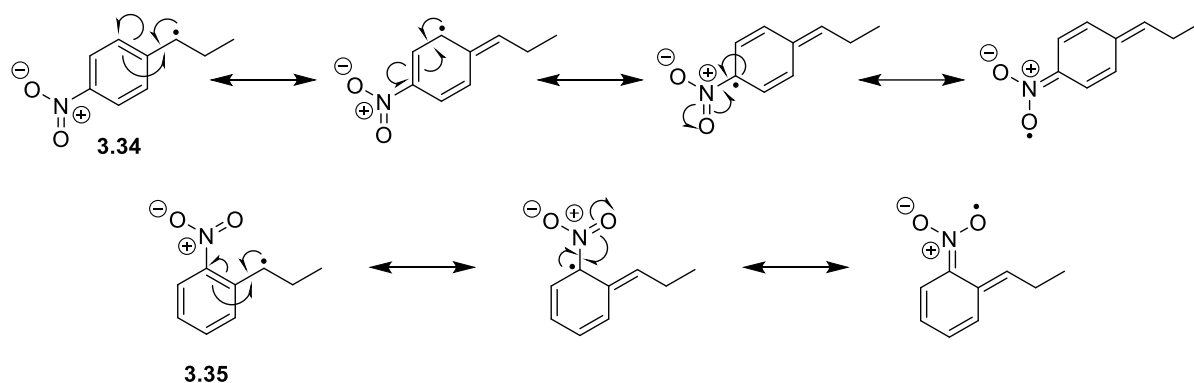
Table 3.8. Yields of the fluorinated products of the substrates investigated. \* Fluorination occurred at the methyl position.

It was found that compounds containing alcohols, i.e. **3.39** and **3.40**, do not result in the desired fluorinated products. Compounds containing alcohols are therefore not suitable for fluorination under the conditions outlined. Protected alcohol species, other than the acetyl esters, have not been tested, e.g. ethers, such as MOM.

1-Nitro-4-*n*-propyl benzene and 1-nitro-2-*n*-propyl benzene were tested as a potential substrates. These substrates did not fluorinate, and no other fluorinated by-products were seen in the reactions. The lack of fluorination is likely due to the increased



stability of the benzylic radical from the resonance effects on the nitro-group (Scheme 3.12).



Scheme 3.12. Resonance of the benzylic radicals stabilised by the *p*-nitro and *o*-nitro-group.

The increased stability of the benzylic radical results in a lack of reactivity, hence the low yields observed. Conducting the reaction using 1-nitro-3-*n*-propyl benzene as the substrate would give an in-depth investigation into the relationship between radical stability and reactivity. Future work would use 1-nitro-3-*n*-propyl benzene as a substrate.

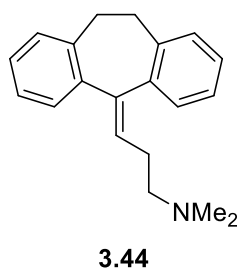


Figure 3.17. Structure of Amitriptyline<sup>TM</sup>.

**3.04** is the precursor molecule in the synthesis of Amitriptyline<sup>TM</sup> **3.44** (Fig. 3.17). Amitriptyline<sup>TM</sup> is a tricyclic antidepressant and is used to treat major depressive disorder and a number of pain syndromes such as fibromyalgia, migraines and neuropathic pain.

An attempt at the fluorination of Amitriptyline<sup>TM</sup> was conducted. Due to the amine and alkene present a number of fluorinated products were observed in the <sup>19</sup>F NMR spectrum. These were present in trace amounts, likely due to the number of potential products under electrophilic fluorination conditions. Therefore, Amitriptyline<sup>TM</sup> would not be a suitable substrate for the electrophilic fluorination method at present, however, further work into the incorporation of the fluorine at early stages within the

Amitriptyline<sup>TM</sup> synthesis may prove a suitable method for the synthesis of fluorinated derivatives.

### 3.5.1. Radical Stability

Following the experiments into the substrate scope, the energies of the radical intermediates were calculated using Spartan18 computational software (Table 3.9).

Entry	Substrate	Fluorination Yield / %	Radical Energies / Hartrees
1	<b>3.04</b>	19	-65.2
2	<b>3.28</b>	10	-537.9
3	<b>3.26</b>	40	-577.2
4	<b>3.29</b>	36	-616.5
5	<b>3.30</b>	13	-655.8
6	<b>3.31</b>	30	-809.0
7	<b>3.32</b>	18	N/A
8	<b>3.33</b>	37	-462.7
9	<b>3.34</b>	0	-553.8
10	<b>3.37</b>	1	-537.9
11	<b>3.38</b>	10	-388.7

Table 3.9. Radical energies and monofluorinated benzylic product yields. Yields are calculated by <sup>19</sup>F NMR using an internal standard of pentafluorotoluene. Radical energies were calculated with Spartan18 using ωB97X-D method with a basis set of 6-31G\*.

The energy of the radicals formed during the reaction have been shown to have little correlation with the yield of the monofluorinated products, the exceptions to this being where the radical can be stabilised by groups on the aromatic ring (e.g. nitro groups, Table 3.9, Entry 9). This suggests that the benzylic fluorination reaction does not seem to require a major stabilisation of the intermediate radical and this, in fact, is detrimental.

This is further supported with the reaction of *p*-cymene which has two possible benzylic sites of fluorination: the methyl- and *iso*-propyl- groups (Fig. 3.18).

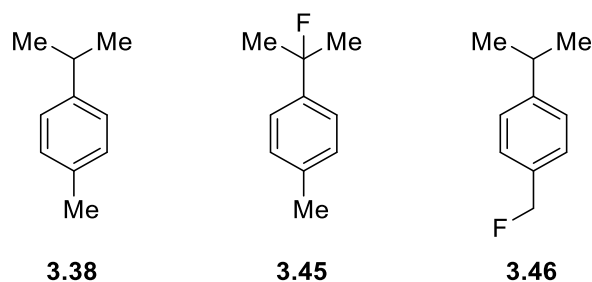


Figure 3.18. *p*-Cymene **3.38** and the two potential fluorinated products.

A radical formed on the *iso*-propyl group would be more stable than a radical formed on the methyl group due to hyperconjugation from the two CH<sub>3</sub> groups. However, when reacted under the optimised fluorination conditions the only product formed was the fluorinated methyl group of *p*-cymene **3.38**.

There is an argument as to whether the stability of the radical formed should dictate the degree of fluorination. A more stable radical would have a greater amount of time to allow for the fluorination but may also be too stable and not react with the Selectfluor™ in the reaction mixture. The less stable radical hence more reactive, could be reactive enough to fluorinate by reaction with the Selectfluor™, however this could be too reactive and result in formation of other products, e.g. hydrogen abstraction resulting in the formation of *p*-cymene, if these have a faster rate of formation than the desired fluorinated product. The stabilisation effect from electron-withdrawing groups on the aromatic ring, e.g. nitro group (Table 3.9, Entry 11) would also result in a more stable radical and the reaction would not result in the formation of the desired product. This would be true for “free radicals” within the reaction. However, the radical formed may be stabilised, and the transition state of this stabilisation allow the formation of the fluorinated products. Closer inspection of the structures shows that the higher yielding fluorination occurs when the structure of the substrate has a group that can allow donation of a lone pair at a distance of 3-4 bonds away from the benzylic position.

### 3.5.2. Chain Length Investigation

The radical stabilisation from the donation of lone pairs was investigated. By looking at the yields of the fluorinated product and the structures of the compounds a pattern was observed. A chain length which allows the formation of 5- or 6-membered rings, between the benzylic radical and a heteroatom which can donate lone pair of electrons

into the iron centre of the radical initiator fluorinate in higher yields than those substrates which can form 4- or 7-membered rings (Fig. 3.19). This is further supported by the difference in yield between (3-chloropropyl)benzene **3.31** and (3-bromopropyl)benzene **3.32**. **3.32**, with a bromine atom at the end of a three-carbon chain (allows the formation of 5-membered ring) fluorinates in a yield of 18%, while **3.31** with a chlorine atom fluorinates in a yield of 30%. Bromine's lone pairs are more diffuse and will be donated to a lesser degree than those of chlorine, which would result in a less stable complex and less fluorination.

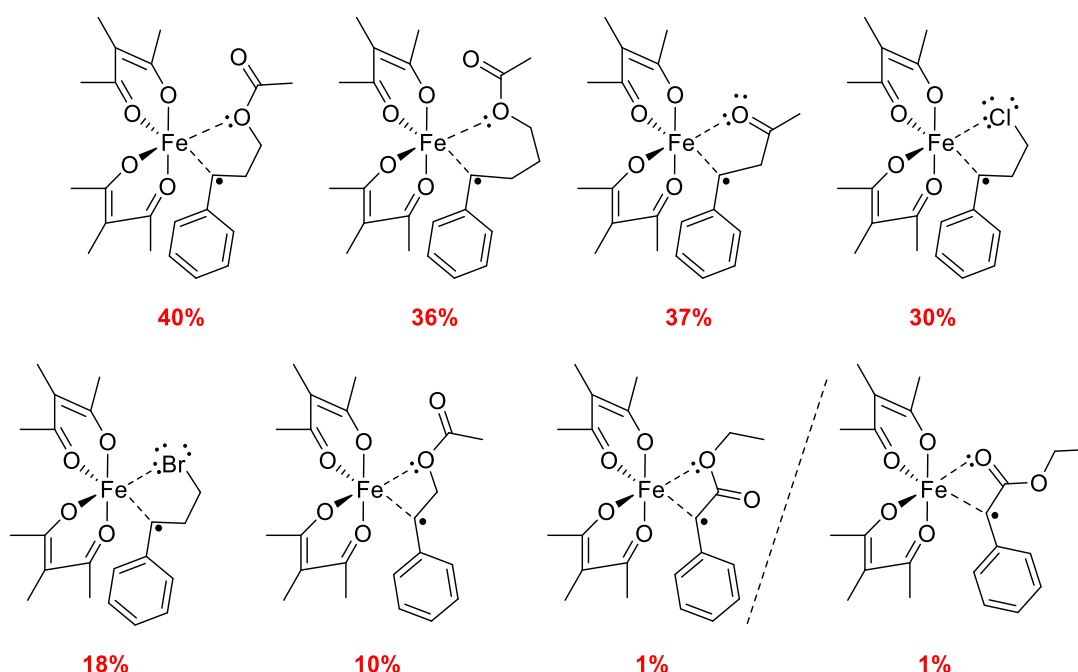


Figure 3.19. Proposed coordination to allow lone pair stabilisation of the radical intermediates.

An argument can also be made for an electronic involvement from the dicationic TEDA<sup>2+</sup> radical. The radical dication formed after the single electron transfer is electron deficient and would preferentially abstract from “electron-rich” C-H bonds, similar to those found in the substrates investigated which gave higher yields (**3.26**, **3.29**, **3.31** and **3.33**). Chen and White used an electrophilic iron catalyst and hydrogen peroxide for aliphatic C-H oxidations which could be predicted using the electronic and steric environment of the C-H bond.<sup>23</sup>

Compounds **3.36**, **3.43** and **3.41** were used to further test different functional groups. Compounds **3.36** and **3.43** did not fluorinate despite the electron density on the nitrogen being incorporated into the amide bonds. As previously mentioned, nitrogen does affect the attempted fluorinations when using Selectfluor<sup>TM</sup> hence the lack of

fluorination observed. **3.41** was investigated as sulfur forms relatively strong bonds with iron.<sup>24</sup> The desired benzylic fluorination occurred in a yield of 6%, however unexpectedly fluorination occurred adjacent to the sulfur atom resulting in the formation of the difluoro-product in a yield of 24%. At first glance this appeared to be a novel fluorination method therefore further investigation into this method was needed and the details of this investigation is reported in Chapter 4.

### 3.6. Conclusion and Future Work

In this chapter, the aim was to investigate an iron (II) acetylacetonate initiated electrophilic fluorination. Although electrophilic fluorination would not be suitable for use with fluorine-18, due to the long reaction time and low specific activity, there may be some merit in when considering a fluorine-19 methodology and designing new fluorinated compounds.

Initial conditions gave low yields of the fluorinated substrates and the fluorinated acetylacetonate ligand was identified. A series of ligands were chosen, and the iron (II) complexes synthesised. There is limited characterisation data for Fe(acac)<sub>2</sub> complexes, and the focus of future work would be to obtain full characterisation. <sup>13</sup>C NMR was collected for three of the seven complexes synthesised and crystallisation data for the iron (II) complexes still eludes this series of work.

Through optimisation of the iron (II) acetylacetonate, **3.21** was identified as the optimal radical initiator. When **3.21** was used alongside the optimal fluorination conditions (Chapter 3.4.4) the yield of the desired fluorinated product of **3.26** increased to 36%. An optimised fluorination process allowed for an in-depth analysis of the mechanism of fluorine transfer. Kinetics data illustrated the reaction proceeds by first order kinetics, with the reaction reaching completion at around 10 h where it then slows.

A variety of substrates were tested using the optimised fluorination conditions, with a range of yields (0-40%). These moderate yields highlight the potential for this method to be used for small molecule fluorination and work was being conducted on the effects of functionalisation within the target molecule on the outcome of the fluorination reaction. Groups at the end of a 3-5 carbon chain with the ability to donate electron density gave higher yields than those unable. Preliminary work was identifying a possible mechanism and the role of the iron (III) within the reaction mixture, however further investigation into the chain length and radical energies is needed.

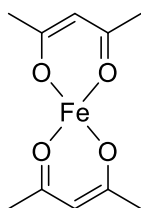
On investigation into ferrophilic sulfur complexes a potentially novel fluorination method was discovered which led to the focus of the work shifting.

### 3.7. Chapter 3 Experimental

Starting materials were purchased from commercial sources and were used without further purification.  $^1\text{H}$ ,  $^{13}\text{C}$  and  $^{19}\text{F}$  NMR spectra were recorded using Bruker Avance II 400 MHz and Bruker Avance III 300 MHz spectrometer, with a residual protic solvent used as the reference for  $^1\text{H}$  and  $^{13}\text{C}$  NMR spectroscopy and an external reference of  $\text{CFCl}_3$  for  $^{19}\text{F}$  NMR studies. Infrared spectroscopy were recorded using Varian 800 FT-IR spectrometer. Melting points were recorded on a Gallenkamp MF-370 melting point apparatus and are uncorrected. LCMS data was recorded on an LCMS Agilent Infinity II R90 UPLC + MSD XT instrument and HRMS data was recorded on a LCMS/MS (QToF) Waters Acquity UPLC + Xevo G2-XS instrument.

Acetonitrile was dried using 3 Å molecular sieves and degassed via freeze-pump-thaw and stored under nitrogen prior to use. The water content was measured (in ppm) using Karl-Fischer Coulometry. Acetonitrile used in the reactions was between 10-80 ppm water content. Solvents used in the synthesis of  $\text{Fe}(\text{acac})_2$  were dried using 3 Å molecular sieves and degassed overnight prior to use and stored under  $\text{N}_2$ . Iron (II) chloride tetrahydrate was bought in fresh and immediately transferred to a Schlenk flask.

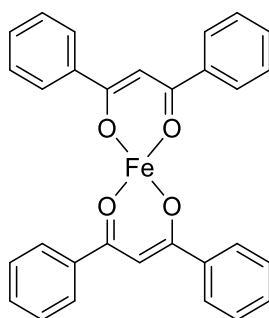
#### Bis(pentane-2,4-dionato) iron (II) 3.18



To an oven-dried Schlenk flask, acetylacetonone (1.27 mL, 12.4 mmol) and piperidine (1.22 mL, 12.4 mmol) were added to water (15 mL) under a  $\text{N}_2$  atmosphere. Iron (II) chloride tetrahydrate (1.23 g, 6.2 mmol) in water (2 mL) was added and the reaction was allowed to stir for 15-30 min. The yellow-brown precipitate that formed was washed within the flask under an  $\text{N}_2$  atmosphere with water (15 mL), followed by ethanol (15 mL) and diethyl ether (15 mL) each being removed by a cannula fitted with a filter before addition of the others. The yellow-brown precipitate was then dried under vacuum for 5-6 h then dried further by heating at 90 °C under vacuum for 6-8 h giving

a reddish-brown powder (1.57 g, 6.2 mmol, 90%).  $\nu_{\max}$  (neat/cm<sup>-1</sup>) 1566, 1519, 1353, 1273, 1015, 928, 770, 665, 548 cm<sup>-1</sup>; <sup>1</sup>H NMR (300 MHz, d<sub>6</sub>-DMSO)  $\delta_{\text{H}}$  28 (2H, br, s, CH), -25 (12H, br, s, CH<sub>3</sub>) ppm; <sup>13</sup>C NMR (400 MHz, d<sub>3</sub>-MeCN, 100,000 scans)  $\delta_{\text{C}}$  1100 (CO), 857 (CH<sub>3</sub>), 657 (CH) ppm;  $m/z$  (HRMS TOF MS AP+) 254.0242 [M]<sup>+</sup>. Found: [M]<sup>+</sup>, 254.0263.

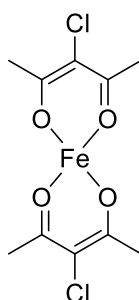
Bis(1,3-diphenylpropan-1,3-dionato) iron (II) 3.19



To an oven-dried Schlenk flask, 1,3-diphenyl-1,3-pentanedione (2.66 g, 11.9 mmol) and piperidine (1.17 mL, 11.9 mmol) were added to ethanol (15 mL) under a N<sub>2</sub> atmosphere and stirred for 10 min giving a yellow solution with some undissolved 1,3-diphenyl-1,3-pentanedione. Iron (II) chloride tetrahydrate (1.23 g, 6.19 mmol) in water (2 mL) was added and the reaction was allowed to stir for 15-30 min. The navy-blue precipitate that formed was washed within the flask under an N<sub>2</sub> atmosphere with ethanol (15 mL), followed by water (15 mL) and diethyl ether (15 mL) each being removed by a cannula fitted with a filter before addition of the others. The dark blue precipitate was then dried under vacuum for 5-6 h then dried further by heating at 50 °C under vacuum for 6 h giving a dark blueish-black powder (2.72 g, 5.41 mmol, 87%).  $\nu_{\max}$  (neat/cm<sup>-1</sup>) 2949, 2734, 1520, 1478, 1453, 1376, 1310, 1226, 1022, 940, 717, 686, 622 cm<sup>-1</sup>;  $m/z$  (TOF MS AP+) 502.0868 [M]<sup>+</sup>. Found: [M]<sup>+</sup>, 502.0863.

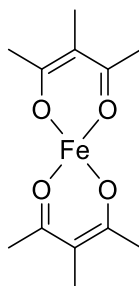


Bis(3-chloropentane-2,4-dionato) iron (II) 3.20



To an oven-dried Schlenk flask, 3-chloro-2,4-pentanedione (1.69 mL, 14.2 mmol) and piperidine (1.40 mL, 14.2 mmol) were added to water (15 mL) under a N<sub>2</sub> atmosphere. Iron (II) chloride tetrahydrate (1.41 g, 7.1 mmol) in water (2 mL) was added and the reaction was allowed to stir for 15-30 min. The brown precipitate that formed was washed within the flask under an N<sub>2</sub> atmosphere with water (15 mL), followed by ethanol (15 mL) and diethyl ether (15 mL) each being removed by a cannula fitted with a filter before addition of the others. The dark brown precipitate was then dried under vacuum for 5-6 h then dried further by heating at 75 °C under vacuum for 6-8 h giving a dark brown powder (2.18 g, 6.8 mmol, 95%).  $\nu_{\max}$  (neat/cm<sup>-1</sup>) 2949, 1560, 1456, 1416, 1359, 1330, 1289, 1042, 918, 685, 637, 436 cm<sup>-1</sup>; <sup>1</sup>H NMR (300 MHz, d<sub>6</sub>-DMSO)  $\delta_{\text{H}}$  -25 (12H, br, s, CH<sub>3</sub>) ppm; m.p 190-195 °C  $m/z$  (HRMS TOF MS AP+) 321.9463 [M]<sup>+</sup>. Found: [M]<sup>+</sup>, 321.9478.

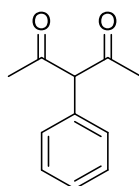
Bis(3-methylpentane-2,4-dionato) iron (II) 3.21



3-Methyl-2,4-pentanedione (3.14 mL, 27 mmol) and piperidine (2.66 mL, 27.0 mmol) were added to water (25 mL) in an oven-dried Schlenk flask under a N<sub>2</sub> atmosphere giving a pale-yellow solution. Iron (II) chloride tetrahydrate (2.68 g, 13.5 mmol) in water

(7.5 mL) was added and the reaction was allowed to stir for 45 min. The reddish-brown precipitate that formed was washed within the flask under N<sub>2</sub> atmosphere with water (20 mL), followed by ethanol (15 mL) and diethyl ether (15 mL) each being removed by a cannula fitted with a filter before the addition of the others. The light reddish-brown precipitate was dried under vacuum for 6 h then dried further by heating at 60 °C under vacuum for 6 h giving a brown powder (3.51 g, 12.4 mmol, 92%).  $\nu_{\max}$  (neat/cm<sup>-1</sup>) 2950, 1570, 1474, 1419, 1357, 1328, 1290, 979, 718, 444 cm<sup>-1</sup>; <sup>1</sup>H NMR (300 MHz, d<sub>6</sub>-DMSO)  $\delta_{\text{H}}$  60 (6H, br, s, CH<sub>3</sub>), -25 (12H, br, s, CH<sub>3</sub>) ppm;  $m/z$  (HRMS TOF MS AP+) 282.0555 [M]<sup>+</sup>. Found: [M]<sup>+</sup>, 282.0541.

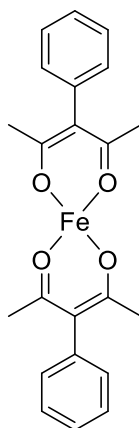
### 3-Phenyl-2,4-pentanedione<sup>25</sup> **3.14**



A mixture of acetylacetone (2.05 mL, 20.0 mmol), iodobenzene (1.09 mL, 9.8 mmol), K<sub>2</sub>CO<sub>3</sub> (4.00 g, 28.9 mmol) and CuI (165 mg, 0.8 mmol, 8 mol%) in DMSO (10 mL) was stirred at 120 °C for 4 h under an N<sub>2</sub> atmosphere. The mixture was poured into HCl (1 M, 20 mL) and extracted with diethyl ether (20 mL) and dried using Na<sub>2</sub>SO<sub>4</sub>. The solvent was removed *in vacuo* giving a pale-yellow oil. The product was isolated by flash column chromatography (0-20% ethyl acetate:petrol) as a white crystalline solid (0.54 g, 2.00 mmol, 32%). <sup>1</sup>H NMR (300 MHz, CDCl<sub>3</sub>)  $\delta_{\text{H}}$  16.68 (1H, s, CH), 7.44 – 7.42 (1H, m, aromatic H), 7.39 – 7.35 (2H, m, aromatic H), 7.19 (2H, dd,  $J = 8.1, 1.7$  Hz, aromatic CH) 1.91 (6H, s, CH<sub>3</sub>) ppm; <sup>13</sup>C NMR (300 MHz, CDCl<sub>3</sub>)  $\delta_{\text{C}}$  190.9 (CO), 136.9 (aromatic C), 131.1 (aromatic CH), 128.8 (aromatic CH), 127.5 (aromatic CH), 115.2 (CH), 24.1 (CH<sub>3</sub>) ppm.  $m/z$  (HRMS TOF MS ES+) 176.0837 [M]<sup>+</sup>. Found: [M+H]<sup>+</sup> 177.0920.

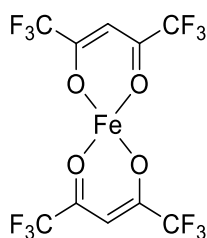
It should be noted that this product mainly resides in the enol tautomeric form.<sup>8</sup>

Bis(3-phenylpentane-2,4-dionato) iron (II) 3.22



To an oven-dried Schlenk flask, 3-phenyl-2,4-pentanedione (0.44 g, 2.5 mmol) and piperidine (0.25 mL, 2.50 mmol) were added to water (15 mL) under a N<sub>2</sub> atmosphere. Iron (II) chloride tetrahydrate (0.22 g, 1.1 mmol) in water (2 mL) was added and the reaction was allowed to stir for 15-30 min. The brown precipitate that formed was washed within the flask under an N<sub>2</sub> atmosphere with water (25 mL), followed by ethanol (25 mL) each being removed by a cannula fitted with a filter before addition of the others. The brown precipitate was then dried under vacuum for 5-6 h then dried further by heating at 75 °C under vacuum for 6-8 h giving dark brown solid (0.40 g, 0.99 mmol, 89%).  $\nu_{\text{max}}$  (neat/cm<sup>-1</sup>) 2920, 1567, 1417, 1314, 1011, 913, 767, 702, 590 cm<sup>-1</sup>; <sup>1</sup>H NMR (300 MHz, d<sub>6</sub>-DMSO)  $\delta_{\text{H}}$  19.11 (4H, s, br, aromatic CH), 13.96 (4H, s, br, aromatic CH), 10.71 (2H, s, br, aromatic CH), -25.18 (12H, s, br, CH<sub>3</sub>) ppm;  $m/z$  (HRMS TOF MS AP+) 406.0868 [M]<sup>+</sup>. Found: [M]<sup>+</sup>, 406.0879.

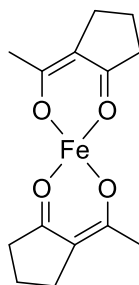
Bis(1,1,1,5,5,5-hexafluoropentane-2,4-dionato) iron (II) 3.23



To an oven-dried Schlenk flask, 1, 1, 1, 5, 5, 5-hexafluoropentane-2,4-dione (1.60 mL, 11.1 mmol) and piperidine (1.10 mL, 11.2 mmol) was added to water (20 mL) under

an N<sub>2</sub> atmosphere. Iron (II) chloride tetrahydrate (1.02 g, 5.1 mmol) in water (2 mL) was added and the reaction mixture was stirred for 15 min at RT. The brown precipitate that formed was washed within the flask under an N<sub>2</sub> atmosphere with water (15 mL), followed by ethanol (15 mL) each being removed by a cannula fitted with a filter before addition of the others. The dark purple precipitate was then dried by heating at 50 °C under vacuum for 6-8 h giving a dark purple solid (1.39 g, 2.96 mmol, 58%).  $\nu_{\max}$  (neat/cm<sup>-1</sup>) 3144, 1628, 1473, 1252, 1194, 1136, 802, 667 cm<sup>-1</sup>; <sup>1</sup>H NMR (300 MHz, d<sub>3</sub>-MeCN)  $\delta_{\text{H}}$  -9.05 (2H, s, br, CH) ppm; <sup>13</sup>C NMR (400 MHz, d<sub>3</sub>-MeCN, 100,000 scans)  $\delta_{\text{C}}$  1455 (CF<sub>3</sub>), 697 (CO), 561 (CH<sub>2</sub>) ppm; <sup>19</sup>F NMR (300 MHz, d<sub>3</sub>-MeCN)  $\delta_{\text{F}}$  -75 (s) ppm; m.p 125-130 °C; *m/z* (HRMS TOF MS AP+) 502.0868 [M]<sup>+</sup>. Found: [M]<sup>+</sup>, 502.0863.

Bis(2-acetylcyclopentane-2,4-dionato) iron (II) 3.24



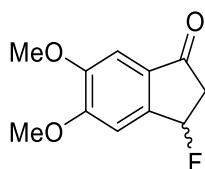
To an oven-dried Schlenk flask, 2-acetylcyclopentanone (1.18 mL, 9.90 mmol) and piperidine (0.98 mL, 9.90 mmol) were added to water (12 mL) under a N<sub>2</sub> atmosphere. Iron (II) chloride tetrahydrate (0.90 g, 4.5 mmol) in water (2 mL) was added and the reaction was allowed to stir for 15-30 min. The brown precipitate that formed was washed within the flask under an N<sub>2</sub> atmosphere with water (25 mL), followed by ethanol (25 mL) each being removed by a cannula fitted with a filter before addition of the others. The brown precipitate was then dried under vacuum for 5-6 h then dried further by heating at 70 °C under vacuum for 6-8 h giving a light brown solid (1.28 g, 4.21 mmol, 93%).  $\nu_{\max}$  (neat/cm<sup>-1</sup>) 2955, 1589, 1480, 1374, 1268, 941, 724, 638 cm<sup>-1</sup>; <sup>1</sup>H NMR (300 MHz, d<sub>6</sub>-DMSO)  $\delta_{\text{H}}$  59.20 (4H, s, br, CH<sub>2</sub>), 18.47 (8H, s, br, CH<sub>2</sub>), -29.69 (6H, s, br, CH<sub>3</sub>) ppm; <sup>13</sup>C NMR (400 MHz, d<sub>3</sub>-MeCN, 100,000 scans)  $\delta_{\text{C}}$  1121 (CO),

998 (CO), 872 (CH<sub>2</sub>), 765 (CH<sub>2</sub>), 631 (CH<sub>3</sub>) ppm; *m/z* (HRMS TOF MS AP+) 306.0555 [M]<sup>+</sup>. Found: [M]<sup>+</sup>, 306.0566.

#### General Procedure for the Electrophilic Fluorination using Fe(x-acac)<sub>2</sub>

Under an atmosphere of N<sub>2</sub>, Selectfluor<sup>TM</sup> (0.55 mmol) and Fe(x-acac)<sub>2</sub> (0.025 mmol, 10 mol%) was added to an oven-dried Schlenk flask followed by degassed anhydrous MeCN (2 mL). The substrate (0.25 mmol) was added, and the mixture was stirred at RT for 24 h. The reaction mixture was diluted with DCM (10 mL) and then washed with water (2 × 10 mL), dried using MgSO<sub>4</sub> and the solvent was removed *in vacuo* to give the crude mixture. Products were separated using various isolation techniques (prepTLC, flash column chromatography and column chromatography).

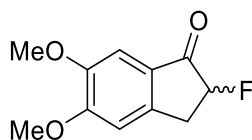
#### (±)-3-Fluoro-5,6-dimethoxy-1-indanone **3.07**



From 5,6-dimethoxy-1-indanone (10.04 g, 52.23 mmol), an off-white solid (0.30 g, 1.43 mmol, 3%). *R*<sub>f</sub> 0.69 (7:3 ethyl acetate:petrol 40-60). <sup>1</sup>H NMR (300 MHz, CDCl<sub>3</sub>) δ<sub>H</sub> 7.20 (1H, s, aromatic H), 7.13 (1H, s, aromatic H), 6.11 (1H, ddd, *J* = 2.1, 6.6, 56.8 Hz, CH), 4.02 (3H, s, OMe), 3.94 (3H, s, OMe), 3.71 (1H, m, CH), 2.83 (1H, m, CH) ppm; <sup>19</sup>F NMR (300 MHz, CDCl<sub>3</sub>) δ<sub>F</sub> -167.7 (1F, ddd, *J* = 11.9, 22.9, 56.2 Hz) ppm.

*Analytical data corresponds with the literature and with a compound isolated by M. Alfasir within M. Carroll Research Group*<sup>26</sup>

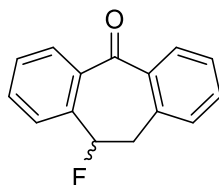
(±)-2-Fluoro-5,6-dimethoxy-1-indanone 3.08



From 5,6-dimethoxy-1-indanone (10.04 g, 52.23 mmol), an off-white solid (3.21 g, 15.27 mmol, 29%).  $R_f$  0.57 (7:3 ethyl acetate:petrol).  $^1\text{H NMR}$  (300 MHz,  $\text{CDCl}_3$ )  $\delta_{\text{H}}$  7.21 (1H, s, aromatic H), 6.86 (1H, s, aromatic H), 5.24 (1H, ddd,  $J = 3.5, 7.2, 51.4$  Hz, CH), 3.98 (3H, s, OMe), 3.92 (3H, s, OMe), 3.53 (1H, m, CH), 3.13 (1H, m, CH) ppm;  $^{19}\text{F NMR}$  (300 MHz,  $\text{CDCl}_3$ )  $\delta_{\text{F}}$  -192.1 (1F, ddd,  $J = 7.6, 22.8, 51.6$  Hz) ppm.

*Analytical data corresponds with the literature and with a compound isolated by M. Alfasir within M. Carroll Research Group<sup>26</sup>*

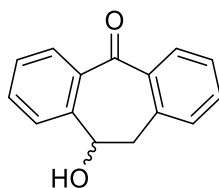
10-Fluoro-10,11-dihydro-5H-dibenzo[a,d][7]annulen-5-one 3.27



**3.27** was isolated using column chromatography as a pale-yellow solid (47 mg, 0.29 mmol, 19%).  $R_f$  0.56 (10% EtOAc:Petrol 40-60)  $^1\text{H NMR}$  (300 MHz,  $\text{CDCl}_3$ )  $\delta_{\text{H}}$  7.98 (1H, d,  $J = 7.7$  Hz, aromatic H), 7.91 (1H, d,  $J = 7.7$  Hz, aromatic H), 7.52 (2H, m, aromatic H), 7.42 (2H, m, aromatic H), 7.29 (2H, m, aromatic H), 5.77 (1H, ddd,  $J = 47.7, 9.7, 2.3$  Hz, CHF), 3.53 (2H, m,  $\text{CH}_2$ ) ppm;  $^{13}\text{C NMR}$  (300 MHz,  $\text{CDCl}_3$ )  $\delta_{\text{C}}$  194.3, 139.1, 138.7, 136.2 (d,  $J = 5$  Hz), 134.2, 132.8, 132.7, 130.7, 130.5, 130.2, 128.8, 127.5, 126.4, 126.4, 126.3, 90.6 (d,  $J = 177$  Hz), 41.1 (d,  $J = 24$  Hz) ppm;  $^{19}\text{F NMR}$  (300 MHz,  $\text{CDCl}_3$ )  $\delta_{\text{F}}$  -168.8 (1F, dd,  $J = 48.8, 26.0$  Hz, CFH) ppm.

*Analytical data corresponds with the literature<sup>27</sup>*

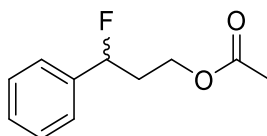
10-Hydroxy-10-11-dihydro-5H-dibenzo[a,d][7]annulen-5-one (By-product)



White solid (4.4 mg, 0.02 mmol, <1%).  $R_f$  0.53 (10% EtOAc:Petrol 40-60).  $^1\text{H NMR}$  (300 MHz,  $\text{CDCl}_3$ )  $\delta_{\text{H}}$  7.97 (1H, d, aromatic CH), 7.89 (1H, d, aromatic CH), 7.48 – 7.46 (1H, m, aromatic CH), 7.44 (t, 1H, aromatic CH), 7.41 (1H, t, aromatic CH), 7.37 – 7.34 (1H, m, aromatic CH), 7.32 (1H, d, aromatic CH), 7.20 (1H, d, aromatic CH), 5.48 (1H, dd,  $J = 1.9, 6.7$  Hz, CH), 3.81 (1H, d,  $J = 15.9$  Hz, CH), 3.48 (1H, dd,  $J = 15.9, 6.8$  Hz, CH) ppm.

*By-product was isolated from a single reaction. HRMS and LCMS was attempted but could not be obtained.*

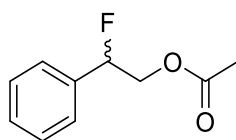
3-Fluoro-3-phenylpropyl acetate **3.27**



As crude mixture (36% based off an internal standard).  $^1\text{H NMR}$  (300 MHz,  $\text{CDCl}_3$ )  $\delta_{\text{H}}$  7.46 – 7.35 (5H, m, aromatic H), 5.60 (1H, ddd,  $J = 48.0, 8.4, 3.9$ , CHF), 4.36 – 4.18 (2H, m,  $\text{CH}_2$ ), 2.51 – 2.37 (2H, m,  $\text{CH}_2$ ), 2.10 (3H, s,  $\text{CH}_3$ ) ppm;  $^{19}\text{F NMR}$  (300 MHz,  $\text{CDCl}_3$ )  $\delta_{\text{F}}$  -177.3 (1F, ddd,  $J = 46.6, 30.1, 14.8$  Hz, CHF) ppm.

*Analytical data corresponds with the literature<sup>1</sup>*

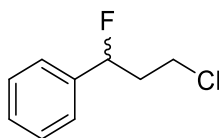
2-Fluoro-2-phenylethyl acetate 3.47



As a crude mixture (10% based off an internal standard).  $^1\text{H}$  NMR (300 MHz,  $\text{CDCl}_3$ )  $\delta_{\text{H}}$  7.48 – 7.36 (5 H, m, aromatic H), 5.60 (1H, ddd,  $J = 48.2, 7.4, 3.6$  Hz, CHF), 2.86 – 2.84 (2H, m,  $\text{CH}_2$ ), 2.23 (3H, s,  $\text{CH}_3$ ) ppm;  $^{19}\text{F}$  NMR (300 MHz,  $\text{CDCl}_3$ )  $\delta_{\text{F}}$  -183.3 (1F, ddd,  $J = 47.1, 31.6, 14.9$  Hz, CHF) ppm.

*Analytical data corresponds with the literature<sup>14</sup>*

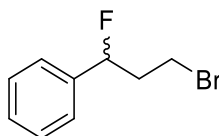
(3-Chloro-1-fluoropropyl)benzene 3.48



As crude mixture (30% based off an internal standard).  $^1\text{H}$  NMR (300 MHz,  $\text{CDCl}_3$ )  $\delta_{\text{H}}$  7.38 – 7.09 (5H, m, aromatic H), 5.61 (1H, ddd,  $J = 47.9, 14.4, 9.0$  Hz, CHF), 3.67 (1H, m,  $\text{CHH}$ ), 3.56 – 3.49 (1H, m,  $\text{CHH}$ ), 2.41 – 2.34 (1H, m,  $\text{CHH}$ ), 2.05 (1H, m,  $\text{CHH}$ ) ppm;  $^{19}\text{F}$  NMR (300 MHz,  $\text{CDCl}_3$ )  $\delta_{\text{F}}$  -179.4 (1F, ddd,  $J = 47.2, 31.1, 14.0$  Hz, CHF) ppm.

*Analytical data corresponds with the literature<sup>28</sup>*

(3-Bromo-1-fluoropropyl)benzene 3.49



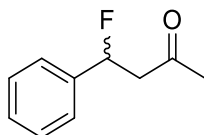
As crude mixture (18% based off an internal standard).  $^1\text{H}$  NMR (300 MHz,  $\text{CDCl}_3$ )  $\delta_{\text{H}}$  7.23 (5H, m, aromatic H), 5.61 (1H, ddd,  $J = 47.9, 14.4, 9.0$  Hz, CHF), 3.69 – 3.65 (1H, m,  $\text{CHH}$ ), 3.55 – 3.52 (1H, m,  $\text{CHH}$ ), 2.38 – 2.34 (1H, m,  $\text{CHH}$ ), 2.07 – 2.03 (1H, m,



CHH) ppm;  $^{19}\text{F}$  NMR (300 MHz,  $\text{CDCl}_3$ )  $\delta_{\text{F}}$  -179.4 (1F, ddd,  $J = 47.2, 31.1, 14.0$  Hz, CHF) ppm.

*Analytical data corresponds with the literature*<sup>1</sup>

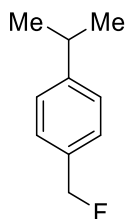
#### 4-Fluoro-4-phenylbutan-2-one 3.50



As crude mixture (37% based off an internal standard).  $^1\text{H}$  NMR (300 MHz,  $\text{CDCl}_3$ )  $\delta_{\text{H}}$  7.35 – 7.07 (5H, m, aromatic H), 5.87 (1H, ddd,  $J = 46.8, 8.8, 4.2$  Hz, CHF), 3.12 (2H, ddd,  $J = 16.6, 14.8, 8.8$  Hz,  $\text{CH}_2$ ), 2.14 (3H, s,  $\text{CH}_3$ ) ppm;  $^{19}\text{F}$  NMR (300 MHz,  $\text{CDCl}_3$ )  $\delta_{\text{F}}$  -174.1 (1F, ddd,  $J = 46.6, 32.1, 14.5$  Hz, CHF) ppm.

*Analytical data corresponds with the literature*<sup>1</sup>

#### 1-(Fluoromethyl)-4-isopropylbenzene 3.46



As crude mixture (10% based off an internal standard).  $^1\text{H}$  NMR (300 MHz,  $\text{CDCl}_3$ )  $\delta_{\text{H}}$  7.23 (2H, d,  $J = 8.2$  Hz, aromatic H), 7.17 (2H, d,  $J = 8.2$  Hz, aromatic H), 5.26 (2H, d,  $J = 51.5$  Hz,  $\text{CH}_2$ ), 2.79 (1H, septet,  $J = 5.9$  Hz, CH), 1.15 (6H, d,  $J = 7.5$  Hz,  $\text{CH}_3$ ) ppm;  $^{19}\text{F}$  NMR (300 MHz,  $\text{CDCl}_3$ )  $\delta_{\text{F}}$  -203.84 (1F, t,  $J = 46.1$  Hz,  $\text{CH}_2\text{F}$ ) ppm.

*Analytical data corresponds with the literature*<sup>1,14</sup>

## References

1. S. Bloom, C. R. Pitts, R. Woltomist, A. Griswold, M. G. Holl and T. Leckta, *Org. Lett.*, 2013, **15**, 1722-1724
2. S. Zheng, H. Tan, X. Zhang, C. Yu and Z. Shen, *Tetrahedron Lett.*, 2014, **55**, 975-978
3. R. D. Chambers, M. P. Greenhall and J. Hutchinson, *Tetrahedron*, 1996, **52**, 1-8
4. J. L. Burdett and M. T. Rogers, *J. Am. Chem. Soc.*, 1964, **86**, 2105-2109
5. K. Okuro, M. Furuune, M. Miura and M. Nomura, *J. Org. Chem*, 1993, **58**, 7606-7607
6. X. Pan, H. Wang, C. Li, J. Z. H. Zhang and C. Ji, *J. Chem. Inf. Model.*, 2021, **61**, 3159-3165
7. T. Mikysek, H. Kvapilová, H. Doušová, F. Josefík, P. Šimonek, Z. Růžičková and J. Ludvík, *Inorganica Chim. Acta*, 2017, **455**, 465-472
8. A. O. Terent'ev, V. A. Vil', I. A. Yaremenko, O. V. Bityukov, D. O. Levitsky, V. V. Chernyshev, G. I. Nikishin and F. Fleury, *New J. Chem.*, 2014, **38**, 1493
9. I. Ullah, M. Sher, R. A. Khera, M. Nawaz, M. Shkoor, I. Iqbal, M. Imran, A. Villinger, C. Fischer and P. Langer, *Tetrahedron*, 2010, **66**, 3824-3835
10. M. E. Lorriss, R. A. Abramovitch, J. Marquet and M. Moreno-Mañas, *Tetrahedron*, 1992, **48**, 6909-6916
11. M. Moriyasu, A. Kato and Y. Hashimoto, *J. Chem. Soc., Perkin Trans 2*, 1986, 515-520
12. J. B. Paine, J. R. Brough, K. K. Buller and E. E. Erikson, *J. Org. Chem.* 1987, **52**, 3986-3993
13. D. A. Buckingham, R. C. Gorges and J. T. Henry, *Aust. J. Chem.*, 1967, **20**, 281-296
14. Z. Xue, J-C. Daran, Y. Champouret and R. Poli, *Inorg. Chem.*, 2011, **50**, 11543-11551
15. J. Christoffers, T. Kauf, T. Werner and M. Rössle, *Eur. J. Org. Chem.*, 2006, **11**, 2601-2608
16. J. A. Bertrand and R. I. Kaplan, *Inorg. Chem.*, 1966, **5**, 489-491
17. J. Laugier and J. P. Mathieu, *Acta Crystallogr., Sect. B*, 1975, **B31**, 631

18. E. J. Hawrelak, W. H. Bernskoetter, E. Lobkovsky, G. T. Yee, E. Bill and P. J. Chirik, *Inorg. Chem.*, 2005, **44**, 3103-3111
19. C. R. Pitts, S. Bloom, R. Woltornist, D. J. Auvenshine, L. R. Ryzhkov, M. A. Siegler and T. Lectka, *J. Am. Chem. Soc.*, 2014, **136**, 9780-9791
20. M. Quaranta, M. Murkovic and I. Klimant, *Analyst*, 2013, **138**, 6243-6245
21. N. Rozatian, I. W. Ashworth, G. Sandford and D. R. W. Hodgson, *Chem. Sci.* 2018, **9**, 8692.
22. V. A. Timoshnikov, T. V. Kobzeva, N. E. Polyakov and G. J. Kontoghiorghes, *Int. J. Mol. Sci.*, 2020, **21**, 3967
23. M. S. Chen and M. C. White, *Science*, 2007, **318**, 783-787
24. D. J. Matthew, E. Tieu and M. D. Morse, *J. Chem. Phys.*, 2017, **146**, 144310
25. K. Okuro, M. Furuune, M. Miura and M. Nomura, *J. Org. Chem*, 1993, **58**, 7606-7607
26. M. Alfasir, PhD Thesis, Newcastle University, 2022
27. X. Huang, W. Liu, H. Ren, R. Neelamegam, J. M. Hooker and J. T. Groves, *J. Am. Chem. Soc.*, 2014, **136**, 6842-6845
28. D. Cantillo, O. de Frutos, J. A. Rincón, C. Mateos and C. O. Kappe, *J. Org. Chem.*, 2014, **79**, 8486-8490

## Chapter 4 - A Practical Route to the Thiodifluoromethylene Group

Following the use of [(3-propylphenyl)thio]benzene **4.1** as a substrate in the electrophilic fluorination reaction using the modified iron (II) acetylacetonate **3.16**, the synthesis of thiodifluoromethylene group was identified as an alternative product (Chapter 3.5.2). A brief review of the literature identified that the synthesis of the thiodifluoromethylene group via direct electrophilic fluorination, is rare and potentially novel using Selectfluor™ and iron (II) acetylacetonates. The majority of the literature for electrophilic fluorination adjacent to sulfur is focused on the fluorination of sulfones rather than thioethers. This information prompted a more in-depth study of the fluorination reaction, including optimisation and substrate scope.

### 4.1 Current Methodology

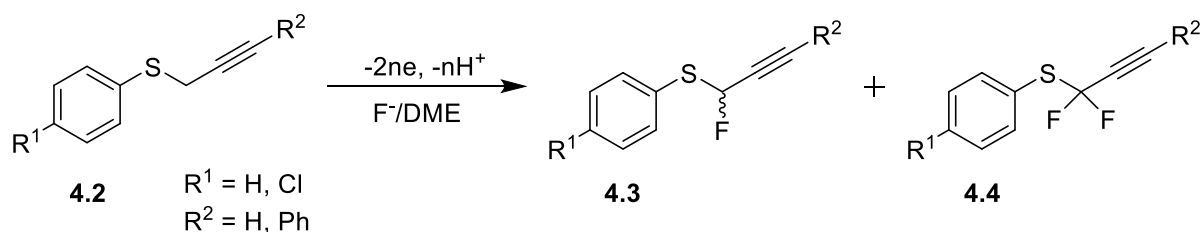
Current methods for the synthesis of difluorothiomethylene groups are limited and there are essentially two types of reaction to introduce this group into a molecule: direct and indirect.

#### 4.1.1 Direct Fluorination

One of the methods of introducing a difluorothiomethylene group is by direct fluorination, i.e. addition of the fluorine into the molecule without the need for further synthetic methods. There are three types of direct fluorination methods reported: electrolysis, nucleophilic and electrophilic fluorination.

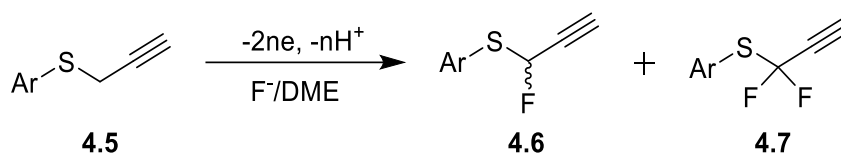
##### 4.1.1.1. Electrolysis

The first method is electrolysis; where an electric current is passed through a reaction medium, via electrodes, containing the fluorinating reagent and substrate. The chemistry for addition of difluorothiomethylene groups using electrolysis, at present, has a limited substrate scope. Anodic mono- and di-fluorination was conducted by T. Fuchigami *et al* on propargyl sulfides (Scheme 4.1), using a constant current, which were converted to the corresponding  $\alpha$ -fluoroallenyl sulfides.<sup>1</sup>



Scheme 4.1. Anodic mono- and difluorination of propargyl sulfides.

The selective formation of the difluorinated compounds was achieved using an excess of constant current passed through DME and the supporting electrolyte  $\text{Et}_3\text{N}\cdot 3\text{HF}$  for prolonged periods. It was found that electron-withdrawing groups markedly facilitated the anodic  $\alpha$ -fluorination of sulfides. Further work by T. Fuchigami *et al* extended the scope of the fluorination to a range of arylthioalkynes, e.g. oxadiazole, thiadiazole, pyrimidines and triazoles (Scheme 4.2).<sup>2</sup>



Scheme 4.2. Anodic fluorination of arylthioalkynes.

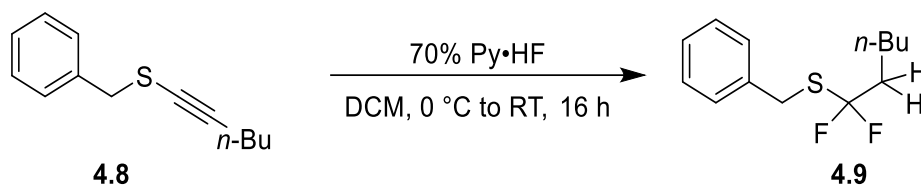
Anodic oxidation at the arylthiol group, using a constant current and platinum electrodes, followed by deprotonation and the subsequent fluorination at the  $\alpha$ -position. Again it was observed that sulfides containing electron-withdrawing groups undergo selective anodic fluorination with good efficiencies. The supporting HF salt,  $\text{Et}_3\text{N}\cdot 3\text{HF}$ , also acted as the base for the deprotonation step for the difluorination.

Electrofluorination has also been conducted on other aromatic compounds containing active methylene groups, such as  $\text{PhSCH}_2\text{COOMe}$ ,  $\text{PhSCH}_2\text{CONH}_2$  and  $\text{PhSCH}_2\text{COOPh}$  by V. Suryanarayanan and M. Noel.<sup>3</sup> However, this is the extent of the substrates that electrofluorination has been tested on for difluorothiomethylene group synthesis.

#### 4.1.1.2. Nucleophilic Fluorination

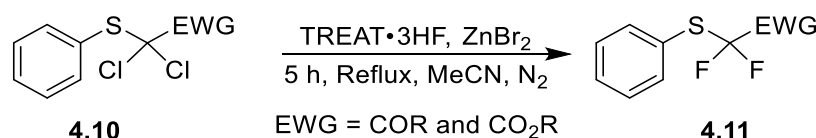
An example of nucleophilic fluorination to form a difluorothiomethylene group is the hydrofluorination of alkynyl sulfides (Scheme 4.3). Initially used to synthesise  $\alpha$ -fluorovinyl thioethers, D. Bello and D. O'Hagan found that using 70%  $\text{Py}\cdot\text{HF}$  lead to

the over fluorination of the alkynyl sulfide to generate the difluoromethylene thioether instead of the desired  $\alpha$ -fluorovinyl thioethers.<sup>4</sup>



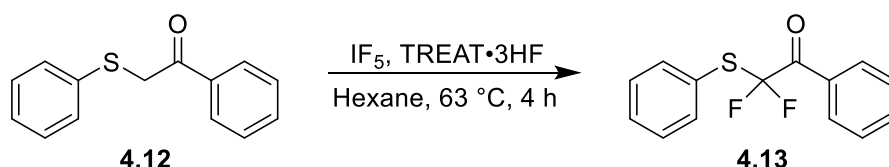
Scheme 4.3. Hydrofluorination of alkynyl sulfides using 70% Py·HF.

*Gem*-difluoroalkylsulfanyl carbonyl compounds have been prepared by halogen exchange reaction using *gem*- $\alpha,\alpha$ -dichloroalkylsulfanyl carbonyl compounds (Scheme 4.4). It was found that rapid exchange of a fluorine atom for the chlorine was achieved by heating at reflux over 1-2 h in MeCN which resulted in the formation of the *gem*-chlorofluoro compounds. In the presence of one equivalent of the Lewis acid ZnBr<sub>2</sub>, the second chlorine atom was displaced to give the *gem*-difluoro compounds.<sup>5</sup>



Scheme 4.4. Halogen exchange reaction using TREAT·3HF to synthesise *gem*-difluoroalkylsulfanyl carbonyl compounds.

A fluorination method using iodine pentafluoride (IF<sub>5</sub>) and triethylamine tris(hydrogen fluoride) (TREAT·3HF) was used to fluorinate 1-phenyl-2-(phenylthio)ethanone in a yield of 45% (Scheme 4.5).<sup>6</sup> IF<sub>5</sub> is a toxic liquid (mp. 9.4 °C, bp 97.9 °C) which reacts vigorously with water to form hydrofluoric acid and iodic acid.

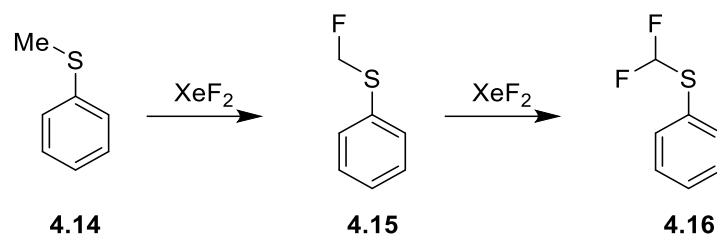


Scheme 4.5. Fluorination using IF<sub>5</sub> and TREAT·3HF.

#### 4.1.1.3. Electrophilic Fluorination

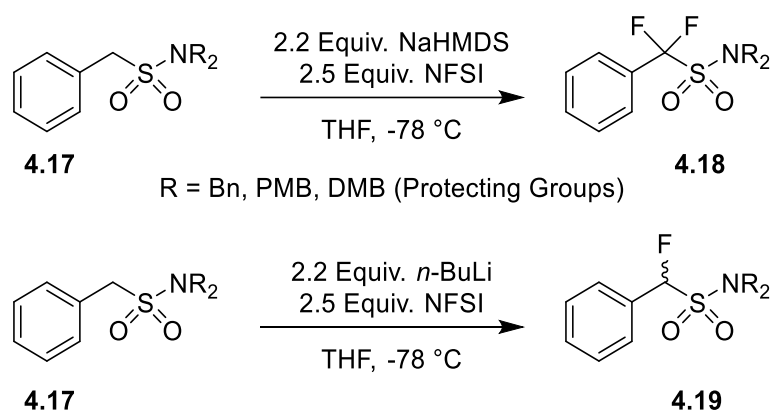
Electrophilic fluorination is the final method used for direct fluorination. Early reactions conducted in the 1970s, used the fluorinating reagents trifluoromethyl hypofluorite and xenon difluoride, XeF<sub>2</sub>, which are no longer available. XeF<sub>2</sub> was introduced to a solution of thioanisole in DCM containing anhydrous hydrogen fluoride. The reaction mixture,

now an orange solution (once colourless), evolved xenon gas yielding the monofluorinated product. Further reaction with an excess of  $\text{XeF}_2$  resulted in the formation of the difluorinated product (Scheme 4.6).<sup>7</sup>



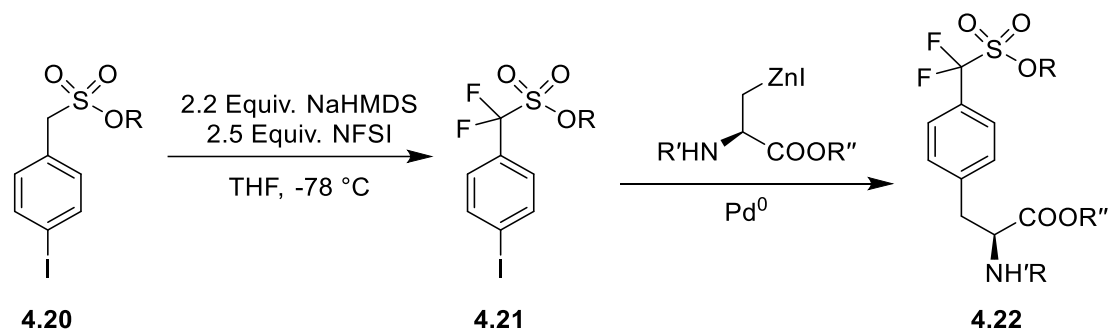
Scheme 4.6. Fluorination of thioanisole with  $\text{XeF}_2$ .

Other electrophilic methods usually utilise a base to abstract the acidic hydrogens and exchange these with fluorine from an electrophilic source, such as NFSI.  $\alpha$ -Fluorosulfonamides have been synthesised by S. Taylor *et al* (Scheme 4.7)<sup>8</sup> by deprotonation using NaHMDS or KHMDS and fluorinating the  $\alpha$ -carbanion species using NFSI. The use of NaHMDS and KHMDS as the base gave exclusively the difluoro product while *n*-BuLi or LDA yielded mainly the mono fluorinated product. It was noted that increasing the size of the cation, increased the yield due to the larger cation being less strongly bound to the anion which results in a stronger base.



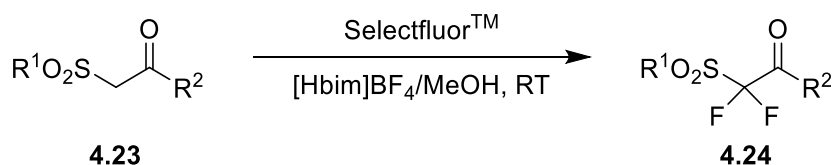
Scheme 4.7. Difluorination of sulfonamides using NaHMDS/KHMDS and NFSI

This work was continued and used to synthesise protected L-4-[sulfonyl(difluoromethyl)]phenylalanine by electrophilic fluorination of a benzylic sulfonate followed by a Pd-catalysed cross-coupling of the fluorinated sulfonate with a zincate of a protected iodoalanine. This was then incorporated into a peptide (Scheme 4.8).<sup>9</sup>



Scheme 4.8. Fluorination and subsequent cross-coupling to form protected L-4-[sulfonyl(difluoromethyl)]phenylalanine.

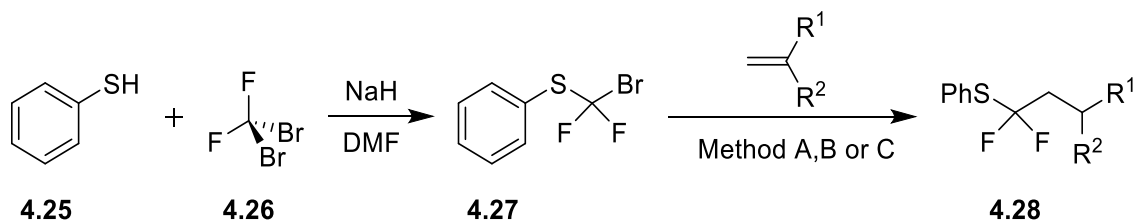
$\beta$ -Ketosulfones have been fluorinated by Selectfluor<sup>TM</sup> promoted by the ionic liquid [Hbm]BF<sub>4</sub> reaction medium and methanol co-solvent under ultrasonic irradiation at ambient conditions.<sup>10</sup> The optimal conditions for this sonochemical synthesis of the difluoro- $\beta$ -ketosulfonone were using the ionic liquid containing 25% MeOH and Selectfluor<sup>TM</sup> (2.1 equiv.) under ambient conditions. (Scheme 4.9).



Scheme 4.9. Synthesis of difluoro- $\beta$ -ketosulfonone using Selectfluor<sup>TM</sup> and [Hbm]BF<sub>4</sub>.

#### 4.1.2 Indirect Synthesis

The most common method for indirect synthesis is via nucleophilic substitution of an organohalide with a thiol in the presence of a base. A multitude of compounds can be synthesised via this method, the limiting factor being the difluorinated-organohalide as these can be difficult to synthesise, have a limited commercial availability and can be very toxic. Some notable examples are detailed below.

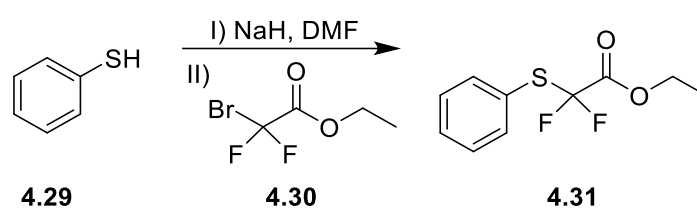


Method A: Sml<sub>2</sub>/THF, Method B: *n*-Bu<sub>3</sub>SnH/AIBN/benzene, Method C: Et<sub>3</sub>B/*n*-Bu<sub>3</sub>SnH/O<sub>2</sub>

Scheme 4.10. Synthesis and application of bromodifluorosulfanylmethane, a gem-difluoromethylene building block.



M. Pohmakotr *et al* demonstrated a versatile *gem*-difluoromethylene building block via the radical reaction of difluorophenylsulfanylmethyl radical with olefins (Scheme 4.10).<sup>11</sup> The building block is synthesised by the reaction of sodium phenylthiolate with dibromodifluoromethane. However, dibromodifluoromethane is a class I ozone depleting substance (ODS) and can be toxic if inhaled or ingested. The difluorophenylphenylsulfanylmethyl radical maybe prepared by three different methods: Method A  $\text{Sml}_2/\text{THF}$ , Method B  $n\text{-Bu}_3\text{SnH}/\text{AIBN}/\text{benzene}$  and Method C  $\text{Et}_3\text{B}/n\text{-Bu}_3\text{SnH}/\text{O}_2$ . The radical is then reacted with electrophilic olefins to give moderate to good yields of the difluorothio-adduct. Non-activated olefins gave low yields which suggests nucleophilic character of the radical formed.



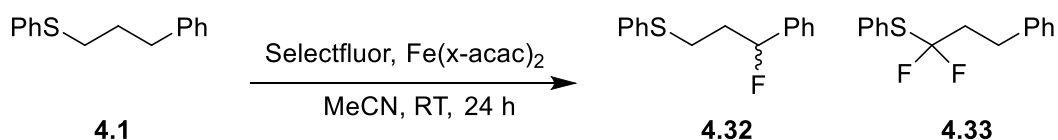
*Scheme 4.11. Synthesis of difluorosulfanylacetate.*

Another example is prepared by the same method as the difluorophenylsulfanyl methane. C. Batisse *et al* has prepared  $\alpha,\alpha$ -difluoro- $\beta$ -sulfanylacetates using thiophenol, in the presence of NaH, and bromodifluoroacetates in DMF. An example of being the use of ethyl bromodifluoroacetate (Scheme 4.11).<sup>12</sup>

The current methods of thiodifluoromethylene synthesis are limited, with some requiring specialist equipment (electrolysis). Despite being a versatile building block, the thiodifluoromethylene group is rare within the literature. The direct difluorination of thioethers by Selectfluor<sup>TM</sup> is potentially a novel synthesis with the scope for a wide range of substrates available to fluorinate, the details of which are outline within this chapter.

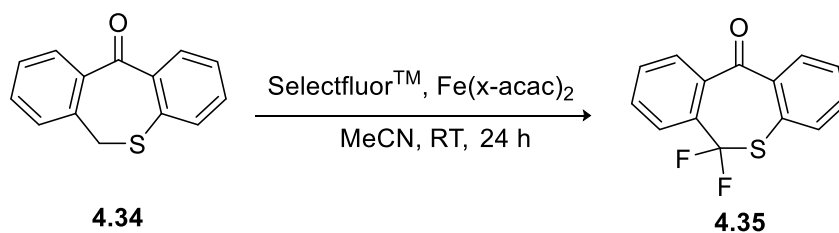
The aim of the work outlined within this chapter is to investigate and develop the difluorothiomethylene formation using electrophilic fluorination techniques, with particular attention to the identification of a potential mechanism of fluorination. Once a method has been established and developed, suitable substrates are to be identified in order to highlight the type of small molecule this fluorination methodology can be utilised for.

## 4.2 Initial Reactions



Scheme 4.12. Structure of the sulfur containing substrate **4.1** and the benzylic product **4.32** and the thiodifluoro-product **4.33**.

Thioarylether **4.1** was used as a substrate to probe the compatibility of functionality with the benzylic fluorination process using  $\text{Fe}(\text{acac})_2$  derivatives as radical initiators. Under these electrophilic fluorination reaction conditions<sup>j</sup> (Chapter 3.4.4 and 3.5.2) the desired product resulting from benzylic fluorination, **4.32** was the minor product of the reaction, in a yield of 6%, while **4.33** occurred in a yield of 24% (Scheme 4.12). The formation of **4.33** is the first occurrence of difluorination under electrophilic conditions using  $\text{Fe}(\text{x-acac})_2$  and Selectfluor<sup>TM</sup> with no mention of this occurrence within the literature.<sup>1,k</sup> It should also be noted that, unlike with some other functional groups, there is an inherent selectivity for the position adjacent to the sulfur over the benzylic position. This suggests a competing reaction in which the major product, the thiodifluoromethylene group is the preferred product.



Scheme 4.13. The reaction of **4.34** with Selectfluor<sup>TM</sup> and  $\text{Fe}(\text{acac})_2$  derivatives.

To explore this reaction further dibenzo[*b,e*]thiepin-11(6*H*)-one **4.34** was also used as a reaction substrate, which led to the formation of the geminal fluorination product adjacent to the sulfur (also a benzylic position and the only option) in an excellent yield of 78% by <sup>19</sup>F NMR spectroscopy (Scheme 4.13). **4.34** was therefore chosen as a model substrate to study this process and due to the structural similarities to dibenzosuberone its potential to access derivatives of Amytryptiline (Chapter 3.5).

<sup>j</sup> 2.2 equiv. Selectfluor<sup>TM</sup>, 10 mol% **3.16**, Anhydrous and FPT-degassed MeCN, RT, 24 h.

<sup>k</sup> it should be noted that sulfur compounds are not included within the compounds tested in the literature

The excellent yield of this initial reaction is likely due to both fluorination pathways directing to the same position – which is adjacent to the sulfur and also benzylic. At this stage, with only these initial reactions conducted, the two reactions could have worked cooperatively producing the high yield seen for the fluorination of **4.34**. Both **4.1** and **4.34** were taken forward as test substrates to be used in the optimisation of this reaction. With no reference to this type of reaction in the literature and the rarity of this specific functional group<sup>1</sup>, the optimisation had very little initial groundwork to build from. Several parameters were identified for the initial optimisation process.

### 4.3 Optimisation

In order to increase the yield of the  $\alpha$ -sulfur geminal fluorination, extensive optimisation was conducted. The first set of parameters, and easiest to investigate, were the reaction conditions.

#### 4.3.1 Reaction Conditions

Initial optimisation reactions focused on the assessing the conditions of the reaction and whether manipulation of conditions, both physical and use of alternative reagents, could increase the yield of the thiodifluoromethylene group and potentially elucidate a mechanism for the fluorination.

##### 4.3.1.1. Practical Measures

In order to improve the yield of the geminal fluorination product the reaction conditions were tested. In the absence of the  $\text{Fe}(\text{3-methyl-acac})_2$ , the difluoro-product **4.35** was synthesised in a yield of 63% by  $^{19}\text{F}$  NMR spectroscopy. This suggests the  $\text{Fe}(\text{x-acac})_2$  is not critical to the reaction and would likely complicate the reaction by increasing the likelihood of by-products occurring when used for other substrates that have the potential for multiple sites of fluorination e.g., a separate benzylic fluorination product.

Reactions that were conducted under an  $\text{N}_2$  atmosphere gave the highest yields of the geminal fluorination of **4.34**, whereas reactions carried out under aerobic conditions still did result in fluorination **4.34** albeit in lower yields (43% compared to 63%). In addition the use of solvent, that had not been degassed, resulted in a large increase in the number of fluorinated products (20-30 compounds) as seen by  $^{19}\text{F}$  NMR

---

<sup>1</sup> Literature focus has been around the use of  $\text{SCF}_2$  as building blocks to further functionalise complex molecules by addition of difluoro-moieties.<sup>5</sup>

spectroscopy suggesting that the presence of oxygen may facilitate uncontrolled radical based mechanisms which could result in the greater number of fluorinated by-products seen. In comparison the use of anhydrous degassed acetonitrile decreased the numbers of the fluorinated by-products which lead to an increase in the yield of the desired fluorinated product. When **4.1** was used as the substrate the yield of **4.33** increased from 24% to 32% with the use of commercial anhydrous acetonitrile<sup>m</sup> (99%+ purity Sigma Aldrich) suggesting that water too may interfere with the reaction. Both of these observations suggest that the reaction is sensitive to oxygen and water, either by facilitating alternative reaction pathways or by preventing the target transformation. This is especially the case with substrates which only give the fluorinated product in low yields as using a solvent that is not dry or degassed results in no fluorination at all.

With the initial reaction conditions requiring two equivalents of Selectfluor<sup>TM</sup> for the formation of the geminal fluorination product, the use of one equivalent was investigated to see if the monofluoro- derivative could be prepared. This study did not result in monofluorination or difluorination products. A potential explanation for this is that the monofluorination product is sensitive to hydroxylation, and therefore the work-up protocol would result in undesired by-products. The <sup>1</sup>H NMR spectrum shows small amounts of aldehyde by-products (singlet peak at 10.07 ppm), which suggests the formation of the SCFH monofluorination product which has then degraded potentially through the formation of a C=S bond. It was noted that prior to work-up there is a distinct colour difference when using one or two equivalents of Selectfluor<sup>TM</sup> with **4.34** as the substrate (Fig. 4.1). The blue colour suggests the formation of the C=S bond as a similar colour is observed with thiobenzophenone (deep blue colour).

---

<sup>m</sup> Karl Fisher analysis of the commercial solvent gave a water content between 14-100 ppm. The solvent was stored in a Schlenk flask under N<sub>2</sub> with activated 3 Å molecular sieves.



Figure 4.1. Colour difference when using one equivalent (left) and two equivalents (right).

The use of more than two equivalents of Selectfluor™ resulted in multiple sites of fluorination rather than just increasing the yield of the difluoromethylene product. This suggests that the formation of the SCF<sub>2</sub> group is relatively quick and easy. When the reaction comes to the limit at which the SCF<sub>2</sub> group is formed the excess Selectfluor™ is available for further reaction e.g. on the aromatic ring.

#### 4.3.1.2. Fluorine Source

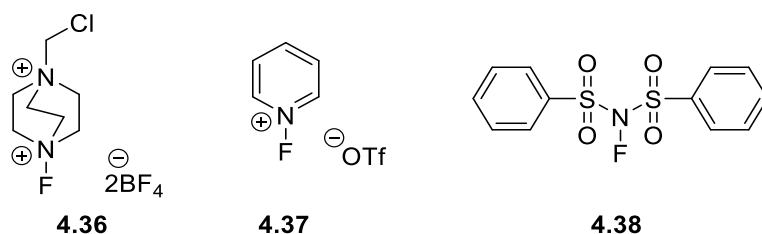


Figure 4.2. Electrophilic fluorinating agents used.

The initial fluorine source used in these reactions was Selectfluor™, following the methodology used in the electrophilic fluorination initiated by Fe(acac)<sub>2</sub> (Chapter 3.4.4). A range of other electrophilic fluorine sources are commercially available, and it was decided to see if a switch in the fluorinating agent had an impact on the outcome: *N*-Fluoropyridinium triflate **4.37** and *N*-fluorobenzenesulfonimide (NFSI) **4.38** are two of the more common commercially available sources (Fig. 4.2) and these were chosen due to them being a mix of stable ionic and neutral, easy to handle solids with different levels of reactivity. The reactivity series of electrophilic fluorinating reagents is shown below (Fig. 4.3) with Selectfluor™ being the most reactive out of the commercially available fluorinating reagents.

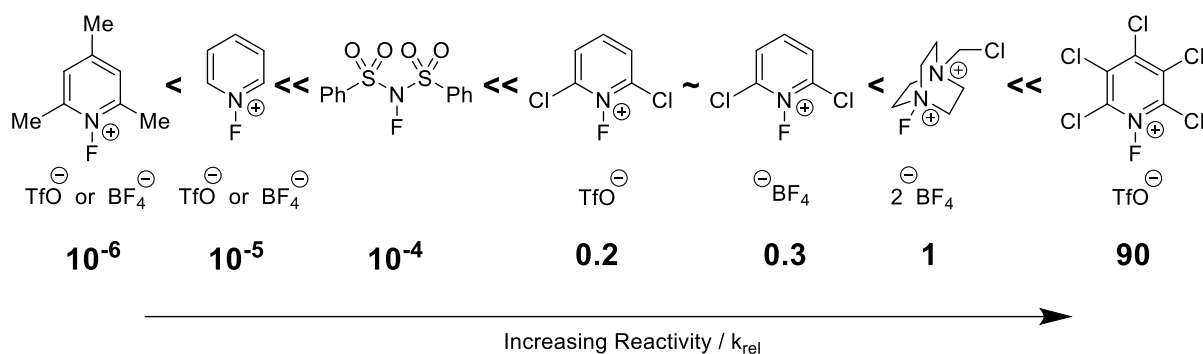
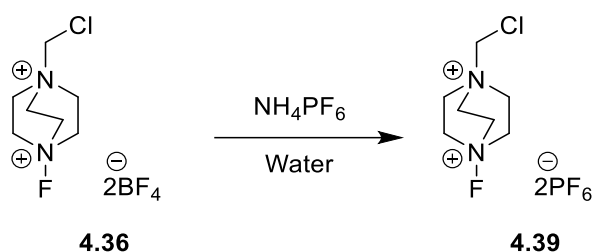


Figure 4.3. Reactivity series for the electrophilic fluorinating reagents.<sup>13</sup>

The ability of these alternative fluorine sources to selectively generate the thiodifluoromethylene group was then tested. NFSI gave a large mixture of fluorinated products, including the desired geminal difluoro fluorination product albeit in a very low yield (<1%). However, the greater mixture of products and the lower yield suggests this fluorine source would complicate the reaction especially in terms of isolation of the target compound. The Selectfluor<sup>TM</sup> reaction by-products are also cationic and hence on work-up these are readily removed while the by-products resulting from the use of NFSI remain in the reaction mixture and need to be removed by further purification e.g. chromatography. NFSI has been identified as being less reactive than Selectfluor<sup>TM</sup> and this lower reactivity could account for the lower levels of indiscriminate fluorination seen as well as the lack of formation of the geminal difluoro product.

*N*-Fluoropyridinium triflate is also less reactive than Selectfluor<sup>TM</sup> and therefore may be expected to give a lower yield of the desired fluorination product. Surprisingly, *N*-fluoropyridinium triflate does not fluorinate either **4.01** or **4.34**. *N*-Fluoropyridinium tetrafluoroborate also did not fluorinate **4.01** or **4.34**. This is further supported by work conducted by T. Fuchigami *et al*, where *N*-fluoropyridinium triflate was tested as a control for the electrochemical geminal fluorination of propargyl sulfides.<sup>1</sup> From these findings this suggests that the Selectfluor<sup>TM</sup> has a greater role within the reaction than just providing the fluorine.

#### 4.3.1.2.1. Alternate Counter-ion to BF<sub>4</sub>



Scheme 4.14. The synthesis of **4.39** by ion exchange using ammonium hexafluorophosphate.

Tetrafluoroborate (BF<sub>4</sub><sup>-</sup>) is the counter ion present in Selectfluor™, and this group may be the source of one or both fluorine atoms in the product and therefore could be intimately involved in the fluorination mechanism, such as seen in the Balz-Schiemann reaction. Currently there are no other commercially available derivatives of Selectfluor™, therefore, to test whether the reaction is counter ion dependant 1-chloromethyl-4-fluoro-1,4-diazoniabicyclo[2.2.2]octane bis(hexafluorophosphate) **4.39** was synthesised from Selectfluor™ by ion exchange using ammonium hexafluorophosphate, in quantitative yield (Scheme 4.14).

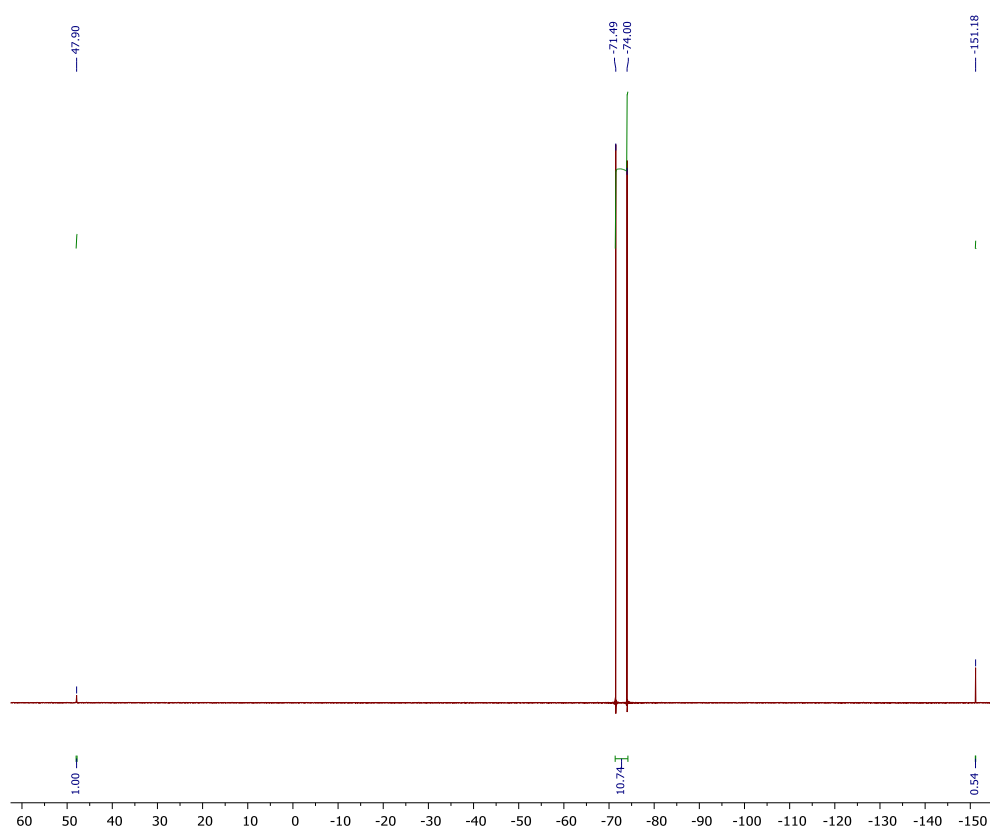


Figure 4.4a. <sup>19</sup>F NMR of **4.39**. Residual BF<sub>4</sub> peak at -151 ppm.

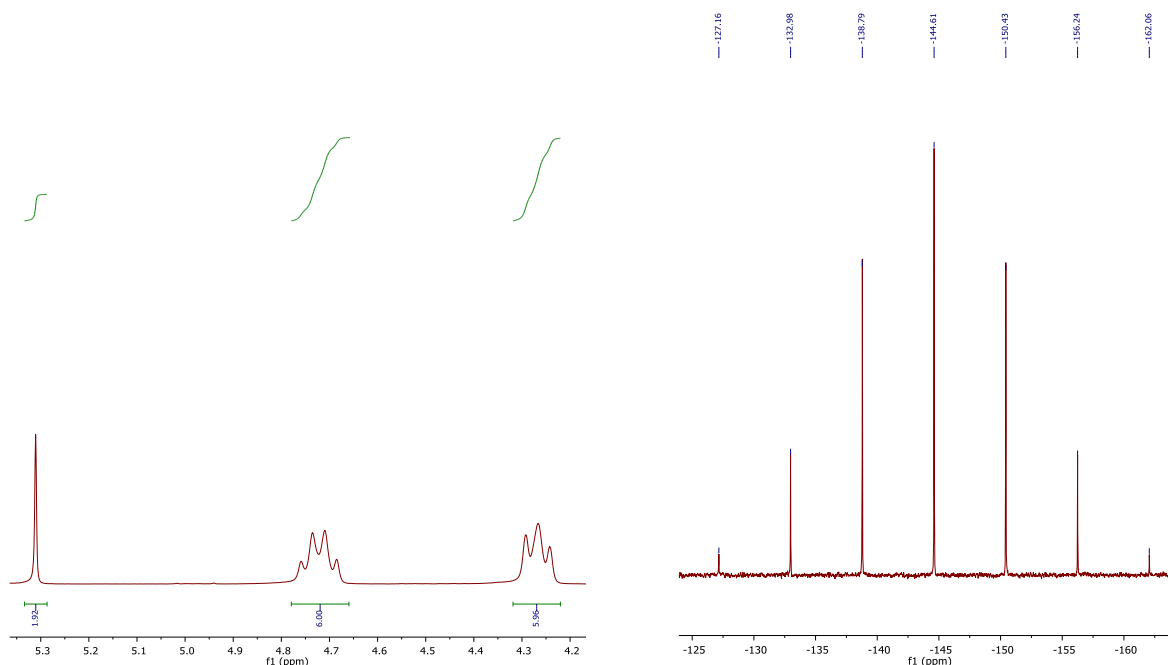


Figure 4b.  $^1\text{H}$  (left) and  $^{31}\text{P}$  (right) NMR of **4.39**.

There was no fluorination of **4.01** or **4.34** when the hexafluorophosphate salt was used as a fluorine source, illustrating that the tetrafluoroborate counter ion is indeed required for fluorination. The hexafluorophosphate ion is considered a poor nucleophile, is classified as a non-coordinating anion and certainly less coordinating than tetrafluoroborate, suggesting that this property could be responsible for the lack of fluorination resulting from the switch of counter-ion. From these findings, it is clear there is a requirement for the tetrafluoroborate counterion being present. Therefore, further work into the need for the tetrafluoroborate was conducted.

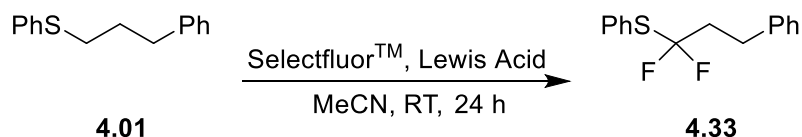
#### 4.3.2 Tetrafluoroborate Counter Ion Investigation

An explanation for the involvement of the tetrafluoroborate counter ion is that it could be stabilising a cationic species which is formed during the reaction. With  $\text{BF}_4^-$  being a small, weakly coordinating anion it could be possible that this is aiding in the stabilisation of a reaction intermediate or transition state, lowering the energy, allowing the reaction to proceed. The  $\text{BF}_4^-$  ion is more soluble in organic solvents than other salts and may therefore be more available for coordination. Another possibility is that the  $\text{BF}_4^-$  ion is a precursor to another species which has an effect on the reaction and allows it to progress to the desired fluorinated product.



#### 4.3.2.1. Lewis Acid Addition

The tetrafluoroborate ion is the conjugate Lewis base of boron trifluoride (BF<sub>3</sub>) and a disadvantage of boron tetrafluoride is that it is slightly sensitive to hydrolysis and decomposition by loss of a fluoride ligand. This loss of fluoride results in a number of boron trifluoride compounds (e.g. BF<sub>3</sub>) which could act as Lewis acids.



Scheme 4.15. Investigation into the Lewis Acid addition using **4.01** as the substrate.

A selection of Lewis acids was therefore investigated, using **4.01** as the substrate, to determine whether their addition would increase the yield of the desired fluorinated products (Scheme 4.15). Boron trifluoride diethyl etherate (BF<sub>3</sub>·OEt<sub>2</sub>), aluminium (III) chloride (AlCl<sub>3</sub>) and iron (III) acetylacetonate were used in catalytic amounts of 5, 10 and 20 mol% (Table 4.1).

<b>Lewis Acid</b>	<b>Catalytic Amount / mol%</b>	<b>Yield / %</b>
None	-	32
BF <sub>3</sub> ·OEt <sub>2</sub>	5	0
	10	14
	20	3
AlCl <sub>3</sub>	5	0
	10	0
	20	0
Fe(acac) <sub>3</sub>	5	8
	10	12
	20	0

Table 4.1. Yields of the geminal difluoroproduct **4.33** with the addition of Lewis acids, following geminal fluorination method.<sup>n</sup>

The lower yields of the geminal fluorination product suggests that Lewis acids do not play a key role in the mechanism of the formation of the fluorinated products and may even hinder the formation of the fluorinated products. The presence of aluminium (III) chloride prevented the formation of the product completely with no fluorination evident,

<sup>n</sup> Yields were calculated from <sup>19</sup>F NMR using an internal standard of pentafluorotoluene

while the  $\text{BF}_3\cdot\text{OEt}_2$  and  $\text{Fe}(\text{acac})_3$  resulted in a lower yield of the products. The lower yield when using  $\text{Fe}(\text{acac})_2$  may also be due to the competing fluorination of the acetylacetonate ligand (see Chapter 3.3.1). The reduced yield with the addition of  $\text{BF}_3\cdot\text{OEt}_2$  is most likely from a reaction with the fluoride anion enhanced by the presence of the Lewis acid. This could interfere with the reaction hence limiting the formation of the desired difluoro-product.

The decomposition of boron tetrafluoride produces boron trifluoride and a fluoride ion. The boron trifluoride may not be the active species of this decomposition and therefore it may be the fluoride ion generated is the cause for the higher yields when additional Lewis acids are not present.

#### 4.3.2.2. Additional Fluoride Sources

To determine whether fluoride ions were responsible for the geminal fluorination the addition of fluoride salts into the reaction, as a co-fluorine source along with Selectfluor™, was also investigated. Potassium fluoride (KF) was used as one source of inorganic fluoride, with Kryptofix® 222 to aid dissolution, and this change resulted in no geminal or benzylic fluorination.

The potassium fluoride derived fluoride may have too much ionic character/different solvation relative to the fluoride formed from the decomposition of  $\text{BF}_4^-$  and therefore triethylamine trihydrofluoride (TREAT·HF) was also used as a source of additional fluoride ions. A yield of 27% was recorded when TREAT·HF was used at 10 mol%, this is within the current range for the yields when using **4.01** as the substrate suggesting that extra fluoride ions are not integral to the reaction mechanism.

#### 4.3.3 Conclusion to Optimised Conditions

In conclusion, the current optimised conditions are as follows:

- Anhydrous MeCN (100>ppm water content), thoroughly degassed using freeze-pump-thaw as the solvent
- 2.2 equivalents Selectfluor™ (boron tetrafluoride salt) as the fluorine source
- Reaction is to be conducted at room temperature and under an  $\text{N}_2$  atmosphere

The reactions were run at room temperature. A focus of future work would be to conduct reactions at varying temperatures in order to assess the affect temperature

has on the yield of the difluoro-product and the formation of fluorinated by-products and impurities.

After conducting work on optimising the reaction and the effect of various additives a mechanistic explanation for the formation of the thiodifluoromethylene group was sought.

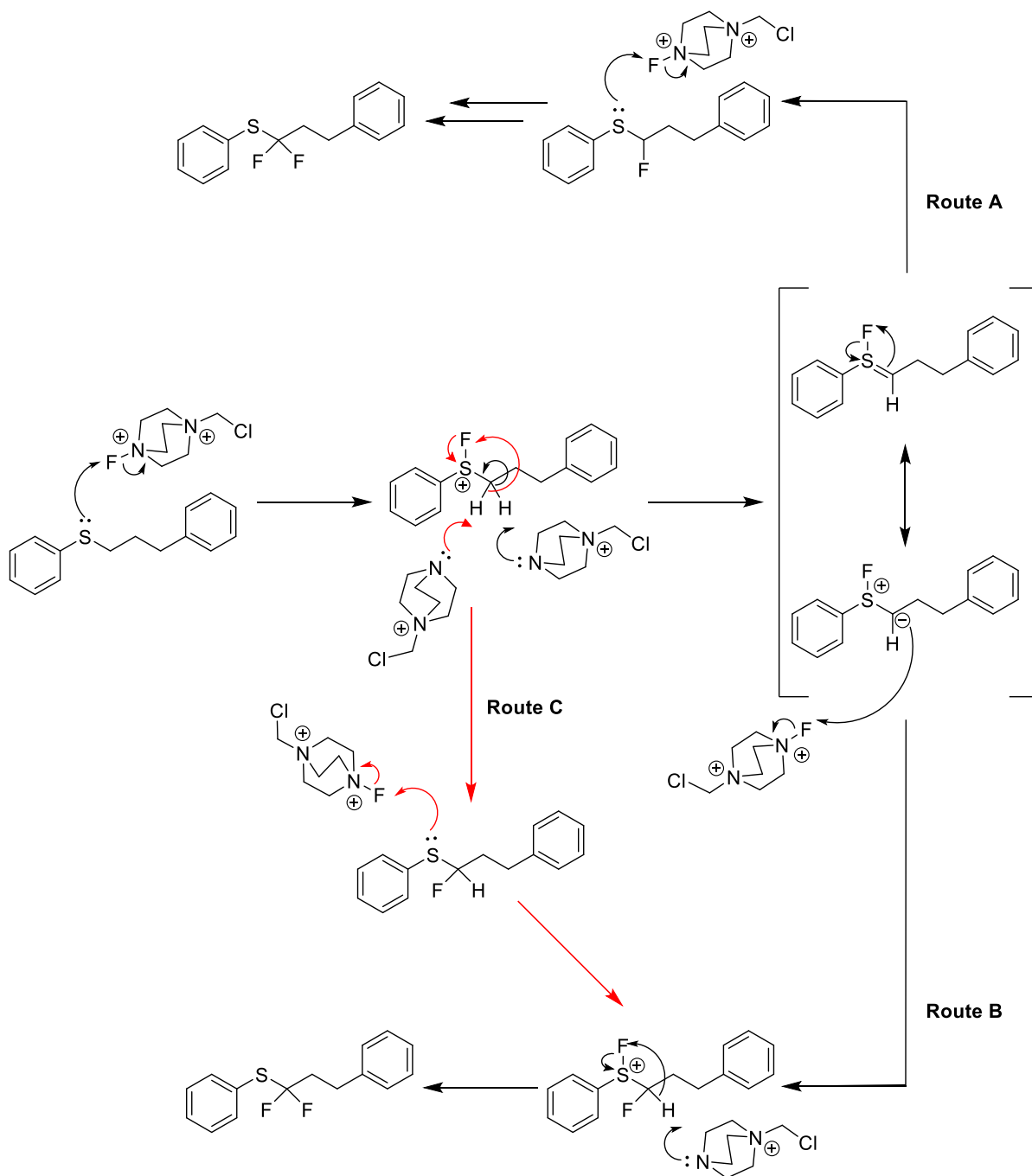
#### 4.4 Mechanism Identification

Potential mechanistic steps for the geminal addition of the fluorine is outlined below (Scheme 4.16). The hypothesis is that the lone pair on the sulfur acts as a nucleophile forming a sulfur-fluorine bond by abstracting the fluorine from Selectfluor™. Deprotonation of the positively charged fluoro-sulfur intermediate at the adjacent carbon gives a sulfur ylide species. Here the reaction can go two different routes:

- Route A: an intramolecular fluorine migration followed by repetition of the previous sequence to give the geminal fluorination product.
- Route B: an abstraction of fluorine from Selectfluor™ by the carbon of the sulfur ylide to form the mono-fluoro group which then deprotonates, and an intramolecular fluorine migration gives the geminal difluorination product.

Another potential route (Route C) is that the S-F compound formed by the initial abstraction undergoes the intramolecular fluorine migration giving the mono-fluoro product. This mono-fluorinated product abstracts fluorine from another molecule of Selectfluor™ and undergoes the intramolecular fluorine migration to form the geminal difluoro-product.

A similar nucleophilic mechanism could not be ruled out by Yang *et al* for the fluorium-initiated dealkylative cyanation of thioethers to thiocyanate.<sup>14</sup> The nucleophilic mechanism proposed follows the same reaction initiation: nucleophilic attack at the fluorine of Selectfluor™ affording the fluorosulfonium intermediate which subsequently reacts further via a dealkylation to form the thiocyanate compound. The sulfide pummerer reaction also follows a similar mechanism, again reported by Yang *et al*.<sup>15</sup>



Scheme 4.16. Potential mechanistic options for the formation of thiodifluoromethylene group-

A base was added in order to test the deprotonation of the S-F complex. DABCO was chosen as an appropriate base due to the structural similarities to that of Selectfluor™. A 10 mol% addition of DABCO gave a yield of 20% for **4.33**. When the DABCO was added after one hour, the yield of **4.33** decreased to 7%. The reduction of yield in both cases, suggests the deprotonation step may be more complex than first hypothesised. However, DABCO, despite the structural similarity, may be mismatched as a base for this reaction.

#### 4.4.1 Sulfone Compounds

The proposed mechanism suggests that nucleophilic attack from the sulfur lone pair initiates the reaction which leads to the formation of an S-F complex. This complex, via a number of potential routes, results in the ultimate formation of the thiodifluoromethylene group. Commercially available substrates containing a sulfone group ( $\text{RSO}_2\text{R}^1$ ) were used to investigate whether the sulfur lone pair was needed in order to synthesise the thiodifluoromethylene desired product. These substrates were (phenylsulfonyl)acetonitrile and benzyl phenylsulfone and neither of these compounds reacted with the Selectfluor<sup>TM</sup> under the optimised fluorination conditions as there were no fluorinated compounds observed by  $^{19}\text{F}$  NMR spectroscopy. In the  $^1\text{H}$  NMR spectrum, only the starting material and Selectfluor<sup>TM</sup> were present in the reaction mixture. The (phenylsulfonyl)acetonitrile does not react with Selectfluor<sup>TM</sup> despite fluorination occurring when 2-(phenylthio)acetonitrile was used as a substrate detailed later within this chapter (Chapter 4.5.1.1).

The lack of fluorination from the sulfones suggests the sulfur lone pair is required for fluorination to occur. With no lone pairs available, the sulfur cannot initiate the fluorine abstraction from Selectfluor<sup>TM</sup> and form the S-F intermediate and thus these observations agree with the proposed mechanism (Scheme 4.16) for the difluorothiomethylene synthesis.

Further focus into the investigation of substrates with different oxidation states with sulfur would be to include experimentation using sulfoxides. Thioanisole sulfone and sulfoxide is commercially available and would be a good indication as to whether the sulfur lone pair is critical to the initiation of the reaction.

#### 4.4.2 Kinetic Studies

An NMR experiment was conducted to determine the kinetics of the reaction using **4.34** as the reaction substrate. The addition of the fluorine is fast; within the first 30 minutes the geminal difluoro product was formed.

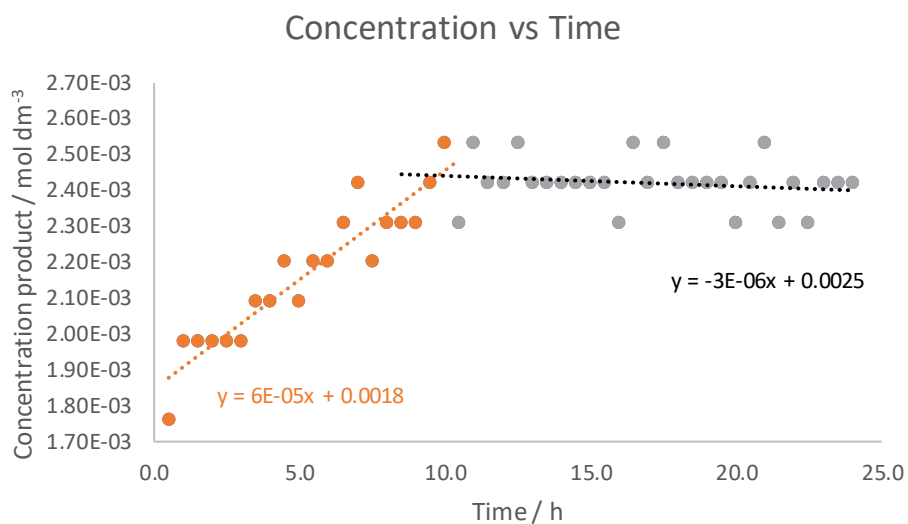


Figure 4.5. Concentration vs time for the fluorination of 4.34 followed by <sup>19</sup>F NMR.

The reaction reaches completion around 10 h, similar to that of the radically initiated fluorination (Chapter 3.4.3.3). The reaction time remained at 24 h to maximise the fluorination and for logistical reasons.

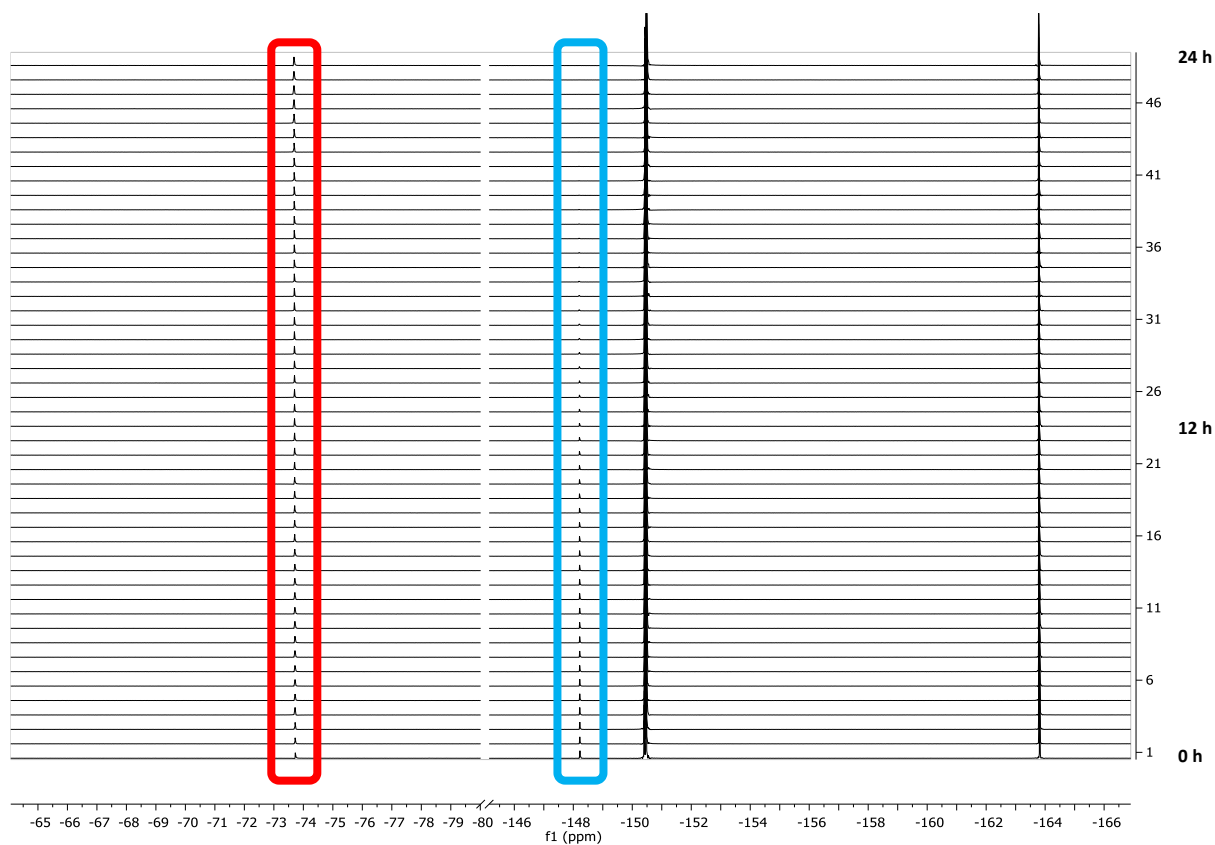


Figure 4.6. <sup>19</sup>F NMR at various time points. Geminal difluoroproduct at -74 ppm (red) and the monofluoro intermediate at -148 ppm (blue). Peaks above -150 ppm are boron tetrafluoride and internal standard hexafluorobenzene.

The monofluorination product can be seen at -148 ppm (doublet, 50 Hz) and over the course of 10-15 h decreases as the geminal difluoro product increases. The formation of the monofluoro-product is very quick, possibly on the timeframe of addition of substrate to the Selectfluor™-MeCN solution, therefore it is very difficult to obtain any kinetic data for the formation as the monofluoro species on the NMR timescale as it is already converting to the difluoro product before the first scan was taken.

Plotting  $-\ln[\text{product}]$  vs time shows a first order relationship for this reaction, if taking the increasing formation separately from the plateau where the reaction slows to completion.<sup>o</sup>

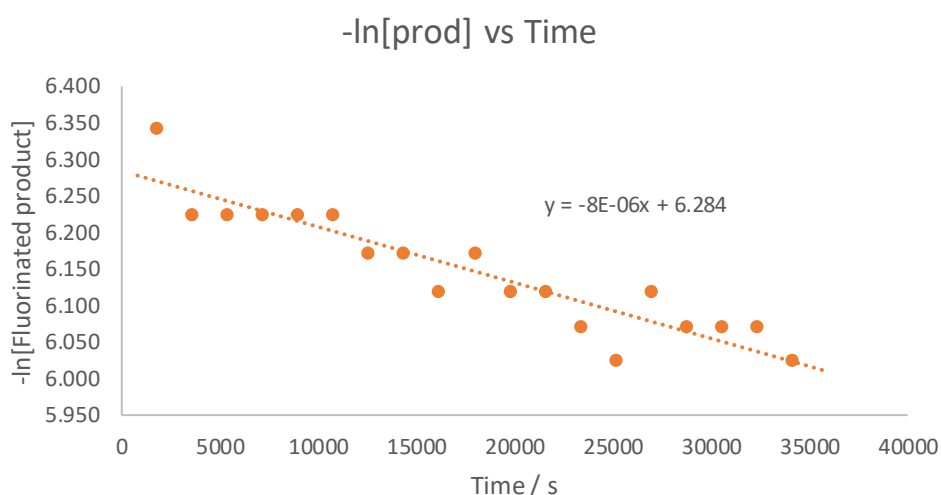


Figure 4.7.  $-\ln[\text{product}]$  vs time for the kinetics reaction of 4.4 (0 h to 10 h).

The linear trend of graph 2 suggests a first order reaction (rate =  $k[A]$  and  $[A] = [A]_0 e^{-kt}$ ). The rate constant of this reaction is  $8 \times 10^{-6} \text{ s}^{-1}$ .

#### 4.4.3 Radical Reactions and Scavengers

To eliminate a single electron process as one of the potential routes to the formation of the difluorothiomethylene group, radical scavengers were used to suppress the formation of this pathway. TEMPO and galvinoxyl were used as the radical scavengers (10 mol%) using 4.1 and 4.34 as the model substrates.

<sup>o</sup> Large deviation from line of best fit due to an intrinsic problem of obtaining integrals from  $^{19}\text{F}$  NMR.

Substrate	Yields of Geminal-difluoro Products / %		
	Control	TEMPO	Galvinoxyl
<b>4.1</b>	32	24	25
<b>4.34</b>	78	68	63

Table 4.2. Yields of the geminal difluoro-products of **4.1** and **4.34** when using radical scavengers. A control, with no radical scavenger added, has been included for comparison.

Compared to the control reaction, when radical scavengers were present during the reaction there is a small reduction in yield of the geminal difluoro-product (24 and 25% from 32% for both TEMPO and galvinoxyl respectively) when using **4.1** as the substrate. When using **4.34** as the substrate there is also a reduction of the geminal difluoro-product (68 and 63% from a control of 78% for both TEMPO and galvinoxyl respectively) (Table 4.2). The scale of the reduction in yield is not significant enough to suggest that the reaction is initiated and propagated via radical mechanisms. There may be some radical components within the reaction, these being the pathways which lead to the formation of the by-products

#### 4.5 Substrate Scope

The synthesis of the difluorothiomethylene group was identified from an investigation into the electrophilic fluorination at benzylic positions. Currently the two substrates used as the model compounds have been relatively simple structures, with only limited functional groups, e.g. the keto group and aromatic rings. As the benzylic position for this particular work is not of interest, this opens the scope for different substrates which undoubtedly include molecules that are polyfunctional. A set of scoping experiments was conducted to determine the suitability of this method for the preparation of SCF<sub>2</sub> building blocks and/or late-stage introduction of the SCF<sub>2</sub> group into a molecule.

##### 4.5.1 Substrates

A variety of substrates were tested with a range of multiple functionalities (Fig. 4.8). The substrates were either commercially available or were synthesised using literature procedures.



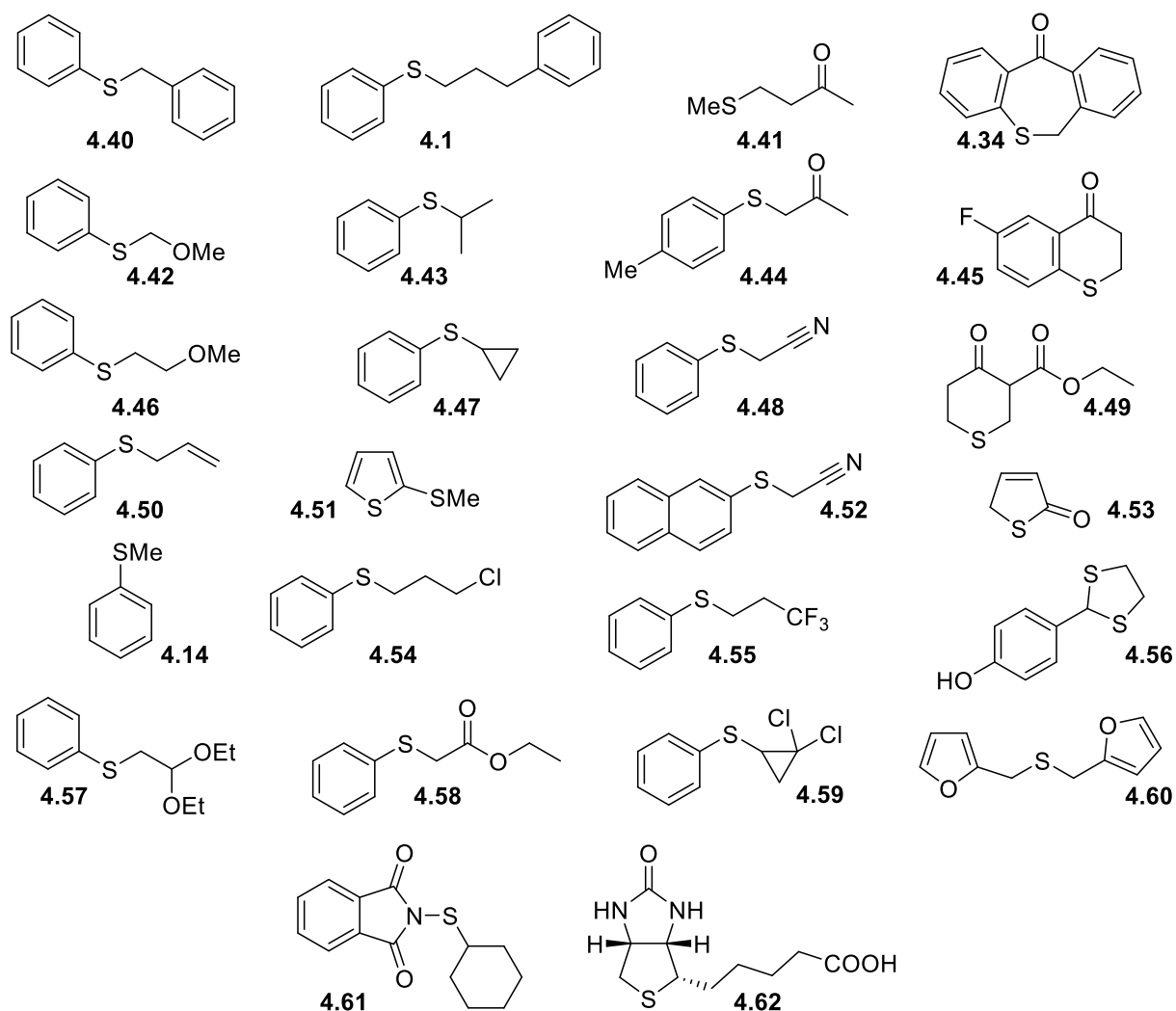


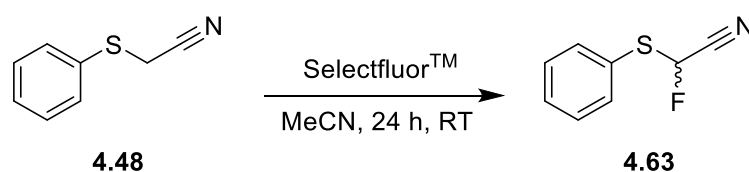
Figure 4.8. The substrates investigated during the substrate scoping experiments. Majority of the compounds were commercially available.

The initial reactions showed that there is a necessity for the thioethers to have an aromatic substituent. The aromatic thioethers fluorinated in variable yields, depending on the substrate. Substrates which contain more reactive aromatic motifs, such as furan or thiophene, were susceptible to polymerisation under the fluorination conditions; brown/black tar formed during the reaction which was insoluble in organic solvents. It should be noted that nitrogen containing heteroaromatic thioethers, e.g. pyrroles and pyridines, were not investigated. However, nitrogen containing molecules have not fluorinated in the desired manner when subjected to the fluorination conditions and tend towards fluorination of the nitrogen which is then subject to hydrolysis on work-up leading to non-fluorinated products. This limits the suitability of this fluorination method to non-heteroaromatic thioethers, i.e. PhSR.

Substrates which contain nucleophilic functional groups, e.g. alkenes, thiophenone, are susceptible to electrophilic fluorination of these functional groups as an alternative reaction pathway. Therefore, this fluorination method is not suitable for the introduction of the difluorothiomethylene functionality directly into substrates containing these groups. Overall this means that the introduction of the difluorothiomethylene group would not be possible as a late-stage functionalisation method due to the issues associated with the presence of certain functional group, however, this method could be used as an early-stage functionalisation and have the non-comptaible groups introduced at a later stage.

Biotin and 4-(1,3-dithiolan-2-yl)phenol were also investigated as possible substrates, however, due to poor solubility in acetonitrile there was no fluorination observed. In order to test these under the optimised fluorination conditions using MeCN, biotin would need to be converted to an alkyl-ester (e.g. methyl or ethyl esters) while the phenol group of the 4-(1,3-diethiolan-2-yl)phenol would require protection e.g. as an OMe group (e.g. using a base and dimethyl sulfate or iodomethane). This would be the focus for future work using these types of substrates.

#### 4.5.1.1. Thioacetonitrile Compounds



*Scheme 4.17. Fluorination of 2-(phenylthio)acetonitrile.*

An attempt to fluorinate 2-(phenylthio)acetonitrile **4.48** (Scheme. 4.17) gave the mono-fluorinated product (doublet, -152.95 ppm; literature value -152 ppm) and potentially the geminal difluoro-product, however, the assigned peak on the  $^{19}\text{F}$  NMR (-68.90 ppm, s) is in disagreement with the literature (-84 ppm, s).<sup>3</sup> This peak does not appear in other reactions and can therefore be ruled out as being a fluorinated by-product of self-fluorination from Selectfluor<sup>TM</sup> (Fig. 4.9). A similar peak is present when using **4.52** as a substrate.

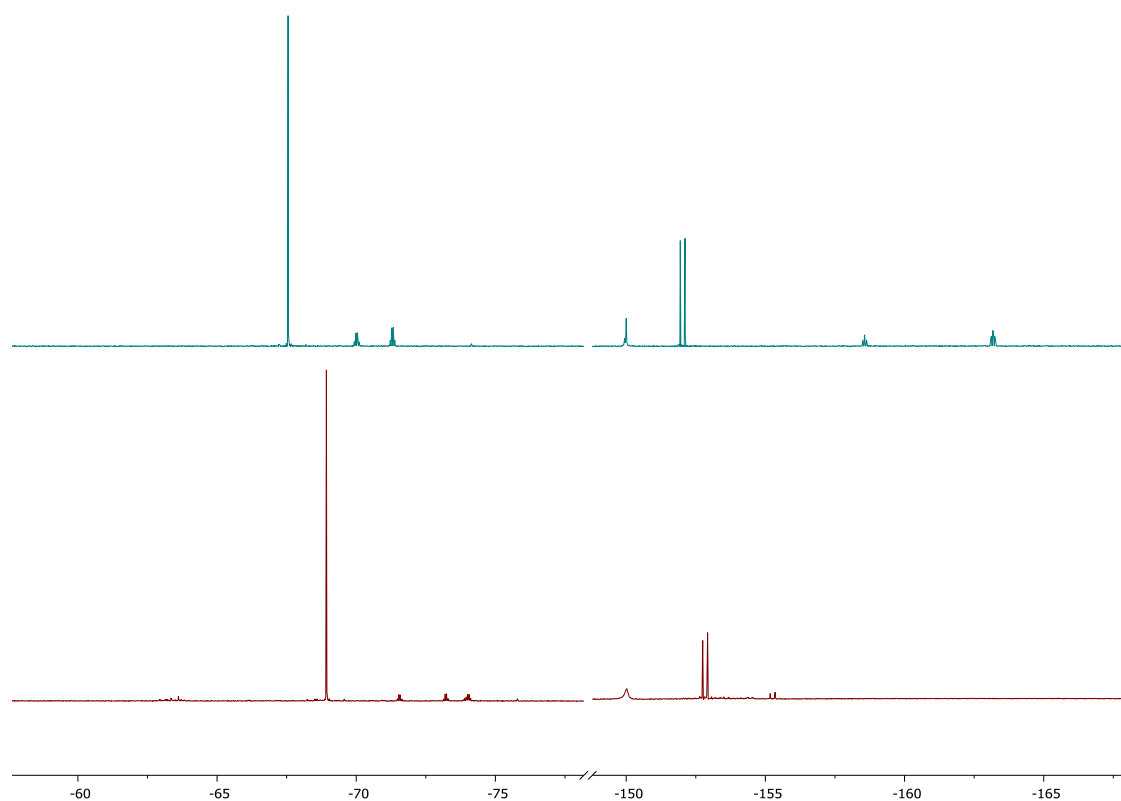


Figure 4.9. Stacked  $^{19}\text{F}$  NMR spectrum of the **4.48** (top) and **4.52** (bottom).

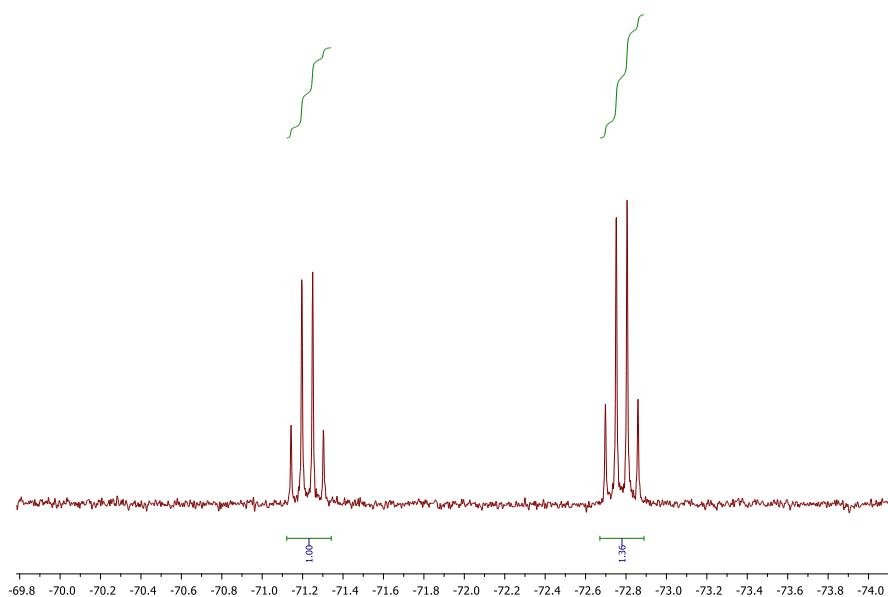


Figure 4.10.  $^{19}\text{F}$  NMR spectrum of the 'rotamers'.

The peaks occurring between -70 and -75 ppm were thought to be rotamers of the S-F intermediate (Fig. 4.10). The quartet observed were initially thought to be overlapping a 2<sup>nd</sup> order multiplet, however this was ruled out using variable

temperature (VT)  $^{19}\text{F}$  NMR. At a temperature of 50 °C the peaks remained a quartet, suggesting that the fluorine is in fact being split by three adjacent hydrogens. Due to the simplicity of **4.48** and **4.52**, the most probable explanation for three adjacent hydrogens is the nitrile group being replaced by a hydrogen atom.

#### 4.5.1.2. Fluorinated Substrates

The substrates which fluorinated in the highest yields, using the optimised conditions stated in Chapter 4.3, are summarised in Table 4.3.

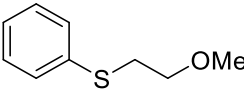
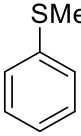
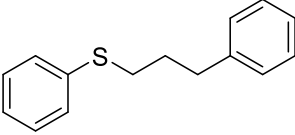
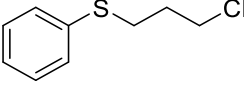
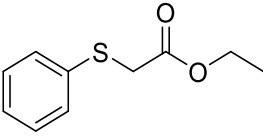
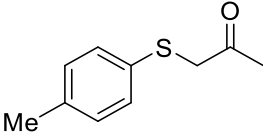
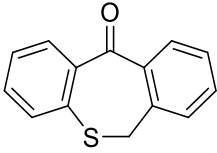
Substrate	No.	Structure	Yield / %
2-Methoxyethyl phenyl sulfide	<b>4.46</b>		37
Thioanisole	<b>4.14</b>		6
[(3-Phenylpropyl)thio]benzene	<b>4.1</b>		32
3-Chloropropyl phenyl sulfide	<b>4.54</b>		9
Ethyl-4-(phenylthio)acetate	<b>4.58</b>		13
1-[4-Methylphenyl]thio]acetone	<b>4.44</b>		15
Dibenzo[ <i>b,e</i> ]thiepin-11(6 <i>H</i> )-one	<b>4.34</b>		73

Table 4.3. The highest yielding substrates.

Substrates which fluorinate in the highest yields have somewhat limited functionalisation, with the majority have electron withdrawing groups. Further investigation into the groups which affect the degree of fluorination was conducted.

#### 4.5.2 Electron Withdrawing Group and Hyperconjugation Effect

Investigation into the substrate scope of the reaction has shown that the higher yields are when electron withdrawing groups are present in the compound, such as esters and ketones **4.58** and **4.44** respectively, and groups which have lone pairs available for donation via hyperconjugation, such as chlorine and oxygen atoms **4.54** and **4.46** respectively.

#### 4.5.3 Effects of Substituents within the Aromatic-Thioether System

The substrate scope studies identified that the presence of an aromatic-thioether system is highly desirable in order to achieve high yields of the difluorothiomethylene group.

The electronic scope of the geminal difluorination was investigated using a wide-range of *para*-substituted aromatic thioethers, derived from **4.1** (Table 4.4). These aromatic *para*-substituted thioethers were synthesised by the addition of 3-phenylpropyl bromide (1.2 equiv.) to the corresponding aromatic substituted thiophenol (1 equiv.) in the presence of a base, either triethylamine or potassium carbonate in EtOH at 25-50 °C for 24-72 h, according to modified literature procedures.<sup>15</sup>

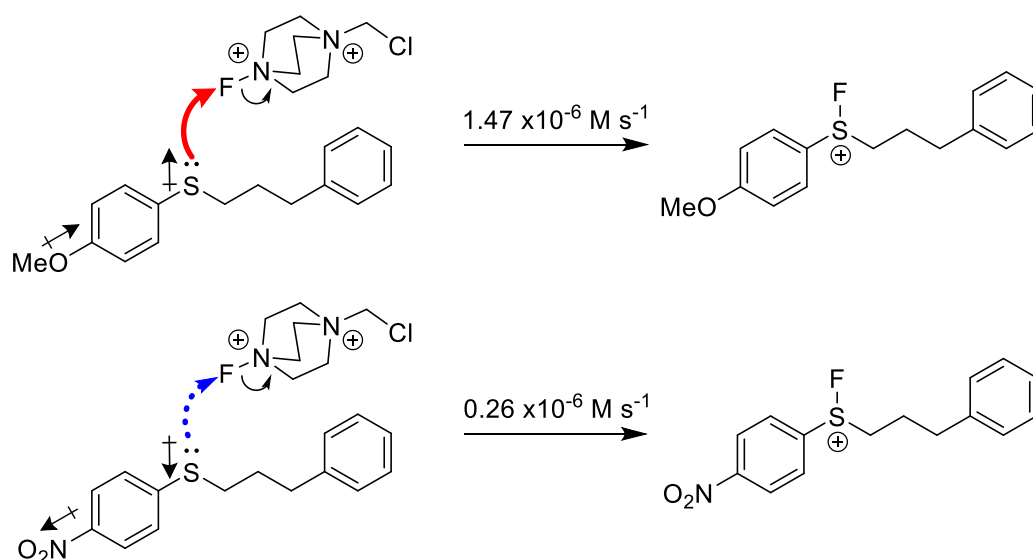
The *para*-substituted aromatic thioethers were subjected to the fluorination conditions and the yields of the geminal fluorination products are recorded in Table 4.4 below. Other by-products and the mono-fluorination (approx. -148 ppm) product have potentially been identified by <sup>19</sup>F NMR spectroscopy but were not isolated. There is limited literature data on the mono- and difluoro-products, therefore the monofluorinated product has been identified by comparison of similar chemical shifts in the <sup>19</sup>F NMR spectrum. This further highlights the rarity of the thiodifluoromethylene groups.

Entry	No.	Substrate	$\sigma^+$	Yield / %
1	4.64		-0.830	<sup>p</sup>
2	4.65		-0.268	42
3	4.66		-0.170	40
4	4.1		0.000	32
5	4.67		+0.227	29
6	4.68		+0.540	19
7	4.69		+0.778	8

Table 4.4. Yields of the difluorothiomethylene products from the *p*-substituted aromatic thioethers.

The electron-donating methoxy group (Entry 4.2, Table 4) resulted in an increase in the yield of the geminal fluorination product (42%) compared to the control **4.1** (32%, Entry 4.4, Table 4). This is likely due to the donation of the oxygen lone pair into the aromatic system which increases the electron density at the sulfur, making the sulfur lone pairs more nucleophilic and thus more reactive towards the electrophilic fluorine on Selectfluor<sup>TM</sup>. This is further supported by entries 3-7. The less electron-donating and more electron-withdrawing a group is, the lower the yield of the geminal difluoro-product is. An extreme example is the *p*-nitro group (Entry 4.7, Table 4) where the electron-withdrawing nature results in a much lower yield (8%) than the control (32%) and the other entries which have a greater degree of electron-donation (Scheme 4.18).

<sup>p</sup> Entry 1 Table 4; N-F (~40 ppm) was formed from the dimethylamine substrate.



Scheme 4.18. The initial nucleophilic attack of the sulfur lone pair on Selectfluor™.

The 4-dimethylamine derivative (Entry 4.1, Table 4) does not fluorinate when subjected to the electrophilic conditions. This is due to the amine present which has been known to complicate the fluorination reactions of previously tested substrates, most likely by acting as an alternative, more reactive nucleophile than the sulfur and abstracting the fluorine from Selectfluor™, the fluorinated product of which will be destroyed upon work-up.

#### 4.5.4 Hammett Plot

The kinetics of the reaction of the 4-substituted derivatives of **4.1** and Selectfluor™ were followed by  $^{19}\text{F}$  NMR spectroscopy. The rates of reaction were obtained for the formation of the difluoro-product and a Hammett plot made to determine the electronic impact on the geminal fluorination (Table 4.5 and Figure 4.11).

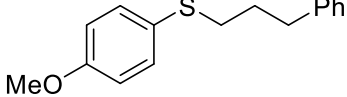
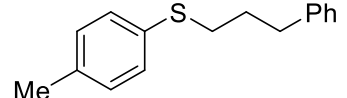
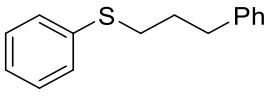
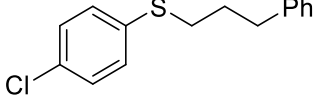
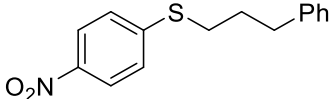
Entry	No.	Substrate	$\sigma$	Rate F2 / M s <sup>-1</sup> (10 <sup>-6</sup> )
1	4.65		-0.268	1.47
2	4.66		-0.170	1.06
3	4.1		0.000	0.80
4	4.67		+0.227	0.37
5	4.69		+0.778	0.26

Table 4.5. Rate of formation of difluoro-product.

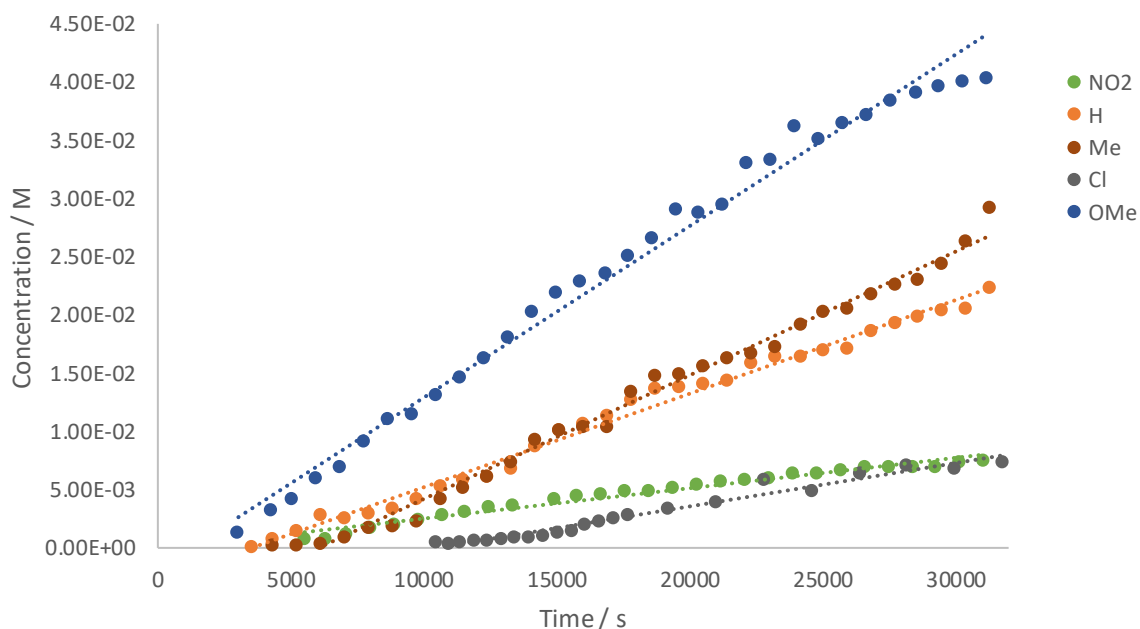


Figure 4.11. Concentration vs time for the *p*-substituted derivatives of 4.1.

The rates were calculated from where the steepest part of the graph occurs and before the plateau for each derivative. The trend in Table 4.5 was also reflected in the rate of reaction and further supported by the colour change of the reaction over time. The 4-methoxy derivative rapidly changes colour, from colourless to orange on addition of



the substrate to the Selectfluor<sup>TM</sup> in MeCN, on a timescale of seconds. Whereas the 4-nitro derivative changes colour on a timescale of approx. 5-10 minutes. The orange colour further supports the formation of the conjugated intermediate hypothesised in the mechanism.

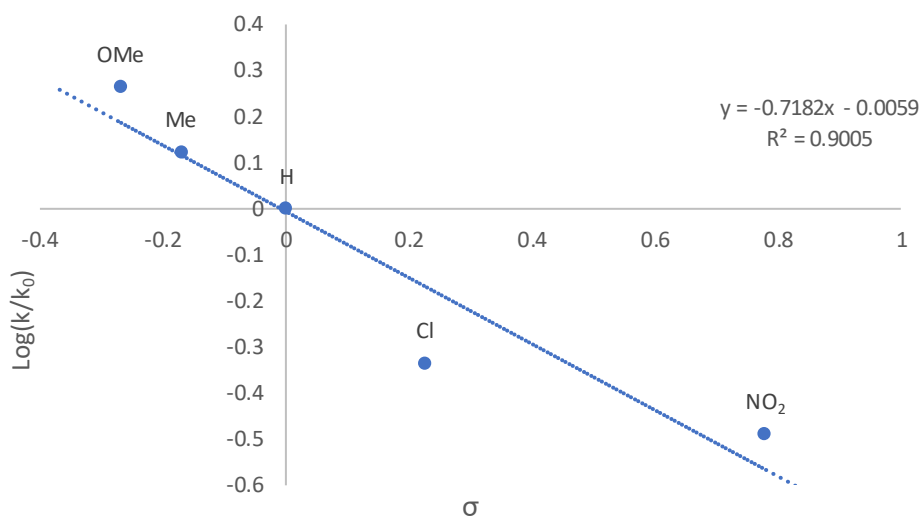
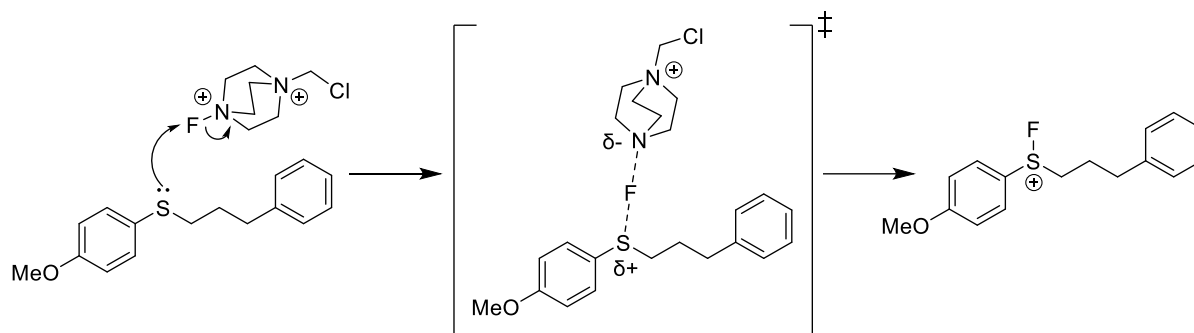


Figure 4.12. Hammett plot for the *p*-substituted derivatives of 4.1.

The linearity of the plot implies that the substituent constants ( $\sigma$ ) are correctly modelling electronic changes taking place in the reaction. The negative reaction constant ( $\rho$ ) value suggests that the formation of the geminal difluoro-product is assisted by a high electron density at the reaction site and that overall, a more electron deficient system is being produced as the reaction progresses. A greater degree of electron density would allow a rapid nucleophilic attack from the sulfur lone pair to the fluorine on Selectfluor<sup>TM</sup> and while this occurs a partial positive charge forms on the sulfur until the S-F bond is formed at which point sulfur has a full positive charge on the atom (Scheme 4.19). The modest size of  $\rho$  could be due to the charge being developed on the sulfur, where due to the large size of sulfur the positive charge is more diffuse.



Scheme 4.19. Formation of the transition state and the S-F bond.

The kinetic data and Hammett plot supports the proposed mechanism with the sulfur abstracting the fluorine from the Selectfluor™ which leads to an intramolecular fluorine migration. The increased electron density resulting from 4-methoxy and 4-methyl substitution led to a faster reaction than the phenyl derivative and those bearing electron-withdrawing substituents which also lends support to the proposed initial step in the mechanism. The formation of the S-F bond and the intramolecular fluorine migration is rapid, as the intermediates are not observed on the NMR timescale.

#### 4.5.5 Electron Rich Ring Systems

The increase yield from the *para*-methoxy derivative of **4.1** directed the investigation of the substrates towards ring systems which were electron-rich, such as those of di- and tri- methoxy and methyl substituted substrates.

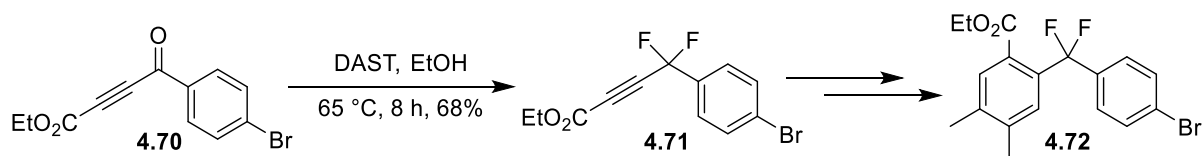
The yields of these derivatives led to trace amounts of the desired thiodifluoromethylene fluorinated products. The influence of the aromatic system is more complicated than originally hypothesised. This, along with the Hammett plot, suggests a potential ceiling effect with regards to the aromatic system. The derivatives which gave the higher yields of the difluoro-product had  $\sigma$  values between +0.227 (Cl) and -0.268 (OMe). Aromatic ring systems which would have a  $\sigma$  outside of this range may not fluorinate as well as previously thought. This could lead to computationally mapping the substrates and aiding in the identification of suitable substrates for this reaction.

## 4.6 Further Functionalisation

The difluoromethylene group has gained interest in the last decade, however less so relative to  $\text{CH}_2\text{F}$  and the trifluoromethylene group, with the potential for use within the areas of agrochemicals, the pharmaceuticals and even the fragrance industry.<sup>17</sup> The difluoromethylene group has the properties associated with a fluorine-containing group (detailed in Chapter 1) but has the advantages of being a bioisostere of hydroxyl, an ether oxygen and thiol groups. In addition, the difluoromethylene group in the terminal position on a chain has a slightly acidic hydrogen which can be incorporated into the design of bioactive molecules.<sup>1</sup>

The current synthetic methods of difluoromethylene groups are not so dissimilar from those of the synthesis of the thiodifluoromethylene group. The methods are, but not limited to, direct fluorination and using a  $\text{CF}_2\text{R}$  building block are the more common methods and a difluoroalkylation strategy.

Difluorination can be achieved using DAST on substrates which have a ketone group. Grée *et al* demonstrated this method in the preparation of *gem*-difluoro-bisarylic derivatives via a *gem*-difluoro-propargylic intermediate (Scheme 4.20).<sup>18</sup>



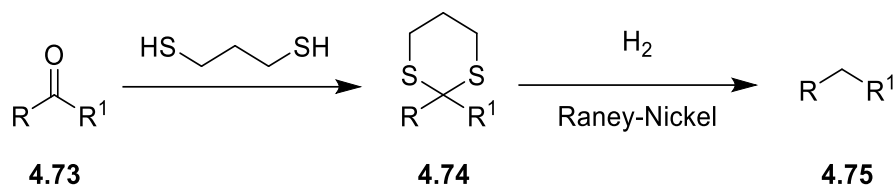
Scheme 4.20. Difluorination to synthesise *gem*-difluoro-bisarylic derivatives.

The thiodifluoromethylene group has the potential to be functionalised to desirable fluorine-containing functional groups.

### 4.6.1 Raney-Nickel Desulfurisation

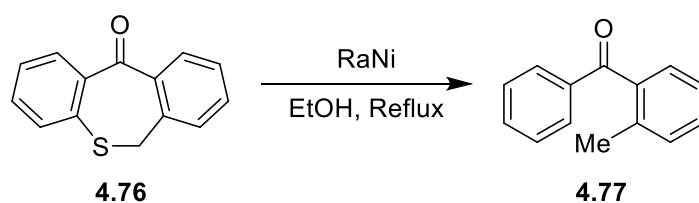
The thiodifluoromethylene group can be a precursor to other functional groups currently not readily attainable through direct fluorination methods. Desulfurisation using Raney-Nickel as a catalyst has been demonstrated, with the most common

example using thioacetals e.g. the last step of the Mozingo reduction (Scheme 4.21).<sup>19,20</sup>



Scheme 4.21. General Mozingo reduction. Formation of a thioacetal followed by desulfurisation to an alkane.

Dibenzo[*b,e*]thiepin-11(6*H*)-one **4.76** was subjected to the desulfurisation conditions using Raney-Nickel in EtOH, heated at reflux, in order to optimise the conditions for the geminal difluorination substrate **4.35** (Scheme 4.22).



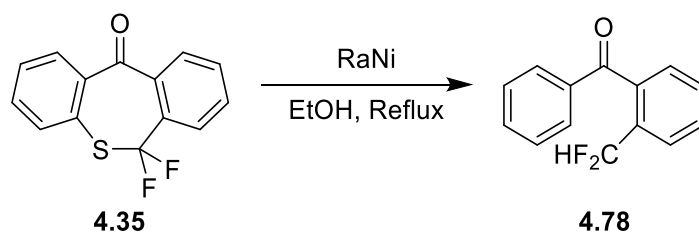
Scheme 4.22. Desulfurisation of **4.76** using Raney-Nickel.

An initial reaction using one equivalent of Raney-Nickel gave trace amounts of the desulfurisation product identified by both TLC and <sup>1</sup>H NMR spectroscopy after 24 h (Table 4.6). When this was left for 48 h only trace amounts were still evident by TLC and <sup>1</sup>H NMR spectroscopy. The loading of Raney-Nickel was increased to approx. 2-2.5 equivalents, which resulted in a conversion of 18% (**4.76** to **4.77**, calculated by <sup>1</sup>H NMR spectroscopy) after 24 h stirring while heating the mixture at reflux. An experiment was set-up where the reaction was monitored by <sup>1</sup>H NMR spectroscopy and GC-MS at intervals of 36, 48, 72 and 168 h (Table 4.6). The reaction reached a conversion of ~35% at 48 h which began to decrease after 1 week. This decrease in yield of **4.77** after 1 week was thought to be due to the over reduction of the carbonyl group of **4.76**, however, the over reduced product is absent from the <sup>1</sup>H NMR spectrum and appears in the GC-MS in trace amounts. The optimised timeframe in which the desulfurisation occurs is about 48 h.

Raney-Nickel Loading / equiv.	Time / h	Conversion / %	
		<sup>1</sup> H NMR	GCMS
1	24	<1	-
1	48	<1	-
2	36	29	18
2	48	36	35
2	72	32	36
2	168	32	29

Table 4.6. The %conversion of **4.76** to **4.77** over a period of 24-168 h.

Using the optimised timeframe, a desulfurisation reaction on the geminal difluoro-compound **4.35** was conducted. The reaction led trace amounts of **4.78** being formed (~4%), however, this is far from an optimised process and <sup>19</sup>F NMR analysis identified 4 other peaks. These compounds were not isolated but could be intermediates of the desulfurisation process.



Scheme 4.23. The desulfurisation reaction of **4.35** to **4.78**.

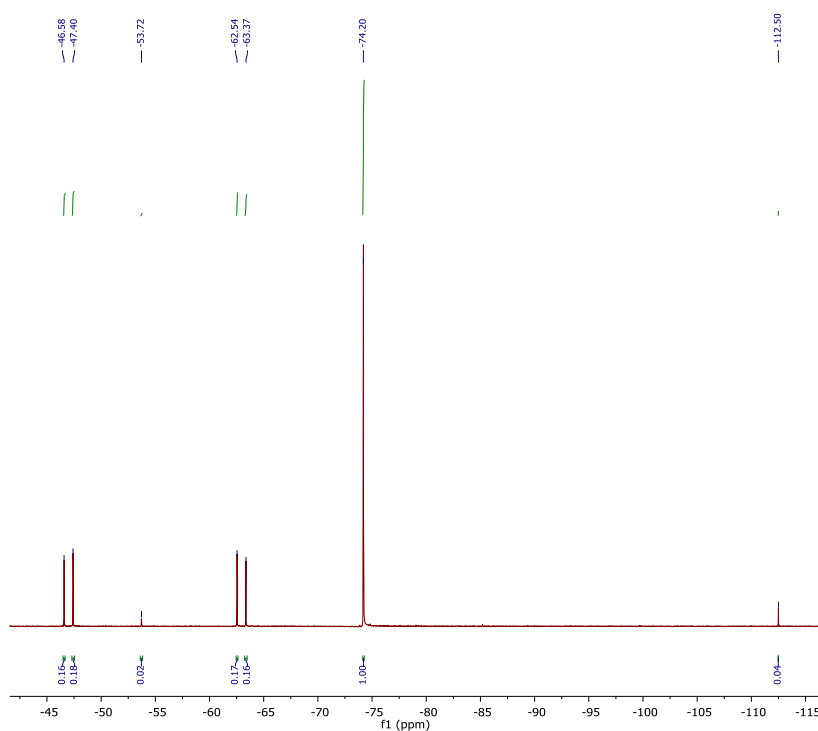


Figure 4.13.  $^{19}\text{F}$  NMR spectrum of the desulfurisation reaction of **4.35**.

Further work into the optimisation of the desulfurisation reaction is needed. An optimised reaction timeframe has been established; however, temperature and Raney-Nickel loading has not been optimised.

#### 4.7 Conclusion and Future Work

The serendipitous discovery of a thiodifluoromethylene group during the testing of sulfur containing substrates when using Selectfluor<sup>TM</sup> and  $\text{Fe}(\text{acac})_2$  complexes has led to the identification of a novel fluorination methodology. This process allows direct access to the thiodifluoromethylene group. Current synthetic methods are limited to a small selection of substrates and more often than not, require specialised equipment and harsh fluorinating conditions.

This chapter focused on two main areas: optimisation of the fluorination process to maximise the yield of the difluoro-product and identification of the mechanism. Early experiments highlighted that the iron (II) acetylacetonate has no role in the reaction allowing for a simple, yet elegant, process to be designed. With thorough degassed and an aerobic, anhydrous environment, moderate to excellent yields of a number of different thiodifluoromethylene groups can be obtained.

A mechanistic investigation into the reaction identified that thioarylethers are more suited to this reaction than other sulfur containing compounds, with the higher yields being associated with an electron-rich aromatic ring system adjacent to the sulfur. A Hammett plot illustrated that the electron rich ring of the *para*-methoxy derivative of **4.01** results in a higher yield compared to other derivatives.

A definitive mechanism has not been identified, while work described in this chapter has highlighted 3 potential routes, it is difficult to confirm which is preferential for the formation of the thiodifluoromethylene group. Further study into the mechanism is needed, which focus being on the use of sulfoxides as substrates. Sulfones have identified the requirement for a lone pair to be able to initiate the nucleophilic attack and fluorine abstraction from the Selectfluor<sup>TM</sup>, however sulfoxides are limited to the one lone pair.

Reactions have been conducted into investigating further functionalisation. This early stage of research focused on the desulfurisation of **4.76** and the fluorinated derivative. The fluorinated derivative **4.35** has showed promising early results however, research moving forward would look to optimise this process and allow access to structurally difficult to obtain CF<sub>2</sub> groups. Preliminary reactions have been conducted into investigating further functionalisation using selenium containing compounds, however results have shown the selenium compounds not to fluorinate.

The next step would be to investigate other functionalisation methods, such as oxidation of the sulfur of the fluorinated compounds to sulfoxides or sulfones. There is a variety of chemical conversions which utilise these species. This would open up synthetic routes to a variety of compounds, using the simple thiodifluoromethylene group as the starting building block.

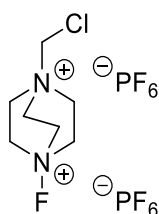
## 4.8 Chapter 4 Experimental

Starting materials were purchased from commercial sources and were used without further purification.  $^1\text{H}$ ,  $^{13}\text{C}$  and  $^{19}\text{F}$  NMR spectra were recorded using Bruker Avance II 400 MHz and Bruker Avance III 300 MHz spectrometer, with a residual protic solvent used as the reference for  $^1\text{H}$  and  $^{13}\text{C}$  NMR spectroscopy and an external reference of  $\text{CFCl}_3$  for  $^{19}\text{F}$  NMR studies. Infrared spectroscopy were recorded using Varian 800 FT-IR spectrometer. Melting points were recorded on a Gallenkamp MF-370 melting point apparatus and are uncorrected. LCMS data was recorded on an LCMS Agilent Infinity II R90 UPLC + MSD XT instrument and HRMS data was recorded on a LCMS/MS (QToF) Waters Acquity UPLC + Xevo G2-XS instrument.

Acetonitrile was dried using 3 Å molecular sieves and degassed via freeze-pump-thaw and stored under nitrogen prior to use. The water content was measured (in ppm) using Karl-Fischer Coulometry. Acetonitrile used in the reactions was between 10-80 ppm water content. Solvents used in the synthesis of  $\text{Fe}(\text{acac})_2$  were dried using 3 Å molecular sieves and degassed overnight prior to use and stored under  $\text{N}_2$ . Iron (II) chloride tetrahydrate was bought in fresh and immediately transferred to a Schlenk flask.

### 1-Chloromethyl-4-fluoro-1,4-diazoniabicyclo[2.2.2]octane bis(hexafluorophosphate)

#### 4.39<sup>21</sup>



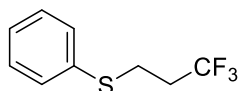
1-Chloromethyl-4-fluoro-1,4-diazoniabicyclo[2.2.2]octane bis(tetrafluoroborate) (1.00 g, 3.00 mmol) was added to water (9 mL) and stirred at RT until dissolved. Ammonium hexafluorophosphate (2.93 g, 18.0 mmol) was added and the reaction was stirred at RT for 2 h. The white precipitate was filtered and then washed with water (5 × 5 mL) and then with diethyl ether (10 mL) to afford the product as a white powder (1.34 g, 2.98 mmol, 100%).  $\nu_{\text{max}}$  (neat/ $\text{cm}^{-1}$ ) 3068, 1470, 1379, 1009, 815, 555, 491, 416  $\text{cm}^{-1}$ ;  $^1\text{H}$  NMR (300 MHz,  $\text{CD}_3\text{CN}$ )  $\delta_{\text{H}}$  5.31 (2H, s,  $\text{CH}_2$ ), 4.72 (6H, dt,  $J = 7.6, 7.2$  Hz,  $\text{CH}_2$ )



4.27 (6H, t,  $J = 7.6$  Hz, CH<sub>2</sub>) ppm; <sup>19</sup>F NMR (300 MHz, CDCl<sub>3</sub>)  $\delta_F$  47.9 (1F, s, NF), -72.8 (12F, d,  $J = 704$  Hz, PF<sub>6</sub>) ppm; <sup>31</sup>P NMR (300 MHz, CDCl<sub>3</sub>)  $\delta_P$  -144.6 (2P, heptet,  $J = 726$  Hz) ppm.

*Analytical data corresponds with the literature*<sup>21</sup>

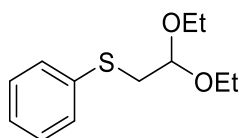
#### Phenyl-3,3,3-trifluoropropyl sulfide 4.55



To a solution of thiophenol (0.46 mL, 4.54 mmol) and triethylamine (0.76 mL, 5.44 mmol) in DCM (10 mL) at 0 °C under an N<sub>2</sub> atmosphere, 1-iodo-3,3,3-trifluoropropane (0.57 mL, 4.99 mmol) was added and the reaction was slowly warmed to RT and left to stir for 24 h. The reaction mixture was poured into ethyl acetate (20 mL) and washed with water (2 × 20 mL), dried with MgSO<sub>4</sub> and the solvent was removed *in vacuo* giving a pale yellow oil (0.88 g, 4.27 mmol, 94%).  $\nu_{\max}$  (neat/cm<sup>-1</sup>) 3070, 2942, 1584, 1481, 1440, 1366, 1237, 1134, 1084, 954, 736, 689, 638 cm<sup>-1</sup>; <sup>1</sup>H NMR (300 MHz, CDCl<sub>3</sub>)  $\delta_H$  7.30-7.20 (4H, m, aromatic H), 7.19-7.12 (1H, m, aromatic H), 3.03 – 2.92 (2H, m, SCH<sub>2</sub>), 2.44 – 2.26 (2H, m, CH<sub>2</sub>CF<sub>3</sub>) ppm; <sup>19</sup>F NMR (300 MHz, CDCl<sub>3</sub>)  $\delta_F$  -66.4 (3F, t,  $J = 10.6$  Hz, CF<sub>3</sub>) ppm.

*Analytical data corresponds with the literature*<sup>22</sup>

#### (Phenylthio)acetaldehyde diethyl acetal 4.57

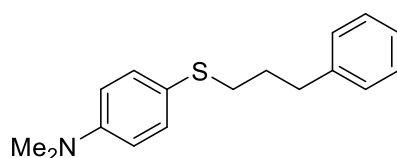


To a solution of thiophenol (0.46 mL, 4.54 mmol) and triethylamine (0.76 mL, 5.44 mmol) in DCM (10 mL) at 0 °C under an N<sub>2</sub> atmosphere, bromoacetaldehyde diethyl acetal (0.75 mL, 4.99 mmol) was added and the reaction was slowly warmed to RT and left to stir for 24 h (Additional DCM (5 mL) was added after 3 h). The reaction mixture was poured into ethyl acetate (20 mL) and washed with water (2 × 20 mL), dried with MgSO<sub>4</sub> and the solvent was removed *in vacuo* giving a colourless oil in a

quantitative yield (1.03 g, 4.54 mmol, 100%).  $\nu_{\max}$  (neat/cm<sup>-1</sup>) 2976, 2881, 1737, 1583, 1439, 1124, 1054, 1023, 737, 688, 474 cm<sup>-1</sup>; <sup>1</sup>H NMR (300 MHz, CDCl<sub>3</sub>)  $\delta_{\text{H}}$  7.33 (2H, d,  $J$  = 8.9 Hz, aromatic H), 7.22 – 7.17 (3H, m, aromatic H), 4.58 (1H, t,  $J$  = 6.4 Hz, CH), 3.64 – 3.54 (2H, m, OCH<sub>2</sub>), 3.55 – 3.45 (2H, m, OCH<sub>2</sub>), 3.28 (2H, d,  $J$  = 5.4 Hz, SCH<sub>2</sub>), 1.15 (6H, t,  $J$  = 7.1 Hz, CH<sub>3</sub>) ppm.

*Analytical data corresponds with the literature*<sup>23</sup>

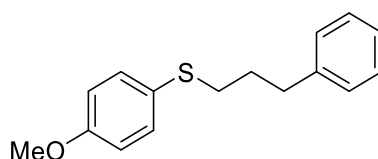
#### *N,N*-Dimethyl-4-((3-phenylpropyl)thio)aniline 4.64



To a solution of 4-(dimethylamino)thiophenol (1.03 g, 6.72 mmol) and triethylamine (1.08 mL, 7.73 mmol) in DCM (25 mL) at 40 °C under an N<sub>2</sub> atmosphere, 3-phenylpropyl bromide (1.08 mL, 7.61 mmol) was added and the reaction was left to stir for 72 h. The reaction was monitored by TLC and on completion the mixture was poured into ethyl acetate (20 mL) and washed with water (2 × 20 mL), dried with MgSO<sub>4</sub> and the solvent was removed *in vacuo* giving an orange oil. The pure product was isolated by column chromatography (9:1 petrol:EtOAc) giving a yellow oil (1.00 g, 3.68 mmol, 55%).  $R_f$  0.64 (9:1 petrol:EtOAc). <sup>1</sup>H NMR (300 MHz, CDCl<sub>3</sub>)  $\delta_{\text{H}}$  7.37 -7.00 (9H, m, aromatic H), 2.80 (6H, s, NMe<sub>2</sub>), 2.66 (2H, t,  $J$  = 7.4 Hz, SCH<sub>2</sub>), 2.61 (2H, t,  $J$  = 7.8 Hz, CH<sub>2</sub>Ph), 1.77 (2H, pent.,  $J$  = 7.8 Hz, CH<sub>2</sub>) ppm.

*Isolated material has <sup>1</sup>H NMR similar to that of other para-substituted compounds synthesised which corresponded with the literature.*

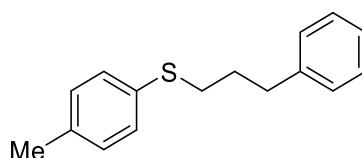
(4-Methoxyphenyl)(3-phenylpropyl)sulfane 4.65



To a solution of 4-methoxythiophenol (0.90 g, 6.44 mmol) and triethylamine (1.08 mL, 7.73 mmol) in DCM (25 mL) at 40°C under an N<sub>2</sub> atmosphere, 3-phenylpropyl bromide (1.08 mL, 7.61 mmol) was added and the reaction was left to stir for 36 h. The reaction was monitored by TLC and on completion the mixture was poured into ethyl acetate (20 mL) and washed with water (2 × 20 mL), dried with MgSO<sub>4</sub> and the solvent was removed *in vacuo* giving an orange oil. The pure product was isolated by column chromatography (Diethyl ether) giving a (1.34 g, 5.19 mmol, 81%). R<sub>f</sub> 0.51 (diethyl ether). <sup>1</sup>H NMR (300 MHz, CDCl<sub>3</sub>) δ<sub>H</sub> 7.25 – 7.18 (2H, m, aromatic H), 7.18 – 7.11 (2H, m, aromatic H), 7.10 – 7.00 (3H, m, aromatic H), 6.74 – 6.67 (2H, m, aromatic H), 3.64 (3H, s, OMe), 2.70 (2H, t, *J* = 7.0 Hz, SCH<sub>2</sub>), 2.61 (2H, t, *J* = 7.4 Hz, CH<sub>2</sub>Ph), 1.78 (2H, pent., *J* = 7.7 Hz, CH<sub>2</sub>) ppm.

*Analytical data corresponds with the literature*<sup>24</sup>

(3-Phenylpropyl)(*p*-tolyl)sulfane 4.66

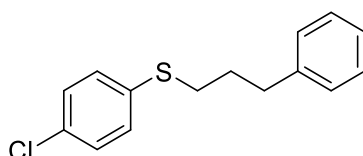


To a solution of 4-methylthiophenol (2.02 g, 16.10 mmol) and triethylamine (2.69 mL, 19.30 mmol) in DCM (35 mL) at 40°C under an N<sub>2</sub> atmosphere, 3-phenylpropyl bromide (2.93 mL, 19.30 mmol) was added and the reaction was left to stir for 36 h. The reaction was monitored by TLC and on completion the mixture was poured into ethyl acetate (20 mL) and washed with water (2 × 20 mL), dried with MgSO<sub>4</sub> and the solvent was removed *in vacuo* giving an yellow oil. The pure product was isolated by column chromatography (Diethyl ether) giving a (3.20 g, 13.20 mmol, 82%). R<sub>f</sub> 0.78 (diethyl ether). <sup>1</sup>H NMR (300 MHz, CDCl<sub>3</sub>) δ<sub>H</sub> 7.18 – 7.10 (4H, m, aromatic H), 7.09 –

7.02 (3H, m, aromatic H), 7.02 – 6.95 (2H, m, aromatic H), 2.21 (3H, s, Me), 2.77 (2H, t,  $J = 7.2$  Hz, SCH<sub>2</sub>), 2.64 (2H, t,  $J = 7.8$  Hz, CH<sub>2</sub>Ph), 1.84 (2H, pent.,  $J = 7.7$  Hz, CH<sub>2</sub>) ppm.

*Analytical data corresponds with the literature*<sup>24</sup>

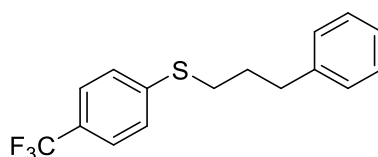
(4-Chlorophenyl)(3-phenylpropyl)sulfane 4.67



To a solution of 4-chlorothiophenol (1.00 g, 6.91 mmol) and triethylamine (1.16 mL, 8.30 mmol) in DCM (10 mL) at 0 °C under an N<sub>2</sub> atmosphere, 3-phenylpropyl bromide (1.08 mL, 7.61 mmol) was added and the reaction was slowly warmed to RT and left to stir for 48 h (Additional DCM (5 mL) was added after 6 h). The reaction was monitored by TLC and on completion the mixture was poured into ethyl acetate (20 mL) and washed with water (2 × 20 mL), dried with MgSO<sub>4</sub> and the solvent was removed *in vacuo* giving an orange oil. The pure product was isolated by column chromatography (petrol 40-60) to give a yellow oil (1.34 g, 5.10 mmol, 74%). R<sub>f</sub> 0.58 (petrol 40-60) <sup>1</sup>H NMR (300 MHz, CDCl<sub>3</sub>) δ<sub>H</sub> 7.38-7.30 (3H, m, aromatic H), 7.29-7.24 (5H, m, aromatic H), 7.23-7.17 (2H, m, aromatic H), 2.92 (2H, t,  $J = 7.7$  Hz, SCH<sub>2</sub>), 2.79 (2H, t,  $J = 7.0$  Hz, CH<sub>2</sub>Ph), 1.99 (2H, pent.,  $J = 7.0$  Hz, CH<sub>2</sub>) ppm; *m/z* (LCMS MS ES+) 262.1 [M]<sup>+</sup>. Found: [M+H]<sup>+</sup>, 263.1

*Analytical data corresponds with the literature*<sup>24</sup>

(3-Phenylpropyl)(4-trifluoromethyl)phenyl)sulfane 4.68

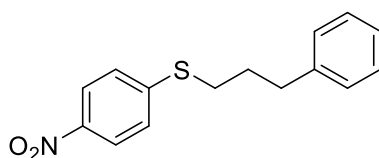


To a solution of 4-methoxythiophenol (0.77 mL, 5.61 mmol) and triethylamine (1.08 mL, 7.73 mmol) in DCM (25 mL) at 40°C under an N<sub>2</sub> atmosphere, 3-phenylpropyl

bromide (1.08 mL, 7.61 mmol) was added and the reaction was left to stir for 48 h. The reaction was monitored by TLC and on completion the mixture was poured into ethyl acetate (20 mL) and washed with water (2 × 20 mL), dried with MgSO<sub>4</sub> and the solvent was removed *in vacuo* giving an orange oil. The pure product was isolated by a silica plug (100% diethyl ether) then allowing the oil to settle and evaporate giving white crystals (1.18 g, 3.98 mmol, 71%). R<sub>f</sub> 0.86 (diethyl ether). <sup>1</sup>H NMR (300 MHz, CDCl<sub>3</sub>) δ<sub>H</sub> 7.46 – 7.29 (3H, m, aromatic H), 7.20 – 7.12 (4H, m, aromatic H), 7.12 – 7.02 (3H, m, aromatic H), 2.82 (2H, t, *J* = 7.1 Hz, SCH<sub>2</sub>), 2.64 (2H, t, *J* = 7.3 Hz, CH<sub>2</sub>Ph), 1.87 (2H, pent., *J* = 7.3 Hz, CH<sub>2</sub>) ppm; <sup>19</sup>F NMR (300 MHz, CDCl<sub>3</sub>) δ<sub>F</sub> -62.6 (3F, s, CF<sub>3</sub>) ppm.

*Analytical data corresponds with the literature*<sup>25</sup>

(4-Nitrophenyl)(3-phenylpropyl)sulfane 4.69



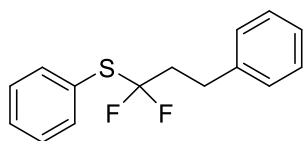
To a solution of 4-nitrothiophenol (1.00 g, 6.44 mmol) and triethylamine (1.08 mL, 7.73 mmol) in DCM (10 mL) at 0 °C under an N<sub>2</sub> atmosphere, 3-phenylpropyl bromide (1.08 mL, 7.09 mmol) was added and the reaction was slowly warmed to RT and left to stir for 24 h. The reaction was monitored by TLC and on completion the mixture was poured into ethyl acetate (20 mL) and washed with water (2 × 20 mL), dried with MgSO<sub>4</sub> and the solvent was removed *in vacuo* giving a yellow solid (1.76 g, 6.44 mmol, 100%)  $\nu_{\text{max}}$  (neat/cm<sup>-1</sup>) 2933, 1571, 1501, 1334, 1069, 835, 738, 700, 497 cm<sup>-1</sup>; <sup>1</sup>H NMR (300 MHz, CDCl<sub>3</sub>) δ<sub>H</sub> 8.02 (2H, d, *J* = 9 Hz, aromatic H), 7.29-7.08 (7H, m, aromatic H), 2.93 (2H, t, *J* = 7.2 Hz, SCH<sub>2</sub>), 2.72 (2H, t, *J* = 7.2 Hz, CH<sub>2</sub>Ph), 1.97 (2H, pent., *J* = 7.5, CH<sub>2</sub>) ppm.

*Analytical data corresponds with the literature*<sup>25</sup>

### General Procedure for the Synthesis of Thiodifluoromethylene Group

To an oven-dried Schlenk flask under an N<sub>2</sub> atmosphere, Selectfluor (0.55 mmol) was added followed by degassed anhydrous MeCN (2 mL). The Selectfluor was allowed to dissolve then substrate (0.25 mmol) was added and the reaction was left to stir for 24 h at room temperature. DCM (25 mL) was added and the reaction as washed with water (2 × 25 mL), dried with MgSO<sub>4</sub> and the solvent removed *in vacuo*. The crude mixture was redissolved in deuterated solvent and an internal standard of pentafluorotoluene (25 μL, 0.395 M) was added.

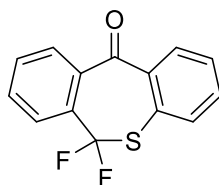
### (1,1-Difluoro-3-phenylpropyl)phenyl sulfane 4.33



<sup>1</sup>H NMR (300 MHz, CDCl<sub>3</sub>) δ<sub>H</sub> 7.29 (2H, d, *J* = 7.1 Hz, aromatic H), 7.24 – 7.15 (4H, m, aromatic H), 7.15 – 7.02 (4H, m, aromatic H), 2.82 (2H, m, SCF<sub>2</sub>CH<sub>2</sub>), 2.30 (2H, m, CH<sub>2</sub>Ph) ppm; <sup>13</sup>C NMR (300 MHz, CDCl<sub>3</sub>) δ<sub>C</sub> 139.6, 136.3, 130.2, 129.6 (t, *J* = 4.3 Hz), 129.0, 128.8, 128.3, 127.1, 126.4, 40.2 (t, *J* = 24.5 Hz), 29.1 (t, *J* = 4.2 Hz) ppm; <sup>19</sup>F NMR (300 MHz, CDCl<sub>3</sub>) δ<sub>F</sub> -73.1 (2F, t, *J* = 14.3 Hz, CF<sub>2</sub>S) ppm.

*Analytical data corresponds with the literature*<sup>26</sup>

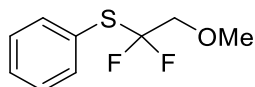
### 6,6-Difluorodibenzo[*b,e*]thiepin-11(6*H*)-one 4.35



Orange solid (2.58 g, 9.84 mmol, 73%). R<sub>f</sub> 0.64 (50:50 DCM:Petrol). ν<sub>max</sub> (neat/cm<sup>-1</sup>) 3065, 1659, 1283, 1026, 925, 753, 729 cm<sup>-1</sup>; <sup>1</sup>H NMR (300 MHz, CDCl<sub>3</sub>) δ<sub>H</sub> 8.08 (1 H, dd, *J* = 7.9, 1.6 Hz, aromatic H), 7.74 (1H, d, *J* = 7.7 Hz, aromatic H), 7.62 (2H, d, *J* = 3.9 Hz, aromatic H), 7.58 – 7.53 (1H, m, aromatic H), 7.53 – 7.45 (1H, dd, *J* = 7.7, 2.0 Hz, aromatic H), 7.39 (1H, dd, *J* = 7.9, 1.5 Hz, aromatic H), 7.35 – 7.24 (1H, m,

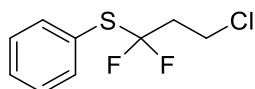
aromatic H) ppm;  $^{13}\text{C}$  NMR (300 MHz,  $\text{CDCl}_3$ )  $\delta_{\text{C}}$  194.4, 136.5, 135.5, 130.2 (t,  $J = 4.7$  Hz), 132.8, 131.8, 131.7, 130.9, 129.7, 129.2, 127.3, 126.4, 122.7, 121.25 (t,  $J = 7.3$  Hz) ppm;  $^{19}\text{F}$  NMR (300 MHz,  $\text{CDCl}_3$ )  $\delta_{\text{F}}$  -74.4 (2F, s,  $\text{CF}_2\text{S}$ ) ppm;  $m/z$  (LCMS MS ES+) 262.0  $[\text{M}]^+$ . Found:  $[\text{M}+\text{H}]^+$ , 263.0

(1,1-Difluoro-2-methoxyethyl)(phenyl)sulfane 4.79



37% by  $^{19}\text{F}$  NMR (pentafluorotoluene internal standard (25  $\mu\text{L}$ , 0.395 M); Rf 0.89 (1:9 EtOAc:Petrol).  $^1\text{H}$  NMR (300 MHz,  $\text{CDCl}_3$ )  $\delta_{\text{H}}$  7.57 (2H, d,  $J = 6.8$  Hz, aromatic H), 7.42-7.27 (3H, m, aromatic H), 3.66 (2H, t,  $J = 11.7$  Hz,  $\text{CH}_2$ ), 3.42 (3H, s,  $\text{CH}_3$ ) ppm;  $^{13}\text{C}$  NMR (300 MHz,  $\text{CDCl}_3$ )  $\delta_{\text{C}}$  136.5, 130.0, 129.1, 128.0 (t,  $J = 279.0$  Hz,  $\text{CF}_2$ ) 126.2 (t,  $J = 2.8$  Hz, quat. C), 73.9 (t,  $J = 29.5$  Hz,  $\text{CH}_2$ ), 60.1 ppm;  $^{19}\text{F}$  NMR (300 MHz,  $\text{CDCl}_3$ )  $\delta_{\text{F}}$  -80.4 (2F, t,  $J = 11.7$  Hz,  $\text{SCF}_2$ ) ppm;  $m/z$  (LCMS MS ES+) 204.0  $[\text{M}]^+$ . Found:  $[\text{M}+\text{H}]^+$ , 205.1.

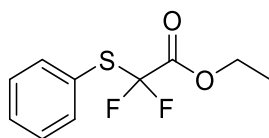
(3-Chloro-1,1-difluoropropyl)(phenyl)sulfane 4.80



9% by  $^{19}\text{F}$  NMR (pentafluorotoluene internal standard (25  $\mu\text{L}$ , 0.395 M); Rf 0.94 (1:9 EtOAc:Petrol).  $^1\text{H}$  NMR (300 MHz,  $\text{CDCl}_3$ )  $\delta_{\text{H}}$  7.63 (2H, d,  $J = 6.6$  Hz, aromatic H), 7.49-7.38 (3H, m, aromatic H), 3.71 (2H, t,  $J = 8.1$  Hz,  $\text{CH}_2\text{Cl}$ ), 2.62 (2H, tt,  $J = 22.0$ , 13.9, 8.1 Hz,  $\text{CF}_2\text{CH}_2$ ) ppm;  $^{13}\text{C}$  NMR (300 MHz,  $\text{CDCl}_3$ )  $\delta_{\text{C}}$  136.2, 130.1, 129.2, 128.0 (t,  $J = 293.6$  Hz,  $\text{CF}_2$ ), 126.2, 41.7 (t,  $J = 24.4$ ,  $\text{CH}_2$ ), 36.9 (t,  $J = 5.0$  Hz,  $\text{CH}_2\text{Cl}$ ) ppm;  $^{19}\text{F}$  NMR (300 MHz,  $\text{CDCl}_3$ )  $\delta_{\text{F}}$  -72.9 (2F, t,  $J = 14.4$  Hz,  $\text{SCF}_2$ ) ppm.

*An attempt at obtaining mass spectrometry data was conducted but was not successful.*

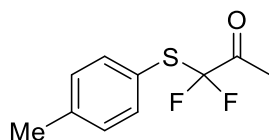
Ethyl 2,2-difluoro-2-(phenylthio)acetate 4.81



13% by  $^{19}\text{F}$  NMR (pentafluorotoluene internal standard (25  $\mu\text{L}$ , 0.395 M);  $^1\text{H}$  NMR (300 MHz,  $\text{CDCl}_3$ )  $\delta_{\text{H}}$  7.62 (2H, d,  $J = 6.7$  Hz, aromatic H), 7.52 (1H, t,  $J = 7.2$  Hz, aromatic H), 7.45 (2H, d,  $J = 8.43$  Hz, aromatic H), 4.25 (2H, q,  $J = 7.3$  Hz,  $\text{CH}_2$ ), 1.26 (3H, t,  $J = 6.9$  Hz,  $\text{CH}_3$ ) ppm;  $^{19}\text{F}$  NMR (300 MHz,  $\text{CDCl}_3$ )  $\delta_{\text{F}}$  -77.1 (2F, s,  $\text{SCF}_2$ ) ppm.

*Analytical data corresponds with the literature<sup>12</sup>*

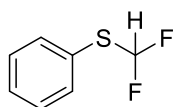
1,1-Difluoro-1-(*p*-tolylthio)propan-2-one 4.82



15% by  $^{19}\text{F}$  NMR (pentafluorotoluene internal standard (25  $\mu\text{L}$ , 0.395 M);  $^1\text{H}$  NMR (300 MHz,  $\text{CDCl}_3$ )  $\delta_{\text{H}}$  7.38 (2H, d,  $J = 8.1$  Hz, aromatic H), 7.12 (2H, d,  $J = 8.0$  Hz), 2.30 (3H, s,  $\text{CH}_3$ ), 2.24 (3H, s,  $\text{CH}_3$ ) ppm;  $^{19}\text{F}$  NMR (300 MHz,  $\text{CDCl}_3$ )  $\delta_{\text{F}}$  -86.1 (2F, s, Hz,  $\text{SCF}_2$ ) ppm.

*Analytical data is similar to that of the para-H derivative within the literature.<sup>27</sup>*

(Difluoromethyl)(phenyl)sulfane 4.83

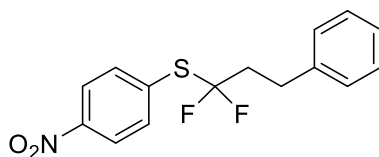


6% by  $^{19}\text{F}$  NMR (pentafluorotoluene internal standard (25  $\mu\text{L}$ , 0.395 M);  $^1\text{H}$  NMR (300 MHz,  $\text{CDCl}_3$ )  $\delta_{\text{H}}$  7.62 (2H, d,  $J = 7.6$  Hz, aromatic H), 7.43 (2H, d,  $J = 7.9$  Hz, aromatic H), 7.34 (1H, t,  $J = 7.3$  Hz, aromatic H), 6.76 (1H, t,  $J = 56.2$  Hz,  $\text{SF}_2\text{H}$ ) ppm;  $^{19}\text{F}$  NMR (300 MHz,  $\text{CDCl}_3$ )  $\delta_{\text{F}}$  -91.4 (2F, d,  $J = 51.1$  Hz,  $\text{SCF}_2$ ) ppm.

*Analytical data corresponds with the literature<sup>28</sup>*

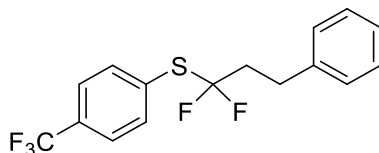


(1,1-Difluoro-3-phenylpropyl)(4-nitrophenyl)sulfane **4.84**



8% by  $^{19}\text{F}$  NMR (pentafluorotoluene internal standard (25  $\mu\text{L}$ , 0.395 M); Rf 0.94 (1:9 EtOAc:Petrol).  $^1\text{H}$  NMR (300 MHz,  $\text{CDCl}_3$ )  $\delta_{\text{H}}$  8.25 (2H, d,  $J = 8.9$  Hz, aromatic H), 7.80 (2H, d,  $J = 8.8$  Hz, aromatic H), 7.37-7.30 (2H, m, aromatic H), 7.29-7.19 (4H, m, aromatic H), 2.95 (2H, tt,  $J = 8.3, 3.0$  Hz,  $\text{CH}_2\text{Ph}$ ), 2.59-2.42 (2H, m,  $\text{SCF}_2\text{CH}_2$ ) ppm;  $^{19}\text{F}$  NMR (300 MHz,  $\text{CDCl}_3$ )  $\delta_{\text{F}}$  -71.7 (2F, t,  $J = 14.7$  Hz,  $\text{SCF}_2$ ) ppm;  $m/z$  (LCMS MS ES+) 273.1  $[\text{M}]^+$ . Found:  $[\text{M}+\text{H}]^+$ , 274.1.

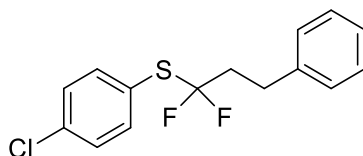
(1,1-Difluoro-3-phenylpropyl)(4-trifluoromethylphenyl)sulfane **4.85**



19% by  $^{19}\text{F}$  NMR (pentafluorotoluene internal standard (25  $\mu\text{L}$ , 0.395 M); Rf 0.90 (1:9 EtOAc:Petrol).  $^1\text{H}$  NMR (300 MHz,  $\text{CDCl}_3$ )  $\delta_{\text{H}}$  7.66 (2H, d,  $J = 9.4$  Hz, aromatic H), 7.55 (2H, d,  $J = 7.5$ , aromatic H), 7.29-7.07 (5H, m, aromatic H), 2.87 – 2.80 (2H, m,  $\text{CH}_2\text{Ph}$ ), 2.40 – 2.35 (2H, m,  $\text{SCF}_2\text{CH}_2$ ) ppm;  $^{19}\text{F}$  NMR (300 MHz,  $\text{CDCl}_3$ )  $\delta_{\text{F}}$  -62.9 (3F, s,  $\text{CF}_3$ ), -72.3 (2F, t,  $\text{SCF}_2$ ) ppm.

*Analytical data fits with proposed structure and is similar to **4.33** and **4.84** (and **4.86**, **4.87** and **4.88**) suggesting a similar structure. Preparative TLC was used to isolate enough material for NMR calibration and testing for Hammett plot experiments therefore mass spectrometry data was not obtained.*

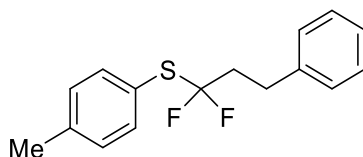
(1,1-Difluoro-3-phenylpropyl)(4-chlorophenyl)sulfane 4.86



29% by  $^{19}\text{F}$  NMR (pentafluorotoluene internal standard (25  $\mu\text{L}$ , 0.395 M);  $R_f$  0.97 (1:9 EtOAc:Petrol).  $^1\text{H}$  NMR (300 MHz,  $\text{CDCl}_3$ )  $\delta_{\text{H}}$  7.48 (2H, d,  $J = 8.9$  Hz, aromatic H), 7.24-7.08 (7H, m, aromatic H), 2.83 (2H, m,  $\text{CH}_2\text{Ph}$ ), 2.33 (2H, m,  $\text{SCF}_2\text{CH}_2$ ) ppm;  $^{13}\text{C}$  NMR (300 MHz,  $\text{CDCl}_3$ )  $\delta_{\text{C}}$  136.2, 130.9, 130.1, 129.2, 128.0 (t,  $J = 275.1$  Hz,  $\text{CF}_2$ ), 126.2, 41.7 (t,  $J = 24$  Hz,  $\text{CH}_2$ ), 36.9 (t,  $J = 5.9$  Hz) ppm;  $^{19}\text{F}$  NMR (300 MHz,  $\text{CDCl}_3$ )  $\delta_{\text{F}}$  -73.1 (2F, t,  $\text{SCF}_2$ ) ppm.

*Analytical data fits with proposed structure and is similar to 4.33 and 4.84 (and 4.85, 4.87 and 4.88) suggesting a similar structure. Preparative TLC was used to isolate enough material for NMR calibration and testing for Hammett plot experiments therefore mass spectrometry data was not obtained.*

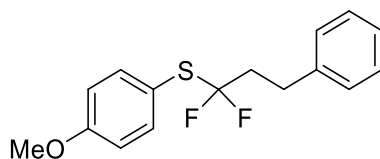
(1,1-Difluoro-3-phenylpropyl)(4-methylphenyl)sulfane 4.87



40% by  $^{19}\text{F}$  NMR (pentafluorotoluene internal standard (25  $\mu\text{L}$ , 0.395 M);  $R_f$  0.96 (9:1 Petrol:EtOAc).  $^1\text{H}$  NMR (300 MHz,  $\text{CDCl}_3$ )  $\delta_{\text{H}}$  7.43 (2H, d,  $J = 8.1$  Hz, aromatic H), 7.20 (2H, d,  $J = 7.2$  Hz, aromatic H), 7.17 – 7.06 (5H, m, aromatic H), 2.83 (2H, m,  $\text{CH}_2\text{Ph}$ ), 2.41 – 2.19 (2H, m,  $\text{SCF}_2\text{CH}_2$ ), 2.29 (3H, s, Me) ppm;  $^{13}\text{C}$  NMR (300 MHz,  $\text{CDCl}_3$ )  $\delta_{\text{C}}$  140.2, 136.2, 129.5 (t,  $J = 277.9$  Hz,  $\text{CF}_2$ ), 128.6, 128.4, 126.2, 41.3 (t,  $J = 24.3$  Hz,  $\text{CH}_2$ ), 29.4 (t,  $J = 3.9$  Hz,  $\text{CH}_2$ ), 21.2 ppm;  $^{19}\text{F}$  NMR (300 MHz,  $\text{CDCl}_3$ )  $\delta_{\text{F}}$  -73.5 (2F, t,  $J = 14.6$  Hz) ppm.

*Analytical data fits with proposed structure and is similar to 4.33 and 4.84 (and 4.85, 4.86 and 4.88) suggesting a similar structure. Preparative TLC was used to isolate enough material for NMR calibration and testing for Hammett plot experiments therefore mass spectrometry data was not obtained.*

(1,1-Difluoro-3-phenylpropyl)(4-methoxyphenyl)sulfane 4.88



42% by  $^{19}\text{F}$  NMR (pentafluorotoluene internal standard (25  $\mu\text{L}$ , 0.395 M);  $R_f$  0.92 (9:1 Petrol 40-60:EtOAc).  $^1\text{H}$  NMR (300 MHz,  $\text{CDCl}_3$ )  $\delta_{\text{H}}$  7.46 (2H, d,  $J = 8.5$  Hz, aromatic H), 7.21 (2H, q,  $J = 6.8$  Hz, aromatic H), 7.11 (3H, t,  $J = 6.9$  Hz, aromatic H), 6.83 (2H, d,  $J = 8.5$  Hz, aromatic H), 3.75 (3H, s,  $\text{OCH}_3$ ), 2.86 – 2.80 (2H, m,  $\text{CH}_2\text{Ph}$ ), 2.34 – 2.28 (2H, m,  $\text{SCF}_2\text{CH}_2$ ) ppm;  $^{13}\text{C}$  NMR (300 MHz,  $\text{CDCl}_3$ )  $\delta_{\text{C}}$  161.1, 140.0, 138.1, 129.5 (t,  $J = 278.2$  Hz,  $\text{CF}_2$ ), 128.6, 128.4, 126.4, 117.5, 114.7, 55.3, 40.3 (t,  $J = 23.1$  Hz,  $\text{CH}_2$ ), 29.3 (t,  $J = 4.1$  Hz,  $\text{CH}_2$ ) ppm;  $^{19}\text{F}$  NMR (300 MHz,  $\text{CDCl}_3$ )  $\delta_{\text{F}}$  -74.2 (2F, t,  $J = 14.2$  Hz,  $\text{SCF}_2$ ) ppm.

*Analytical data fits with proposed structure and is similar to 4.33 and 4.84 (and 4.85, 4.86 and 4.87) suggesting a similar structure. Preparative TLC was used to isolate enough material for NMR calibration and testing for Hammett plot experiments therefore mass spectrometry data was not obtained.*

General Procedure for Desulfurisation Reaction using Raney-Nickel

To a heterogeneous mixture of Raney-Nickel (8.83 mmol) in EtOH (10 mL), the substrate (4.42 mmol) was added and the reaction was stirred at reflux for 48 h. An aliquot was taken and analysed using GC-MS or  $^1\text{H}$  and/or  $^{19}\text{F}$  NMR spectroscopy.

## References

1. S. M. Riyadh, H. Ishii and T. Fuchigami, *Tetrahedron Lett.*, 2001, **42**, 3009-3011
2. S. Kuribayashi, N. Shida, S. Inagi and T. Fuchigami, *Tetrahedron*, 2016, **72**, 5343-5349
3. V. Suryanarayanan and M. Noel, *J. Fluorine Chem.*, 1998, **92**, 177-180
4. D. Bello and D. O'Hagan, *Beilstein J. Org. Chem.*, 2015, **11**, 85-91
5. S. Gouault, C. Guérin, L. Lemoucheux, T. Lequeux and J-C. Pommelet, *Tetrahedron Lett.*, 2003, **44**, 5061-5064
6. Y. Narihiko and F. Tsuyoshi, *Chemistry Letters*, 2001, **3**, 222-223
7. M. Zapun, *J. Fluor. Chem.*, 1976, **8**, 305-309
8. B. Hill, Y. Liu and S. D. Taylor, *Org. Lett.*, 2004, **6**, 4285-4288
9. S. Lui, C. Dockendorff and S. D. Taylor, *Org. Lett.*, 2001, **3**, 1571-1574
10. M. R. P. Heravi, *Chin. Chem. Lett.*, 2010, **21**, 1399-1402
11. V. Reutrakul, T. Thongpaisanwong, P. Tuchinda, C. Kuhakarn and M. Pohmakotr, *J. Org. Chem.*, 2004, **69**, 6913-6915
12. C. Batisse, D. Céspedes, F. Maria, M. Castello, A. Messara, B. Vivet, G. Marciniak, A. Panossian, G. Hanquet and F. R. Leroux, *Tetrahedron*, 2019, **75**, 3063-3079
13. N. Rozatian, I. W. Ashworth, G. Sandford and D. R. W. Hodgson, *Chem. Sci.*, 2018, **9**, 8692
14. Y. Chen, H. Qi, N. Chen, D. Ren, J. Xu and Z. Yang, *J. Org. Chem.*, 2019, **84**, 9044-9050
15. Z. Yang, S. Yang and J. Xu, *Tetrahedron*, 2017, **73**, 3240-3248
16. D. Zhang, H. Wang, H. Cheng, J. G. Hernández and C. Bolm, *Adv. Synth. Catal.*, 2017, **359**, 4274-4277
17. F. Gao, B. Li, Y. Wang, Q. Chen, Y. Li, K. Wang and W. Yan, *Org. Chem. Front.*, 2021, **8**, 2799-2819
18. A. Khalaf, D. Grée, H. Abdallah, N. Jaber, A. Hachem and R. Grée, *Tetrahedron*, 2011, **67**, 3881-3886
19. H. Hauptmann and W. F. Walter, *Chem. Rev.*, 1962, **62**, 47-404
20. F. A. Carey and R. J. Sundberg, *Advanced Organic Chemistry: Reactions and Synthesis*, Springer, 452-454

21. T. Furuya, A. E. Strom and T. Ritter, *J. Am. Chem. Soc.*, 2009, **131**, 1662-1663
22. Y-F. Yang, J-H. Lin and J-C. Xiao, *Org. Lett.*, 2021, **23**, 9277-9282
23. S. Zhang, D. Yi, F. Li, L. Li, G. Zhao and Z. Tang, *Tetrahedron Lett.*, 2021, **62**, 152688
24. F. Wang, W. Rao and S-Y. Wang, *J. Org. Chem.*, 2021, **86**, 8970-8979
25. J. Y. Mo, M. Epifanov, J. W. Hodgson, R. Dubois and G. M. Sammis, *Chem. Eur. J.*, 2020, **26**, 4958-4962
26. V. Reutrakul, T. Thongpaisan, P. Tuchinda, C. Kuhakarn and M. Pohmakotr, *J. Org. Chem.*, 2004, **69**, 6913-6915
27. B. Yin, S. Inagi and T. Fuchigami, *Beilstein J. Org. Chem.*, 2015, **11**, 85-91
28. J. Wu, Y. Gu, X. Leng and Q. Shen, *Angew. Chem., Int. Ed.*, 2015, **127**, 7758-7762

## Appendix

Appendix A. Crystal Structure Refinement for compound **2.25**.

### Crystal structure determination of: **mac190013\_fa** (C<sub>14</sub>H<sub>14</sub>O)

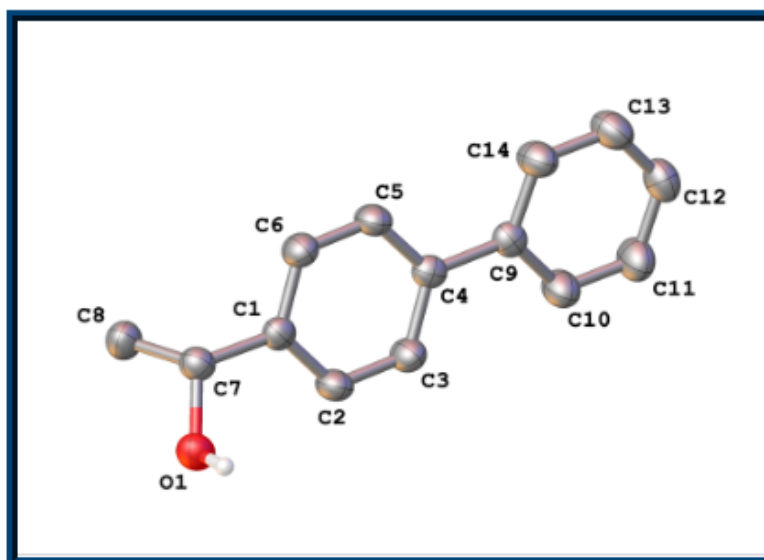


Table 1 : Crystal data and structure refinement for mac190013\_fa.

Identification code	mac190013_fa
Empirical formula	C <sub>14</sub> H <sub>14</sub> O
Formula weight	198.25
Temperature/K	200.0(2)
Crystal system	triclinic
Space group	P-1
a/Å	5.6786(3)
b/Å	7.9801(4)
c/Å	23.8726(13)
$\alpha$ /°	80.513(5)
$\beta$ /°	83.876(4)
$\gamma$ /°	89.419(4)
Volume/Å <sup>3</sup>	1060.89(10)
Z	4
$\rho_{\text{calc}}/\text{cm}^3$	1.241
$\mu/\text{mm}^{-1}$	0.593
F(000)	424.0
Crystal size/mm <sup>3</sup>	0.31 × 0.16 × 0.02
Radiation	CuK $\alpha$ ( $\lambda$ = 1.54184)
2 $\theta$ range for data collection/°	7.552 to 133.916
Index ranges	-5 ≤ h ≤ 6, -9 ≤ k ≤ 9, -27 ≤ l ≤ 28
Reflections collected	14964
Independent reflections	3762 [R <sub>int</sub> = 0.0411, R <sub>sigma</sub> = 0.0318]
Data/restraints/parameters	3762/0/279
Goodness-of-fit on F <sup>2</sup>	1.042

Final R indexes [ $I > 2\sigma(I)$ ]  $R_1 = 0.0445$ ,  $wR_2 = 0.1142$   
Final R indexes [all data]  $R_1 = 0.0637$ ,  $wR_2 = 0.1297$   
Largest diff. peak/hole /  $e \text{ \AA}^{-3}$  0.26/-0.19

#### Experimental

Crystal structure data for mac190013\_fa was collected on a Xcalibur, Atlas, Gemini ultra diffractometer equipped with a fine-focus sealed X-ray tube ( $\lambda_{\text{CuK}\alpha} = 1.54184 \text{ \AA}$ ) and an Oxford Cryosystems CryostreamPlus open-flow  $N_2$  cooling device. Cell refinement, data collection and data reduction were undertaken via software CrysAlisPro 1.171.38.42b (Rigaku OD, 2015). Intensities were corrected for absorption using CrysAlisPro 1.171.38.42b (Rigaku Oxford Diffraction, 2015). Analytical numeric absorption correction using a multifaceted crystal model based on expressions derived by R.C. Clark & J.S. Reid. (Clark, R. C. & Reid, J. S. (1995). Acta Cryst. A51, 887-897) Empirical absorption correction using spherical harmonics, implemented in SCALE3 ABSPACK scaling algorithm.

Using Olex2 (Dolomanov, 2009), the structure was solved using XT (Sheldrick, 2015) and refined by XL (Sheldrick, 2008).

Dolomanov, O.V., Bourhis, L.J., Gildea, R.J., Howard, J.A.K. & Puschmann, H. (2009). *J. Appl. Cryst.* 42, 339-341.  
Sheldrick, G.M. (2008). *Acta Cryst.* A64, 112-122.  
Sheldrick, G.M. (2015). *Acta Cryst.* A71, 3-8.

#### Crystal structure determination of [mac190013\_fa]

Crystal Data for  $C_{14}H_{14}O$  ( $M = 198.25 \text{ g mol}^{-1}$ ): triclinic, space group P-1 (no. 2),  $a = 5.6786(3) \text{ \AA}$ ,  $b = 7.9801(4) \text{ \AA}$ ,  $c = 23.8726(13) \text{ \AA}$ ,  $\alpha = 80.513(5)^\circ$ ,  $\beta = 83.876(4)^\circ$ ,  $\gamma = 89.419(4)^\circ$ ,  $V = 1060.89(10) \text{ \AA}^3$ ,  $Z = 4$ ,  $T = 200.0(2) \text{ K}$ ,  $\mu(\text{CuK}\alpha) = 0.593 \text{ mm}^{-1}$ ,  $D_{\text{calc}} = 1.241 \text{ g cm}^{-3}$ , 14964 reflections measured ( $7.552^\circ \leq 2\theta \leq 133.916^\circ$ ), 3762 unique ( $R_{\text{int}} = 0.0411$ ,  $R_{\text{sigma}} = 0.0318$ ) which were used in all calculations. The final  $R_1$  was 0.0445 ( $I > 2\sigma(I)$ ) and  $wR_2$  was 0.1297 (all data).

#### Special details of refinement:

?

#### Comments:

The diffraction pattern observed from crystals of this sample exhibited layer defects at low temperature hence data were collected at 200 K.

**Table 2 Fractional Atomic Coordinates ( $\times 10^4$ ) and Equivalent Isotropic Displacement Parameters ( $\text{\AA}^2 \times 10^3$ ) for mac190013\_fa.  $U_{eq}$  is defined as 1/3 of the trace of the orthogonalised  $U_{IJ}$  tensor.**

Atom	x	y	z	U(eq)
O1	3257 (2)	6082.1 (17)	598.0 (5)	42.6 (3)
O2	6349 (2)	3376.6 (15)	594.5 (5)	44.6 (3)
C1	867 (3)	6138.6 (19)	1509.4 (6)	32.4 (3)
C2	2677 (3)	6934 (2)	1711.4 (7)	39.6 (4)
C3	2548 (3)	7169 (2)	2276.5 (7)	39.8 (4)
C4	606 (3)	6610.8 (18)	2665.2 (6)	31.4 (3)
C5	-1207 (3)	5799 (2)	2457.3 (7)	39.1 (4)
C6	-1076 (3)	5572 (2)	1895.7 (7)	39.5 (4)
C7	925 (3)	5890 (2)	891.6 (7)	36.5 (4)
C8	-649 (3)	7138 (3)	559.8 (8)	46.2 (4)
C9	491 (3)	6821.8 (18)	3277.8 (6)	33.1 (4)
C10	2156 (3)	7802 (2)	3468.9 (8)	46.7 (4)
C11	2075 (4)	7981 (3)	4037.0 (8)	53.1 (5)
C12	329 (3)	7194 (2)	4431.3 (8)	46.8 (4)
C13	-1349 (4)	6231 (3)	4252.8 (8)	52.0 (5)
C14	-1269 (3)	6037 (2)	3686.3 (8)	46.7 (4)
C15	5787 (3)	1548.5 (19)	1492.0 (7)	34.7 (4)
C16	7527 (3)	807 (2)	1815.3 (7)	40.4 (4)
C17	7422 (3)	864 (2)	2394.2 (7)	40.1 (4)
C18	5572 (3)	1664.6 (18)	2677.3 (6)	31.5 (3)
C19	3793 (3)	2344 (2)	2352.3 (7)	41.1 (4)
C20	3896 (3)	2282 (2)	1776.0 (7)	42.1 (4)
C21	5955 (3)	1621 (2)	853.5 (7)	39.7 (4)
C22	3788 (4)	937 (3)	647.6 (8)	53.9 (5)
C23	5494 (3)	1813.2 (18)	3294.6 (7)	33.1 (4)
C24	7146 (3)	1032 (2)	3638.7 (8)	46.4 (4)
C25	7046 (4)	1184 (3)	4209.3 (8)	53.1 (5)
C26	5308 (3)	2121 (2)	4454.4 (8)	47.3 (4)
C27	3672 (4)	2925 (3)	4120.0 (8)	53.4 (5)
C28	3762 (3)	2773 (2)	3551.1 (7)	47.2 (4)

**Table 3 Anisotropic Displacement Parameters ( $\text{\AA}^2 \times 10^3$ ) for mac190013\_fa. The Anisotropic displacement factor exponent takes the form:**

$$-2\pi^2[h^2a^{*2}U_{11}+2hka^*b^*U_{12}+...].$$

Atom	$U_{11}$	$U_{22}$	$U_{33}$	$U_{23}$	$U_{13}$	$U_{12}$
O1	39.7 (7)	48.4 (7)	39.1 (6)	-8.0 (5)	-0.1 (5)	5.7 (5)
O2	58.4 (8)	39.0 (6)	34.2 (6)	-3.4 (5)	1.0 (5)	-0.9 (5)
C1	31.0 (8)	32.0 (8)	33.7 (8)	-4.3 (6)	-3.8 (6)	4.4 (6)
C2	34.1 (9)	47.5 (9)	35.7 (9)	-7.0 (7)	3.2 (6)	-6.8 (7)
C3	35.9 (9)	46.9 (9)	37.9 (9)	-10.7 (7)	-2.9 (7)	-8.4 (7)
C4	32.3 (8)	27.1 (7)	34.4 (8)	-4.6 (6)	-2.0 (6)	2.8 (6)
C5	34.1 (9)	45.5 (9)	36.2 (9)	-6.1 (7)	2.7 (6)	-7.9 (7)
C6	35.4 (9)	44.6 (9)	39.2 (9)	-9.0 (7)	-4.1 (7)	-7.1 (7)
C7	35.4 (8)	39.1 (8)	34.9 (9)	-7.4 (7)	-0.7 (6)	0.1 (7)



C8	40.6 (10)	58.0 (11)	39.4 (9)	-5.3 (8)	-6.6 (7)	6.7 (8)
C9	36.1 (9)	28.5 (8)	34.2 (8)	-4.7 (6)	-3.1 (6)	4.8 (6)
C10	49.1 (10)	52.2 (10)	37.9 (9)	-6.2 (8)	-1.7 (7)	-13.4 (8)
C11	59.7 (12)	61.2 (12)	40.8 (10)	-12.0 (8)	-8.6 (8)	-13.7 (9)
C12	58.7 (11)	48.9 (10)	33.6 (9)	-9.6 (7)	-3.7 (8)	2.2 (8)
C13	56.1 (11)	58.9 (11)	39.6 (10)	-11.0 (8)	6.8 (8)	-10.0 (9)
C14	45.5 (10)	53.9 (11)	41.1 (10)	-13.4 (8)	2.9 (7)	-11.9 (8)
C15	39.2 (9)	29.4 (7)	35.3 (8)	-5.5 (6)	-2.9 (6)	-1.3 (6)
C16	36.5 (9)	47.0 (9)	37.2 (9)	-7.4 (7)	-1.4 (7)	10.0 (7)
C17	36.3 (9)	45.9 (9)	37.6 (9)	-4.4 (7)	-6.2 (7)	10.1 (7)
C18	33.6 (8)	27.5 (7)	32.2 (8)	-2.4 (6)	-2.0 (6)	-2.0 (6)
C19	38.2 (9)	45.6 (9)	40.6 (9)	-11.6 (7)	-4.1 (7)	12.3 (7)
C20	42.2 (9)	46.8 (9)	40.0 (9)	-10.3 (7)	-12.2 (7)	13.0 (7)
C21	47.3 (10)	35.2 (8)	36.6 (9)	-6.1 (7)	-4.4 (7)	7.3 (7)
C22	72.9 (13)	47.8 (10)	42.8 (10)	-6.7 (8)	-14.7 (9)	-7.9 (9)
C23	34.7 (8)	29.1 (8)	34.4 (8)	-3.0 (6)	-1.9 (6)	-3.8 (6)
C24	48.3 (10)	51.0 (10)	43.3 (10)	-13.7 (8)	-12.1 (8)	13.6 (8)
C25	62.8 (12)	56.0 (11)	44.4 (10)	-10.9 (8)	-20.8 (9)	12.6 (9)
C26	60.8 (12)	48.3 (10)	33.1 (9)	-7.8 (7)	-4.6 (8)	-5.7 (8)
C27	54.3 (11)	64.9 (12)	40.6 (10)	-13.6 (9)	2.8 (8)	11.3 (9)
C28	45.7 (10)	59.2 (11)	36.0 (9)	-6.5 (8)	-3.8 (7)	13.8 (8)

**Table 4 Bond Lengths for mac190013\_fa.**

Atom Atom Length/Å			Atom Atom Length/Å		
O1	C7	1.428 (2)	C13	C14	1.382 (3)
O2	C21	1.444 (2)	C15	C16	1.386 (2)
C1	C2	1.383 (2)	C15	C20	1.385 (2)
C1	C6	1.388 (2)	C15	C21	1.509 (2)
C1	C7	1.517 (2)	C16	C17	1.385 (2)
C2	C3	1.387 (2)	C17	C18	1.395 (2)
C3	C4	1.390 (2)	C18	C19	1.391 (2)
C4	C5	1.398 (2)	C18	C23	1.494 (2)
C4	C9	1.494 (2)	C19	C20	1.380 (2)
C5	C6	1.376 (2)	C21	C22	1.512 (3)
C7	C8	1.513 (2)	C23	C24	1.388 (2)
C9	C10	1.392 (2)	C23	C28	1.393 (2)
C9	C14	1.395 (2)	C24	C25	1.382 (3)
C10	C11	1.383 (3)	C25	C26	1.372 (3)
C11	C12	1.372 (3)	C26	C27	1.374 (3)
C12	C13	1.374 (3)	C27	C28	1.379 (3)

**Table 5 Bond Angles for mac190013\_fa.**

Atom Atom Atom Angle/°				Atom Atom Atom Angle/°			
C2	C1	C6	117.38 (14)	C16	C15	C21	122.15 (14)
C2	C1	C7	122.76 (14)	C20	C15	C16	117.28 (15)
C6	C1	C7	119.86 (14)	C20	C15	C21	120.53 (14)
C1	C2	C3	121.30 (14)	C17	C16	C15	121.16 (15)

C2	C3	C4	121.65 (15)	C16	C17	C18	121.73 (15)
C3	C4	C5	116.57 (15)	C17	C18	C23	122.43 (14)
C3	C4	C9	121.73 (14)	C19	C18	C17	116.44 (15)
C5	C4	C9	121.68 (14)	C19	C18	C23	121.13 (14)
C6	C5	C4	121.63 (14)	C20	C19	C18	121.73 (15)
C5	C6	C1	121.48 (15)	C19	C20	C15	121.56 (15)
O1	C7	C1	112.23 (13)	O2	C21	C15	107.26 (13)
O1	C7	C8	107.34 (13)	O2	C21	C22	109.91 (14)
C8	C7	C1	112.13 (13)	C15	C21	C22	113.95 (15)
C10	C9	C4	121.43 (14)	C24	C23	C18	122.18 (14)
C10	C9	C14	116.79 (15)	C24	C23	C28	116.67 (16)
C14	C9	C4	121.78 (15)	C28	C23	C18	121.14 (14)
C11	C10	C9	121.60 (16)	C25	C24	C23	121.40 (17)
C12	C11	C10	120.55 (18)	C26	C25	C24	120.91 (17)
C11	C12	C13	119.01 (17)	C25	C26	C27	118.70 (17)
C12	C13	C14	120.74 (17)	C26	C27	C28	120.55 (17)
C13	C14	C9	121.31 (17)	C27	C28	C23	121.76 (17)

**Table 6 Hydrogen Bonds for mac190013\_fa.**

D	H	A	d(D-H)/Å	d(H-A)/Å	d(D-A)/Å	D-H-A/°
O1	H1	O2	0.88 (3)	1.94 (3)	2.7696 (17)	157 (2)
O2	H2A	O1 <sup>1</sup>	0.90 (3)	1.91 (3)	2.7931 (17)	170 (2)

<sup>1</sup>1-x,1-y,z

**Table 7 Hydrogen Atom Coordinates (Å×10<sup>4</sup>) and Isotropic Displacement Parameters (Å<sup>2</sup>×10<sup>3</sup>) for mac190013\_fa.**

Atom	x	y	z	U(eq)
H1	4090 (40)	5170 (30)	696 (10)	64
H2A	6500 (40)	3420 (30)	215 (12)	67
H2	4007	7319	1463	47
H3	3792	7714	2398	48
H5	-2534	5403	2705	47
H6	-2316	5027	1772	47
H7	361	4737	886	44
H8A	-47	8270	536	69
H8B	-2228	7059	751	69
H8C	-670	6875	182	69
H10	3350	8350	3208	56
H11	3215	8641	4153	64
H12	281	7309	4814	56
H13	-2551	5705	4516	62
H14	-2412	5370	3575	56
H16	8786	262	1640	49
H17	8616	355	2600	48
H19	2501	2855	2528	49
H20	2666	2743	1574	51

H21	7332	961	736	48
H22A	2411	1532	777	81
H22B	3609	-252	797	81
H22C	3969	1097	238	81
H24	8345	393	3482	56
H25	8173	643	4430	64
H26	5237	2210	4839	57
H27	2496	3577	4279	64
H28	2635	3325	3333	57

#### Refinement model description

Number of restraints - 0, number of constraints - unknown.

#### Details:

1. Fixed Uiso
  - At 1.2 times of:
    - All C(H) groups
  - At 1.5 times of:
    - All C(H,H,H) groups, All O(H) groups
- 2.a Ternary CH refined with riding coordinates:
  - C7(H7), C21(H21)
- 2.b Aromatic/amide H refined with riding coordinates:
  - C2(H2), C3(H3), C5(H5), C6(H6), C10(H10), C11(H11), C12(H12), C13(H13), C14(H14), C16(H16), C17(H17), C19(H19), C20(H20), C24(H24), C25(H25), C26(H26), C27(H27), C28(H28)
- 2.c Idealised Me refined as rotating group:
  - C8(H8A,H8B,H8C), C22(H22A,H22B,H22C)

This report has been created with Olex2, compiled on May 29 2018 13:30:08 for OlexSys. Please [let us know](#) if there are any errors or if you would like to have additional features.

Appendix B. Crystal Structure Refinement for compound **2.30**.

### Crystal structure determination of: mac200001\_fa (C<sub>20</sub>H<sub>22</sub>FMnN<sub>2</sub>O<sub>3</sub>)

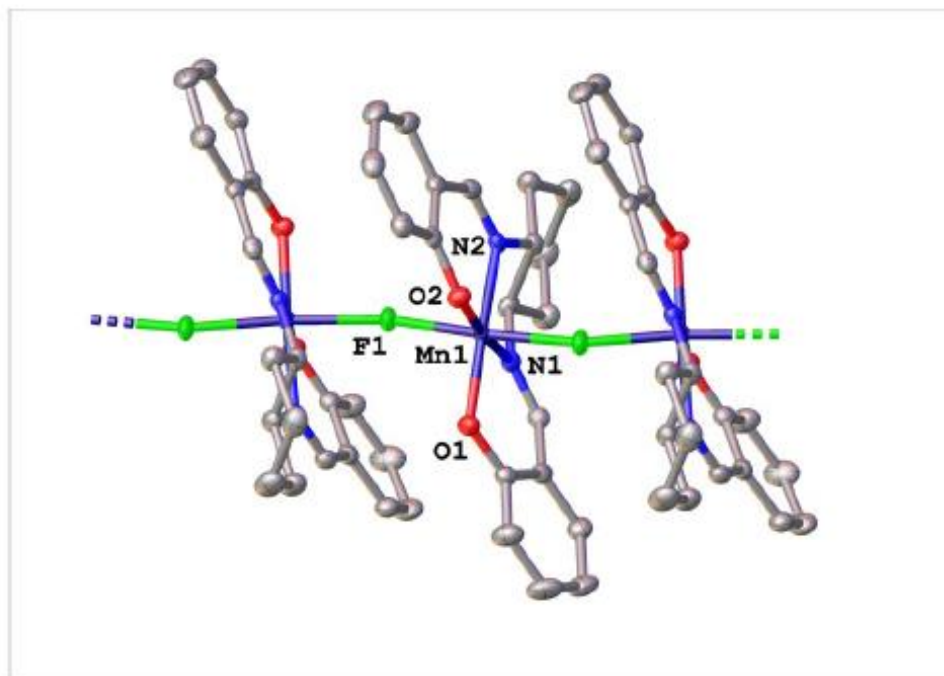


Table 1 : Crystal data and structure refinement for mac200001\_fa.

Identification code	mac200001_fa
Empirical formula	C <sub>20</sub> H <sub>22</sub> FMnN <sub>2</sub> O <sub>3</sub>
Formula weight	412.33
Temperature/K	150.0(2)
Crystal system	orthorhombic
Space group	Pbca
a/Å	18.0243(4)
b/Å	8.00887(19)
c/Å	25.6482(9)
α/°	90
β/°	90
γ/°	90
Volume/Å <sup>3</sup>	3702.43(18)
Z	8
ρ <sub>calc</sub> /cm <sup>3</sup>	1.479
μ/mm <sup>-1</sup>	6.086
F(000)	1712.0

Crystal size/mm <sup>3</sup>	0.32 × 0.03 × 0.02
Radiation	CuKα (λ = 1.54184)
2θ range for data collection/°	6.892 to 133.792
Index ranges	-21 ≤ h ≤ 20, -6 ≤ k ≤ 9, -30 ≤ l ≤ 29
Reflections collected	14052
Independent reflections	3279 [R <sub>int</sub> = 0.0491, R <sub>sigma</sub> = 0.0382]
Data/restraints/parameters	3279/0/250
Goodness-of-fit on F <sup>2</sup>	1.035
Final R indexes [I >= 2σ (I)]	R <sub>1</sub> = 0.0339, wR <sub>2</sub> = 0.0772
Final R indexes [all data]	R <sub>1</sub> = 0.0499, wR <sub>2</sub> = 0.0857
Largest diff. peak/hole / e Å <sup>-3</sup>	0.24/-0.32

### Experimental

Crystal structure data for mac200001\_fa was collected on a Xcalibur, Atlas, Gemini ultra diffractometer equipped with a fine-focus sealed X-ray tube (λ<sub>CuKα</sub> = 1.54184 Å) and an Oxford Cryosystems CryostreamPlus open-flow N<sub>2</sub> cooling device. Cell refinement, data collection and data reduction were undertaken via software CrysAlisPro 1.171.38.42b (Rigaku OD, 2015). Intensities were corrected for absorption using CrysAlisPro 1.171.38.42b (Rigaku Oxford Diffraction, 2015) Analytical numeric absorption correction using a multifaceted crystal model based on expressions derived by R.C. Clark & J.S. Reid. (Clark, R. C. & Reid, J. S. (1995). Acta Cryst. A51, 887-897) Empirical absorption correction using spherical harmonics, implemented in SCALE3 ABSPACK scaling algorithm..

Using Olex2 (Dolomanov, 2009), the structure was solved using ShelXT (Sheldrick, 2015) and refined by XL (Sheldrick, 2008).

Dolomanov, O.V., Bourhis, L.J., Gildea, R.J, Howard, J.A.K. & Puschmann, H. (2009), J. Appl. Cryst. 42, 339-341.  
 Sheldrick, G.M. (2008). Acta Cryst. A64, 112-122.  
 Sheldrick, G.M. (2015). Acta Cryst. A71, 3-8.

### Crystal structure determination of [mac200001\_fa]

Crystal Data for C<sub>20</sub>H<sub>22</sub>FMnN<sub>2</sub>O<sub>3</sub> (M = 412.33 g/mol): orthorhombic, space group Pbca (no. 61), a = 18.0243(4) Å, b = 8.00887(19) Å, c = 25.6482(9) Å, V = 3702.43(18) Å<sup>3</sup>, Z = 8, T = 150.0(2) K, μ(CuKα) = 6.086 mm<sup>-1</sup>, D<sub>calc</sub> = 1.479 g/cm<sup>3</sup>, 14052 reflections measured (6.892° ≤ 2θ ≤ 133.792°), 3279 unique (R<sub>int</sub> = 0.0491, R<sub>sigma</sub> = 0.0382) which were used in all calculations. The final R<sub>1</sub> was 0.0339 (I > 2σ(I)) and wR<sub>2</sub> was 0.0857 (all data).

### Special details of refinement:

?

### Comments:

This structure is a 1D coordination polymer propagating along the crystallographic [010] direction.



**Table 2 Fractional Atomic Coordinates ( $\times 10^4$ ) and Equivalent Isotropic Displacement Parameters ( $\text{\AA}^2 \times 10^3$ ) for mac200001\_fa.  $U_{eq}$  is defined as 1/3 of the trace of the orthogonalised  $U_{ij}$  tensor.**

Atom	x	y	z	U(eq)
Mn1	7578.9 (2)	3817.4 (4)	6271.0 (2)	14.62 (11)
F1	7309.5 (8)	1346.3 (13)	6266.2 (5)	22.8 (3)
O1	8322.0 (9)	3671.6 (17)	5733.7 (6)	21.0 (3)
O2	8253.6 (9)	3542.7 (17)	6837.5 (6)	21.1 (3)
O3	9613.7 (12)	4656 (3)	6398.9 (11)	53.0 (6)
N1	6785.1 (10)	4217 (2)	5739.9 (7)	18.0 (4)
N2	6711.1 (10)	3968.1 (19)	6760.2 (7)	17.1 (4)
C1	6036.8 (13)	3925 (3)	5948.6 (9)	20.3 (5)
C2	6036.6 (13)	4631 (3)	6505.4 (9)	20.1 (5)
C3	5299.5 (13)	4290 (3)	6775.0 (9)	23.7 (5)
C4	4665.2 (14)	5036 (3)	6454.5 (10)	30.3 (6)
C5	4662.4 (14)	4332 (3)	5902.8 (10)	33.5 (6)
C6	5399.4 (13)	4630 (3)	5629.6 (10)	27.4 (5)
C7	6914.5 (13)	4911 (3)	5298.7 (9)	20.0 (5)
C8	7637.1 (14)	5207 (3)	5078.7 (9)	20.3 (5)
C9	8299.4 (13)	4542 (3)	5292.8 (9)	20.3 (5)
C10	8958.4 (15)	4782 (3)	5012.9 (10)	32.0 (6)
C11	8974.4 (16)	5685 (4)	4555.0 (10)	36.9 (6)
C12	8329.8 (15)	6394 (3)	4355.7 (10)	31.5 (6)
C13	7669.6 (15)	6130 (3)	4613.0 (9)	25.3 (5)
C14	6711.8 (13)	3356 (3)	7219.8 (9)	21.4 (5)
C15	7355.8 (14)	2726 (3)	7490.4 (9)	21.4 (5)
C16	8090.3 (13)	2886 (3)	7296.5 (9)	19.6 (5)
C17	8674.5 (15)	2327 (3)	7615.3 (9)	25.7 (5)
C18	8541.8 (16)	1605 (3)	8097.7 (10)	29.9 (6)
C19	7821.2 (16)	1440 (3)	8284.8 (10)	32.2 (6)
C20	7242.6 (15)	2008 (3)	7985.1 (9)	28.6 (6)

**Table 3 Anisotropic Displacement Parameters ( $\text{\AA}^2 \times 10^3$ ) for mac200001\_fa. The Anisotropic displacement factor exponent takes the form:  $-2\pi^2[h^2a^{*2}U_{11}+2hka^*b^*U_{12}+\dots]$ .**

Atom	$U_{11}$	$U_{22}$	$U_{33}$	$U_{23}$	$U_{13}$	$U_{12}$
Mn1	14.93 (18)	12.96 (18)	15.96 (19)	0.57 (13)	0.18 (14)	0.93 (13)
F1	29.3 (7)	12.0 (6)	27.1 (7)	0.2 (5)	1.1 (6)	0.4 (5)
O1	19.3 (8)	22.7 (7)	21.0 (8)	2.2 (6)	2.3 (7)	4.3 (7)
O2	18.4 (8)	25.3 (7)	19.4 (8)	2.5 (6)	-0.2 (6)	-1.3 (6)
O3	28.3 (12)	65.5 (14)	65.2 (16)	4.9 (12)	5.6 (11)	-9.8 (10)
N1	17.4 (10)	16.8 (8)	19.8 (10)	-0.5 (7)	-1.1 (8)	-0.6 (7)

N2	16.4(10)	14.1(8)	20.9(10)	-2.4(7)	1.4(8)	0.5(7)
C1	17.5(12)	20.5(11)	22.9(12)	3.5(9)	-1.7(9)	-4.2(9)
C2	18.6(12)	16.7(10)	24.9(12)	-0.7(9)	0.6(10)	0.0(9)
C3	19.6(12)	24.7(11)	26.7(12)	1.7(10)	2.4(10)	1.5(9)
C4	18.3(12)	30.9(12)	41.5(15)	6.0(11)	5.5(11)	-0.5(10)
C5	18.0(13)	45.0(14)	37.4(15)	9.6(12)	-5.4(11)	-2.3(11)
C6	19.4(13)	34.5(13)	28.3(13)	4.8(10)	-3.1(10)	0.7(10)
C7	18.9(12)	21.8(10)	19.3(11)	-0.8(9)	-3.0(9)	1.4(9)
C8	23.2(12)	19.6(10)	18.2(11)	-2.1(9)	0.4(10)	-2.7(10)
C9	21.4(12)	21.4(11)	18.2(11)	-1.3(9)	0.7(9)	-0.1(9)
C10	22.2(12)	48.0(15)	25.9(13)	6.2(11)	1.8(11)	1.3(11)
C11	24.2(14)	60.5(17)	26.0(13)	6.2(12)	6.1(11)	-6.7(12)
C12	33.2(14)	42.1(14)	19.2(12)	6.1(10)	1.6(11)	-6.4(12)
C13	27.8(13)	28.7(12)	19.3(11)	1.3(9)	-2.3(10)	-0.2(11)
C14	22.6(12)	19.4(10)	22.3(12)	-3.2(9)	4.6(10)	-2.0(9)
C15	28.8(13)	17.8(10)	17.8(11)	-2.2(9)	1.3(10)	-0.4(10)
C16	24.3(12)	14.6(9)	20.0(11)	-4.0(9)	-1.2(10)	-0.6(9)
C17	28.6(14)	23.9(11)	24.6(13)	-2.2(9)	-4.5(11)	-0.4(10)
C18	37.3(15)	26.7(12)	25.8(13)	-1.1(10)	-10.9(11)	2.0(11)
C19	46.5(17)	31.0(12)	19.0(12)	5.8(10)	-3.1(12)	-1.7(12)
C20	34.7(16)	27.2(12)	23.8(12)	1.2(10)	3.6(11)	-2.4(11)

**Table 4 Bond Lengths for mac200001\_fa.**

Atom	Atom	Length/Å	Atom	Atom	Length/Å
Mn1	F1 <sup>1</sup>	2.0354(11)	C4	C5	1.523(4)
Mn1	F1	2.0378(11)	C5	C6	1.521(3)
Mn1	O1	1.9253(16)	C7	C8	1.439(3)
Mn1	O2	1.9074(16)	C8	C9	1.418(3)
Mn1	N1	2.0013(19)	C8	C13	1.406(3)
Mn1	N2	2.0089(19)	C9	C10	1.401(3)
F1	Mn1 <sup>2</sup>	2.0354(11)	C10	C11	1.379(4)
O1	C9	1.329(3)	C11	C12	1.391(4)
O2	C16	1.323(3)	C12	C13	1.377(4)
N1	C1	1.470(3)	C14	C15	1.443(3)
N1	C7	1.282(3)	C15	C16	1.420(3)
N2	C2	1.479(3)	C15	C20	1.408(3)
N2	C14	1.277(3)	C16	C17	1.406(3)
C1	C2	1.536(3)	C17	C18	1.386(3)
C1	C6	1.519(3)	C18	C19	1.391(4)
C2	C3	1.522(3)	C19	C20	1.373(4)
C3	C4	1.530(3)			

<sup>1</sup>3/2-X,1/2+Y,+Z; <sup>2</sup>3/2-X,-1/2+Y,+Z

**Table 5 Bond Angles for mac200001\_fa.**

Atom	Atom	Atom	Angle/°	Atom	Atom	Atom	Angle/°
F1 <sup>1</sup>	Mn1	F1	171.85 (2)	N2	C2	C3	116.90 (18)
O1	Mn1	F1 <sup>1</sup>	89.27 (6)	C3	C2	C1	110.90 (19)
O1	Mn1	F1	95.89 (6)	C2	C3	C4	109.77 (19)
O1	Mn1	N1	91.14 (7)	C5	C4	C3	110.9 (2)
O1	Mn1	N2	172.93 (7)	C6	C5	C4	111.5 (2)
O2	Mn1	F1	92.55 (6)	C1	C6	C5	110.7 (2)
O2	Mn1	F1 <sup>1</sup>	93.23 (6)	N1	C7	C8	125.6 (2)
O2	Mn1	O1	95.44 (7)	C9	C8	C7	123.3 (2)
O2	Mn1	N1	173.08 (7)	C13	C8	C7	117.2 (2)
O2	Mn1	N2	91.58 (7)	C13	C8	C9	119.5 (2)
N1	Mn1	F1 <sup>1</sup>	84.68 (6)	O1	C9	C8	123.5 (2)
N1	Mn1	F1	88.90 (6)	O1	C9	C10	118.8 (2)
N1	Mn1	N2	81.88 (8)	C10	C9	C8	117.6 (2)
N2	Mn1	F1	82.91 (6)	C11	C10	C9	121.7 (2)
N2	Mn1	F1 <sup>1</sup>	91.20 (6)	C10	C11	C12	120.6 (3)
Mn1 <sup>2</sup>	F1	Mn1	160.53 (8)	C13	C12	C11	118.9 (2)
C9	O1	Mn1	123.77 (14)	C12	C13	C8	121.6 (2)
C16	O2	Mn1	125.59 (15)	N2	C14	C15	125.4 (2)
C1	N1	Mn1	112.51 (14)	C16	C15	C14	123.4 (2)
C7	N1	Mn1	122.69 (16)	C20	C15	C14	117.4 (2)
C7	N1	C1	123.86 (19)	C20	C15	C16	119.2 (2)
C2	N2	Mn1	112.69 (13)	O2	C16	C15	123.7 (2)
C14	N2	Mn1	123.56 (16)	O2	C16	C17	118.5 (2)
C14	N2	C2	123.1 (2)	C17	C16	C15	117.8 (2)
N1	C1	C2	106.28 (17)	C18	C17	C16	121.5 (3)
N1	C1	C6	116.03 (18)	C17	C18	C19	120.6 (2)
C6	C1	C2	111.34 (19)	C20	C19	C18	119.0 (2)
N2	C2	C1	106.18 (17)	C19	C20	C15	122.0 (3)

<sup>1</sup>3/2-X,1/2+Y,+Z; <sup>2</sup>3/2-X,-1/2+Y,+Z

**Table 6 Hydrogen Bonds for mac200001\_fa.**

D	H	A	d(D-H)/Å	d(H-A)/Å	d(D-A)/Å	D-H-A/°
O3H3C	O2	O	0.85 (4)	2.18 (5)	2.841 (3)	134 (4)
O3H3D	O1	O	0.83 (4)	2.20 (5)	2.992 (3)	159 (4)

**Table 7 Torsion Angles for mac200001\_fa.**

A	B	C	D	Angle/°	A	B	C	D	Angle/°
---	---	---	---	---------	---	---	---	---	---------



Mn1 O1 C9 C8	-22.9 (3)	C6 C1 C2 N2	$\bar{175.42 (17)}$
Mn1 O1 C9 C10	159.06 (17)	C6 C1 C2 C3	56.6 (2)
Mn1 O2 C16 C15	-18.8 (3)	C7 N1 C1 C2	-129.3 (2)
Mn1 O2 C16 C17	161.89 (15)	C7 N1 C1 C6	-4.9 (3)
Mn1 N1 C1 C2	39.82 (18)	C7 C8 C9 O1	-4.3 (3)
Mn1 N1 C1 C6	164.18 (15)	C7 C8 C9 C10	173.7 (2)
Mn1 N1 C7 C8	12.5 (3)	C7 C8 C13 C12	-176.1 (2)
Mn1 N2 C2 C1	36.69 (18)	C8 C9 C10 C11	2.4 (4)
Mn1 N2 C2 C3	161.00 (15)	C9 C8 C13 C12	0.6 (3)
Mn1 N2 C14 C15	11.0 (3)	C9 C10 C11 C12	0.1 (4)
O1 C9 C10 C11	-179.4 (2)	C10 C11 C12 C13	-2.3 (4)
O2 C16 C17 C18	$\bar{179.10 (19)}$	C11 C12 C13 C8	2.0 (4)
N1 C1 C2 N2	-48.2 (2)	C13 C8 C9 O1	179.21 (19)
N1 C1 C2 C3	$\bar{176.16 (17)}$	C13 C8 C9 C10	-2.7 (3)
N1 C1 C6 C5	$\bar{176.68 (19)}$	C14 N2 C2 C1	-134.6 (2)
N1 C7 C8 C9	9.5 (3)	C14 N2 C2 C3	-10.3 (3)
N1 C7 C8 C13	-174.0 (2)	C14 C15 C16 O2	-3.9 (3)
N2 C2 C3 C4	$\bar{179.04 (18)}$	C14 C15 C16 C17	175.44 (19)
N2 C14 C15 C16	7.4 (3)	C14 C15 C20 C19	-177.0 (2)
N2 C14 C15 C20	-176.4 (2)	C15 C16 C17 C18	1.6 (3)
C1 N1 C7 C8	$\bar{179.44 (19)}$	C16 C15 C20 C19	-0.7 (3)
C1 C2 C3 C4	-57.2 (2)	C16 C17 C18 C19	-1.2 (3)
C2 N2 C14 C15	$\bar{178.63 (19)}$	C17 C18 C19 C20	-0.2 (4)
C2 C1 C6 C5	-55.0 (3)	C18 C19 C20 C15	1.1 (4)
C2 C3 C4 C5	57.4 (3)	C20 C15 C16 O2	-179.9 (2)
C3 C4 C5 C6	-56.8 (3)	C20 C15 C16 C17	-0.6 (3)
C4 C5 C6 C1	55.3 (3)		

**Table 8 Hydrogen Atom Coordinates ( $\text{\AA} \times 10^4$ ) and Isotropic Displacement Parameters ( $\text{\AA}^2 \times 10^3$ ) for mac200001\_fa.**

Atom	x	y	z	U(eq)
H3C	9360 (30)	4510 (50)	6677 (17)	79
H3D	9350 (30)	4330 (50)	6157 (17)	79
H1	5965	2715	5974	24
H2	6094	5845	6479	24
H3A	5303	4782	7121	28
H3B	5228	3096	6812	28
H4A	4196	4786	6622	36

H4B	4719	6240	6440	36
H5A	4564	3143	5916	40
H5B	4268	4855	5704	40
H6A	5392	4102	5289	33
H6B	5472	5819	5579	33
H7	6506	5253	5104	24
H10	9397	4321	5139	38
H11	9421	5820	4378	44
H12	8344	7036	4054	38
H13	7235	6573	4475	30
H14	6260	3313	7395	26
H17	9161	2444	7500	31
H18	8938	1228	8298	36
H19	7733	953	8608	39
H20	6761	1916	8113	34

#### Refinement model description

Number of restraints - 0, number of constraints - unknown.

#### Details:

1. Fixed Uiso  
 At 1.2 times of:  
 All C(H) groups, All C(H,H) groups  
 At 1.5 times of:  
 All O(H,H) groups  
 2.a Ternary CH refined with riding coordinates:  
 C1(H1), C2(H2)  
 2.b Secondary CH2 refined with riding coordinates:  
 C3(H3A,H3B), C4(H4A,H4B), C5(H5A,H5B), C6(H6A,H6B)  
 2.c Aromatic/amide H refined with riding coordinates:  
 C7(H7), C10(H10), C11(H11), C12(H12), C13(H13), C14(H14), C17(H17),  
 C18(H18),  
 C19(H19), C20(H20)

Appendix C. Crystal Structure Refinement for compound **Fe(acac)<sub>3</sub>**.

07/01/2021

mac200005\_tables.html



**Crystal structure  
determination of:  
82888775\_shelxt  
(C<sub>15</sub>H<sub>21</sub>FeO<sub>6</sub>)**

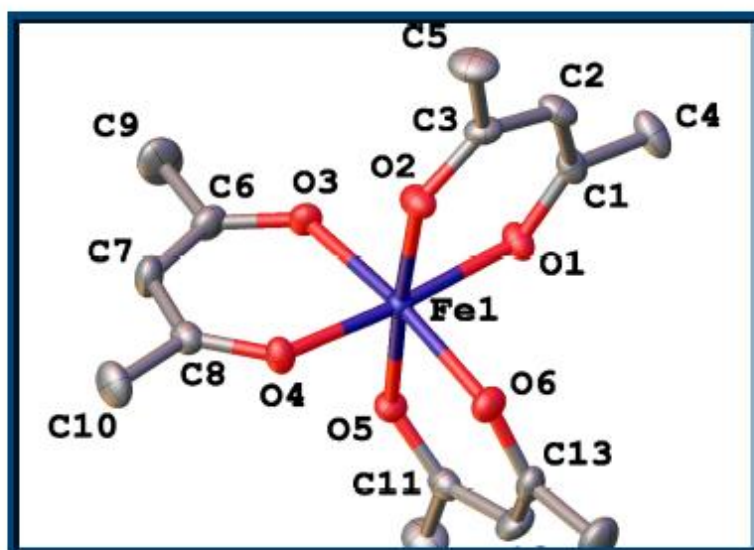


**Table 1 : Crystal data and structure refinement for 82888775\_shelxt.**

Identification code	82888775_shelxt
Empirical formula	C <sub>15</sub> H <sub>21</sub> FeO <sub>6</sub>
Formula weight	353.17
Temperature/K	100.0(2)
Crystal system	orthorhombic
Space group	Pbca
a/Å	16.36570(10)
b/Å	15.19040(10)
c/Å	13.39230(10)
α/°	90
β/°	90
γ/°	90
Volume/Å <sup>3</sup>	3329.35(4)
Z	8

$\rho_{\text{calc}}/\text{cm}^3$	1.409
$\mu/\text{mm}^{-1}$	0.924
F(000)	1480.0
Crystal size/ $\text{mm}^3$	0.116 × 0.102 × 0.059
Radiation	Synchrotron ( $\lambda = 0.6889$ )
2 $\theta$ range for data collection/ $^\circ$	4.826 to 63.772
Index ranges	-23 ≤ h ≤ 15, -18 ≤ k ≤ 17, -19 ≤ l ≤ 8
Reflections collected	13940
Independent reflections	4744 [ $R_{\text{int}} = 0.0408$ , $R_{\text{sigma}} = 0.0461$ ]
Data/restraints/parameters	4744/0/205
Goodness-of-fit on $F^2$	1.080
Final R indexes [ $I > 2\sigma(I)$ ]	$R_1 = 0.0371$ , $wR_2 = 0.1014$
Final R indexes [all data]	$R_1 = 0.0436$ , $wR_2 = 0.1056$
Largest diff. peak/hole / $e \text{ \AA}^{-3}$	0.43/-0.81

### Experimental

Crystal structure data for 82888775\_shelxt was collected on a DLS\_I19\_upgrade diffractometer equipped with a Synchrotron ( $\lambda_{\text{Synchrotron}} = 0.6889 \text{ \AA}$ ) and an Oxford Cryosystems CryostreamPlus open-flow  $\text{N}_2$  cooling device. Cell refinement, data collection and data reduction were undertaken via software ?. Intensities were corrected for absorption using ?.

Using Olex2 (Dolomanov, 2009), the structure was solved using ShelXT (Sheldrick, 2015) and refined by ShelXL (Sheldrick, 2015).

Dolomanov, O.V., Bourhis, L.J., Gildea, R.J., Howard, J.A.K. & Puschmann, H. (2009), *J. Appl. Cryst.* 42, 339-341.

Sheldrick, G.M. (2008). *Acta Cryst.* A64, 112-122.

Sheldrick, G.M. (2015). *Acta Cryst.* A71, 3-8.

### Crystal structure determination of [82888775\_shelxt]

Crystal Data for  $\text{C}_{15}\text{H}_{21}\text{FeO}_6$  ( $M = 353.17 \text{ g/mol}$ ): orthorhombic, space group  $Pbca$  (no. 61),  $a = 16.36570(10) \text{ \AA}$ ,  $b = 15.19040(10) \text{ \AA}$ ,  $c = 13.39230(10) \text{ \AA}$ ,  $V = 3329.35(4) \text{ \AA}^3$ ,  $Z = 8$ ,  $T = 100.0(2) \text{ K}$ ,  $\mu(\text{Synchrotron}) = 0.924 \text{ mm}^{-1}$ ,  $D_{\text{calc}} = 1.409 \text{ g/cm}^3$ , 13940 reflections measured ( $4.826^\circ \leq 2\theta \leq 63.772^\circ$ ), 4744 unique ( $R_{\text{int}} = 0.0408$ ,  $R_{\text{sigma}} = 0.0461$ ) which were used in all calculations. The final  $R_1$  was 0.0371 ( $I > 2\sigma(I)$ ) and  $wR_2$  was 0.1056 (all data).

### Special details of refinement:

?

### Comments:

These data represent a redetermination of a structure for which data are available in the CSD (CSD Refcode: FEACAC).

**Table 2 Fractional Atomic Coordinates ( $\times 10^4$ ) and Equivalent Isotropic Displacement Parameters ( $\text{\AA}^2 \times 10^3$ ) for 82888775\_shelxt.  $U_{\text{eq}}$  is defined as 1/3 of the trace of the orthogonalised  $U_{\text{ij}}$  tensor.**

Atom	x	y	z	U(eq)
Fe1	2545.6 (2)	6429.0 (2)	7259.2 (2)	15.35 (8)
O1	2524.7 (6)	5424.7 (8)	8225.9 (8)	22.1 (2)

O2	1801.2 (6)	5733.2 (8)	6401.5 (7)	22.6 (2)
O3	1644.6 (6)	7016.3 (8)	8002.0 (7)	21.6 (2)
O4	2473.4 (6)	7392.5 (8)	6248.5 (7)	20.5 (2)
O5	3317.6 (6)	7062.5 (7)	8177.3 (7)	20.0 (2)
O6	3540.9 (6)	5958.9 (8)	6570.2 (8)	22.7 (2)
C1	2137.9 (10)	4701.4 (10)	8186.9 (9)	20.0 (3)
C2	1638.4 (10)	4450.4 (11)	7383.4 (10)	23.0 (3)
C3	1497.2 (8)	4965.8 (11)	6545.9 (10)	21.3 (3)
C4	2220.0 (12)	4104.1 (12)	9073.2 (11)	29.1 (4)
C5	938.3 (10)	4646.2 (13)	5731.1 (12)	34.3 (4)
C6	1342.7 (9)	7780.2 (12)	7857.7 (11)	24.7 (3)
C7	1499.0 (10)	8305.4 (12)	7037.3 (12)	28.3 (4)
C8	2034.0 (9)	8081.2 (10)	6257.1 (10)	20.5 (3)
C9	772.0 (13)	8096.3 (14)	8661.3 (14)	44.2 (5)
C10	2092.1 (12)	8670.5 (12)	5362.3 (12)	30.5 (4)
C11	4078.9 (9)	6945.2 (10)	8306.3 (10)	21.5 (3)
C12	4564.9 (10)	6407.5 (12)	7710.7 (12)	28.4 (4)
C13	4283.4 (9)	5975.6 (11)	6857.7 (11)	23.5 (3)
C14	4461.1 (11)	7466.4 (13)	9142.5 (12)	34.4 (4)
C15	4882.5 (11)	5510.2 (14)	6190.5 (14)	37.8 (4)

**Table 3 Anisotropic Displacement Parameters ( $\text{\AA}^2 \times 10^3$ ) for 82888775\_shelxt. The Anisotropic displacement factor exponent takes the form:**

$$-2\pi^2[h^2a^{*2}U_{11}+2hka^*b^*U_{12}+...].$$

Atom	$U_{11}$	$U_{22}$	$U_{33}$	$U_{23}$	$U_{13}$	$U_{12}$
Fe1	16.49 (13)	14.13 (17)	15.42 (11)	-1.29 (7)	-0.75 (6)	0.41 (7)
O1	32.1 (6)	15.6 (7)	18.6 (4)	-0.8 (4)	-5.1 (4)	-2.3 (4)
O2	24.7 (5)	22.3 (7)	20.7 (4)	1.1 (4)	-6.2 (4)	-4.7 (5)
O3	20.2 (5)	23.7 (7)	20.9 (4)	1.8 (4)	5.8 (4)	1.6 (5)
O4	26.5 (6)	17.4 (7)	17.6 (4)	0.3 (4)	3.1 (3)	2.9 (4)
O5	20.6 (5)	18.2 (6)	21.3 (4)	-4.7 (4)	-2.0 (4)	-1.6 (4)
O6	21.5 (5)	23.6 (7)	22.9 (5)	-6.3 (4)	0.1 (4)	4.1 (4)
C1	27.8 (8)	15.4 (9)	16.7 (5)	-3.1 (5)	2.2 (5)	0.4 (6)
C2	27.6 (8)	19.9 (9)	21.5 (6)	-1.6 (5)	0.7 (5)	-9.2 (7)
C3	16.9 (7)	27.1 (10)	19.9 (6)	-3.2 (6)	-1.5 (5)	-4.4 (6)
C4	51.7 (10)	16.7 (9)	18.8 (6)	-0.1 (6)	-0.3 (7)	-4.1 (8)
C5	30.1 (9)	42.6 (12)	30.3 (7)	-2.8 (8)	-10.3 (6)	-14.2 (8)
C6	19.8 (7)	27.6 (10)	26.5 (7)	-3.6 (6)	5.0 (5)	4.2 (7)
C7	30.2 (9)	22.3 (10)	32.4 (7)	4.2 (7)	5.2 (6)	9.9 (7)
C8	23.4 (7)	19.6 (9)	18.5 (6)	1.4 (5)	-4.4 (5)	-1.8 (6)
C9	44.7 (11)	39.8 (13)	48.2 (10)	-3.8 (9)	27.9 (9)	8.5 (9)
C10	43.6 (10)	25.2 (10)	22.6 (7)	6.8 (6)	-4.8 (7)	1.3 (8)
C11	24.5 (7)	20.1 (9)	19.8 (6)	3.4 (5)	-4.3 (5)	-3.2 (6)
C12	17.2 (8)	35.0 (11)	33.1 (8)	0.5 (7)	-5.9 (6)	2.9 (7)
C13	21.9 (8)	22.0 (9)	26.7 (7)	3.5 (6)	4.3 (5)	7.3 (6)
C14	36.7 (9)	37.4 (11)	29.1 (7)	-2.9 (7)	-13.6 (7)	-7.7 (8)
C15	30.5 (9)	41.0 (13)	41.8 (9)	-2.8 (8)	10.8 (7)	13.9 (8)

**Table 4 Bond Lengths for 82888775\_shelxt.**

Atom Atom Length/ $\text{\AA}$  Atom Atom Length/ $\text{\AA}$

Fe1	O1	2.0012 (12)	C1	C2	1.404 (2)
Fe1	O2	1.9801 (10)	C1	C4	1.500 (2)
Fe1	O3	1.9900 (10)	C2	C3	1.387 (2)
Fe1	O4	1.9971 (11)	C3	C5	1.5043 (19)
Fe1	O5	2.0084 (10)	C6	C7	1.382 (2)
Fe1	O6	2.0037 (10)	C6	C9	1.504 (2)
O1	C1	1.2692 (19)	C7	C8	1.405 (2)
O2	C3	1.2821 (19)	C8	C10	1.499 (2)
O3	C6	1.276 (2)	C11	C12	1.391 (2)
O4	C8	1.2695 (19)	C11	C14	1.507 (2)
O5	C11	1.2704 (18)	C12	C13	1.396 (2)
O6	C13	1.2750 (18)	C13	C15	1.503 (2)

**Table 5 Bond Angles for 82888775\_shelxt.**

Atom	Atom	Atom	Angle/°	Atom	Atom	Atom	Angle/°
O1	Fe1	O5	88.85 (4)	O1	C1	C2	123.85 (13)
O1	Fe1	O6	92.30 (5)	O1	C1	C4	116.51 (13)
O2	Fe1	O1	87.58 (4)	C2	C1	C4	119.63 (14)
O2	Fe1	O3	94.21 (5)	C3	C2	C1	124.29 (15)
O2	Fe1	O4	87.80 (4)	O2	C3	C2	124.78 (13)
O2	Fe1	O5	176.28 (5)	O2	C3	C5	114.83 (13)
O2	Fe1	O6	92.44 (4)	C2	C3	C5	120.37 (14)
O3	Fe1	O1	90.33 (4)	O3	C6	C7	125.02 (14)
O3	Fe1	O4	88.08 (4)	O3	C6	C9	114.99 (15)
O3	Fe1	O5	86.87 (5)	C7	C6	C9	119.99 (16)
O3	Fe1	O6	172.94 (5)	C6	C7	C8	124.52 (15)
O4	Fe1	O1	174.99 (4)	O4	C8	C7	124.02 (13)
O4	Fe1	O5	95.80 (5)	O4	C8	C10	116.67 (13)
O4	Fe1	O6	89.84 (4)	C7	C8	C10	119.30 (14)
O6	Fe1	O5	86.64 (4)	O5	C11	C12	124.40 (13)
C1	O1	Fe1	129.93 (9)	O5	C11	C14	115.75 (14)
C3	O2	Fe1	129.54 (9)	C12	C11	C14	119.80 (14)
C6	O3	Fe1	128.23 (9)	C11	C12	C13	123.81 (15)
C8	O4	Fe1	129.14 (9)	O6	C13	C12	124.84 (14)
C11	O5	Fe1	129.27 (10)	O6	C13	C15	115.64 (14)
C13	O6	Fe1	128.94 (10)	C12	C13	C15	119.49 (15)

**Table 6 Torsion Angles for 82888775\_shelxt.**

A	B	C	D	Angle/°	A	B	C	D	Angle/°
Fe1	O1	C1	C2	2.1 (2)	O1	C1	C2	C3	-1.1 (3)
Fe1	O1	C1	C4	-176.61 (11)	O3	C6	C7	C8	-2.0 (3)
Fe1	O2	C3	C2	0.4 (2)	O5	C11	C12	C13	4.3 (3)
Fe1	O2	C3	C5	179.05 (11)	C1	C2	C3	O2	-0.2 (3)
Fe1	O3	C6	C7	11.2 (2)	C1	C2	C3	C5	-178.82 (15)
Fe1	O3	C6	C9	-169.38 (12)	C4	C1	C2	C3	177.62 (15)
Fe1	O4	C8	C7	1.2 (2)	C6	C7	C8	O4	-4.5 (3)
Fe1	O4	C8	C10	-177.73 (10)	C6	C7	C8	C10	174.38 (16)
Fe1	O5	C11	C12	9.4 (2)	C9	C6	C7	C8	178.60 (17)
Fe1	O5	C11	C14	-173.28 (10)	C11	C12	C13	O6	-6.3 (3)
Fe1	O6	C13	C12	-5.7 (2)	C11	C12	C13	C15	171.78 (16)
Fe1	O6	C13	C15	176.23 (12)	C14	C11	C12	C13	-172.90 (16)

**Table 7 Hydrogen Atom Coordinates ( $\text{\AA} \times 10^4$ ) and Isotropic Displacement Parameters ( $\text{\AA}^2 \times 10^3$ ) for 82888775\_shelxt.**

Atom	<i>x</i>	<i>y</i>	<i>z</i>	U(eq)
H2	1380.27	3890.95	7415.35	28
H4A	2757.7	4188.89	9380.57	44
H4B	2163.67	3490.63	8857.41	44
H4C	1792.3	4242.54	9560.7	44
H5A	422.34	4972.75	5758.68	51
H5B	830.18	4016.92	5823.19	51
H5C	1198.3	4740.89	5080.74	51
H7	1225.92	8856.16	6998.03	34
H9A	280.5	7727.83	8667.25	66
H9B	618.5	8708.9	8529.29	66
H9C	1045.15	8058.08	9311.06	66
H10A	2638.65	8621.19	5068.45	46
H10B	1993.97	9281.28	5565.16	46
H10C	1681.84	8494.41	4868.12	46
H12	5120.75	6329.93	7895.41	34
H14A	4524.94	8081.06	8934.37	52
H14B	4998.02	7218.3	9303.26	52
H14C	4108.96	7438.66	9733.49	52
H15A	4751.73	4880.9	6169.58	57
H15B	5436.89	5590.19	6451.8	57
H15C	4849.47	5756.1	5515.19	57

#### Refinement model description

Number of restraints - 0, number of constraints - unknown.

#### Details:

1. Fixed Uiso
  - At 1.2 times of:
    - All C(H) groups
  - At 1.5 times of:
    - All C(H,H,H) groups
- 2.a Aromatic/amide H refined with riding coordinates:
  - C2(H2), C7(H7), C12(H12)
- 2.b Idealised Me refined as rotating group:
  - C4(H4A,H4B,H4C), C5(H5A,H5B,H5C), C9(H9A,H9B,H9C), C10(H10A,H10B,H10C), C14(H14A,H14B,H14C), C15(H15A,H15B,H15C)



Appendix D. Crystal Structure Refinement for compound **Fe(3-chloroacetylacetonate)<sub>3</sub>**.



Crystal structure  
determination of:  
**mac210003**  
(**C<sub>15</sub>H<sub>18</sub>Cl<sub>3</sub>FeO<sub>6</sub>**)

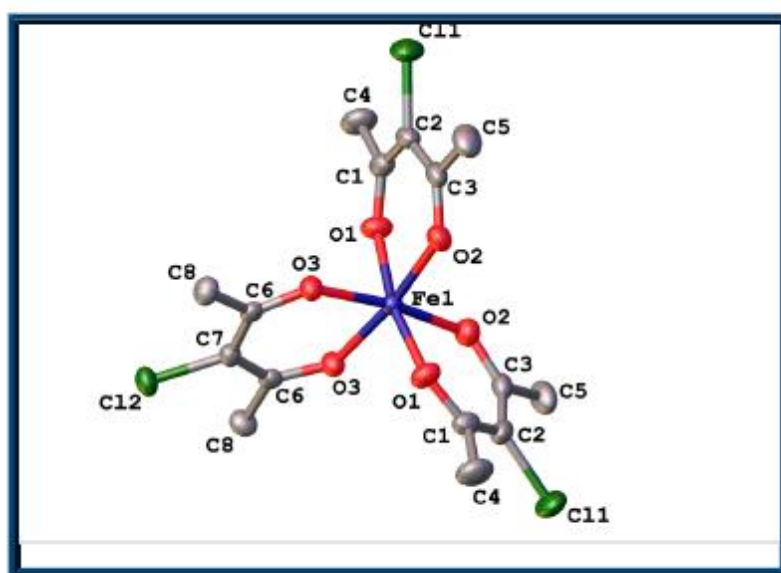
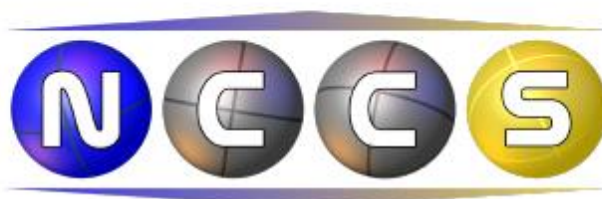


Table 1 : Crystal data and structure refinement for mac210003.

Identification code	mac210003
Empirical formula	C <sub>15</sub> H <sub>18</sub> Cl <sub>3</sub> FeO <sub>6</sub>
Formula weight	456.49
Temperature/K	150.0(2)
Crystal system	monoclinic
Space group	C2/c
a/Å	15.7218(4)
b/Å	9.4101(2)
c/Å	12.8074(3)
α/°	90
β/°	99.772(2)
γ/°	90



Volume/Å <sup>3</sup>	1867.28(8)
Z	4
$\rho_{\text{calc}}/\text{g}/\text{cm}^3$	1.624
$\mu/\text{mm}^{-1}$	10.690
F(000)	932.0
Crystal size/mm <sup>3</sup>	0.22 × 0.16 × 0.09
Radiation	Cu K $\alpha$ ( $\lambda = 1.54184$ )
2 $\theta$ range for data collection/°	11 to 133.664
Index ranges	-14 ≤ h ≤ 18, -11 ≤ k ≤ 11, -15 ≤ l ≤ 14
Reflections collected	12950
Independent reflections	1655 [ $R_{\text{int}} = 0.0491$ , $R_{\text{sigma}} = 0.0224$ ]
Data/restraints/parameters	1655/0/118
Goodness-of-fit on F <sup>2</sup>	1.064
Final R indexes [ $I \geq 2\sigma(I)$ ]	$R_1 = 0.0348$ , $wR_2 = 0.0932$
Final R indexes [all data]	$R_1 = 0.0356$ , $wR_2 = 0.0945$
Largest diff. peak/hole / e Å <sup>-3</sup>	0.53/-0.48

### Experimental

Crystal structure data for mac210003 was collected on a Xcalibur, Atlas, Gemini ultra diffractometer equipped with an fine-focus sealed X-ray tube ( $\lambda_{\text{Cu K}\alpha} = 1.54184 \text{ \AA}$ ) and an Oxford Cryosystems CryostreamPlus open-flow N<sub>2</sub> cooling device. Cell refinement, data collection and data reduction were undertaken via software CrysAlisPro 1.171.40.82a (Rigaku OD, 2020). Intensities were corrected for absorption using CrysAlisPro 1.171.40.82a (Rigaku Oxford Diffraction, 2020) Empirical absorption correction using spherical harmonics, implemented in SCALE3 ABSPACK scaling algorithm..

Using Olex2 (Dolomanov, 2009), the structure was solved using SHELXT 2014/5 (Sheldrick, 2014) and refined by XL (Sheldrick, 2008).

Dolomanov, O.V., Bourhis, L.J., Gildea, R.J., Howard, J.A.K. & Puschmann, H. (2009), *J. Appl. Cryst.* 42, 339-341.  
 Sheldrick, G.M. (2008). *Acta Cryst. A* 64, 112-122.  
 Sheldrick, G.M. (2015). *Acta Cryst. A* 71, 3-8.

### Crystal structure determination of [mac210003]

Crystal Data for C<sub>15</sub>H<sub>18</sub>Cl<sub>3</sub>FeO<sub>6</sub> ( $M = 456.49 \text{ g/mol}$ ): monoclinic, space group C2/c (no. 15),  $a = 15.7218(4) \text{ \AA}$ ,  $b = 9.4101(2) \text{ \AA}$ ,  $c = 12.8074(3) \text{ \AA}$ ,  $\beta = 99.772(2)^\circ$ ,  $V = 1867.28(8) \text{ \AA}^3$ ,  $Z = 4$ ,  $T = 150.0(2) \text{ K}$ ,  $\mu(\text{Cu K}\alpha) = 10.690 \text{ mm}^{-1}$ ,  $D_{\text{calc}} = 1.624 \text{ g}/\text{cm}^3$ , 12950 reflections measured ( $11^\circ \leq 2\theta \leq 133.664^\circ$ ), 1655 unique ( $R_{\text{int}} = 0.0491$ ,  $R_{\text{sigma}} = 0.0224$ ) which were used in all calculations. The final  $R_1$  was 0.0348 ( $I > 2\sigma(I)$ ) and  $wR_2$  was 0.0945 (all data).

### Special details of refinement:

?

### Comments:

These data represent a low-temperature redetermination of a structure for which room temperature data are available in the CSD (CSD Refcode: PAYRAK).

**Table 2 Fractional Atomic Coordinates ( $\times 10^4$ ) and Equivalent Isotropic Displacement Parameters ( $\text{\AA}^2 \times 10^3$ ) for mac210003.  $U_{\text{eq}}$  is defined as**

1/3 of the trace of the orthogonalised  $U_{IJ}$  tensor.

Atom	x	y	z	U(eq)
Fe1	5000	2883.8 (5)	7500	21.61 (17)
Cl1	2050.5 (4)	975.3 (8)	5849.6 (7)	57.5 (3)
Cl2	5000	8349.0 (8)	7500	36.1 (2)
O1	3853.8 (10)	2681.8 (19)	7942.5 (13)	32.5 (4)
O2	4546.1 (10)	1530.2 (16)	6333.5 (13)	30.5 (4)
O3	5348.2 (10)	4444.3 (16)	8536.8 (12)	26.9 (4)
C1	3150.4 (15)	2183 (2)	7453 (2)	31.6 (5)
C2	3078.4 (15)	1508 (2)	6468 (2)	33.8 (5)
C3	3772.8 (16)	1187 (2)	5953.4 (19)	31.1 (5)
C4	2382.4 (17)	2345 (4)	8002 (3)	46.8 (7)
C5	3649 (2)	397 (3)	4917 (2)	46.9 (7)
C6	5297.0 (13)	5797 (2)	8461.2 (17)	23.6 (5)
C7	5000	6491 (3)	7500	24.8 (6)
C8	5576.0 (16)	6611 (3)	9462.9 (18)	31.6 (5)

**Table 3 Anisotropic Displacement Parameters ( $\text{\AA}^2 \times 10^3$ ) for mac210003. The Anisotropic displacement factor exponent takes the form:**

$$-2\pi^2[h^2a^{*2}U_{11}+2hka^*b^*U_{12}+...].$$

Atom	$U_{11}$	$U_{22}$	$U_{33}$	$U_{23}$	$U_{13}$	$U_{12}$
Fe1	19.0 (3)	20.4 (3)	25.0 (3)	0	2.63 (18)	0
Cl1	32.3 (4)	47.5 (4)	83.2 (6)	-12.1 (4)	-17.7 (3)	-4.6 (3)
Cl2	40.8 (5)	20.4 (4)	46.0 (5)	0	4.0 (3)	0
O1	23.0 (8)	43.1 (10)	31.5 (9)	-3.6 (7)	4.6 (7)	-4.7 (7)
O2	33.0 (9)	24.6 (8)	33.8 (8)	-2.9 (6)	5.1 (7)	-2.6 (7)
O3	29.9 (8)	23.2 (8)	25.9 (8)	1.3 (6)	-0.1 (6)	-1.2 (6)
C1	23.4 (12)	29.8 (13)	40.8 (13)	8.7 (9)	2.7 (10)	-1.0 (9)
C2	26.4 (11)	25.5 (12)	45.1 (14)	1.7 (10)	-6.6 (10)	-4.7 (9)
C3	36.7 (13)	18.2 (10)	34.6 (12)	0.7 (9)	-5.0 (10)	-2.0 (9)
C4	24.7 (13)	59.6 (18)	57.4 (18)	5.6 (14)	10.4 (12)	-3.3 (12)
C5	60.1 (18)	31.1 (13)	43.1 (15)	-11.2 (11)	-9.3 (13)	2.7 (12)
C6	15.7 (10)	26.0 (11)	29.3 (11)	-1.1 (8)	4.2 (8)	-1.7 (8)
C7	22.5 (14)	20.0 (15)	32.4 (16)	0	5.8 (12)	0
C8	35.5 (12)	31.5 (12)	27.4 (12)	-4.8 (9)	3.9 (9)	-4.0 (10)

**Table 4 Bond Lengths for mac210003.**

Atom	Atom	Length/\AA	Atom	Atom	Length/\AA
Fe1	O1	1.9878 (16)	O2	C3	1.272 (3)
Fe1	O1 <sup>1</sup>	1.9878 (16)	O3	C6	1.278 (3)
Fe1	O2 <sup>1</sup>	2.0005 (16)	C1	C2	1.399 (4)
Fe1	O2	2.0005 (16)	C1	C4	1.505 (4)
Fe1	O3	1.9931 (16)	C2	C3	1.401 (4)
Fe1	O3 <sup>1</sup>	1.9931 (15)	C3	C5	1.504 (3)
Cl1	C2	1.748 (2)	C6	C7	1.402 (3)
Cl2	C7	1.749 (3)	C6	C8	1.495 (3)
O1	C1	1.266 (3)			

**Table 5 Bond Angles for mac210003.**

Atom	Atom	Atom	Angle/°	Atom	Atom	Atom	Angle/°
O1	Fe1	O1 <sup>1</sup>	169.02 (11)	C6	O3	Fe1	132.58 (14)
O1 <sup>1</sup>	Fe1	O2 <sup>1</sup>	85.77 (7)	O1	C1	C2	123.1 (2)
O1 <sup>1</sup>	Fe1	O2	87.24 (7)	O1	C1	C4	115.7 (2)
O1	Fe1	O2 <sup>1</sup>	87.24 (7)	C2	C1	C4	121.2 (2)
O1	Fe1	O2	85.77 (7)	C1	C2	C11	117.76 (19)
O1	Fe1	O3	92.31 (7)	C1	C2	C3	124.9 (2)
O1 <sup>1</sup>	Fe1	O3 <sup>1</sup>	92.31 (7)	C3	C2	C11	117.35 (19)
O1 <sup>1</sup>	Fe1	O3	95.77 (7)	O2	C3	C2	122.4 (2)
O1	Fe1	O3 <sup>1</sup>	95.77 (7)	O2	C3	C5	115.8 (2)
O2	Fe1	O2 <sup>1</sup>	100.90 (9)	C2	C3	C5	121.8 (2)
O3	Fe1	O2	171.69 (7)	O3	C6	C7	122.5 (2)
O3	Fe1	O2 <sup>1</sup>	87.06 (6)	O3	C6	C8	116.10 (19)
O3 <sup>1</sup>	Fe1	O2 <sup>1</sup>	171.69 (7)	C7	C6	C8	121.4 (2)
O3 <sup>1</sup>	Fe1	O2	87.06 (6)	C6 <sup>1</sup>	C7	C12	117.77 (14)
O3	Fe1	O3 <sup>1</sup>	85.09 (9)	C6	C7	C12	117.77 (14)
C1	O1	Fe1	130.71 (17)	C6 <sup>1</sup>	C7	C6	124.5 (3)
C3	O2	Fe1	130.10 (16)				

**Table 6 Torsion Angles for mac210003.**

A	B	C	D	Angle/°	A	B	C	D	Angle/°
Fe1	O1	C1	C2	6.8 (3)	O1	C1	C2	C3	6.1 (4)
Fe1	O1	C1	C4	-173.73 (18)	O3	C6	C7	C12	-177.72 (15)
Fe1	O2	C3	C2	-14.2 (3)	O3	C6	C7	C6 <sup>1</sup>	2.28 (15)
Fe1	O2	C3	C5	166.36 (16)	C1	C2	C3	O2	-2.3 (4)
Fe1	O3	C6	C7	-4.7 (3)	C1	C2	C3	C5	177.1 (2)
Fe1	O3	C6	C8	175.50 (14)	C4	C1	C2	C11	4.6 (3)
C11	C2	C3	O2	179.78 (18)	C4	C1	C2	C3	-173.3 (2)
C11	C2	C3	C5	-0.9 (3)	C8	C6	C7	C12	2.1 (2)
O1	C1	C2	C11	-175.96 (19)	C8	C6	C7	C6 <sup>1</sup>	-177.9 (2)

**Table 7 Hydrogen Atom Coordinates ( $\text{Å} \times 10^4$ ) and Isotropic Displacement Parameters ( $\text{Å}^2 \times 10^3$ ) for mac210003.**

Atom	x	y	z	U(eq)
H4A	2570.82	2729.97	8714.47	70
H4B	2111.32	1415.8	8053.03	70
H4C	1964.98	2995.65	7595.23	70
H5A	3344.28	1007.42	4354.88	70

H5B	3307.71	-462.58	4974.03	70
H5C	4212.58	132.97	4748.31	70
H8A	5096	7197.64	9612.74	47
H8B	6065.3	7222.87	9383.42	47
H8C	5749.63	5945.81	10049.16	47

#### Refinement model description

Number of restraints - 0, number of constraints - unknown.

#### Details:

1. Fixed Uiso  
At 1.5 times of:  
All C(H,H,H) groups  
2.a Idealised Me refined as rotating group:  
C4 (H4A, H4B, H4C), C5 (H5A, H5B, H5C), C6 (H6A, H6B, H6C)

This report has been created with Olex2, compiled on 2020.12.01 svn:r5660950 for OlexSys. Please [let us know](#) if there are any errors or if you would like to have additional features.